Study of the effects of macroautophagy deficiency on mitochondrial function, energy metabolism and cell fate

Lucia Sedlackova

Doctor of Philosophy

Campus for Ageing and Vitality
Institute for Cell and Molecular Biosciences
Newcastle University

September 2019

Published Materials & Conference Attendance

Published manuscripts:

Sedlackova, Lucia, and Viktor I. Korolchuk. "Mitochondrial quality control as a key determinant of cell survival." *Biochimica et Biophysica Acta (BBA)-Molecular Cell Research* (2018)

Conference attendance and contributions:

1. **10th Annual Alliance for Healthy Ageing**
   Newcastle upon Tyne, UK, October 2019. Poster presentation: *Autophagy Promotes Cell/Organismal Survival by Maintaining NAD+/NADH Levels*.

2. **Redox Signalling in Physiology, Ageing and Disease**
   Newcastle upon Tyne, UK, July 2019. Poster presentation and session co-chair: *Study of Autophagy-Mitochondria-ETC axis in cell fate determination.* Poster prize awarded from BSRA and the Biochemical society.

3. **Keystone Symposia J2 Mitochondria in Aging and Age-Related Disease**
   Keystone, CA, USA, January 2019. Poster presentation: *Investigations of the autophagy-mitochondria axis in cell survival.* Travel to conference was supported by a Keystone Symposia Scholarship and a Biochemical society general travel grant.

4. **8th Annual Alliance for Healthy Ageing**
   Groningen, NE, November 2017. Poster presentation: *Autophagy impairment plays a role in mitochondrial dysfunction and the pathology of NPC1*. Travel to conference was supported by Newcastle University Institute for Ageing (NUIA) travel fund.

5. **Mitochondrial Patient Day**
   Newcastle Upon Tyne, UK, October 2016. Held a researcher table to communicate my research to patients suffering from mitochondrial disease and to their families.

Thesis Abstract

Functional cellular metabolism underpins healthy ageing by sustaining cellular signalling and organelle function. In turn, cellular metabolism critically depends on macronutrient availability and organelle health, which are maintained by cellular catabolic pathways, and by autophagy in particular. Importantly, decline in autophagy flux and mitochondrial dysfunction are observed in a variety of age-related chronic disorders and neurodegenerative diseases. I hypothesized that autophagy impairment stands at the root of age-related pathology and set out to test my hypothesis in a genetic model of autophagy deficiency. I have established a model where autophagy 5 (*Atg5*) knockout cells are forced to produce ATP via oxidative phosphorylation (OXPHOS) in culture and uncovered a rapid loss of viability accompanied by a reduction in nucleotides. In particular, loss of nicotinamide adenine dinucleotide (NAD(H)) levels were most predictive of cellular viability. NADH functions as a cofactor in cellular metabolism, maintenance of mitochondrial membrane potential and ATP production. I identified several compounds that rescue loss of cellular viability due to autophagy dysfunction, of which NAD(H) level normalization by precursor supplementation proved most effective.

I tested the translational potential of my findings in cellular models of Niemann Pick Type C1 (NPC1) disease that is characterized by altered lipid metabolism and autophagy impairment, and its clinical presentations include spleen and liver enlargement, and progressive neurodegeneration. In immortalized *NPC1* knockout cell lines, NAD(H) precursor treatment rescued cell death in conditions of enforced OXPHOS respiration. Furthermore, I identified NAD(H) depletion and increased susceptibility to exogenous oxidative stress in primary human fibroblasts isolated from NPC1 patients. Corroborating results from other models tested in my study, NAD(H) precursor supplementation successfully boosted NAD(H) levels and improved resistance to oxidative stress in patient cells.

In summary, I have demonstrated that autophagy promotes a healthy nucleotide and NAD(H) metabolism and that NAD(H) precursor supplementation could protect cells and tissues affected by autophagy dysfunction.

Acknowledgements

First of all, I would like to express my gratitude to the Medical Research Council for funding not only this PhD project, but also an international laboratory visit to the Trushina Group at the Mayo Clinic as a part of the DiMeN Doctoral Training Partnership. Furthermore, many thanks to the EU COST action PROTEOSTASIS for funding my short-term scientific mission to Carracedo Group at the CICbioGUNE institute.

My greatest appreciation belongs to my main supervisor Dr Viktor I Korolchuk for his constructive suggestions, advice and support throughout this project, as his guidance and mentoring helped me grow into a resilient and confident researcher. I also greatly appreciate the advice, continuous support and constructive feedback that was invaluable throughout my studies from my second supervisor, Prof Alberto Sanz Montero. Sincere thanks to Dr Laura Greaves and Prof Thomas von Zglinicki, members of my progression panel for their valuable guidance and helpful suggestions. I am particularly grateful to Dr Arkaitz Carracedo and Prof Eugenia Trushina for their kindness, mentorship and guidance during my laboratory visits. I would also like to acknowledge their many lab members who helped me adjust to the local culture and lab environment and made my visits an altogether unforgettable experience.

I would like to express my gratitude to past lab members Dr Elsje G. Otten, Dr Yoana Rabanal Ruiz, Dr Alvaro Martinez Guimera, Dr Bernadette Carroll, Dr Graeme Hewitt, Dr Diego Manni, Dr Alison Howard, current lab members George Kelly and Elise Bennett, and visiting scientists Francesca Urselli and Tetsushi Kataura for their help, support and contributions to my work. A big thank you to the countless collaborators who contributed to this project. I would especially like to thank the undergraduate students I mentored along the way, for their company and help during long days spent in the lab, and for helping me grow as a researcher and as a mentor.

Finally, my greatest appreciation goes to my family and friends for their unwavering love and support throughout my studies and a very special thanks belongs to Mr Matthew Snowdon for his love, his skills as a motivator and for ‘dealing with my crazy’.

Table of Contents

List of Figures

List of Tables

List of Abbreviations

$\bullet NO_2$	nitrogen dioxide
$\bullet O_2$	superoxide
•QH	ubisemiquinone
2-DG	2-deoxy glucose
3-MA	3-methyladenine
3-NT	3-nitrotyrosine
ACMS	α-amino-β-carboxymuconate-ε-semialdehyde
ACMSD	α-amino-β-carboxymuconate-ε-semialdehyde decarboxylase
AD	Alzheimer's disease
ADP	adenine diphosphate
ADPR	ADP ribose
AEC	adenylate energy charge
ALS	amyotrophic lateral sclerosis
AMBRA1	activating molecule in beclin 1-regulated autophagy protein 1
AMP	adenine monophosphate
AMPK	AMP-activated protein kinase
ANT	adenine nucleotide translocase
ApoE	apolipoprotein E
ARH3	ADP-ribosylhydrolase 3
ARTD1	ADP-ribosyltransferase diphtheria toxin-like 1
ATF4/5	activating transcription factor 4/5
ATFS-1	activating transcription factor associated with stress-1
ATG	autophagy
ATM	ataxia-telangiectasia mutated
ATP	adenosine triphosphate
BBB	blood brain barrier
BCL-2	B-cell lymphoma 2
BNIP3	BCL-2/adenovirus E1B 19 kDa protein-interacting protein 3
BNIP3L (NIX)	BNIP3-like
BN-PAGE	blue native polyacrylamide gel electrophoresis
Ca^{2+}	calcium
cADPR	cyclic ADP-ribose
CALCOCO2	Ca2+-binding and coiled-coil domain-containing protein 2
c-Cbl	cellular Casitas B-lineage lymphoma
CHIP	C-terminus of heat shock cognate 71 kDa-interacting protein
CKD	chronic kidney disease
CL	cardiolipin
ClpP	caseinolytic peptidase proteolytic subunit
CMA	chaperone mediated autophagy
CoQ	coenzyme Q
CRISPR	clustered regularly interspaced short palindromic repeats
CSB	Cockayne syndrome group B protein
cyt *c*	cytochrome *c*
DHODH	dihydroorotate dehydrogenase

Dig	digitonin
DMT2	diabetes mellitus type 2
DRP1	dynamin related protein 1
DTAB	dodecyltrimethylammonium bromide
DTT	dithiothreitol
DUB	deubiquitylase
ECAR	extracellular acidification rate
ENT	equilibrative nucleoside transporters
ER	endoplasmic reticulum
ETC	electron transport chain
ETF	electron transfer flavoprotein
FAD	flavin adenine dinucleotide
FBS	foetal bovine serum
FCCP	carbonyl cyanide-*4*-(trifluoromethoxy)phenylhydrazone
FDR	false discovery rate
FIS1	mitochondrial fission 1 protein
FMN	flavin mononucleotide
FOXO	forkhead box group O
FUNDC1	FUN14 domain-containing protein 1
GABARAP	γ-aminobutyric acid receptor-associated protein
GAPARAPL1/2	γ-aminobutyric acid receptor-associated protein like 1 and 2
GPDH	glycerol-3-phosphate dehydrogenase
gRNA	guide RNA
GTPase	guanosine triphosphatase
GTZ	glitazone
H2DCFDA	2′,7′-dichlorodihydrofluorescein diacetate, acetyl ester
H_2O_2	hydrogen peroxide
HD	Huntington's disease
HDAC6	histone deacetylase 6
HPβCD	2-hydroxypropyl-β-cyclodextrin
HRP	horseradish peroxidase
HSC70	heat shock cognate 71 kDa
I/R	ischaemia-reperfusion
IMM	mitochondrial inner membrane
IMS	intermembrane space
KD	knockdown
KEGG	Kyoto Encyclopaedia of Genes and Genomes
LAMP2A	lysosome-associated membrane protein 2
LIR	LC3-interacting region
L-OPA1	long peptide OPA1
LRP1	lipoprotein receptor-related protein
MAM	mitochondria-associated membranes
MAP1LC3/LC3	microtubule associated protein 1 light-chain 3
MB	mitochondrial biogenesis
MCI	mild cognitive impairment
MCU	mitochondrial calcium uniporter
MD	mitochondrial disease

MDV	mitochondria-derived vesicle
MEF	mouse embryonic fibroblast
MFF	mitochondrial fission factor
Mfn1	mitofusin 1
Mfn2	mitofusin 2
MICOS	mitochondrial contact site and cristae organising system
MID49/51	mitochondrial dynamics protein of 49kDa/51kDa
MiDAS	mitochondrial-dysfunction-associated senescence
MIRO-1	mitochondrial Rho GTPase1
mMP	mitochondrial membrane potential (ΔΨm)
MOMP	mitochondrial outer membrane permeabilization
MPC	mitochondrial pyruvate carrier
MPP+	1-methyl-4-phenylpyridinium
MPT	mitochondrial permeability transition
MQC	mitochondrial quality control
mRNA	messenger RNA
mtDNA	mitochondrial DNA
MTG	mitotracker green
mTORC1	mammalian target of rapamycin complex I
MTS	mitochondria targeting sequence
MTT	methylthiazolyldiphenyl-tetrazolium bromide
NA	nicotinic acid
NAAD	NA adenine dinucleotide
NAADP	nicotinic acid-adenine dinucleotide phosphate
NAC	N-acetylcysteine
NAD(P)	nicotinamide adenine dinucleotide phosphate (oxidised)
NAD(P)H	nicotinamide adenine dinucleotide phosphate (reduced)
NAD+	nicotinamide adenine dinucleotide (oxidised)
NADH	nicotinamide adenine dinucleotide (reduced)
NADSYN	NAD^+ synthase
NAFDL	non-alcoholic fatty liver disease
NAM	nicotinamide
NAMN	NA mononucleotide
NAMPT	nicotinamide phosphoribosyltransferase
NBR1	neighbour of breast cancer 1
NCLX	sodium/calcium/lithium exchanger pump
ND	neurodegenerative disorder
NDI1	non-proton translocating single-subunit NADH–ubiquinone reductase
nDNA	nuclear DNA
NDP52	nuclear domain 10 protein 52
NDUF	NADH Ubiquinone oxidoreductase Fe-S protein
NFE2L2	nuclear erythroid 2-like 2
NFT	neurofibrillary tangles
NLS	nuclear localization sequence
NMN	nicotinamide mononucleotide
NMNAT	NMN adenylyltransferase

NNMT	NAM *N*-methyltransferase
NO	nitric oxide
NPC	Niemann Pick Type C
NPC1/2	Niemann Pick Type C1/2
NR	nicotinamide riboside
NRBF2	nuclear receptor binding factor 2
NRF1/2	nuclear respiratory factor 1/2
NRK1/2	nicotinamide riboside kinase 1/2
OARD1	*O*-acyl-ADP-ribose deacylase 1
OCR	oxygen consumption rate
OMM	mitochondrial outer membrane
$ONOO^-$	peroxynitrite
OPA1	optic atrophy 1
OPTN	optineurin
OXPHOS	oxidative phosphorylation
p62	sequestosome 1 (SQSTM1)
PA	picolinic acid
PAR	poly(ADP-ribose)
PARG	PAR glycohydrolase
PARL	presenilin-associated rhomboid-like protease
PARP	poly-(ADP-ribose) polymerase
PCA	principal component analysis
PD	Parkinson's disease
PE	phosphatidylethanolamine
PGC-1α	PPARγ coactivator 1α
PGC-1β	PPARγ coactivator 1β
P_i	inorganic phosphorus
PI(3)P	phosphatidylinositol 3-phosphate
PINK1	PTEN-induced kinase 1
PKB (AKT)	protein kinase B
PM	pyruvate and malate
pmf	proton motive force
PPARγ	peroxisome proliferator-activated receptor γ
PPP	pentose phosphate pathway
Prdx-SO3	peroxiredoxin-SO3
PRPP	5-phosphoribosyl-α-1-pyrophosphate
PTM	post-translational modifications
Q	ubiquinone
QA	quinolinic acid
QH	ubisemiquinone
QH_2	ubiquinol
RCR	respiratory control ratio
RET	reverse electron transport
RISP	Rieske iron-sulphur protein
RNS	reactive nitrogen species
ROS	reactive oxygen species
SC	supercomplex

S.E.M	standard error of the mean
S1QEL2.2	suppressor of site Iq electron leak
SD	standard deviation
SDH	succinate dehydrogenase
SDHA	SDH subunit A
SDHB	SDH subunit B
SDHC	SDH subunit C
SDHD	SDH subunit D
SIRT	sirtuin
SOD	superoxide dismutase
S-OPA1	soluble short peptide OPA1
SP	sodium pyrvuate
TAX1BP1	Tax1 binding protein 1
TCA	tricarboxylic acid
TEM	transmission electron microscopy
TMRM	tetramethylrhodamine, methyl ester
TOLLIP	toll interacting protein
TSC1/2	tuberous sclerosis complex
TX-100	triton X-100
TZD	thiazolidinedione
Ub	ubiquitin
UMP	uridine monophosphate
UPR^{mt}	mitochondrial unfolded protein response
UPS	ubiquitin-proteasome system
UQCRFS1	ubiquinol-cytochrome *c* reductase iron-sulphur subunit 1
USP15/30	ubiquitin carboxyl-terminal hydrolase 15/30
UVRAG	UV radiation resistance associated protein
VDAC	voltage-dependent anion channel
VPS35	vacuolar protein sorting-associated protein 35
WIPI	WD repeat domain phosphoinositide-interacting protein 1
XPC	xeroderma pigmentosum
Z-VAD-fmk	Z-VAD-fluoromethylketone

Chapter 1. Introduction

1.1 Ageing: A primer

Age is the major risk factor for development of chronic illnesses and their comorbidities, including but not limited to cancer, cardiovascular disease, diabetes, arthritis and neurodegeneration. Age-related cellular and metabolic changes however, are not limited to the scope of any single disease, thus adding complexity to the research of underlying ageing-promoting processes (Guarente, 2014). On a molecular level, ageing is associated with metabolic alterations (López-Otín *et al.*, 2016) coupled to the complexity of global dysregulation and dysfunction (López-Otín *et al.*, 2013). Particularly vulnerable to the effect of time are the post-mitotic tissues of heart, muscle and brain (Ferrucci *et al.*, 2015).

In contrast, healthy ageing is underpinned by a functional metabolism. Major processes involved in metabolism control include proteostasis; energy generation and sensing; and nicotinamide adenine dinucleotide (NAD(H)) metabolism (Cantó, Menzies and Auwerx, 2015; López-Otín *et al.*, 2016). First, control of the abundance and correct folding of all cellular proteins is necessary to maintain a healthy cytosolic environment (Morimoto and Cuervo, 2014). Proteasome-mediated degradation and autophagy pathways act in concert to maintain quality control and functional proteome, thus mediating proteostasis (Tanaka and Matsuda, 2014). In addition to proteostasis, autophagy maintains a healthy cytoplasm by executing degradation of dysfunctional organelles and bulky protein aggregates (Klionsky and Emr, 2000).

Second, initial stages of energy generation occur in the cytoplasm and link to mitochondrial tricarboxylic acid (TCA) cycle, which leads to total substrate oxidation and release of electrons that feed the electron transport chain (ETC) and assist in energy generation in the form of an adenine triphosphate (ATP) molecule. In addition to energy generation, mitochondria are the hubs of amino acid, fatty acid and carbon metabolism, iron-sulphur cluster (Fe-S) generation, intracellular calcium (Ca^{2+}) and redox signalling, and play a central role in regulation of apoptotic cell death (Weinberg and Chandel, 2014; Galluzzi *et al.*, 2018). Mitochondrial health is thus key to cellular metabolic fitness and survival.

Lastly, involvement of a co-enzyme and a co-substrate of metabolic and redox reactions, the NAD(H) molecule (Verdin, 2015), has been explored in its role as a substrate for enzymes that help protect cells from age-related decline (Houtkooper, Pirinen and Auwerx, 2012; Cantó, Menzies and Auwerx, 2015). Enzymes that require NAD^+ as a co-factor include sirtuins (SIRTs), known to improve metabolic efficiency in conditions of nutrient stresses such as exercise, caloric restriction and fasting (Cantó, Menzies and Auwerx, 2015). In addition, poly(ADP-ribose) polymerases (PARPs) consume NAD^+ to aid DNA damage repair and contribute to metabolic adaptation by affecting the rate of glycolysis (Chaitanya, Steven and Babu, 2010; Cantó, Menzies and Auwerx, 2015). While SIRT activation has been linked to the protective effect of caloric restriction on the pathology of ageing, PARP inhibitors are currently explored as a target for cancer treatment (Cantó, Menzies and Auwerx, 2015).

It is now understood that together, these pathways have evolved to control, sense and react to the overall metabolic status of the cell and their individual function as well as their crosstalk are necessary for homeostasis maintenance. On the flip side, dysregulation of any of the pathways potentiates the development of age-related diseases such as neurodegeneration.

1.2 Proteostasis

Protein sentinels monitor the health of the entirety of the cellular protein population, the proteome, which is vital for the structural and catalytic integrity of the cell. The structure of the proteome is different in various cell types and undergoes changes during development, upon various insults, and in response to nutrient availability (Huang *et al.*, 2015; Harper and Bennett, 2016). Interestingly, the abundance of protein orthologs appears to be conserved across species (Vogel and Marcotte, 2012). Thus, cells contain multiple pathways of proteome monitoring, health maintenance and degradation in response to changes in environmental ques to achieve true adaptation and prevent onset of disease (Balch *et al.*, 2008). Loss of proteostasis has been described as one of the hallmarks of ageing and has been linked to the pathology of many neurodegenerative diseases, including Parkinson's disease (PD), Huntington's disease (HD), and Alzheimer's disease (AD) (Wong and Cuervo, 2010; López-Otín *et al.*, 2013).

1.2.1 Ubiquitin-proteasome system

The true complexity of a cellular proteome arises from the sheer number of genes transcribed in any given cell type, which has been approximated to ten thousand transcripts (Harper and Bennett, 2016). Proteins can exist in several forms as a consequence of alternative messenger RNA (mRNA) splicing, complex formation, and post-translational modification (PTM); and localize to various subcellular compartments (Harper and Bennett, 2016). Maintenance of the cellular proteome starts at surveillance of the fidelity of mRNA translation and involves a rapid response to misfolding, and degradation (Balch *et al.*, 2008; Harper and Bennett, 2016). Protein misfolding and dysfunction often occurs as a result of genetic mutations or stress (i.e. oxidation, thermal shock, radiation), which lead to loss of native structure. Proteins initially adopt their secondary and tertiary structure upon synthesis. Protein folding patterns are based on the primary amino acid sequence and the folding process is assisted by molecular chaperones, often referred to as heat shock proteins (Labbadia and Morimoto, 2015). Upon misfolding, chaperones are recruited to mediate re-folding, often in an ATP-dependent folding process (Kim *et al.*, 2013). If the protein damage is beyond repair, chaperones can also participate in protein delivery for degradation (Arndt, Rogon and Höhfeld, 2007). Specifically, the C-terminus of heat shock cognate 71 kDa-interacting protein (CHIP) acts as the switch between re-folding and proteasome-mediated degradation via its E3-ubiquitin ligase activity (Murata, Chiba and Tanaka, 2003).

Ubiquitin (Ub) is a small, 8.5kDa, highly conserved protein in eukaryotes, which is covalently linked to lysine residues of proteins in an ATP-depended process that requires three distinct classes of enzymes, called E1 (ubiquitin-activating enzymes), E2 (ubiquitin-conjugating enzymes) and E3 (ubiquitin-ligating enzymes) (Figure 1.1). (Welchman, Gordon and Mayer, 2005). Protein ubiquitylation serves a diverse set of functions in DNA repair, protein transcription, endocytosis and signal transduction (reviewed in (Welchman, Gordon and Mayer, 2005)). Additional linkage of more Ubs aided by E2, E3 and accessory factors (E4) results in formation of a ubiquitin chain (polyubiquitylation), which is opposed by the function of a class of deubiquitylating enzymes (DUBs) (Nijman *et al.*, 2005; Huang and Dixit, 2016). The nature of ubiquitin linkage via its seven lysine (K) residues determines the function of protein ubiquitylation due to chain recognition by ubiquitin-binding domain adaptor proteins(Kwon and Ciechanover, 2017). Formation of a polyubiquitin chain via

homotypic K48 (Chau *et al.*, 1989; Finley *et al.*, 1994) or heterotypic K48 and K11 linkages (Xu *et al.*, 2009) (a minimum of four Ubs) is sufficient for recognition by the ubiquitin-proteasome system (UPS) and targets proteins for degradation (Figure 1.1) (Welchman, Gordon and Mayer, 2005).

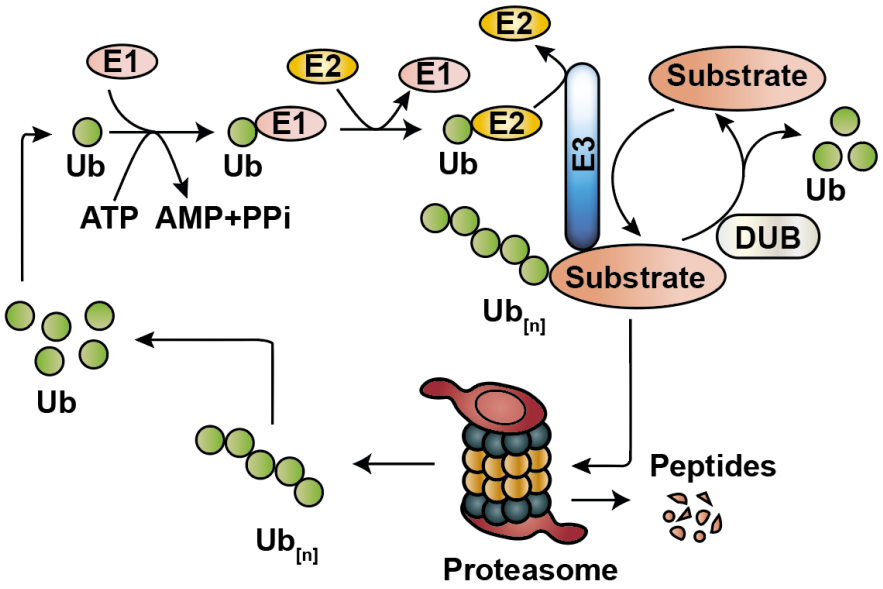

Figure 1. 1 Mechanism of protein ubiquitination

Protein modification by ubiquitin (Ub) is achieved by a catalytic cascade of three classes of enzymes: E1 (ubiquitin activation), E2 (ubiquitin conjugation) and E3 (ubiquitin ligation). Two known E1 enzymes, UBA1 and UBA6 form a thioester bond with ubiquitin. Approximately 38 E2 enzymes add specificity to the ubiquitylation pathway. E2s are viewed as Ub carriers between E1s and E3s via an active site cysteine residue. Approximately 700 proteins form the E3 family transfer charged Ub onto a lysine residue of the substrate protein. E2 and E3 enzymes aid the formation of poly-Ub chains. Ubiquitylation is opposed by a family of over 100 deubiquitylases (DUBs).

In UPS, ubiquitylated proteins are delivered to the 26S proteasome, a large protein complex consisting of a core particle (20S) and regulatory subunits (19S) located both in the cytoplasm and the nucleus (Finley, Chen and Walters, 2016; Collins and Goldberg, 2017). CryoEM resolution of the 19S subunits revealed their assembly into a ‘lid&base’ model hypothesized to wrap around the core subunit and regulate substrate recognition and entry. Delivery of protein cargo to the 26S proteasome is followed by its deubiquitylation and ATP-assisted unfolding by the 19S subunits and translocation to the core 20S unit for proteolysis (Finley, Chen and Walters, 2016). Due to the narrow translocation channel, properly folded or aggregated proteins are

excluded from entry into the core. Once inserted, unfolded protein chains are threaded through the core particle and undergo cleavage into smaller amino acid peptides that are either further processed for amino acid recycling, or, upon interferon activation, externalized on the plasma membrane to serve a role in adaptive cell-mediated immunity (Finley, 2009; Collins and Goldberg, 2017).

Importantly, if protein misfolding leads to oligomer and aggregate formation, i.e. when hydrophobic residues get exposed, and the resulting complexes cannot be unravelled, the complexes are sequestered in a double membraned vesicle and transported to lysosomes, a process referred to as macroautophagy (Zhang *et al.*, 2016) (Discussed in sections 1.2.2-1.2.4).

1.2.2 Autophagy

Autophagy refers to a set of evolutionarily conserved catabolic pathways that are together essential for the physiological pathways of cellular differentiation, development, homeostasis maintenance, immunity and ultimately, for survival (Mizushima *et al.*, 2008). On the flip side, autophagy has also been linked to pathophysiological roles in cancer, ageing and neurodegeneration (Mizushima *et al.*, 2008). Autophagy (self-eating) occurs in the cytoplasm whereby a dynamic membrane rearrangement and cargo engulfment/transport lead to lysosomal degradation of a variety of cytosolic targets (proteins, organelles, extracellular organisms) (Klionsky and Emr, 2000). Three forms of autophagy have been described to date: microautophagy, chaperone-mediated autophagy (CMA) and macroautophagy (Figure 1.2). It is now recognized that all forms of autophagy can act in a non-selective (bulk) or a highly selective manner assisted by receptors and chaperones. Although the mechanisms of cargo delivery and translocation to the lysosomal lumen differ, the end stage of autophagy, defined as cargo breakdown and recycling in the lysosomes, is common to all three forms. Chaperone-mediated autophagy refers to entry of cytosolic proteins into lysosomes via a protein translocation system (Tasset and Cuervo, 2016). In contrast to macroautophagy and microautophagy, CMA does not involve membrane re-organization. Rather, CMA cargo proteins that contain a KFERQ-like sequence (approximately 45% of mammalian proteome) are delivered to lysosomes by cytosolic heat shock cognate 71 kDa (HSC70), and enter the lumen through a protein

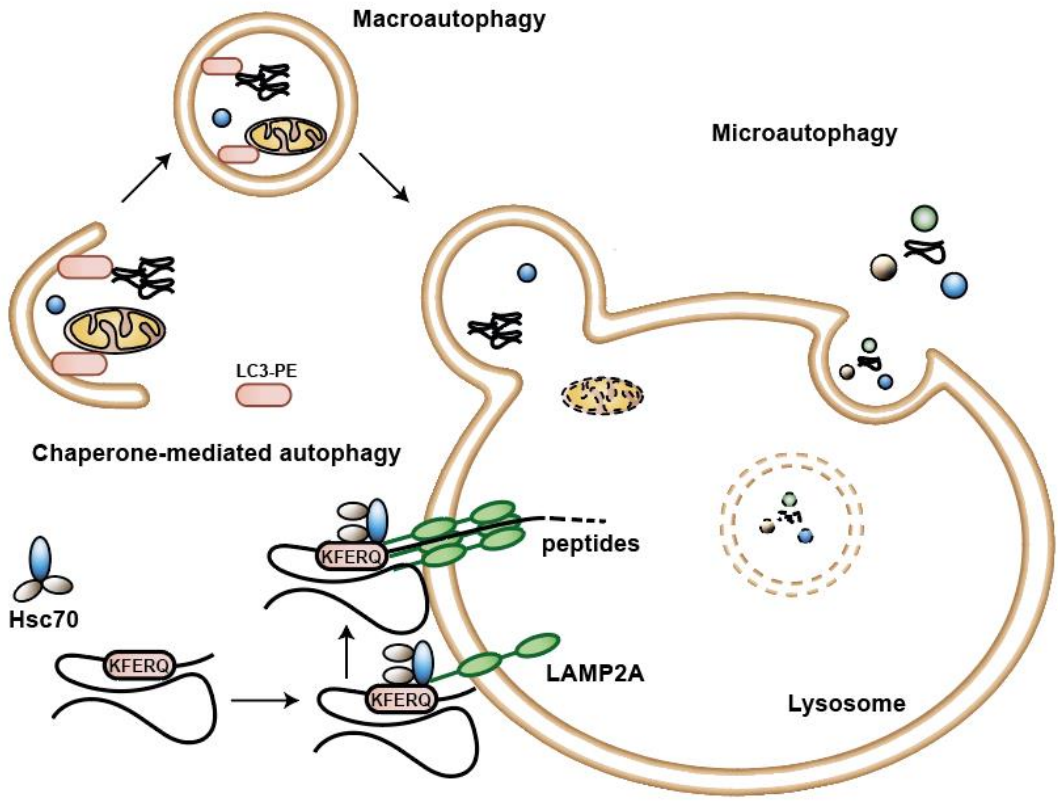

Figure 1. 2 The three forms of autophagy

Microautophagy: the inward invagination of lysosomal membrane results in engulfment of neighbouring cytosolic components. Chaperone-mediated autophagy: KFERQ-like motif containing proteins are delivered to the lysosome in a selective manner and translocate into the lumen via a LAMP2A oligomer. Macroautophagy: cytoplasmic cargo is recognized, engulfed into autophagoasomes and transported to lysosomes along the microtubules. Cargo is degraded within the lysosome following autophagosome-lysosome fusion.

translocation complex consisting of a lysosome-associated membrane protein type 2A (LAMP2A) oligomer (Tasset and Cuervo, 2016; Kirchner *et al.*, 2019). Therefore, CMA mediates degradation of proteins only, and was long considered to be a specific cellular response aimed to selectively replenish amino acid pools during periods of starvation. Proteins are protected from CMA-mediated degradation by multiple strategies: by sub-compartmentalization within the cell; by shielding their KFERQ-motif via adapting a tertiary structure; by interaction with other proteins or substrates; or by post-translational modifications to amino acids within or flanking the motif (Cuervo, 2010; Kirchner *et al.*, 2019). However, as explored in a review by Tasset and Cuervo, and research from the Cuervo group, CMA is likely to play a more specific role in energy metabolism homeostasis by targeted degradation of enzymes involved in glucose metabolism and promotion of lipolysis (Schneider, Suh and Cuervo, 2014; Tasset and Cuervo, 2016).

Microautophagy refers to a direct engulfment of cytoplasmic contents located in the proximity of endosomes and lysosomes. Microautophagy, when triggered by starvation, proceeds via tubular invaginations of the endosomal/lysosomal membranes (Mijaljica, Prescott and Devenish, 2011). Selective forms of microautophagy often require involvement of Hsc70. Other proteins involved in microautophagy were identified in yeast models and include clathrins and the Niemann-Pick Type C (NPC) protein family (summarized in (Tekirdag and Cuervo, 2018)). Selective microautophagy was reported in degradation of peroxisomes in yeast growing on glucose (pexophagy) (Dunn William A. *et al.*, 2005), in piecemeal nuclear degradation upon cell division or in carbon and nitrogen starvation (nucleophagy) (Roberts *et al.*, 2002) and upon discovery of mitochondria-derived vesicles (MDVs) that bud off the mitochondria and translocate to late endosomes (micromitophagy) (Neuspiel *et al.*, 2008; Sugiura *et al.*, 2014; McLelland and Fon, 2018).

1.2.3 Macroautophagy Overview

Macroautophagy refers to an autophagy pathway that involves a dynamic re-arrangement of cellular membranes to engulf cytoplasmic cargo, vesicle trafficking to- and fusion with- the lysosome. In contrast to the other two autophagy pathways and the UPS, macroautophagy is involved in the quality control of long-lived proteins, cytoplasmic organelles and bulky cytoplasmic aggregates (Zhang *et al.*, 2016). Multiple forms of macroautophagy, from herein referred to as autophagy, have been explored. From a metabolic standpoint, low levels of autophagy can occur in unstressed cells (basal autophagy), which are rapidly boosted by metabolic, oxidative or genotoxic stresses (bulk autophagy). In terms of function, autophagy can be highly selective or indiscriminate. Selective autophagy functions to maintain cellular fitness by degrading invading organisms (xenophagy), misfolded and aggregated proteins (aggrephagy) and dysfunctional/surplus organelles (pexophagy, ribophagy, mitophagy). In contrast, indiscriminate autophagy is activated at times when nutrient (amino acids, fatty acids, nucleotides) recycling is required for biosynthesis or for further catabolic processing to generate energy necessary for cell survival (Levine and Yuan, 2005).

1.2.4 Macroautophagy Mechanism

Formation and elongation of a cup-shaped double-layered membrane (isolation membrane, phagophore) marks initiation of autophagy. The origin of this membrane is a matter of debate and isolation membranes are likely to arise from multiple sources, including the endoplasmic reticulum (ER), the Golgi apparatus, the plasma membrane and during starvation perhaps also from organelles like mitochondria (Ravikumar *et al.*, 2010; Zhao and Zhang, 2019). Published data also supports a strong link between formation and maturation of the isolation membrane and the ER. This link was first shown by amino-acid starvation triggered re-localization of key autophagy initiation components to the ER and membrane curvature into an Ω (omegasome) shape (Axe *et al.*, 2008) and later visualised by electron microscopy as an ER cradle model, where the isolation membrane sits between two ER sheets and is neither assembled *de novo* nor completely identical to the ER (Hayashi-Nishino *et al.*, 2009).

Although autophagy was first discovered in mammals, it was subsequent studies in *Saccharomyces cerevisiae* that identified a set of autophagy (*ATG*) genes involved in orchestration of the entire process (Tsukada and Ohsumi, 1993; Thumm *et al.*, 1994; Suzuki *et al.*, 2007). The autophagy proteins often associate in complexes with distinct functions (Table 1.1) (Figure 1.3). The earliest complex, complex I or, Unc-51-like kinase 1 (ULK1)-ATG13-ATG101-focal adhesion kinase family interacting protein of 200kD (FIP200) (or ULK1-ATG13-ATG101-FIP200) (Hara *et al.*, 2008; Chan *et al.*, 2009; Ganley *et al.*, 2009; Hosokawa *et al.*, 2009; Jung *et al.*, 2009) is regulated by cellular energy sensor kinases including mammalian target of rapamycin complex I (mTORC1), protein kinase B (PKB, AKT) and adenine monophosphate (AMP)-activated protein kinase (AMPK), largely due to phosphorylation of ULK1. Additional layer of regulation is achieved by the tuberous sclerosis 1-2 complex (TSC1-TSC2 complex) inhibitory association with FIP200 (Wesselborg and Stork, 2015). Upon activation, autophagy complex I relocates to the ER and interacts with members of autophagy complex II, or VPS34-VPS15-Beclin1 (Kihara *et al.*, 2001).

Similarly to autophagy complex I, mTORC1, AMPK and AKT kinases are upstream regulators of complex II due to their interactions with all three components of the core complex (Wesselborg and Stork, 2015). The core element of autophagy complex II, Beclin1, also interacts with a number of regulatory proteins, including ATG14, nuclear receptor binding factor 2 (NRBF2), UV radiation resistance associated protein

(UVRAG), Rubicon, activating molecule in beclin 1-regulated autophagy protein 1 (AMBRA1) and B-cell lymphoma 2 (BCL-2) (Wesselborg and Stork, 2015). Beclin1 association with ATG14 is considered crucial for autophagosome formation (Zhong *et al.*, 2009). Complex II produces phosphatidylinositol 3-phosphate (PI(3)P), a lipid which assists with positive membrane curvature, and is likely to help the initiation membrane in adopting its cup-shaped form. PI(3)P formation also initiates recruitment of PI(3)P-binding proteins of the WIPI(1-4) family and by extension a trio of ATG proteins, ATG16L1 and a complex of ATG5-ATG12, which mark the site of autophagosome formation (Bento et al., 2016).

Table 1. 1 Eukaryotic ATG protein complex identity

Protein ID	Full Name	Yeast Homolog	Complex Identity
ULK1	Unc-51-like kinase 1	Atg1	Complex I
ATG13	Autophagy 13	Atg13	Complex I
FIP200	Focal adhesion kinase family interacting protein of 200kD	Atg17	Complex I
ATG101	Autophagy 101		Complex I
Beclin1/ BECN1	Beclin 1	Atg6/VPS30	Complex II
VPS34/ PIK3C3	Vacuolar protein sorting-associated protein 34/ Phosphatidylinositol 3-kinase catalytic subunit type 3	Vps34	Complex II
VPS15/ PIK3R4	Vacuolar protein sorting-associated protein 15/ Phosphoinositide 3-kinase regulatory subunit 4	Vps15	Complex II
ATG14	Autophagy 14, Barkor	Autophagy 14	Complex II
ATG9	Autophagy 9	Atg9	
WIPI	WD-repeat protein interacting with phosphoinosides	Atg18	Complex III
ATG2A/B	autophagy 2	Atg2	Complex III
ATG5	autophagy 5	Atg5	Complex IV
ATG12	autophagy 12	Atg12	Complex IV
ATG7	autophagy 7	Atg7	Complex IV (E1)
ATG10	autophagy 10	Atg10	Complex IV (E2)
ATG16L	autophagy 16-like	Atg16	Complex IV
ATG4A-D	autophagy 4	Atg4	
LC3	microtubule-associated protein light chain 3	Atg8	

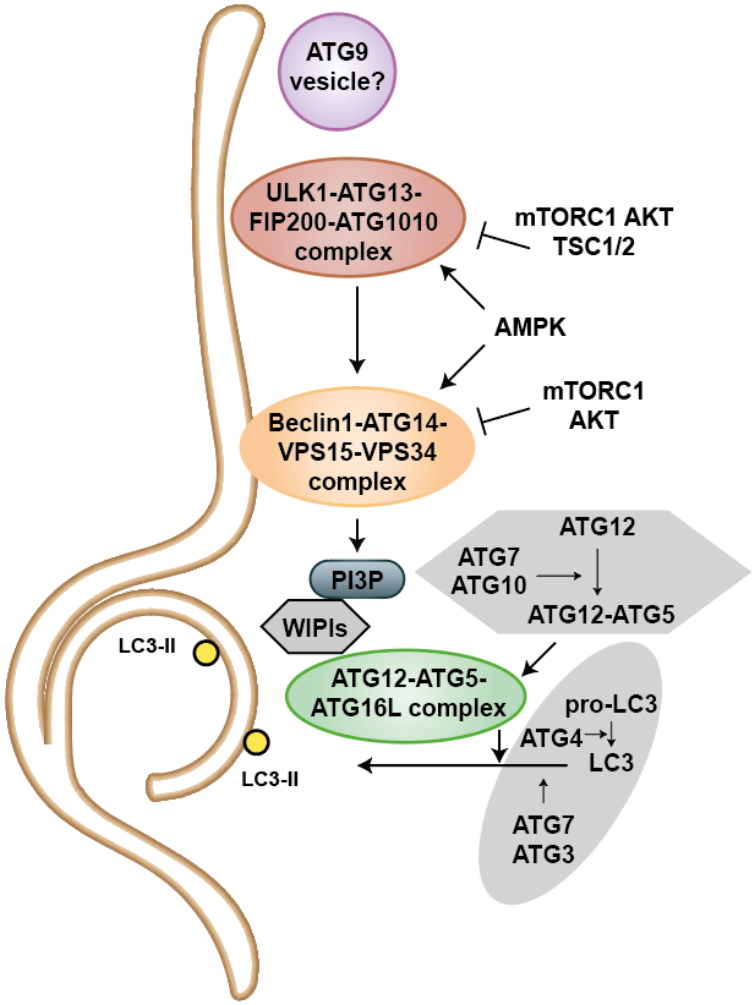

Figure 1. 3 The hierarchy of ATG complexes involved in autophagosome formation

Signals including nutrient and energy depletion, oxidative stress, hypoxia or protein aggregation converge on sensor kinases (mTORC1, AMPK, AKT), which activate the ULK1-ATG13-FIP200-ATG101 complex (complex I) through PTMs of its members. Members of complex I and sensor kinases phosphorylate members of VPS34-VPS15-Beclin1 complex (complex II), which activate local phosphatidylinositol-3-phosphate (PI(3)P) production. PI(3)P-binding protein WIPI then recruits ATG2 to the nascent phagophore, which is elongated upon membrane donation from ATG9-containing vesicles. WIPI also recruits the ATG16L-ATG5-ATG12 complex (complex III) and by extension the ATG3-LC3 complex. Pro-LC3 is cleaved by ATG4 and conjugated to phosphatidylethanolamine (PE), thus creating a membrane bound form. LC3 then acts to recruit autophagic cargo via the LC3-interacting region (LIR) of autophagy receptor proteins, but is also required for phagophore maturation, enclosure and trafficking to- and fusion with the lysosome.

Extension of the isolation membrane and its growth and maturation into an autophagosome seems to be linked to vesicles containing the membrane-spanning ATG9 protein (Yamamoto *et al.*, 2012; Bento *et al.*, 2016). Recent studies in yeast point towards the role of ATG9 in establishing contact sites between the ER and phagophore via its interaction formation with the ATG2-WIPI complex (Gómez-Sánchez *et al.*, 2018). The ATG2-WIPI complex is targeted to early phagophores upon PI(3)P formation by the PI(3)P binding domain of the WIPI(1-4) protein (Bento *et al.*, 2016). Although the exact role of WIPI(1-4) remains a mystery, a recent study of its complex partner, ATG2, provides an insight into ATG2 functioning as a membrane tether via its two membrane-spanning domains and acts to dock the nascent isolation membrane to the ER (Kotani *et al.*, 2018). In addition, it is hypothesized that the ATG2-WIPI complex is responsible for ATG9 recycling (Reggiori *et al.*, 2004; Zhao and Zhang, 2019).

The final of autophagy complexes recruited to the site of phagophore formation are the members of the ATG16L-ATG5-ATG12 complex and the ATG3-LC3 conjugate (Bento *et al.*, 2016). First, ATG12, a ubiquitin-like protein, is covalently bound to ATG5 in a process assisted by ATG7 (E1-like enzyme) and ATG10 (E2-like enzyme). The ATG5-ATG12 associates in a complex with ATG16L via ATG5-ATG16 interaction (Mizushima, Noda and Ohsumi, 1999). The ATG16L-ATG5-ATG12 complex is recruited to the phagophore by a direct binding between WIPI2 and ATG16L (Dooley *et al.*, 2014). Importantly, ATG16L-ATG5-ATG12 complex dissociates from the structure upon autophagosome formation and is often used to track early autophagy events. By its action as an E3 ubiquitin ligase and the ubiquitin-like nature of ATG12, the ATG16L1-ATG5-ATG12 complex recruits ATG3 (E3 like enzyme) of the ATG3-ATG8 complex (Noda *et al.*, 2013). Human orthologs of the yeast Atg8 proteins include three microtubule associated protein 1 light-chain 3 proteins (MAP1LC3A-C/LC3A-C), the γ-aminobutyric acid receptor-associated protein (GABARAP), and the γ-aminobutyric acid receptor-associated protein like 1 and 2 (GAPARAPL 1/2) (Lee and Lee, 2016). MAP1LC3, hereafter referred to as LC3-I, is cleaved by ATG4 to expose its C-terminal glycine residue. ATG7 (E1-like enzyme), ATG3 (E2-like enzyme) and ATG16L-ATG5-ATG212 (E3-like enzyme) facilitate the conjugation of LC3-I to a membrane-resident phosphatidylethanolamine (PE), thus resulting in formation of a membrane bound form of LC3 (LC3-II) (Scherz-Shouval *et al.*, 2007). The spatial

closeness of ATG3-LC3-I and ATG16L-ATG5-ATG12 required for LC3 processing is mediated by specific binding between ATG3 and ATG12 (Noda *et al.*, 2013).

The role of LC3 in selective autophagy arises through its specific association with autophagy receptor proteins that contain an LC3-interacting region, a LIR motif, and a ubiquitin binding domain that spatially link ubiquitylated cargo to the autophagic machinery (Stolz, Ernst and Dikic, 2014). In addition, LC3 and the ATG core machinery have been linked to autophagosome biogenesis, cargo recognition, autophagosome closure, transport and fusion with lysosomes (Bento *et al.*, 2016). As the research is still ongoing, it is clear that much more needs to be understood about autophagosome formation and closure and specifically the multiple roles of and interactions between the ATG proteins.

1.2.5 Selective Macroautophagy

Of the two conjugates that localize to early phagophore, the ATG5-ATG12 conjugate, dissociates from the phagophore and is not directly involved in the later stages of the autophagy pathway. In contrast, LC3 conjugation to the inner membrane component of the phagophore remains unchallenged for the entirety of the vesicle biogenesis, and thus turns LC3 into a substrate designed for degradation upon autophagosome fusion with the lysosome (Wesselborg and Stork, 2015). Experimental evidence led to discovery of an 8-residue long motif that allows proteins to recognize and bind to LC3, and identification of the binding motif in protein sequences led to the description of autophagy receptor proteins that link specific cargo to the autophagy pathway in a process termed selective autophagy (Johansen and Lamark, 2011). Autophagy receptors are proteins that fulfil three required features: direct interaction with LC3 via an LC3-interacting region (LIR), ability to recognize substrates, and an inherent ability to polymerize or aggregate. Canonical autophagy receptors include p62 (sequestosome 1 (SQSTM1)), neighbour of breast cancer 1 (NBR1), optineurin (OPTN), nuclear domain 10 protein 52 (NDP52; or Ca2+-binding and coiled-coil domain-containing protein 2, CALCOCO2), Tax1 binding protein 1 (TAX1BP1), Toll interacting protein (TOLLIP) and cellular Casitas B-lineage lymphoma (c-Cbl) (Wesselborg and Stork, 2015; Mancias and Kimmelman, 2016). Other non-canonical autophagy receptors include proteins that bind either Ub (histone deacetylase 6 (HDAC6)) or LC3 (BCL2/adenovirus E1B 19 kDa protein-interacting protein 3 **(**BNIP3), BNIP3-like (BNIP3L/NIX), FUN14 domain-containing protein 1 (FUNDC1) and others)

(Johansen and Lamark, 2011). Due to their association with LC3 and/or cargo, the receptor proteins become autophagy substrates themselves. Although a degree of redundancy is built into substrate recognition and multiple autophagy receptors are recruited to identical substrates, a degree of specificity exists where different combinations of receptors aid degradation of the same cargo in response to different triggers (Mancias and Kimmelman, 2016). This phenomenon holds particularly true to selective degradation of mitochondria (discussed in section 1.3.5)

1.3 Mitochondria

Mitochondria are a dynamic network of tubular organelles of a bacterial origin, separated from the rest of the cell by a double membrane coat. Since the first fusion event of an eubacteria-like endo-symbiont with an archaea host, the bacteria lost a major part of their integral function, became dependent on the host cell for the majority of its proteome and developed into the mitochondria I recognize today (Balaban, Nemoto and Finkel, 2005). Akin to bacteria, mitochondria contain their own DNA in a form of a circular molecule (mtDNA), which encodes a small part of the mitochondrial proteome. Thus, mitochondria largely depend on proteins encoded by the host's nuclear DNA (nDNA) for their function, replication and recycling (Balaban, Nemoto and Finkel, 2005). Likewise, the host cell became reliant on energy generation and signalling by the mitochondrial network (Balaban, Nemoto and Finkel, 2005; Frezza, 2017). Intermediates, terminal molecules and by-products of mitochondrial metabolism escape the organelle and influence the adaptability, metabolic state and survival of the host cell (Frezza, 2017). In addition, mitochondria play a key role in the maintenance of cellular and organismal fitness by acting as metabolic hubs that integrate a plethora of intra- and extra-cellular signals (Sedlackova and Korolchuk, 2018).

1.3.1 Mitochondrial structure and dynamics

Two functionally distinct membranes, the outer mitochondrial membrane (OMM) and the inner mitochondrial membrane (IMM) separate mitochondria from the cytosol. The OMM is a smooth and highly porous membrane permeable to small solutes through the voltage–dependent anion channels (VDACs) (Cogliati, Enriquez and Scorrano, 2016). The OMM acts as a barrier to the cytoplasmic proteins and is also a site of interaction with other organelles, most notably the endoplasmic reticulum (ER) (Cogliati, Enriquez and Scorrano, 2016). OMM forms an interface for docking and

interaction with cytosolic proteins involved in mitochondria-dependent cell fate determination (Cogliati, Enriquez and Scorrano, 2016; Sedlackova and Korolchuk, 2018). In addition, insertion and stabilization of a subset of cytosolic proteins or externalization of the most abundant lipid of the IMM, the cardiolipin (CL) on the OMM, act as signals for mitochondrial recycling via macroautophagy (Sedlackova and Korolchuk, 2018). In contrast, the IMM is impermeable to ions and larger molecules and contains a multitude of carriers that facilitate a controlled transport of metabolites (Cogliati, Enriquez and Scorrano, 2016). In addition, IMM and the protein complexes embedded within it are the sites of mitochondrial energy generation that is aided by the double-membrane nature of the organelle (discussed in section 1.3.2). Thus, two metabolically distinguishable compartments are formed within the mitochondrion, an intermembrane space (IMS) and a mitochondrial matrix.

Invaginations and stabilized curvature of the IMM, referred to as cristae formation, can also lead to a functionally distinct portion of the IMS, the cristae lumen. A large proportion of the IMM in healthy mitochondria adopts the cristae formation (Cogliati, Enriquez and Scorrano, 2016). Cristae are stabilised by the mitochondrial contact site and cristae organising system (MICOS, also known as MitOS and MINOS) as a tight tubular junction on the site proximal to the OMM and by ATP synthase dimer rows at the distal region (Strauss *et al.*, 2008; Pfanner *et al.*, 2014). Cristae structure changes in response to intra- and extra-mitochondrial cues and, in turn, regulates the efficiency of mitochondrial metabolism and plays a role in mitochondrial dynamics and programmed cell death (Cogliati, Enriquez and Scorrano, 2016).

Mitochondria associate into dynamic networks to facilitate inter-organelle exchange of metabolites and DNA and to dilute toxins (Detmer and Chan, 2007). In contrast, separation of dysfunctional regions is required for organelle distribution to sub-cellular locations, particularly in neurons, and for maintenance of mitochondrial fitness via their fission-assisted removal from the pool and sequestration for degradation via macroautophagy (Lazarou *et al.*, 2015). The flexibility of mitochondrial networks is determined by the balance of fusion and fission events and its plasticity can vary in different cell types and subcellular locations (Detmer and Chan, 2007). At steady state, the mitochondrial network undergoes balanced fusion and fission events to maintain its overall morphology. Experimental perturbation of either of the two processes and cellular energy availability revealed the rapid rate at which mitochondrial networks

adopt either a hyperfused or a fragmented state accompanied by a condensed and relaxed cristae morphology, respectively (Detmer and Chan, 2007). Physiologically, mitochondria tend to become hyperfused in conditions of low nutrient availability, presumably to dilute the available metabolites and avoid recycling via macroautophagy (Rambold *et al.*, 2011). In contrast, a balance shift toward the fragmented mitochondrial morphology is observed in pancreatic β cells cultured in nutrient excess (Molina *et al.*, 2009) and pathological states including apoptosis (Arnoult, 2007), ischaemia/reperfusion injury (I/R) (Ong *et al.*, 2010).

Guanosine triphosphatases (GTPases) conserved from yeast to mammal, are located at the IMM and the OMM and regulate the fusion and fission processes (Koshiba *et al.*, 2004; Westermann, 2010). Mitochondrial fusion is dependent on the proton potential across the IMM (mitochondrial membrane potential, mMP) and proceeds in three distinct phases. Firstly, fusion requires spatial proximity between two adjacent organelles followed by inter-OMM tethering made possible by the action of dynamin-related guanosine triphosphatases, mitofusin 1 and its paralog mitofusin 2 (Mfn1 and Mfn2), which are docked at the OMM via their C-terminal domains (Rojo *et al.*, 2002). Approximated membranes are tethered by inter-organelle mitofusin oligomerisation (Koshiba *et al.*, 2004). Upon tethering, mitofusins mediate OMM fusion in an action dependent on their N-terminal GTPase domain to give rise to a short-lived intact mitochondrion with two separate cristae compartments (Koshiba *et al.*, 2004). Finally, IMM fusion within the mitochondrion is assisted by optic atrophy 1 (OPA1) GTPase (Song *et al.*, 2007). OPA1 is an IMM protein involved in a multitude of mitochondrial processes, including but not limited to cristae reorganization, apoptotic signalling and IMM fusion. Upon import to the intermembrane space, OPA1 adopts two distinct peptide structures, a long peptide anchored to the IMM (L-OPA1) and a soluble short peptide (S-OPA1), which remains in the IMS (Song *et al.*, 2007). While L-OPA1 homo-oligomer assembly is involved in cristae stabilization and thus plays a role in ETC efficiency, L-OPA1 interaction with CL, a phospholipid unique to the mitochondrial IMM and predominantly located in the inner leaflet, mediates IMM fusion (Ban *et al.*, 2017). The role of S-OPA1 in fusion is unclear. Several studies report the possible involvement of excessive levels S-OPA1, due to L-OPA1 cleavage, in increased levels of fission (Ishihara *et al.*, 2006; Anand *et al.*, 2014). It is however unclear whether S-OPA1 directly participates in fission, or whether the shift towards fission occurs as an indirect consequence of L-OPA1 loss. First indications of S-OPA1 direct involvement

in fission come from studies, which report that in mouse embryonic fibroblasts (MEFs) transfected with S-OPA1 constructs, S-OPA1 localized to OMM fission sites and accelerated mitochondrial fragmentation (Anand *et al.*, 2014).

Another conserved GTPase, dynamin related protein 1 (DRP1), regulates mMP-independent mitochondrial fission. The triggers of DRP1 recruitment to mitochondria are not well understood, but are thought to occur via its PTMs, specifically via phosphorylation (Ni, Williams and Ding, 2015). What is known is that DRP1 recruitment to mitochondria is mediated by interactions with several OMM proteins including fission 1 (FIS1), mitochondrial fission factor (MFF) and mitochondrial dynamics proteins of 49kDa and 51kDa (MID49 and MID51) (Losón *et al.*, 2013). Upon recruitment, DRP1 forms oligomeric constriction rings along the OMM and splits the intact mother organelle into two daughters. DRP1 oligomerisation primes its GTPase domain for GTP binding and hydrolysis, which provides the necessary energy to induce conformational changes in the protein and mediates the ring constriction and thus the scission event (Mears *et al.*, 2011).

1.3.2 Mitochondrial energy generation

The most-widely studied function of the mitochondrial network is its contribution to cellular bioenergetics by oxidation of carbon substrates that precedes a process referred to as oxidative phosphorylation (OXPHOS). Complete oxidation of the pyruvate molecule via the tricarboxylic acid (TCA, Krebs) cycle, beta-oxidation of fatty acids and oxidation of amino acids occur in the mitochondrial matrix and each liberate electrons (e^-). Released e^- are then loaded onto carriers including NAD^+ and flavin adenine dinucleotide (FAD) to form their reducing equivalents (NADH and $FADH_2$) (Balaban, Nemoto and Finkel, 2005; Watmough and Frerman, 2010). The next step of energy generation occurs at the IMM. Proteins expressed from two distinct genomes (the nDNA and mtDNA) localise to the IMM to form four multimeric IMM-docked and -embedded protein complex structures collectively referred to as the electron transport chain (ETC) (Watt *et al.*, 2010). ETC is designed to direct the flow of e^- donated by NADH and $FADH_2$ to O_2, the terminal acceptor. Electron flow across the complexes is accompanied by pumping of hydrogen ions (H^+, protons) across the IMM at complexes I, III and IV of the ETC. H^+ pumping across the IMM creates a local electrochemical gradient also referred to as the mMP ($\Delta\Psi m$) (Watt *et al.*, 2010). The resulting transmembrane potential of -160mV and concentration of protons in the cristae lumen

drives proton flow through the F_0 subunit of the F_1F_0ATP synthase to provide the rotational energy for ATP synthesis at the F_1 subunit. Aerobic respiration via the coupling of ETC together with ATP-synthase activity is collectively referred to as OXPHOS (Watt *et al.*, 2010). OXPHOS is also ultimately dependent on adenine nucleotide translocases (ANTs) responsible for exchange of adenine diphosphate (ADP) and inorganic phosphorus (Pi) from the cytosol and ATP from the mitochondrial matrix (Stepien *et al.*, 1992). Once ATP is formed, it is released from mitochondria and its high-energy bond is cleaved to release energy required to assist cellular catalytic reactions.

Electron entry into the ETC

The ETC in the majority of eukaryotes consists of four large membrane embedded complexes (C I-IV) and two mobile carriers, ubiquinone and cytochrome *c.* Complexes I and II and quinone facilitate e^- entry into the ETC system and link metabolic oxidation in the matrix to the Q cycle (Van Vranken *et al.*, 2015; Formosa *et al.*, 2018). Complex I (CI), or NADH:ubiquinone oxidoreductase, is the largest of the ETC complexes and represents the entry point for the majority of e^- to the ETC. In mammals, CI consists of 44 unique subunits expressed from both mtDNA (7)- and nDNA (37)-encoded genes. CI assembly proceeds via subunit assembly into three modules, N-, Q- and P-module, each consisting of core and accessory subunits (Formosa *et al.*, 2018). A fully assembled CI complex adopts an L-shape with P-module forming the hydrophobic membrane embedded arm and Q- and N-modules extending into the mitochondrial matrix. N-module forms the tip of the matrix arm and is the site of NADH interaction with N-module-associated flavin mononucleotide (FMN) in the matrix arm of CI. e^- released from NADH at the FMN site then flow through a series of iron sulphur (Fe-S) clusters embedded within the core complex subunits of the Q module. e^- then flow into the matrix arm (P-module) embedded in the IMM, and load onto ubiquinone at its P-module binding site within the IMM. Energy released by the transfer of $2e^-$ along the P-module is harvested to assist translocation of $4H^+$ atoms from the matrix into the cristae lumen via four antiporter channels opened by redox-state linked conformational changes in CI subunits (Jones *et al.*, 2017; Ramsay, 2019). P-module also contains all of the mtDNA-encoded CI subunits, which were likely preserved in the mtDNA due to their extreme hydrophobicity (Johnston and Williams, 2016). Altogether, CI assembly

into a functional complex requires several routes of subunit transcription, folding and subcomplex formation assisted by multiple assembly factors (Formosa *et al.*, 2018).

Complex II (CII), or succinate dehydrogenase (SDH), represents an entry point for e^- delivered by a CII-associated FAD molecule (Ramsay, 2019). It is the only enzyme of the ETC involved in the TCA. CII participates in the TCA cycle by catalysing oxidation of succinate into fumarate, thus liberating e^- in the proximity of its FAD co-factor (Al Rasheed, Rizwan and Tarjan, 2018). In contrast to CI, CII is a small tetrameric protein complex, and the only complex of the ETC that is entirely encoded by nDNA (Van Vranken *et al.*, 2015). The catalytic core of the complex consists of subunits A and B (SDHA, SDHB). SDHA harbours the covalently bound FAD molecule and a succinate-binding pocket and catalyses e^- liberation. SDHB harbours three Fe-S clusters that mediate e- flow from FAD to the membrane complex subunits. The membrane docking subunits C and D (SDHC, SDHD) contain a heme *b* co-factor and two ubiquinone binding sites (Van Vranken *et al.*, 2015; Al Rasheed, Rizwan and Tarjan, 2018). Lastly, CII-mediated e^- delivery to ubiquinone is not linked to proton translocation across the IMM.

Electron flow and exit from the ETC

Ubiquinone, or coenzyme Q (CoQ), is an IMM associated mobile e^- carrier composed of a quinoid moiety tethered to the IMM by a long carbon hydrophobic tail (50 carbons in mammals) (Ramsay, 2019). CoQ adopts three redox states as a fully oxidized molecule (Q), a partially reduced ubisemiquinone (•QH) and a fully reduced ubiquinol (QH_2). Upon full reduction by CI, CII or alternative mitochondrial donors (glycerol-3-phosphate dehydrogenase (GPDH) and electron transfer flavoprotein (ETF)), all QH_2 molecules become re-oxidized by complex III ((CIII), or ubiquinol-cytochrome *c* oxidoreductase) that passes e^- onto cytochrome *c* (cyt *c*), the second mobile e^- carrier of the ETC (Ramsay, 2019).

CIII is an 11-subunit protein complex that assembles into a homodimer within the IMM (Cogliati *et al.*, 2018). CIII harbours a catalytic core, which consists of a single mtDNA encoded subunit, cytochrome *b* and two nDNA-encoded subunits, cytochrome *c1* and the Rieske iron-sulphur protein (RISP or ubiquinol-cytochrome *c* reductase iron-sulphur subunit 1 (UQCRFS1)) (Cogliati *et al.*, 2018). Two e^- released during QH_2 re-oxidation into Q are loaded onto two separate e^- flow chains, a high potential chain of

RISP and a tightly bound cytochrome *c1*, which load the reduction potential onto cyt *c* and a low-potential cytochrome *b* chain, respectively. The low-potential chain links to proton pumping across the IMM, though the exact mechanism remains unknown (Bazil *et al.*, 2013; Ramsay, 2019). The e^- separation into the two-flow chains results in $1e^-$ transfer to cyt *c* and $1e^-$ transfer to Q at the cyt *b* site of CIII. Two cycles of QH_2 re-oxidation complete this cycle, whereby $2e^-$ are loaded onto cyt *c*, $2e^-$ are accepted by Q to form a fully reduced QH_2 and $4H^+$ are pumped across the IMM, together referred to as the Q-cycle (Bazil *et al.*, 2013; Ramsay, 2019).

Cytochrome *c* is a multifunctional small hydrophobic protein that locates to the outer leaflet of the IMM within the cristae lumen (Zaidi *et al.*, 2014). Despite the relatively low number of evolutionarily conserved residues within the protein, its structural stability is retained in the majority of studied species (Zaidi *et al.*, 2014). Cyt *c* facilitates e^- transfer from CIII to CIV of the ETC via its covalently bound and protected heme cofactor (Ramsay, 2019).

Complex IV ((CIV), or cytochrome *c* oxidase), links oxidative mechanism and e^- flow through the ETC to reduction of O_2 into H_2O (Zong *et al.*, 2018; Ramsay, 2019). Although published literature disagrees on the number of protein subunits, varying from 7 to 13, three core subunits are encoded in mtDNA and form the catalytic core (Yoshikawa *et al.*, 2012; Ramsay, 2019). The complex core subunit 1 and 2 contain two heme ($heme_A$, $heme_B$) and two copper redox sites (Cu_A, Cu_B), which catalyse a directional Cu_A, $heme_A$, $heme_B$, Cu_B e^- transfer. Subunit 3 does not contain a redox active metal co-factor, but was hypothesized to facilitate the terminal step of the ETC, the O_2 binding and reduction (Yoshikawa *et al.*, 2012). It is not known where the proton-transfer across the IMM occurs within CIV, though several hypotheses suggest a link to the O_2 reduction site within subunit 3 and acidic amino acid-lined channels (Yoshikawa and Shimada, 2015; Ramsay, 2019).

ETC complexes normally assemble to form highly-ordered stable structures of CI monomer associated with a CIII dimer and a variable number of CIV complexes (Jha, Wang and Auwerx, 2016). Additionally, CI homodimerization is hypothesized to lead to the assembly of a high-molecular ordered structure referred to as the respirasome (Jha, Wang and Auwerx, 2016). Supercomplex (SC) and respirasome assembly is thought to stabilize the CI-CIV structure, increase the efficiency of e^- transfer due to a

tighter ETC confirmation and lesser distances between mobile carrier binding sites and thus lower risk of e^- escape into matrix from reaction intermediates (Ramsay, 2019).

1.3.3 Additional mitochondrial functions

Mitochondria perform a set of diverse yet interconnected functions beyond their role of energy generation. As discussed above, intermediates of mitochondrial metabolism re-routed to the cytosol contribute to cellular anabolism and influence cellular adaptation to stresses (Frezza, 2017). Other mitochondrial biosynthetic functions include Fe-S cluster maturation and a minor, yet essential role in pyrimidine synthesis (Lill and Kispal, 2000; Gattermann *et al.*, 2004). Fe-S clusters are protein co-factors that assist with protein catalytic functions, e^- transfer and regulation of gene expression (Lill and Kispal, 2000). Studies in a yeast model identified a eukaryotic Fe-S cluster synthesis pathway, conserved from bacteria to mammals, which does not proceed in the absence of mMP and requires mitochondrial matrix enzymes and IMM transporters for the export into the cytosol (Lill and Kispal, 2000). Similarly, the majority of pyrimidine biosynthesis occurs in the cytosol, the *de novo* synthesis pathway depends on an IMM enzyme, dihydroorotate dehydrogenase (DHODH), which was hypothesized to interact with ETC SCs (Gattermann *et al.*, 2004; Fang *et al.*, 2013). DHODH faces the IMS and catalyses oxidation of dihydroorotate into orotate, a uridine monophosphate (UMP) precursor, by channelling e^- from the dihydroorotate to Q via its resident FMN molecule (Fang *et al.*, 2013).

Mitochondria also functionally interact with other cellular organelles, as explored in a recent review (Lackner, 2019). The most widely studied interactions are between mitochondria and the ER through mitochondria-associated membranes (MAMs), which are involved in the regulation of Ca^{2+} signalling. Mitochondrial Ca^{2+} intake is dependent on mMP and the organelle's close proximity to the ER via MAMs, which provide a platform for microdomain signalling highly enriched in key signalling molecules. Efflux and influx pathways maintain overall mitochondrial levels of Ca^{2+}. The OMM is permeable, though directed calcium import into the IMS was shown to be mediated and directed by VDACs at MAMs (Gincel, Zaid and Shoshan-Barmatz, 2000). Ca^{2+} uptake into the mitochondrial matrix is orchestrated by the mitochondrial calcium uniporter complex (MCU) and its regulators (Baughman *et al.*, 2011; De Stefani *et al.*, 2011). Ca^{2+} efflux across the IMM is maintained by the coordinated action of sodium/calcium/lithium exchanger pump (NCLX) and a direct Ca^{2+}/H^+ antiporter that

exchanges Ca^{2+} for protons across the membrane at the expense of the proton motive force (pmf) for ATP synthesis (De Marchi *et al.*, 2014; Jaquenod De Giusti, Roman and Das, 2018). Mitochondria can protect cells from short aberrant Ca^{2+} peaks by importing Ca^{2+} into their matrix and thus respond to increased metabolic demand via increased ATP generation due to Ca^{2+}-dependent stimulation of TCA rate-limiting enzymes: pyruvate, isocitrate and α-ketoglutarate dehydrogenases (Denton, 2009). However, Ca^{2+} overload that can result from high level of transfer from the ER stores, or increased levels or sensitivity of Ca^{2+} transporters can lead to toxicity, dissipation of the mMP and cell death (Ichas and Mazat, 1998; Galluzzi *et al.*, 2018).

Cell death initiation occurs upon a persistent chemical or physical insult to the cell. Cell death can occur as a programmed event, apoptosis, or an accidental event, necrosis (Galluzzi *et al.*, 2018). Mitochondria directly or indirectly participate in cell death execution via six of the twelve described cell death pathways, including direct mitochondria-executed intrinsic apoptosis via mitochondrial outer membrane permeabilization (MOMP) or mitochondrial permeability transition (MPT) upon loss of IMM integrity (Galluzzi *et al.*, 2018). Mitochondria also indirectly participate in extrinsic apoptosis, parthanatos, ferroptosis and lysosome-dependent cell death (Galluzzi *et al.*, 2018). The intrinsic apoptosis pathway consists of an ATP-dependent, highly ordered and regulated event governed by pro- and anti-apoptotic members of a BCL-2 protein family that transiently or permanently localize to the OMM (Sedlackova and Korolchuk, 2018). MOMP is characterized by increased cyt *c* solubility (Kagan *et al.*, 2004), its dissociation from the IMM into the IMS and escape into the cytosol via OMM pores created by insertion of pro-apoptotic BCL-2 family members (Galluzzi *et al.*, 2018). Upon release from mitochondria, cyt *c* interacts with its cytosolic binding partners and participates in the formation of a multimeric protein structure, called the apoptosome, that cleaves caspase 3 and thus initiates an apoptotic signalling cascade (Galluzzi *et al.*, 2018). MPT-driven necrotic cell death is associated with a sudden increase of IMM permeability by channel formation in response to a burst of Ca^{2+} or ROS, which leads to an increased H_2O intake, loss of cristae formation, loss of mMP, mitochondrial swelling and cell death (Berghe *et al.*, 2014).

1.3.4 Mitochondrial quality control

Mitochondria utilize H^+ and e^- released by oxidation of dietary sources to generate an electrochemical gradient across the IMM by selectively pumping H^+ into the IMS and

channelling e^- to reduce O_2 into H_2O at CIV of the ETC. However, e^- that leak from the ETC interact with nearby O_2 molecules and lead to production of free radical species, particularly the superoxide ($\bullet O_2$) (Ramsay, 2019). The $\bullet O_2$ is normally detoxified to a more stable species hydrogen peroxide (H_2O_2), by mitochondrial matrix and IMS superoxide dismutases (SODs), MnSOD and Cu/ZnSOD respectively (Wallace, 2005). On one hand, ROS released from the ETC due to stalled e^- flow in conditions of calorie excess (leading to ETC over-reduction) or mitochondrial dysfunction can act as signalling molecules and promote cellular adaptation to such stresses (Scialò *et al.*, 2016). On the other hand, dysfunction of ETC complexes can lead to increased ROS release in the form $\bullet O_2$ that can react with H_2O and give rise to a highly reactive and damaging hydroxyl radicals ($\bullet OH$) that interact with their immediate environment and damage mitochondrial and cellular proteins, lipids and DNA and promote further ROS release in neighbouring mitochondria via a ROS-induced ROS release mechanism (Wallace, 2005; Zorov, Juhaszova and Sollott, 2006). In addition, $\bullet O_2$ can interact with nitric oxide (NO), present in mitochondria in an abundance reaching μM concentrations, to form a peroxynitrite species ($ONOO^-$), a highly damaging reactive nitrogen species (RNS) (Murray *et al.*, 2003).

Mitochondrial dysfunction in dividing cells promotes establishment of an irreversible cellular arrest, senescence, and was shown to contribute to tissue ageing (discussed in section 1.5.2). In addition, mitochondrial health is particularly crucial in post-mitotic cells and tissues, in which the load of dysfunctional organelles cannot by diluted by mitotic cell division, and in neurons specifically, due to the distance the mitochondria have to travel for efficient recycling in the cell body (Wallace, 2005; Lin and Beal, 2006). Therefore, eukaryotic cells developed tight monitoring of mitochondrial function and efficient quality control systems to prevent damage accumulation and further dysfunction (Sedlackova and Korolchuk, 2018).

Mitochondrial quality control (MQC) mechanisms are triggered by several perturbations. First, the majority of mitochondrial proteome is encoded in the nuclear DNA and nascent amino acids chains require efficient transport to and import into mitochondria (Balaban, Nemoto and Finkel, 2005). Mitochondrial protein import machinery was shown to be dependent on the organelle's bioenergetic state, as functional import machinery requires mMP and ATP (Martin, Mahlke and Pfanner, 1991; Harbauer *et al.*, 2014). Thus, protein import acts as a sensor of mitochondrial

function and loss of mMP due to loss of substrate or inefficient ETC results in import deficiency (Martin, Mahlke and Pfanner, 1991). Depending on the severity and length of import perturbation, the same signal can initiate two distinct pathways of MQC.

Mild import inefficiency results in the activation of mitochondrial unfolded protein response (UPR^{mt}) via an activating transcription factor associated with stress-1 (ATFS-1) in *C. elegans*; and activating transcription factors 4 and 5 (ATF4 and ATF5) in mammals (Shpilka and Haynes, 2017). ATFS-1 is a nucleus-encoded protein, first identified in *C. elegans* (Martinus *et al.*, 1996), which contains two localisation signals, a mitochondrial targeting sequence (MTS) and a nuclear localisation sequence (NLS) (Nargund *et al.*, 2012). The MTS of ATFS-1 was shown to be weak and highly responsive to mitochondrial protein import dysfunction (Nargund *et al.*, 2012). Efficient protein import promotes ATFS1 entry into the mitochondrial matrix, followed by cleavage by Lon, a mitochondrial protease, and ATFS1 degradation (Nargund *et al.*, 2012). In contrast, loss of mitochondrial protein import results in ATFS-1 translocation to the nucleus (Nargund *et al.*, 2012). ATFS-1-initiated gene expression promotes synthesis of chaperones, ROS detoxification systems and mitochondrial import machinery (Nargund *et al.*, 2012; Shpilka and Haynes, 2017). Thus, the ATFS-1 mediated UPR^{mt} response is dampened when the improvement of mitochondrial function leads to reconstituted ATFS-1 import. Similarly to ATFS-1, PTEN-induced kinase 1 (PINK1) is normally imported into the mitochondrial matrix and cleaved by the presenilin-associated rhomboid-like (PARL) protease (Jin *et al.*, 2010). Prolonged perturbation of mitochondrial protein import leads to PINK1 accumulation and stabilization at the OMM, thus marking the first step of whole-organelle degradation in a process of selective autophagy, termed mitophagy (Jin *et al.*, 2010) (discussed in section 1.3.5). Altogether, mitochondrial stress presenting as loss of protein import triggers two distinct, but complementary pathways. While ATFS-1 mediates transcriptional adaptation to mitochondrial dysfunction, PINK1/Parkin mediate degradation of dysfunctional mitochondria to protect cells from excessive stress from depolarised organelles (Jin *et al.*, 2010; Nargund *et al.*, 2012).

Recent advances in EM imaging led to the discovery of small, uniform vesicles budding from mitochondria. Termed MDVs, these structures contain selected mitochondrial cargo destined for inter-organellar signalling and trafficking to peroxisomes and lysosomes (Neuspiel *et al.*, 2008; Sugiura *et al.*, 2014; McLelland and Fon, 2018).

MDVs shed in the proximity of protein import sites independently of the mitochondrial fission machinery, and are trafficked in a PINK1/Parkin or vacuolar protein sorting-associated protein 35 (VPS35) dependent manner, determined by their final destination (Neuspiel *et al.*, 2008; McLelland *et al.*, 2014). In addition, MDVs participate in mitochondrial dynamics, by turnover of membrane sites enriched in DRP1 (Wang *et al.*, 2015), in movement, by releasing mitochondria from their docking sites (Lin *et al.*, 2017) and in immune response by mitochondrial antigen presentation (Matheoud *et al.*, 2016; McLelland and Fon, 2018). Enrichment of oxidised proteins in MDV vesicles also hints at MDV role in the mitochondrial quality control (Soubannier *et al.*, 2012; McLelland and Fon, 2018). Importantly, MDV formation by budding off functional organelles means its cargo is fully enclosed in a single or double membrane and does not require the autophagic machinery to facilitate vesicle trafficking and recycling. Indeed, a study of MDV formation and trafficking found that MDV delivery to lysosomes is independent of both, ATG5 and LC3 proteins (Soubannier *et al.*, 2012).

In summary, researchers have so far identified three main models of MQC subject to the scale and severity of mitochondrial dysfunction. Short-term perturbations in mitochondrial protein import active a UPR^{mt}–dependent transcription program; oxidative damage can trigger small scale mitochondrial recycling and signalling via MDVs; while persistent and severe insults result in whole organelle degradation by the process of selective autophagy (mitophagy) (Jin *et al.*, 2010; Nargund *et al.*, 2012; McLelland and Fon, 2018).

1.3.5 Mitophagy

Mitophagy is a form of MQC that leads to whole organelle recycling. Several forms of mitophagy have been identified, though they all proceed through a common pathway of LC3 interaction region (LIR) stabilization on the OMM, recruitment of the autophagic machinery and ultimately, engulfment and trafficking of the dysfunctional organelle to the lysosome for recycling. The most-widely studied form of whole organelle recycling is a pathway dependent on large-scale OMM protein ubiquitylation in response to mitochondrial depolarization, referred to as the ubiquitin- or PINK1/Parkin-mediated mitophagy (Lazarou *et al.*, 2015). The involvement of PINK1 and Parkin proteins in selective mitochondrial recycling was first reported in studies of pharmacological induction of mMP collapse and protein overexpression (Narendra *et al.*, 2008, 2010; Matsuda *et al.*, 2010) and (Matsuda *et al.*, 2010; Narendra *et al.*, 2010) investigations

of the PINK1/Parkin pathway have since relied on the same concept of overexpression of either of the two proteins or large-scale acute mitochondrial depolarization (Whitworth and Pallanck, 2017). It is difficult to estimate how such methods, although effective in elucidating the underlying MQC mechanisms, relate to physiological conditions and further study is required to identify this pathway's triggers *in vivo* (Whitworth and Pallanck, 2017). Other forms of stress-induced mitophagy proceed in the absence of protein ubiquitylation and require an alternative set of autophagy receptors that are expressed in response to specific stresses including hypoxia and oxidative stress (Figure 1.4).

Ubiquitin-mediated mitophagy

Mitochondrial depolarization triggers two sets of interconnected events at the IMM and at the OMM. First, mitochondrial fusion, fission and cristae structure depend on the balance of long and short isoforms of OPA1 (Ishihara *et al.*, 2006; Song *et al.*, 2007; Anand *et al.*, 2014; Ban *et al.*, 2017). Loss of mMP results in excessive OPA1 cleavage by an intermembrane ATP-dependent zinc metalloprotease, Yme1L, and promotes mitochondrial fragmentation (Ishihara *et al.*, 2006; Song *et al.*, 2007). Second, stalled protein import in the absence of mMP leads to PINK1 to stabilisation at the OMM and its autophosphorylation (Figure 1.4A).

Activated PINK1 then phosphorylates ubiquitin and activates Parkin, and E3 enzyme, thus leading to a feed-forward loop of OMM protein ubiquitylation (Okatsu *et al.*, 2012; Koyano *et al.*, 2014; Harper, Ordureau and Heo, 2018), which is opposed by the action of mitochondrial ubiquitin carboxyl-terminal hydrolases 15 and 30 (USP15 and USP30) (Bingol *et al.*, 2014; Van Humbeeck *et al.*, 2014). Mitochondrial movement along actin filaments and fusion with other organelles are stalled due to ubiquitylation and proteasome-mediated degradation of mitochondrial Rho GTPase1 (MIRO-1) (Wang *et al.*, 2015) and Mfn1/2 (Tanaka *et al.*, 2010), respectively. Collectively, these events lead to separation of the depolarized organelle from its network by loss of inner and outer membrane fusion and motility impairment and thus prepare it for sequestration by the autophagy machinery.

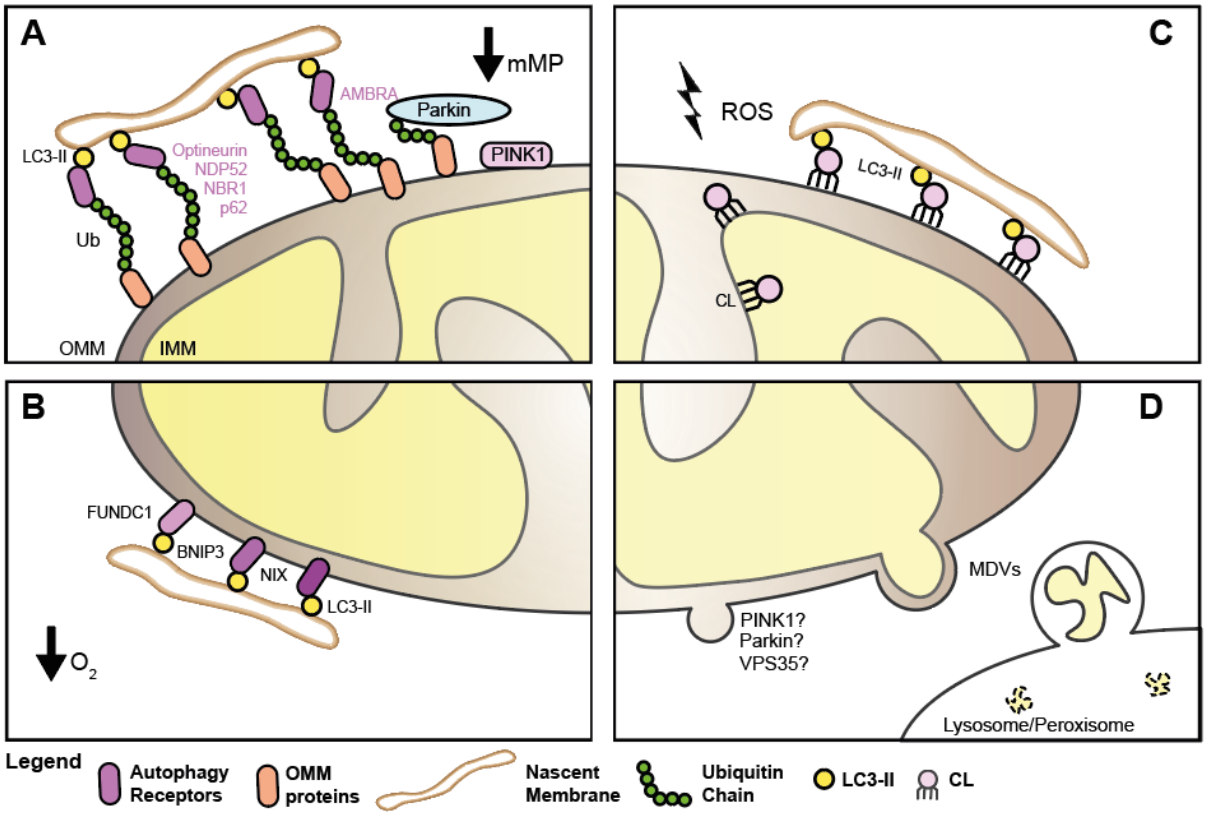

Figure 1. 4 The multiple forms of mitochondrial quality control

(A-C) Mitophagy mediates whole-organelle degradation upon physical interaction of autophagy receptors with LC3-II to facilitate nascent membrane recruitment, autophagosome formation and organelle engulfment. (A) Canonical autophagy receptors (optineurin, NDP52, NBR1, p62, AMBRA) localize to depolarized mitochondria due to PINK1 stabilization, parkin recruitment and OMM protein ubiquitylation. (B) Expression and OMM insertion of non-canonical autophagy receptors including FUNDC1, BNIP3 and NIX, increases upon O_2 depletion. (C) Oxidation of cardiolipin (CL), an IMM resident lipid, promotes its externalization to the OMM, its recognition by LC3-II and recruitment of a nascent membrane. (D) Additional form of MQC occurs via membrane budding to form mitochondria-derived vesicles (MDVs) that carry mitochondrial contents and signalling molecules to multiple sub-cellular compartments including lysosomes and peroxisomes.

Figure modified from (Sedlackova and Korolchuk, 2018).

Finally, Parkin-mediated ubiquitylation of other mitochondrial targets including VDACs, B-cell lymphoma 2 (BCL-2), components of the mitochondrial protein import system (TOM70, TOM40, TOM20) and DRP1 recruits mitophagy receptors, OPTN, NDP52 and TAX1BP1 via their ubiquitin binding domains (Lazarou *et al.*, 2015). Another mitophagy receptor, AMBRA1, is recruited to mitochondria via its interaction with Parkin (Van Humbeeck *et al.*, 2011). Autophagy receptors recruitment to the OMM spatially links dysfunctional mitochondria to the autophagy machinery via their LIR domains and mediate the formation of an autophagic vesicle around the organelles (Johansen and Lamark, 2011). Altogether, studies of the PINK1/Parkin pathway identify a system of rapid recognition, separation, sequestration and recycling of mitochondria damaged beyond repair.

Ubiquitin-Independent Autophagy

Efficient mitochondrial clearance is required in conditions of insufficient levels of O_2, the ETC terminal e^- acceptor (Figure 1.4B). Hypoxia, or oxygen depletion, promotes expression of three non-canonical mitophagy receptors- FUNDC1, BNIP3 and NIX (Bruick, 2000; Fei *et al.*, 2004; Li *et al.*, 2014). BNIP3 and NIX are two atypical pro-apoptotic members of the BCL-2 protein family thought to participate in mitophagy by homodimer formation, insertion into the OMM and direct LC3 recruitment (Zhang and Ney, 2009; Novak *et al.*, 2010). Similarly to the BNIP3 and NIX, FUNDC1 inserts into the OMM and recruits LC3 via its cytoplasm-facing LIR domain (Liu *et al.*, 2012). In addition, FUNDC1 interaction with LC3 is regulated by phosphorylation of a tyrosine 18 residue within its LIR domain, which becomes dephosphorylated in hypoxia as a result of an upstream kinase inactivation (Liu *et al.*, 2012).

Oxidative stress, which results in lipid peroxidation, induces mitophagy in a mechanism dependent on CL externalization to OMM (Figure 1.4C). CL is a phospholipid unique to the inner leaflet of the IMM and by its unique conical structure contributes to IMM fluidity (Unsay *et al.*, 2013; Pointer and Klegeris, 2017). In healthy organelles, CL is implicated in supporting ETC assembly and efficiency, in H^+ pumping, IMM fusion and cristae stabilisation (Pointer and Klegeris, 2017). Upon increased peroxidation, CL interacts with phospholipid scramblase 3 to facilitate its externalization on the OMM. Externalized CL is recognized by LC3 via its CL-recognition sequence and thus leads to the recruitment of the autophagic machinery (Liu *et al.*, 2003; Chu *et al.*, 2013).

A little explored form of ubiquitin/PINK1/parkin-independent mitophagy was first identified in an autophagy-based screen adapted for mitophagy (Allen *et al.*, 2013). Depletion of iron by cell treatment with iron chelators resulted in a ROS-independent and mMP-independent mitophagy induction (Allen *et al.*, 2013). It was since reported that iron depletion induces mitophagy in a *Caenorhabditis elegans* model (Schiavi *et al.*, 2015), in a pathogenic yeast strain *Candida glabrata* (Nagi *et al.*, 2016), and in a *Drosophila melanogaster* model (Lee *et al.*, 2018). However, at least the nematode study reports the dependence of iron-chelation-induced mitophagy on the PINK1, Parkin and BNIP3 homologs (Schiavi *et al.*, 2015). The difference in models, length of treatment and type of iron chelators used could all underlie the contradictory reports. Specifically, deferiprone, an iron chelator used in the original screen is thought to initiate mitophagy without inducing a collapse in mMP, a characteristic that is not replicated in the nematode study (Allen *et al.*, 2013; Schiavi *et al.*, 2015). Finally, if DFP is indeed confirm to induce mitophagy independently of PINK1 and Parkin as the authors suggest, it could provide an alternative therapeutic route to promoting MQC in patients suffering from Parkinson's disease (Allen *et al.*, 2013).

Basal Mitophagy

A vast amount of research was for decades focused on the discovery of MQC pathways in stress conditions *in vitro* which led to an increased interest in mitophagy as a housekeeping process implicated in health and disease. To visualise mitophagy *in vivo* and address the existence of mitochondrial recycling in absence of significant stressors, basal mitophagy, Ganley group developed a mito-QC transgenic mouse model (McWilliams and Ganley, 2016; McWilliams *et al.*, 2016). Steady state mitophagy events and mitophagy dynamics can be studied in any fixed or live tissue of this mouse, thanks to incorporation of a pH-sensitive mitochondrial signal, which differentiates between mitochondria residing in the cytoplasm with an innate pH of 7.8 in the matrix and mitochondria engulfed in lysosomes at pH 4.5-5. Initially, study of heart and kidney tissue uncovered regions with increased number of mitophagy events (McWilliams *et al.*, 2016). Further study into the underlying mechanisms reports that basal mitophagy is not dependent on PINK1 (McWilliams *et al.*, 2018). The lack of PINK1/Parkin involvement in basal mitophagy was further confirmed in mito-QC and mt-Keima *Drosophila* studies, in which levels of mitophagy were readily detectable in dopaminergic neurons and other cell types of control, *PINK1* and *parkin* null flies (Lee

et al., 2018). Authors of a study from a second mitophagy mouse model based on a pH-sensitive fluorescent reporter, the mt-Keima from Finkel group, report that approximately 80% of basal mitophagy events in the Purkinje cells of the cerebellum are Atg5-dependent, and basal mitophagy in the embryonic liver and brain of *Atg7*$^{-/-}$ mouse was greatly diminished (Sun *et al.*, 2015). Studies from the two mouse models highlight a great heterogeneity of mitophagy levels between and within tissues. It is also becoming clear that a considerable amount of mitochondrial recycling in basal conditions occurs independently of autophagy and is perhaps mediated directly by MDVs (Figure 1.4D).

1.3.6 Mitochondrial Biogenesis

Mitochondrial biogenesis (MB) maintains the health and abundance of the mitochondrial network in times of increased degradation. Successful MB has to integrate newly synthesized lipids with a mitochondria-targeted nucleus-encoded proteome (Ploumi, Daskalaki and Tavernarakis, 2017). Adding further complexity, assembly of a functional ETC requires independent expression of two genomes and tight coordination and quality control to prevent proteotoxic stress (Ramsay, 2019). A variety of intra- and extra-cellular stimuli converge on a small number of nuclear transcription factors and their co-activators to promote large-scale nuclear gene expression programmes. The nuclear respiratory factors 1 and 2 (NRF1 and NRF2) and the nuclear erythroid 2-like 2 (NFE2L2) are among the best-characterized nuclear transcription factors, which regulate transcription of mitochondrial import and transcription machinery, several ETC subunits and detoxification response and thus contribute to the coordination of nuclear and mitochondrial genome expression (Scarpulla, 2011; Ploumi, Daskalaki and Tavernarakis, 2017). Peroxisome proliferator-activated receptor γ (PPARγ) coactivators PGC-1α and PGC-1β are known tissue specific positive regulators of MB, initially identified in adipocyte differentiation signalling, though the complexity of upstream and downstream signalling, as well as interactions with other regulators of MB remains to be elucidated (Ploumi, Daskalaki and Tavernarakis, 2017). Interestingly, PGC-1α can bind to NRF1 directly and act as an upstream transcriptional inducer (Scarpulla, 2011). Further exploration of PGC-1α uncovered its role in the integration of multiple metabolic signalling pathways via PTMs by AMPK and by an NAD^+-dependent deacetylase sirtuin 1 (SIRT1) (discussed in section 1.4.2) (Scarpulla, 2011).

1.4 Nicotinamide adenine dinucleotide

1.4.1 NAD^+: a co-enzyme in redox reactions

Nicotinamide adenine dinucleotide (NAD^+) is a ubiquitous molecule crucial for cellular energy metabolism, protein transcription, and protein post-translational modification pathways (Cantó, Menzies and Auwerx, 2015). According to the Kyoto Encyclopaedia of Genes and Genomes (KEGG) reaction database, NAD^+ participates in over a quarter (2378 of 9972) of all identified enzymatic reactions as a co-enzyme or a co-substrate (*DBGET Search Result: REACTION NAD*, no date). NAD^+ consists of two nucleobases, an adenine and a nicotinamide (NAM), connected by two phosphate-ribose groups (Figure 1.5). In all living cells, NAD exists in two forms, an oxidised form (NAD^+) and a reduced form (NADH) (Cantó, Menzies and Auwerx, 2015). As a co-enzyme, NAD^+ accepts hydride equivalents from the major energy-producing catabolic pathways including glycolysis, β-oxidation and the TCA cycle to form NADH. Thus, NAD^+ abundance directly influences the activity of metabolic enzymes and adjusts the rate of metabolic flux to the rate of NADH consumption. NADH is re-oxidized primarily by CI of the ETC and thus links substrate oxidation to energy generation by donating the e^- necessary for ATP production within mitochondria (Cantó, Menzies and Auwerx, 2015).

Although little is known about the true dynamics of subcellular-compartment-specific NAD^+ biosynthesis and consumption, it is recognized that organelles contain distinct pools of NAD(H) and that cells protect the redox potential carried by NAD^+/NADH within mitochondria (Yang *et al.*, 2007). It is important to note that the mammalian IMM was long thought to be impermeable to both NAD^+ and NADH and to contain no direct transport systems for the nucleotide cofactors (Lin and Guarente, 2003; Davila *et al.*, 2018). It was also believed that cells had overcome this particular challenge by an indirect transfer of reducing equivalents across the IMM in the form of the glycerol-phosphate shuttle, ethanol-acetaldehyde and the malate-aspartate shuttle. However, recently published work challenges these concepts and supports the theory that, similarly to yeast and plant mitochondria, mammalian IMM contains an unidentified NAD(H) transporter (Davila *et al.*, 2018). It is also worth considering that redox reactions that utilise NAD^+ as a co-enzyme alter its oxidation/reduction ratio, but have no effect on total NAD(H) levels.

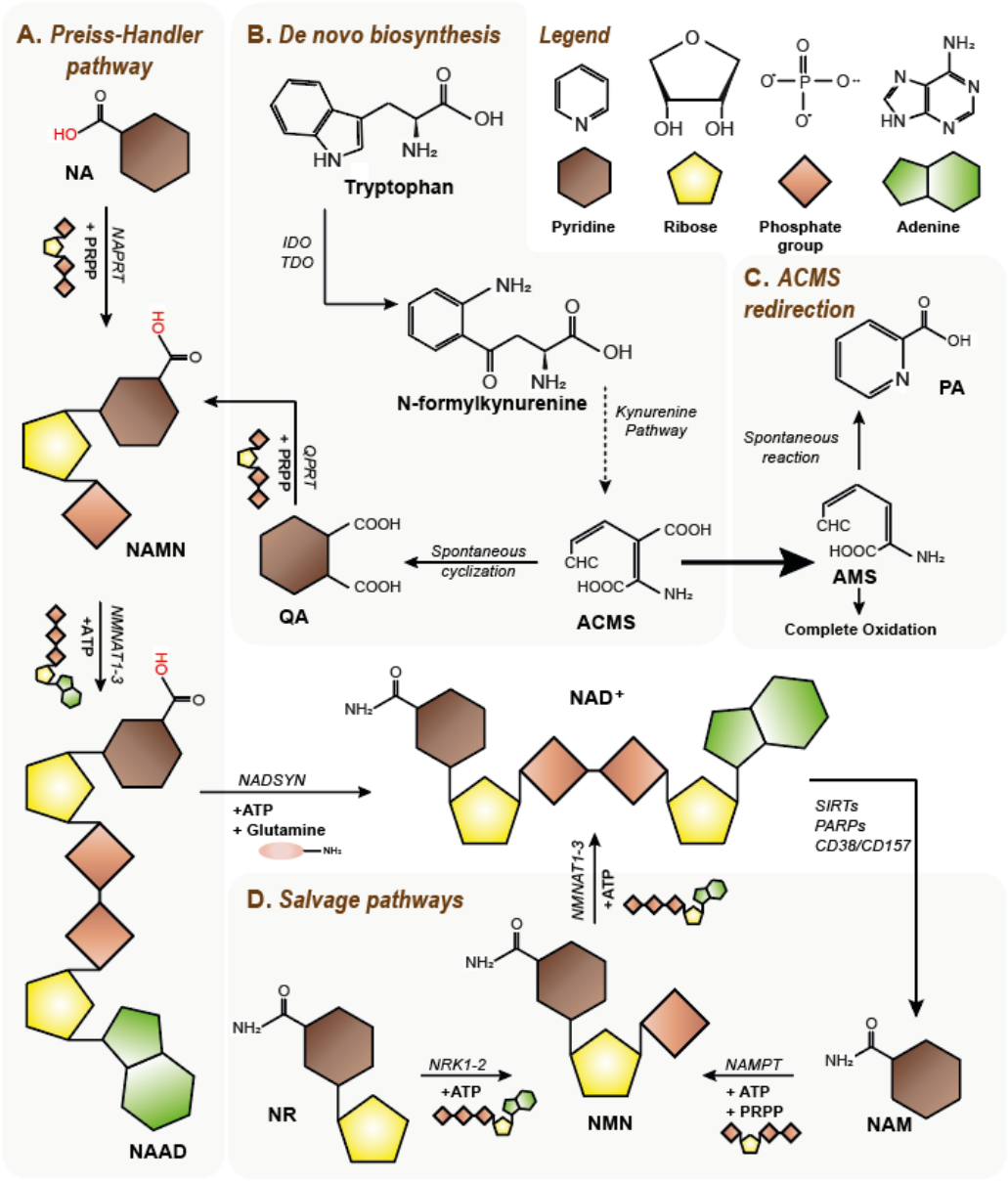

Figure 1. 5 NAD⁺ synthesis and degradation

Distinct metabolic pathways utilize precursors L-tryptophan and three forms of vitamin B3 (NA, NAM and NR) to synthesize NAD^+. (A) NA is converted to NAD^+ by the Preiss-Handler pathway, which utilizes PRPP, ATP and glutamine as donors of ribose-1-phosphate group, adenine nucleotide, and an NH_2 group in three sequential enzyme-assisted steps to form NAMN, NAAD and NAD^+, respectively. (B) L-Tryptophan enters the kynurenine pathway to form an unstable ACMS, which undergoes nonenzymatic cyclization to QA. QA feeds into the Preiss-Handler pathway via PRPP-dependent QPRT-catalysed formation of NAMN. (C) ACMS is enzymatically re-directed from QA formation to form AMS, which either undergoes total oxidation or spontaneously converts to PA. (D) NAD^+ precursors NR and NAM enter the NAD^+ salvage pathway. Both are converted to NMN upon cellular entry by NRK1-2 and NAMPT, respectively. The NMNAT1-3 enzymes catalyse synthesis of NAD+ NMN by adding an adenine nucleotide to NMN.

1.4.2 NAD^+: a co-substrate to NAD^+-consuming enzymes

In contrast, NAD^+ alone acts as a co-substrate to non-redox cellular enzymes that cleave NAD^+ to ADP-ribose and NAM (Figure 1.5). NAD^+ links cellular metabolic status to protein post-translational modifications (PTMs) by regulating the activity of SIRTs, an NAD^+-dependent highly conserved class of deacetylases; and poly(ADP-ribose) polymerases (PARPs; also referred to as ADP-ribosyltransferase diphtheria toxin-like 1 (ARTD1)). In addition, cyclic ADP-ribose (cADPR) synthases located on the plasma membrane, including CD38 and CD157, cleave NAD^+ to produce a secondary messenger involved in Ca^{2+} and insulin signalling and in cell cycle progression (Malavasi *et al.*, 2008; Cantó, Menzies and Auwerx, 2015). The two products of NAD^+ cleavage perform distinct functions. The NAM moiety locally exerts feedback inhibition on NADases in distinct mechanisms. SIRT function is inhibited by NAM-mediated reversal of NAD+ cleavage in a reaction termed nicotinamide exchange (Avalos, Bever and Wolberger, 2005). In PARPs, NAM occupies the NAD^+ binding pocket and thus prevents its catalytic activity (Henning, Bourgeois and Harbison, 2018). Nicotinamide role in CD38 inhibition is not known. It is also important to note that nicotinamide is a precursor for NAD^+ recycling (discussed in section 1.4.4), and due to its rapid conversion to NAD^+ is unlikely to inhibit NADases *in vivo* when administered externally (Hwang and Song, 2017). In contrast to NAM, ADP-ribose participates in the enzymatic activity of NADases either as a terminal sidechain acceptor (SIRTs) or as a metabolic precursor (PARPs, CD38/CD157).

NAD^+-dependent deacetylases

Seven sirtuin enzymes are known in mammals, three of which reside in mitochondria (SIRT3, SIRT4 and SIRT5), one is principally cytoplasmic (SIRT2) and three reside predominantly within the nucleus (SIRT1, SIRT6 and SIRT7) (Cantó, Menzies and Auwerx, 2015). Sirtuins, aided by NAD+, catalyse acyl moiety removal from protein lysine residues in a six-step reaction described in detail by Sauve (Sauve, 2010), which is initiated by NAD^+ association with the SIRT binding pocket. Computer-based modelling provides a model whereby NAD^+ interaction with two active residues of the binding site leads to its destabilization, nicotinamide bond cleavage and release of ADP-ribose, which accepts the acetyl group from the target acetyl-lysine residue to form *O*-acetyl-ADP-ribose. Of the seven known sirtuins, one sirtuin in each subcellular location (SIRT1, SIRT2 and SIRT3) possesses a strong deacetylase potential. Other

sirtuins possess a varied set of abilities including NAD^+-dependent lipoamidase (SIRT4), NAD^+-dependent mono-ADP-ribosyltransferase (SIRT6), desuccinylase /demalonylase/deglutarylase (SIRT5) and, lastly, p53 NAD^+-dependent deacetylase (SIRT7). In physiological terms, sirtuins are activated by increased NAD^+ levels in response to exercise, fasting and calorie restriction and promote cellular catabolism (Cantó, Menzies and Auwerx, 2015).

Extensive study of the best understood of sirtuins, SIRT1, has been carried out in mouse models of genetic manipulation via silencing, knockout or overexpression. Although reports present contradictory results, the general consensus dictates that increased SIRT1 activity leads to improvements of metabolic adaptation and mimics the benefit of caloric restriction on the symptoms of metabolic syndrome (Boutant and Cantó, 2014). Among SIRT1 targets are nuclear histones, the deacetylation of which increases histone binding, DNA condensation and represses transcription. In addition, activated SIRT1 removes acyl residues from proteins involved in DNA damage response and repair proteins and regulators including p53 (represses transcriptional activity); Ku70 (increased DNA repair, sequestration of BAX); FOXL2 (promotes cell cycle progression), Werner helicase (decreases helicase and exonuclease activity), xeroderma pigmentosum C (XPC, enhances XPC-mediated nucleotide excision repair). SIRT1 also enhances activity of transcription factors including, but not limited to forkhead box group O (FOXO) (increased transcriptional activity); heat shock factor 1 (increased transcription of heat shock proteins); PPARγ (fat mobilization), PGC-1α (increased gluconeogenesis and fatty acid oxidation). Importantly, SIRT1 also mediates inhibitory deacetylation of PARP1 to protect cells from parthanatos, PARP-induced cell death by NAD^+ depletion in response to extensive DNA damage (Rajamohan *et al.*, 2009; Cantó, Menzies and Auwerx, 2015). Furthermore, SIRT1 is also implicated in repression of PARP1 gene expression (Rajamohan *et al.*, 2009).

Poly-(ADP-ribose) polymerases

Original research of the PARP enzymes largely focused on their role in DNA damage repair inflammation and cell death. Following DNA damage, PARPs detect single- and double-strand breaks via their DNA-binding domain and undergo a conformational change that leads to NAD^+ cleavage. ADP-ribose released upon NAD^+ cleavage is then used by PARPs as a substrate for generation of poly(ADP-ribose) (PAR) and

PARP and histone PARylation. Protein PARylation then leads to recruitment of the DNA repair machinery. Protein PARylation is a reversible PTM, which is rapidly (2-5 min after formation) opposed by PAR glycohydrolase (PARG), ADP-ribosylhydrolase 3 (ARH3) and O-acyl-ADP-ribose deacylase 1 (OARD1) (Bernardi *et al.*, 1997; Ray Chaudhuri and Nussenzweig, 2017). Proteins which contain a PAR-binding domain are then recruited to the DNA break to mediate its repair (Okano *et al.*, 2003). The majority of research is focused on PARP1 and PARP2 thought to account for the majority of PAR activity in the cell (Cantó, Menzies and Auwerx, 2015). Beyond its role in DNA damage response and parthanatos-induced cell death, PARP1 also has an impact on cell fate determination by mediating PARylation of p53. Covalent attachment of PAR to p53 conceals its nuclear export signal thereby blocking recognition by a nuclear export factor, which results in p53 sequestration in the nucleus and increased gene expression of p53 gene targets (Kanai *et al.*, 2007). Further research of PARPs and ADP-ribose transferases uncovers diverse functions of the 18 or so family members, many of which need further characterization, but may include regulation of chromatin modulation, ubiquitylation, and glucose metabolism (Fouquerel *et al.*, 2014; Gupte, Liu and Kraus, 2017)

Cyclic ADP-ribose synthases

Cyclic ADP-ribose synthases, CD38 and CD157, reside on and span the plasma membrane and, in contrast to SIRTs and PARPs, can consume both extra- and intra-cellular NAD^+ pools (Cantó, Menzies and Auwerx, 2015). CD38 was discovered first and remains the more intensively studied member of the protein family (Reinherz *et al.*, 1980; Malavasi *et al.*, 2008). Although initially discovered on the plasma membrane of immune cells, CD38 is also expressed in various non-immune cells and in tissues including muscle, brain and liver (Malavasi *et al.*, 2008; Cantó, Menzies and Auwerx, 2015). The traditional view of CD38 is that of a type II membrane protein with its C-terminal catalytic $NAD(P)^+$ binding pocket exposed to the extracellular environment (Malavasi *et al.*, 2008). Opposing that view are reports of CD38 adopting the opposite membrane orientation (a type III membrane protein) and thus expose its C-terminus to the cytoplasm and act intracellularly (Zhao, Lam and Lee, 2012; Matalonga *et al.*, 2017). Studies by the Lee group first demonstrated that the catalytic site of CD38 folds correctly and remains fully functional when exposed to the intracellular environment (Zhao *et al.*, 2011) and later found that the determinants of CD38 membrane

orientation are four positively-charged amino acid residues located on the N-terminus (Y. J. Zhao *et al.*, 2015). Accordingly, it is then entirely possible that CD38 can consume both intra- and extra-cellular $NAD(P)^+$ levels and influence both environments.

CD38 and CD157 cleave NAD^+ and $NADP^+$ into NAM and via their hydrolase, cyclase and nicotinamide transferase activity generate Ca2+ mobilizing second messengers: ADP-ribose (ADPR) and cyclic ADP-ribose (cADPR) by NAD^+ cleavage and nicotinic acid-adenine dinucleotide phosphate (NAADP) by $NADP^+$ cleavage (Malavasi *et al.*, 2008). In addition, recent studies report that CD38 can also cleave nicotinamide mononucleotide (NMN) (Grozio *et al.*, 2013; Camacho-Pereira *et al.*, 2016), an intermediate metabolite of NAD synthesis/salvage pathway and thus limiting NMN pools available for NAD^+ synthesis, which can have implications for NAD^+-boosting therapeutic strategies (discussed in section 6.2).

NAD^+ cleavage by SIRTs, PARPs and CD38 leads to release of ADP-ribose, which participates in their enzymatic activity and can act as a second messenger, and in NAM that is recycled into NAD^+ through a series of enzyme-assisted steps referred to as the NAD^+ salvage pathway (Cantó, Menzies and Auwerx, 2015). Through their concerted action, SIRTs, PARPs and CD38 aid cellular and/or tissue adaptation to intra- and extra-cellular stresses at the expense of the available NAD^+ pools. SIRT1/3/5 activity is tightly linked to NAD^+ levels as determined by their Michaelis constant K_m (Cantó, Menzies and Auwerx, 2015). In contrast, PARP activity is not regulated by NAD^+ levels, but rather by levels of DNA damage. The indiscriminate action of PARPs can thus lead to severe depletion of NAD^+ to 10-20% of normal levels upon large scale DNA damage induced by genotoxic treatments (Goodwin *et al.*, 1978; Skidmore *et al.*, 1979; Barbosa *et al.*, 2007). The impact of CD38 on intra- and extracellular NAD^+ pools was demonstrated in a *CD38* knockout mouse model, in which loss of CD38 alone results in a 10- to 20-fold increase in NAD^+ in studies liver, muscle, brain and heart tissue (Aksoy *et al.*, 2006). This avid consumption of short-lived NAD^+ pools by PARPs and CD38 leads to competition with and limitation of SIRT activity in the cytoplasmic and nuclear compartments. In addition, PARP1 was also found to localize to mitochondria and participate in mtDNA repair (Rossi *et al.*, 2009) and is thus likely to also affect mitochondrial NAD^+ pools and carbon metabolism.

1.4.3 NAD$^+$/NADH in subcellular compartments

Accurate measurement of the NAD$^+$:NADH ratio is critical for understanding the interdependence of the two functions of NAD$^+$ as a co-factor to metabolic pathways and as a co-substrate to PTM-modulating enzymes. Although it is recognized that the NAD$^+$:NADH ratio fluctuates in response to energy demands, the true estimation of NAD$^+$:NADH ratio is complex due to technological limitations, i.e. detection of protein-free and protein-bound NAD(H) molecules, and indirect form of measurement (pyruvate:lactate ratio as a reflection of NAD$^+$:NADH ratio) (Sun *et al.*, 2012). Pyruvate reduction to lactate occurs when glucose catabolism exceeds the capacity of the mitochondrial TCA cycle and leads to the oxidation of a single NADH molecule to NAD$^+$. Sun and colleagues argue that the P/L ratio is highly labile and not reflective of the true NAD$^+$:NADH ratio (Sun *et al.*, 2012). Despite the technical considerations, it is widely accepted that in mammalian cells and tissues, the total NAD$^+$:NADH ratio is approximately 10:1 while the cytoplasmic protein-free NAD$^+$:NADH ratio reaches as high as 700:1, thus favouring use of NAD$^+$ as a cofactor in oxidation reactions (Lin and Guarente, 2003; Anderson *et al.*, 2017). In addition, the published estimate of mitochondrial protein-free NAD$^+$:NADH ratio of 7:1 points to the existence of discreet NAD$^+$:NADH pools, which are resistant to depletion even in treatments which drastically deplete cytosolic and nuclear NAD$^+$ (Yang *et al.*, 2007; Pittelli *et al.*, 2010)

1.4.4 NAD$^+$ biosynthesis

The balance between NAD$^+$ consumption and NAD$^+$ biosynthesis governs the cellular NAD$^+$ pool. NAD$^+$ undergoes rapid fluctuations and is subject to a constant cycle of synthesis, degradation and recycling (Rajman, Chwalek and Sinclair, 2018). Due to its rapid utilization, studies from the 1960s-1980s indicate that NAD$^+$ has a relatively short half-life (up to 10h in mammals) (Elhassan, Philp and Lavery, 2017). NAD$^+$ and its pyridine precursors (L-tryptophan, nicotinic acid (NA), nicotinamide riboside (NR) and NAM) are extracted from dietary sources in the small intestine (Gross and Henderson, 1983; Cantó, Menzies and Auwerx, 2015). To enter circulation, NAD$^+$ is cleaved into its precursor NMN and further processed into NR and NAM (Gross and Henderson, 1983). Mammalian cells, with the exception of neurons, cannot import NAD$^+$ directly and must therefore synthesize it locally from circulating precursors, NR, NMN and NAM that enter cells via nucleoside transporters and feed into NAD$^+$ salvage pathway (Cantó, Menzies and Auwerx, 2015). In contrast, L-tryptophan and NA feed into NAD$^+$

de novo synthesis pathways mainly in the kidney and the liver (Figure 1.5A,B) (Cantó, Menzies and Auwerx, 2015; Katsyuba *et al.*, 2018). For local NAD^+ synthesis that combats its consumption, cells rely on recycling NAD^+ cleavage by-product, NAM, by the salvage pathway (Figure 1.5D) (Rajman, Chwalek and Sinclair, 2018). Both, *de novo* and salvage pathways require a ribose phosphate moiety from 5-phosphoribosyl-α-1-pyrophosphate (PRPP), the rate-limiting substrate of purine synthesis formed from ribose-5-phosphate, a product and an intermediate of the pentose phosphate pathway (PPP) and glycolysis (Hove-Jensen *et al.*, 2017). In addition, both, *de novo* and salvage pathways, also require ATP, from which an adenine nucleoside moiety is liberated to form the purine component of NAD^+ and can therefore only occur in conditions of ATP surplus (Figure 1.5B,D) (Cantó, Menzies and Auwerx, 2015; Rajman, Chwalek and Sinclair, 2018).

De novo NAD⁺ biosynthesis

NA, also known as niacin or vitamin B3, and the essential amino acid L-tryptophan stand at the root of *de novo* NAD^+ biosynthesis (Figure 1.5A), (Cantó, Menzies and Auwerx, 2015). Taken up from the diet, L-tryptophan feeds into the kynurenine pathway (Rajman, Chwalek and Sinclair, 2018). In the rate-limiting step of the pathway, L-tryptophan undergoes modification to an unstable intermediate, α-amino-β-carboxymuconate-ε-semialdehyde (ACMS). ACMS constitutes a branch point in the *de novo* synthesis pathway and can either undergo spontaneous cyclisation into quinolinic acid (QA), an NAD^+ precursor, or enzyme-assisted redirection towards total oxidation or production of picolinic acid (PA) in kidney and liver (Figure 1.5C) (Katsyuba *et al.*, 2018). The enzyme required is a conserved α-amino-β-carboxymuconate-ε-semialdehyde decarboxylase (ACMSD) and it is hypothesized that only when its enzymatic activity is saturated does ACMS proceed to spontaneously form QA (Grant, Coggan and Smythe, 2009). Next, QA and NA enter the Preiss-Handler pathway by accepting a ribose-1-phosphate group from PRPP and an adenine nucleotide from ATP to sequentially form NA mononucleotide (NAMN) and NA adenine dinucleotide, respectively (NAAD) (Figure 1.5A) (Cantó, Menzies and Auwerx, 2015). In the latter step, ATP cleavage and adenine nucleotide transfer onto NAMN is catalysed by a family of NMN adenylyltransferases (NMNATs) that also participate in the NAD^+ salvage pathway (Cantó, Menzies and Auwerx, 2015). In mammals, three isoforms of NMNATs (NMNAT1-3) localize to nucleus, cytoplasm (cytosolic face of the Golgi

apparatus), or mitochondria, respectively (Berger *et al.*, 2005). Last step of NAD^+ *de novo* synthesis requires ATP- and glutamine-dependent NAAD amidation by NAD^+ synthase (NADSYN). It is important to note that *de novo* NAD^+ synthesis is likely to occur mainly in tissues, which express high levels of the rate-limiting enzymes (ACMSD, NADSYN), including but not limited to the liver and the kidney (Cantó, Menzies and Auwerx, 2015; Katsyuba *et al.*, 2018).

NAD recycling via the salvage pathway

NAD^+ salvage pathway is key to maintenance of cellular NAD^+ levels and utilises two other forms of vitamin B3, NAM (also known as niacinamide) and NR, as initial inputs (Figure 1.5D). NR and NAM enter the cell via ubiquitously expressed equilibrative nucleoside transporters (ENTs), plasma membrane channels that facilitate influx and efflux of nucleosides and nucleobases (Boswell-Casteel and Hays, 2017). Upon entry into cells, NR is converted to NMN by the ubiquitous ATP-dependent nicotinamide riboside kinases (NRK1 and NRK2). Similarly, NAM is converted to NMN in an ATP- and PRPP- dependent catalytic step by NAMPT (Cantó, Menzies and Auwerx, 2015). NAMPT-mediated conversion of NAM into NMN is the rate-limiting step of the NAD^+ salvage pathway route from NAM that can be targeted by an NAMPT specific inhibitor FK866 (Hasmann and Schemainda, 2003; Khan, Tao and Tong, 2006; Pittelli *et al.*, 2010). Additionally, conversion of NAM to NMN, and ultimately to NAD^+, relieves NAM-mediated inhibition PARP and SIRT activity (Avalos, Bever and Wolberger, 2005; Henning, Bourgeois and Harbison, 2018). NMN conversion to NAD^+ requires addition of an adenine nucleoside that is catalysed by NMNATs, a family of enzymes shared between the salvage and the *de novo* NAD^+ synthesis pathways (Berger *et al.*, 2005).

1.5 Age-related dysfunction of autophagy, mitochondrial bioenergetics and NAD^+ metabolism

1.5.1 Loss of proteostasis and autophagy impairment

In young and healthy cells, the proteostasis network ensures correct protein expression, folding, function and recycling. Over time, intra- and extra-cellular stressors, including heat stress, oxidative stress and toxins, impact on protein conformation and can result in partial unfolding and exposure of hydrophobic regions to the cytosolic environment and aggregation (Hipp, Kasturi and Hartl, 2019). Protein aggregate formation can arise by chaotic interaction due to exposure of hydrophobic amino acid residues or ordered by interaction between β-sheet-assisted formation of toxic oligomers and fibrils (Moreno-Gonzalez and Soto, 2011). It is still debated whether it is the soluble (oligomer) or insoluble (fibril) aggregate form, which is toxic to the cellular environment (Ross and Poirier, 2005; Winklhofer, Tatzelt and Haass, 2008). Protein aggregation is challenged by the action of cellular chaperones that shield affected regions from interaction, attempt re-folding and, if facing unresolvable protein aggregation, promote aggregate sequestration into protein aggresomes and eventually into insoluble intracellular inclusions (Hipp, Kasturi and Hartl, 2019).

Analyses of aggresomes and insoluble fractions revealed presence of protein chaperones, proteasome subunits, ubiquitin and autophagy receptors, a sign that the misfolding/aggregation was recognised, but their clearance was unsuccessful (Kopito, 2000; Xia *et al.*, 2008; Henderson *et al.*, 2017). Interestingly, existing evidence supports two distinct models of disease onset. Firstly, accumulation of mutated or chronically misfolded proteins overwhelms the proteostasis systems, and leads to both, loss-of-function and gain-of-function phenotypes leading to cellular dysfunction (Balchin, Hayer-Hartl and Hartl, 2016; Hipp, Kasturi and Hartl, 2019). Secondly, age-related disruption in degradation pathways could underlie the toxicity of accumulating disease-associated proteins in both, wild-type and mutant form, which can lead to impairment of RNA homeostasis or disruption of recycling pathways by sequestration of their components (Balchin, Hayer-Hartl and Hartl, 2016).

Age-related loss of the proteostatic capacity, expression of mutant proteins with unusual folding patterns or altered stability and protein aggregate formation have all been linked to proteinopathies and neurodegenerative disorders (NDs) (Labbadia and

Morimoto, 2015). In addition, an ever increasing number of NDs is characterised by protein aggregate accumulation in insoluble cellular or extracellular aggregates and by perturbations in the protein degradation pathways (Labbadia and Morimoto, 2015; Sweeney *et al.*, 2017). Most notably, autophagy impairment at various stages of the pathways was identified in multiple NDs including Alzheimer's disease (AD), Parkinson's disease (PD), Huntington's disease (HD), and amyotrophic lateral sclerosis (ALS) and in disorders presenting with early onset neurodegeneration, including lysosomal storage disorders (LSD) like Niemann Pick Type C1 (NPC1) disease (Wong and Cuervo, 2010; Guo *et al.*, 2018). Reduction in autophagy initiation (AD), enhanced autophagy repression (HD), altered cargo recognition (HD, PD), impaired autophagosome trafficking (HD, ALS), inefficient autophagosome fusion with lysosomes (LSD) and loss of lysosomal function (AD, LSD) have all been implicated in NDs (Wong and Cuervo, 2010; Nah, Yuan and Jung, 2015)

In vivo studies have provided evidence for the causal role of autophagy in cellular health, homeostasis, and survival. Conversely, autophagy perturbation has been implicated in ageing, cell death and neurodegeneration. Mouse models of 14 core autophagy gene knockouts have been generated to date, of which genes encoding ATG conjugation proteins show disease-relevant phenotypes as neonates or adults (Kuma, Komatsu and Mizushima, 2017). Firstly, the generation of an *Atg5* knockout mouse clarified the importance of autophagy as a protective nutrient liberation process in periods of severe starvation (Kuma *et al.*, 2004). Although mice survive the early embryonic stage thanks to the maternal contribution of Atg5 RNA (Tsukamoto *et al.*, 2008), the pups die shortly after birth presumably due to inability to survive the post-natal starvation period upon separation from the placental nutrient supply prior to first feeding (Kuma *et al.*, 2004). In addition, *Atg5* knockout mice also showed a neurological defect presenting as suckling failure, which can be alleviated by neuron-specific expression of ATG5 (Yoshii *et al.*, 2016). Other phenotypes of autophagy mouse models include delayed clearance of apoptotic cells in *Atg5* deficient mouse embryonic stem cells in culture (Qu *et al.*, 2007); and altered mitochondrial morphology, peroxisome accumulation and increased levels of ubiquitylated proteins and protein aggregates in *Atg7* deficient mice (Komatsu *et al.*, 2005). Furthermore, tissue specific autophagy perturbations in these mouse models led to understanding of autophagy in tissue homeostasis. Both, systemic *Atg5* mosaic deficiency and a liver-specific *Atg7* deletion led to increased tumorigenesis in the liver (Takamura *et al.*,

2011). Although the exact mechanism of tumour formation is unknown, the authors hypothesized that tumorigenesis occurs due to constitutive Nrf2 activation as an indirect result of p62 accumulation in autophagy-deficiency. In addition, a neuron specific *Atg5* knockout results in motor and behavioural aberrations (Hara *et al.*, 2006). On a molecular level, absence of autophagy in neuronal cells led to formation of intracellular inclusions positive for ubiquitin, and ultimately resulted in swelling and loss of Purkinje cells in the cerebellum and in increased apoptosis of granular cells in the neighbouring granular layer (Hara *et al.*, 2006). *Atg* mutant mice and cells isolated from these animals thus provide a good model to study the pathology of autophagy-impairment on organellar health and metabolism.

1.5.2 Mitochondrial dysfunction

Mitochondrial dysfunction, the resulting production of ROS and damage to cellular macromolecules were long thought to drive ageing and age-related pathology. Initially proposed by Harman (Harman, 1972), the mitochondrial free-radical theory of ageing as a single cause of age-related dysfunction is now challenged and a more complex picture of ageing is emerging, which spans beyond macromolecule damage and includes dysregulation of cellular signalling as a contributor (Theurey and Pizzo, 2018). Due to the involvement of mitochondria in cellular homeostasis and central metabolic pathways they are still considered to be major contributors to the ageing phenotype and feature in the majority of proposed theories of ageing. First, the chronic exposure of mtDNA to ROS, a lack of protective histones and the higher error rate of mtDNA polymerase lead to a time-dependent increase in mtDNA mutation load (Wallace, 2005). Deleterious mutations, although originally diluted within the mitochondrial population, can over time drift towards WT or mutant and undergo clonal expansion and compromise mitochondrial ATP production (Greaves *et al.*, 2014). In addition, age-related increase of mtDNA insertion into nDNA centromeric regions was observed in a study of healthy young and aged rat tissue, though the physiological role and potential pathogenesis have not been explored (Caro *et al.*, 2010). However, mtDNA liberation from the organelle and interaction with cytosolic DNA sentinels as a stimulus of inflammation is currently under investigation. In addition, increased levels of circulating mtDNA was detected in samples from aged humans and correlated with the expression of pro-inflammatory molecules (Pinti *et al.*, 2014).

Second, three pathogenic alterations of cardiolipin (CL) have been described, altogether encompassing CL damage by oxidation; CL level alteration by altered biosynthetic and degradation pathways; and aberrant CL modelling (Chicco and Sparagna, 2007). CL functions at the IMM include stabilization of ETC complexes and spatial organization of cristae (Paradies *et al.*, 2010). A study of aged rat tissue identified a link between age-related increase in CL oxidation levels and CI dysfunction (Petrosillo *et al.*, 2008). It is since appreciated that many mitochondrial membrane complexes and transporters require healthy and abundant CL pools for optimal function (Chicco and Sparagna, 2007; Böttinger *et al.*, 2012). Importantly, although not yet experimentally confirmed, it is logical to suspect that increased CL oxidation may result in CL depletion through upregulation of its recycling pathway (Chicco and Sparagna, 2007). Decreased levels of CL were first reported from healthy aged rat brain tissue (Ruggiero *et al.*, 1992) and since identified in multiple models of age-related pathology (Chicco and Sparagna, 2007). Decrease in mitochondrial CL content seems to be particularly important for the pathogenesis of PD. One of the proteins implicated in the development of PD, α-synuclein, directly associates with CL, adopts an α-helical fold in its unstructured region and becomes less prone to aggregation (Ghio *et al.*, 2016). Therefore, age-related loss of CL could destabilize α-synuclein and result in aggregate formation. Interestingly, association between α-synuclein and mitochondria can lead to a range of mitochondrial phenotypes, including but not limited to mitochondrial fragmentation, decreased CI activity, increased ROS release and mitophagy activation (Nakamura, 2013)

Furthermore, mitochondria were shown to perform an essential role in stabilization of a tumour-suppressive mechanism termed cellular senescence. Cell senescence is defined as an irreversible cell cycle arrest associated with a pro-inflammatory and pro-oxidant secretory phenotype (Correia-Melo *et al.*, 2016). Beyond its role in cancer prevention, senescence contributes to age-related decline by imposing the senescent phenotype on neighbouring healthy cells and thus spreading dysfunction, oxidative damage and inflammation (Coppé *et al.*, 2008; Childs *et al.*, 2015). In a proof of concept study, Correia-Melo and colleagues demonstrated that senescence-induction and stabilisation does not occur in cells which lack mitochondria altogether (Correia-Melo *et al.*, 2016). Although healthy mitochondria are capable of adopting a pro-oxidant state to establish senescence (Correia-Melo *et al.*, 2016), mitochondrial dysfunction in proliferating human cells and a mouse progeria model drives a form of senescence

termed the mitochondrial-dysfunction-associated senescence (MiDAS) (Wiley *et al.*, 2016). Importantly, decrease in cytoplasmic NAD^+/NADH ratio, ATP depletion, AMPK activation and p53 phosphorylation are key to the establishment of cell cycle arrest and senescence secretory phenotype in response to mitochondrial dysfunction (Wiley *et al.*, 2016). Mitochondrial dysfunction leads to excessive NAD^+ reduction to NADH, which in turn deactivates glycolysis and glycolytic ATP production. Supplementation of cell permeable pyruvate, maintenance of a normal cytoplasmic NAD^+/NADH ratio by pyruvate reduction to lactate, and glycolysis activation prevent senescence in cells with dysfunctional mitochondria (Wiley *et al.*, 2016). These studies confirm that dysfunctional mitochondria might drive age-related phenotypes not only via increased oxidative damage, but more importantly, by negatively affecting cellular metabolism and signalling pathways.

1.5.3 Age-related NAD^+ depletion

NAD^+ is a co-factor of cellular redox reactions in the cytoplasmic and mitochondrial pathways of glucose oxidation (glycolysis and TCA cycle) and a substrate for plasma membrane, nuclear, cytoplasmic and mitochondrial enzymes (Cantó, Menzies and Auwerx, 2015). The involvement of cellular metabolism in ageing was explored upon identification of the key role of a small set of evolutionarily conserved longevity and stress-response pathways in yeast, worm, fly and rodent models during the 20th century, and further confirmed in primate models in 2009 (Campisi *et al.*, 2019). These studies had contributed not only to our understanding of the plasticity of ageing via lifespan extension, but also led to a realization that modulation of healthspan is achievable. Limiting calorie excess by dietary restriction and by exercise are the most robust metabolic interventions, which lead to lifespan and healthspan extension. Multiple studies have since confirmed the metabolic link between these interventions to increased NAD^+ availability due to rapid NADH oxidation, and thus to modulation of SIRT expression/activity and the downstream protein PTMs and transcription programmes (Bonkowski and Sinclair, 2016). In addition to SIRTs, the role of PARPs and cyclic ADP-ribose synthases in contributing to age-related defects has been explored in cellular and mouse models, in which both protein families indiscriminately consume NAD^+ when activated (Cantó, Menzies and Auwerx, 2015).

NAD^+ decline with age is a phenomenon that was reported as a result of increased PARP activity (Pacher and Szabo, 2008), increased CD38 expression (Camacho-

Pereira *et al.*, 2016) and decreased flux through the NAM-mediated salvage pathway (Stein and Imai, 2014). Age-dependent increase in PARP activity due to increased levels of DNA damage and increased expression of CD38 deplete the intra-cellular pool of available NAD^+. Combined with the age-dependent reduction of NAMPT activity (Stein and Imai, 2014), these conditions perpetuate the perfect storm of NAD depletion, loss of NAM recycling and thus SIRT inactivation. Study of human tissue samples at different ages partially supports this hypothesis (Massudi *et al.*, 2012). In this study, an age-dependent increase in DNA damage correlated with an increase in PARP activity, depletion of NAD^+ and, in the elderly, in reduction in SIRT1 activity. It is important to mention that stronger correlations were observed in the male population than in females and might warrant further study with increased statistical power. Another study utilised the power of magnetic resonance-based non-invasive *in vivo* imaging of human brain and revealed an age-dependent decrease in total NAD^+ levels, concomitant with reduction in NAD^+ and an increase in NADH levels, indicative of metabolic dysfunction (Zhu *et al.*, 2015).

Building on discoveries of the last decade, NAD^+ decline is now considered as one of the hallmarks of ageing. The ever-increasing understanding of cellular, tissue specific and circulatory NAD^+ metabolism offers a multitude of possible 'biomarkers' of NAD^+ metabolism for exploration in disease pathology. Indeed, as a key player in metabolism, disruption of NAD^+ levels was reported in a plethora of diseases associated with metabolic syndrome, including cancer, obesity, diabetes mellitus type 2, non-alcoholic fatty liver disease, atherosclerosis and depression (Okabe *et al.*, 2019). In addition, dysregulated NAD^+ metabolism and loss of SIRT function is implicated in neurodegeneration. First, although no single common source of cellular disruption is conclusively linked to Alzheimer's disease, metabolic disruption and deficient DNA repair were both implicated in disease onset and progression (Obulesu and Rao, 2010; Yin *et al.*, 2016). Moreover, *NMNAT2* mRNA levels negatively correlate with AD in human post-mortem brain tissue (Ali *et al.*, 2016). These findings, combined with the high failure rate of AD clinical trials focusing anti-amyloid compounds (Cummings, 2018), substantiated the rationale of repurposing NAM, an FDA approved supplement for treatment of several skin conditions, as an NAD^+-boosting strategy to slow or reverse the disease progression.

Similarly to AD, analysis of blood samples from PD patients and aged-matched healthy control group revealed a decrease in NAD^+:NADH ratio (white blood cells), a reduced NAD^+:$NADP^+$ ratio (red blood cells), and decreased levels of total circulating NA metabolites, expressed as a sum of NA, NAM and uric acid (plasma) (Wakade *et al.*, 2014). Correspondingly, two novel small-molecule activators of NAMPT prevent loss of dopaminergic neurons in a rat model of PD (De Jesús-Cortés *et al.*, 2015). Conversely, increased levels of NAM *N*-methyltransferase (NNMT) were detected in post-mortem brain tissue of PD patients (Parsons *et al.*, 2002). NNMT catalyses formation of *N*-methyl-NAM, a degradation metabolite destined for clearance, although novel hypotheses of *N*-methyl-NAM as a signalling metabolite are explored (Pissios, 2017). Importantly, *N*-methyl-NAM was hypothesized to be toxic to mitochondrial CI function due to its structural similarity to a known CI toxin that induces parkinsonism by selectively poisoning dopaminergic neurons, the 1-methyl-4-phenylpyridinium (MPP+) (Williams and Ramsden, 2005). This observation is relevant to modelling and therapeutic targeting of PD, but could also explain the anecdotal toxicity of high doses of NAD^+-precursor supplementation in cellular and animal models and might become a cautionary tale in future NAD^+-boosting strategies aimed to combat age-related NAD^+ decline.

1.5.4 Correlation and causality relationships in age-related dysfunction

Autophagy deficiency vs. mitochondrial health

Autophagy plays a crucial role in MQC, particularly stress-induced whole organelle recycling (Narendra *et al.*, 2008, 2010; Sedlackova and Korolchuk, 2018). Stress-induced and basal autophagy maintain mitochondrial health and are crucial for healthy ageing (Figure 1.6). In one particular example, study of a cardiomyocyte-specific *Bnip3* and *Nix* double knockout mouse model study identified their role in what authors referred to as ‘mitochondrial pruning’, a life-long basal autophagy activation that prevents the development of cardiomyopathy (Dorn, 2010). Deficient mitochondrial clearance as a cause of age-related dysfunction is best demonstrated in familial PD, particularly where *PINK1* and *Parkin* mutations underpin the disease (Pickrell and Youle, 2015), but also in sporadic cases, in which accumulation of α-synuclein interferes with autophagosome maturation and autophagosome-lysosome fusion, resulting in autophagy flux impairment, dysfunctional organelle accumulation and disease pathology (Tanik *et al.*, 2013).

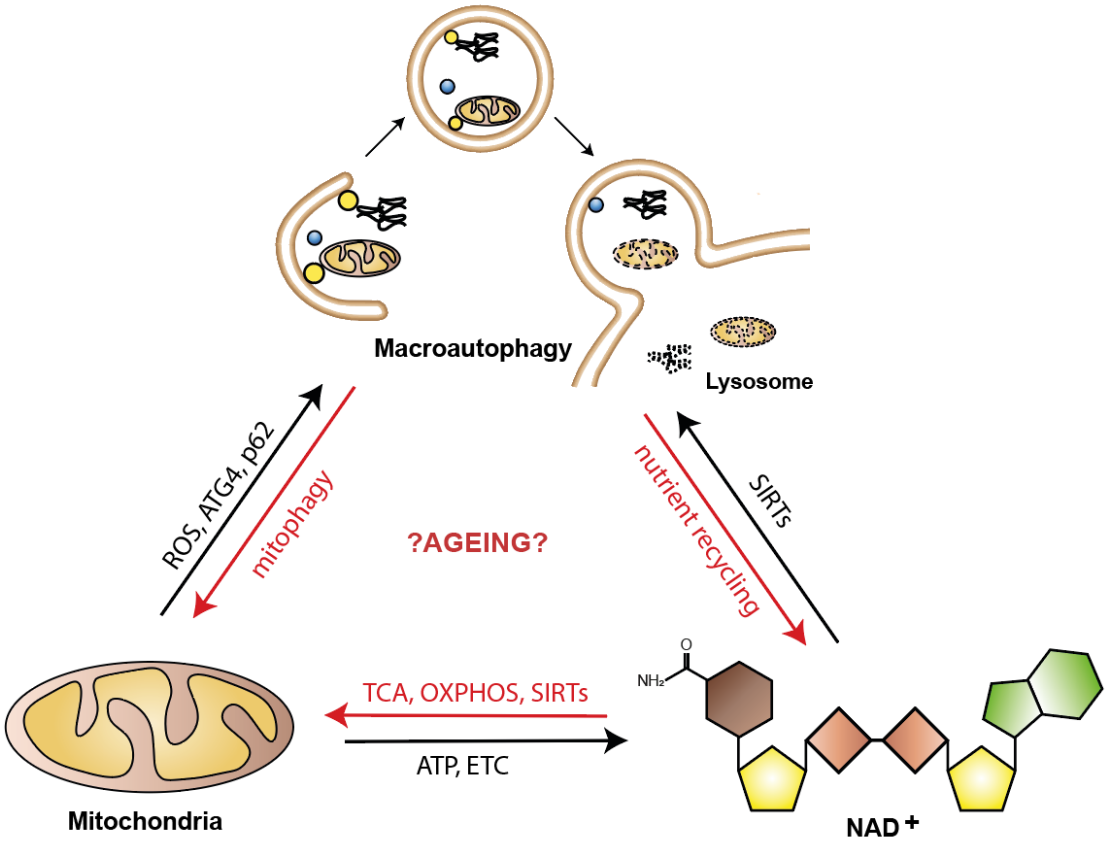

Figure 1. 6 Interrelatedness of age-related dysfunction

Autophagy flux, mitochondrial function, and NAD^+ levels all decline with age and underpin some of the hallmarks of ageing. It is unclear which hallmark is disturbed first in ageing and/or pathology. Current research indicates that decline of each of the three hallmarks in isolation compromises cellular function. Knowledge of pathways and enzymes that promote interrelatedness between the three hallmarks is limited.

Strong evidence supports the idea that mitochondrial ROS promote starvation-induced autophagy. The first line of evidence comes from HeLa cell models, in which depletion of mtDNA (ρ°) or SOD2 prevent starvation-induced ROS-mediated AMPK activation and autophagy stimulation (Lionaki *et al.*, 2015). ROS also modulate autophagy and other cellular processes by modifying cysteine residues and thus promoting formation of intra- and inter-protein disulphide bonds that affect protein conformation and function. In particular, two proteins involved in distinct stages of the autophagy pathway are regulated by disulphide bond formation. First, ATG4 is responsible for LC3-I cleavage prior to conjugation to PE and later for LC3-II recycling upon autophagosome fusion with lysosome. ATG4 de-lipidation activity is decreased upon disulphide bond formation in response to ROS, whereas its initial LC3-I cleavage remains thus leading to increased levels of autophagosome formation (Scherz-Shouval *et al.*, 2007). Second, disulphide bond formation promotes p62 oligomerisation and confers oxidative stress resistance by autophagy promotion (Figure 1.6) (Carroll *et al.*, 2018). Finally, mounting evidence now suggests an interplay of excessive mitochondrial ROS production and autophagy initiation in establishment of cancer metabolism, whereby excessive activation of autophagy promotes cancer cell survival (Li *et al.*, 2011).

NAD^+ deficiency vs. mitochondrial function

A correlation between NAD^+ depletion due to PARP hyperactivation and mitochondrial dysfunction was first observed in human neurodegenerative progeria syndromes. Studies of XPA (Fang *et al.*, 2014), Cockayne syndrome group B protein (CSB) (Scheibye-Knudsen *et al.*, 2012) and ataxia-telangiectasia mutated (ATM) protein (Valentin-Vega *et al.*, 2012) report dysregulated mitochondrial bioenergetics and recycling as a result of SIRT1 inactivity. Importantly, PARP inhibition by AZD2281 (olaparib) and NAD^+ precursor supplementation both rescued the mitochondrial pathology and progeria phenotypes in models of all three syndromes (Cantó, Menzies and Auwerx, 2015). A similar concept was also confirmed in *CD38* knockout mice, which maintain mitochondrial function, measured as respiration-driven ATP synthesis, better than their WT littermates (Camacho-Pereira *et al.*, 2016). In addition, CD38 transfection into a cell line model led to acute depletion of cellular NAD^+ and NADH levels; aberrations in mitochondrial morphology and function; and metabolic re-wiring towards aerobic glycolysis (Camacho-Pereira *et al.*, 2016). This study also reiterated the crucial role of mitochondrial SIRT3 activation as the mediator of the beneficial

effects of elevated NAD^+, which leads to SIRT3-mediated deacetylation of ETC subunits to promote OXPHOS and in a more direct fashion, deacetylation of SOD2 to activate $\cdot O_2$ detoxification (van de Ven, Santos and Haigis, 2017). Furthermore, the involvement of age-related NAD^+ decline in mitochondrial dysfunction was demonstrated in a mouse study where aged and *SIRT1* KO animals presented with lower mtDNA-encoded gene expression that was demonstrated to rely on nuclear NAD^+ availability (Gomes *et al.*, 2013).

In turn, age-related mitochondrial dysfunction and elevated levels of e^- leakage from the ETC results in decreased coupling of substrate (NADH, $FADH_2$) oxidation and ATP production. Loss of ATP, a key donor of adenine moiety in NAD^+ biosynthesis, limits the flux through NAD^+ biosynthetic and salvage pathways (Figure 1.5D, Figure 1.6) (Pinson *et al.*, 2019). Additionally, chronic loss of OXPHOS function decreases the NAD^+:NADH ratio, deactivates SIRT1-mediated mitochondrial biogenesis and SIRT3-mediated detoxification, and in a vicious cycle potentiates further ATP depletion and loss of cellular function and viability (Wallace, 2005).

Maintenance of NAD^+ levels vs. autophagy

Autophagy was identified as a contributor to age-related neurodegeneration and implicated in the pathology of AD, PD, ALS and HD. The main role of autophagy as a nutrient liberation pathway, links autophagy to cellular biosynthetic pathways by providing the building blocks and precursors for macromolecule synthesis. More specifically, study of *Atg7* WT and *Atg7*-deficient tumours revealed the crucial role of autophagy in the maintenance of glutamine/glutamate levels, cellular energy charge and total adenosine, uridine and cytidine levels (Guo *et al.*, 2016). Interestingly, glutamine supplementation prevented the exhaustion of all nucleosides in *Atg7*-deficient tumours. Although not explored in this study, depletion of glutamine and adenosine may contribute to altered NAD^+ metabolism and might warrant further research in cancer and age-related models of autophagy deficiency (Figure 1.6).

Conversely, NAD^+-mediated SIRT promotes autophagy induction. First, transient SIRT1 overexpression leads to increased levels of autophagy flux by mimicking nutrient starvation. Importantly, SIRT1-mediated autophagy stimulation is dependent on its deacetylase activity (Lee *et al.*, 2008). First, deacetylation of transcription factors including members of the forkhead box protein O (FoxO) protein family promotes

expression of multiple core autophagy genes (Webb and Brunet, 2014). Second, direct SIRT1-mediated deacetylation of ATG proteins, including ATG5, ATG7 and LC3, is required for starvation-induced autophagy at the stage of phagophore expansion (Huang *et al.*, 2015). Moreover, PARP1 activation was linked to autophagy initiation in response to DNA damage via signalling through AMPK (Muñoz-Gámez *et al.*, 2009; Chen *et al.*, 2015). In the earlier study, concurrent pharmacological inhibition of autophagy and stimulation of DNA damage-PARP1 axis led to cell death and suggests a protective role of autophagy-mediated recycling in DNA damage repair (Muñoz-Gámez *et al.*, 2009).

1.5.5 Niemann Pick type C1 disease: an example of interplay between autophagy and mitochondrial dysfunction

Niemann Pick type C1 (NPC1) disease is a rare and fatal autosomal recessive LSD, which presents with accumulation of unesterified cholesterol in the liver, spleen and central nervous system (Vanier, 2010). The disease is caused by a mutation in one of two genes NPC1 or NPC2. NPC1 and NPC2 genes encode membrane-anchored and soluble lysosomal lipid transporters, respectively. Mutations of NPC2 account for only 5% of the diagnosed cases (Wassif *et al.*, 2016). The more commonly affected protein, NPC1, is a transmembrane protein of the late endosome and lysosome. Loss of function mutations of NPC1 lead to sphingolipid, mostly cholesterol, sphingomyelin and glycosphingolipid, accumulation in late endosomes and lysosomes (Vanier, 2010). The age of onset and disease progression in NPC1 patients is heterogeneous and varies from a neonatal rapidly fatal disease to an adult-onset chronic neurodegenerative disorder (Vanier, 2010). The classic juvenile NPC patients present with early onset neuropathology as motor deficits progressing into cognitive decline, dementia, ataxia and seizures (Berry-Kravis *et al.*, 2018). Molecular neuropathological defects lead to formation of Alzheimer's-like neurofibrillary tangles, degeneration, axonal dystrophy and demyelination (Vanier, 2010). Complicating the search for an effective intervention in NPC1 is the lack of understanding of molecular mechanisms at the root of disease onset that explains the biochemistry and clinical presentations of this disease (Lloyd-Evans and Platt, 2010).

Sphingolipid accumulation was long thought to be the root cause of the molecular pathology of NPC1 and was the target of therapeutic treatment research. Miglustat (*N*-butyldeoxynojirimycin, Zavesca®; Actelion Pharmaceuticals), a reversible inhibitor of

glycosphingolipid biosynthesis capable of crossing the blood-brain barrier (BBB), is currently the only approved treatment for NPC disease shown to consistently slow neurological disease progression and improve patient survival (Lachmann *et al.*, 2004; Patterson *et al.*, 2012; Pineda, Walterfang and Patterson, 2018). 2-hydroxypropyl-β-cyclodextrin (HPβCD, VTS-270), a cholesterol binding and liberating compound, was successfully tested in a small phase 1-2a study (Ory *et al.*, 2017) and is currently tested for safety and efficacy in a multinational, randomized, double-blind phase 2b/3 trial (clinicaltrials.gov, NCT02534844). The largest drawback of HPβCD as a potential treatment of NPC1 is its exclusion by the BBB and thus it's direct impact on cholesterol accumulation in neurons is less than optimal (Pontikis *et al.*, 2013). The latest therapeutic approach to enter clinical trials is treatment with histone deacetylase inhibitors (HDACi). The underlying basis of HDACi use is to promote NPC1 expression and studies using mouse embryonic fibroblasts expressing NPC1 ^{I1061T}, the most common NPC1 allele mutation, and other missense NPC1 mutant proteins, show success in NPC1 stabilization and in cholesterol decrease (Pipalia *et al.*, 2017). One such HDACi molecule, vorinostat, is currently under evaluation in a completed phase1/2a trial (clinicaltrials.gov, NCT02124083).

Studies of *NPC1* knockout cell lines and NPC1 patient fibroblast have identified additional molecular pathologies, which associate with the disease. First, a defect in autophagic flux was shown in multiple models of NPC1 disease and in fibroblasts from NPC1 patients (Sarkar *et al.*, 2013). Second, a study of fibroblasts from healthy subjects and NPC1 patients revealed abnormal mitochondrial morphology, bioenergetics and membrane cholesterol content in NPC cells (Woś *et al.*, 2016). Third, NPC1 disease is characterized by an accumulation of cholesterol in neuronal and hepatocyte mitochondria. The exact mechanism of cholesterol trafficking and its intracellular origin are not fully elucidated (reviewed in (Torres *et al.*, 2017)), and neither is the resulting mitochondrial dysfunction. Nevertheless, increased cholesterol in mitochondrial membranes could lead to alterations in membrane fluidity, a shift towards mitochondrial fragmentation, and deficient OXPHOS, and subsequently result in increased oxidative stress and loss of mMP (Vázquez *et al.*, 2012; Torres *et al.*, 2017). HPβCD-assisted release of cholesterol from mitochondrial membranes is sufficient to rescue inhibition of the ATP synthase observed in *NPC1* KO cells (Kennedy *et al.*, 2014). Changes associated with cholesterol accumulation in mitochondrial membranes are consistent with findings of an increased glycolytic

phenotype (Kennedy *et al.*, 2014). Although the role of NAD^+ metabolism in NPC1 disease has not yet been investigated, one small mouse study of infantile NPC1 disease has demonstrated that NAM supplementation leads to improvement of cognitive function, as demonstrated by a passive avoidance shock chamber test (Marshall, Borbon and Erickson, 2017). Although the search of NPC1 therapy has so far focused on cholesterol and other lipid trafficking, studies in cellular and mouse models of the disease expanded the knowledge of other mechanisms potentially contributing to disease pathology, including autophagy impairment and dysregulated mitochondrial function. Further understanding of the cause and effect relationships and contribution to disease pathology of any or all of these pathways could contribute to the development of therapeutics that may alleviate liver disease and neurodegeneration symptoms of NPC1.

1.6 Aims & Objectives

Age is the main risk factor for prevalent chronic late-onset diseases in developed countries. Research over the last decade has contributed to our understanding of molecular pathology and metabolic dysfunction that correlate with disease pathology and clinical symptoms, but the underlying cause of disease onset and progression is still largely unknown. Concurrent with previous theories of age-related damage accumulation and newer theories of metabolic dysregulation, mitochondrial bioenergetics dysfunction was identified in multiple disorders. Similarly, autophagy impairment and NAD^+ depletion positively correlate with neurodegeneration and metabolic disorders. It is becoming clear that the study of these pathways should not happen in isolation and the wider impact of developed therapeutics should be considered. I hypothesized that autophagy dysfunction stands at the root of age-related molecular dysfunction and through loss of recycling results in aberrations of MQC and NAD^+ metabolism. Within the scope of this study I approached this complex issue by utilizing a genetic model of autophagy impairment, the immortalized *Atg5*$^{-/-}$ MEFs to characterize the downstream effect of autophagy abolition on mitochondrial function and the dynamics of NAD^+ metabolism. To investigate the relationship and interdependence of autophagy, mitochondrial quality control, NAD^+ metabolism and cellular function I designed the following aims:

Main aim 1: Establish whether autophagy abolition alone is sufficient to cause dysfunction of mitochondrial bioenergetics and NAD^+ metabolism.

Specific aim 1.1: Characterise mitochondrial structure and function changes in *Atg5*$^{-/-}$ MEFs cultured in a glucose-based medium.

Specific aim 1.2: Investigate the ability of *Atg5*$^{-/-}$ MEFs to adapt to increased OXPHOS demand by culture in a galactose-based medium.

Specific aim 1.3: Characterize metabolic changes in *Atg5*$^{-/-}$ MEFs.

Specific aim 1.4: Investigate main findings from *Atg5*$^{-/-}$ MEFs in autophagy-deficient and disease-relevant *NPC1*$^{-/-}$ MEFs.

Specific aim 1.5: Upon identification of common pathways of dysfunction, study the underlying cause by genetic and pharmacological means.

Main aim 2: Identify potential therapeutic compounds to target dysfunction and translate findings to NPC1 patient fibroblasts.

Specific aim 2.1: Identify small compounds that target autophagy/mitochondrial /NAD^+ metabolism aberrations.

Specific aim 2.2. Study the relevance of findings and therapeutics from immortalized MEF models in human patient fibroblasts.

Chapter 2. Materials & Methods

2.1 Cell lines obtained

Immortalized *Atg5*$^{+/+}$ and *Atg5*$^{-/-}$ mouse embryonic fibroblasts (MEFs) were kindly provided by Dr Noboru Mizushima, Tokyo, Japan (Kuma *et al.*, 2004). Immortalized *Npc1*$^{+/+}$ and *Npc1*$^{-/-}$ MEFs were a kind gift from Dr Peter Lobel, New Jersey, USA (Loftus et al 1997, Sarkar et al 2013). HEK293GPG and primary WT and *Npc1*^{KII1061T} MEFs, were a gift from Dr Daniel Ory, St. Louis, USA (Ory, Neugeboren and Mulligan, 1996; Praggastis *et al.*, 2015). HEK293T cells were obtained from the American Type Culture Collection. Control young human female fibroblasts (10705, 10763, 10632, 10263, 10156) were a kind gift from Dr Devin Oglesbee, Rochester, USA and Npc1 patient fibroblasts (GM17912, GM17924, GM18387, GM18402 and GM18417) were obtained from Coriell Cell Repositories.

Table 2. 1 Mouse and human model cell lines

Cell Line	Cell type	Source	Reference
MEF *Atg5*$^{+/+}$	immortalised	Dr Noboru Mizushima (Tokyo Medical and Dental University)	(Kuma et al., 2004)
MEF *Atg5*$^{-/-}$	immortalised		(Kuma et al., 2002)
MEF *Npc1*$^{+/+}$	immortalised	Dr Sovan Sarkar (University of Birmingham, UK)	(Sarkar *et al*., 2013).
MEF *Npc1*$^{-/-}$	immortalised		(Sarkar *et al*., 2013).
HEK293GPG	immortalised	Dr Daniel Ory (Washington University in St. Louis, USA)	Ory *et al*., 1996
HEK293T	immortalised	ATCC	CRL-3216™

Table 2. 2 Human control and NPC1 patient fibroblasts

Study Label	Catalogue ID	Gender	Age	Disease Affected	Allele 1 Mutation Allele 2 Mutation
CTRL (1)	10176	Female	24	no	none
CTRL (2)	10263	Female	21	no	none
CTRL (3)	10632	Female	22	no	none
CTRL (4)	10705	Female	26	no	none
CTRL (5)	10763	Female	21	no	none
NPC1 (1)	GM17912	Female	11	yes	[P1007A]^{L};[T1036M)]^{L}
NPC1 (2)	GM17924	Female	21	yes	c.451_452delAG^{L};[Y825C]^{C}
NPC1 (3)	GM18387	Female	33	yes	[D874V]^{L};[Y890X]^{L}
NPC1 (4)	GM18402	Female	10	yes	[D700N]^{TM};[F1221fsX]^{L}
NPC1 (5)	GM18417	Female	25	yes	[I1061T]^{L}; [I1061T]^{L}

2.2 Cell stock maintenance

Cells were maintained in DMEM (Sigma) supplemented with 10% FBS (Sigma), 100Uxml^{-1} penicillin/streptomycin (Sigma) and 2mM L-glutamine (Sigma). Control and NPC1 patient primary fibroblasts were cultured as above, except with 15% FBS. All cells were cultured in atmospheric oxygen conditions at 37°C and 5% CO_2 in a humidified incubator. HEK293GPG virus packaging cells require various culture supplements further described in section 2.3.1.

Table 2. 3 Cell culture: consumables

Consumable	Manufacturer/Vendor	Catalogue Number
75 cm² TC treated flask with filter cap	Greiner-Bio one	658175
175 cm² TC treated flask with filter cap	Greiner-Bio one	661175
6-well cell culture plates	Fisher	11825275
12-well cell culture plates	Fisher	TKB-100-110R
24-well cell culture plates	Fisher	TKB-100-115H
CELLview cell culture slide	Greiner-Bio one	543079
10cm TC plates (TPP yellow edge)	Helena biosciences	93100
Serological pipettes 10 ml	Sarstedt	86.1254.001
Serological pipettes 25 ml	Sarstedt	86.1685.001
Serological pipettes 5 ml	Sarstedt	86.1253.001
Glass Pasteur pipettes 230 mm	VWR	612-1702
0.6 ml 'Crystal Clear' microcentrifuge tube	Starlab	E1405-0600
1.5 ml microcentrifuge tubes	Starlab	S1615-5500
2 ml 'Crystal Clear' Microcentrifuge Tube	Starlab	E1420-2000
15 ml Centrifuge Tube, Conical (Sterile), Loose	Starlab	E1415-0200
50 ml Centrifuge Tube, Conical (Sterile), Loose	Starlab	E1450-0200
CryoTube vials	Fisher Scientific	377267
Mr. FrostyTM freezing container	Fisher Scientific	5100-0001
Coverglass 13 mm/0.16 mm	VWR	631-0150
Nalgene™ 25mm Syringe Filters, 0.2µm pore size	Fisher Scientific	15352388
0.45 µm Membrane Filter, PTFE (Sterile)	Starlab	P7166-6800
BD Discardit™ Eccentric Luer-Slip Two-Piece Syringe	Fisher Scientific	10345844
Slide-A-Lyzer# 2K MWCO Dialysis Cassettes	Fisher Scientific	10127483

Table 2. 4 Cell culture maintenance: reagents

Reagent	Manufacturer/Vendor	Catalogue Number
20x PBS	New England BioLabs	9808
Acryl Aquaclean	WAK-Chemie Medical GmbH	WAK-AQA-250-50L
DMEM	Sigma	D6546
Foetal Bovine Serum (FBS)	Sigma	F0804
L-glutamine solution	Sigma	G7513
Penicillin/Streptomycin	Sigma	P4333
Rely+On™ Virkon™	VWR	148-0202
Trypsin-EDTA solution	Sigma	T3924

2.3 Stable and transient cell line generation

2.3.1 Retroviral transduction

Stable expression of the ATG gene in the *Atg5*$^{-/-}$ MEFs was carried out by Dr Bernadette Carroll (current affiliation at School of Biochemistry, University of Bristol, University Walk, Bristol, UK) using a retroviral transduction protocol with the pMXs-IP-eGFP-mAtg5 construct (Addgene 38196). The viruses were packaged in HEK293T. 293T cells were seeded in a 10cm dish ($6x10^6$/10ml/dish) in antibiotic-free culture medium with 0.1mM MEM non-essential amino acid solution (Sigma) and 1mM sodium pyruvate (Sigma). Next day, cells were transfected with plasmids containing the packaging (Gag/Pol) and envelope (VSV-G) genes (kindly gifted by Michael Lazarou) and the pMXs-IP-eGFP-mAtg5 construct with the Lipofectamine 2000 reagent (Fisher Scientific) in OptiMEM (Invitrogen) as per manufacturer's instruction. Following overnight transfection, culture medium was replaced with fresh antibiotic-free medium that was collected after 24h. The virus containing medium was filtered through 0.45µm pore-size filter and overlayed, on 70% confluent *Atg5*$^{-/-}$ MEFs for 24h in the presence of 10µgxml^{-1} polybrene (Sigma). Cells stably expressing the mAtg5 gene were optimized for protein expression via puromycin selection (2µgxml^{-1}). Stable cell lines were maintained in lower levels of puromycin (1µgxml^{-1}) until seeding for experimental purposes.

Stable expression of NPC1 in *Npc1*$^{-/-}$ MEFs was achieved via retroviral transduction. HEK293GPG cells were cultured in high glucose DMEM (Sigma) supplemented with 10% FBS (Sigma), 50Uxml^{-1} penicillin/streptomycin (Sigma), 4mM L-glutamine (Sigma), 1mM sodium pyruvate (Sigma), 0.1mM MEM non-essential amino acid solution (Sigma), 1µg/mL tetracycline (Sigma), 2µgxml^{-1} puromycin (Santa Cruz

biotechnology) and 0.3mgxml^{-1} G418 (Enzo Life Sciences), referred to as 293GPG medium. HEK293GPG cells were seeded into 10cm dishes (5.5x10^6/10ml/dish) 48h prior to DNA transfection. When cell growth reached approximately 90% confluency, 293GPG medium was replaced with tetracycline-free, 293GPG medium, to allow for expression of viral packaging components. Cells were then transfected with either Δ U3BstX empty or NPC1 retroviral expression plasmid (Ory et al., 1996; Wu et al., 2004) with 4µg of DNA using Lipofectamine 2000 (Fisher Scientific) in OptiMEM (Invitrogen) according to manufacturer instruction. Transfection medium was replaced with tetracycline-free, 20% FBS containing 293GPG medium 16h later. Virus-containing medium was collected 48h post transfection and was filtered through a 0.45µm membrane filter (Starlab). Viral transduction was performed by overlaying 70% confluent *Npc1*$^{-/-}$ MEFs seeded in a 6-well plate with 1ml of virus-containing medium mixed with 1ml full nutrient medium in the presence of 8µgxml^{-1} polybrene (Sigma). Following overnight incubation, diluted virus-containing medium was replaced with fresh full nutrient medium supplemented with 200µgxml^{-1} hygromycin B (InvivoGen) for selection of transduced cells. Medium with antibiotic was replaced every 2-3 days to keep transduced cells in antibiotic selection for 10 days. Stable cell lines were maintained in lower levels of hygromycin B (20µgxml^{-1}) until seeding for experimental purposes.

Table 2. 5 Retroviral transduction: reagents

Reagent/Consumable	Manufacturer/Vendor	Catalogue Number
10cm TC plates (TPP yellow edge)	Helena biosciences	93100
0.45 µm Membrane Filter, PTFE (Sterile)	Starlab	P7166-6800
Hexadimethrine bromide (Polybrene)	Sigma	H9268
Hygromycin B Gold	InvivoGen	ant-hg-1
L-glutamine solution	Sigma	G7513
Lipofectamine® 2000	Fisher Scientific	10696153
MEM Non-essential Amino Acid Solution	Sigma	M7145
Neomycin (G418 Sulfate)	Enzo Life Sciences	ALX-380-013-G005
OptiMEM	Invitrogen	11058021
Penicillin/Streptomycin	Sigma	P4333
Puromycin	Santa Cruz biotechnology	sc-108071A
Sodium Pyruvate	Sigma	S8636
Tetracycline	Sigma	87128

2.3.2 siRNA transfection

ON-TARGETplus SMARTpool siRNA against mouse Ndufs3, Sdha, Uqcrfs1 or non-targeting control were purchased from GE Healthcare's Dharmacon (Table 2.4). Final siRNA concentration of 100nM was used for silencing, and transfections were performed with Lipofectamine 2000 (Fisher Scientific) in OptiMEM (Invitrogen) on *Atg5*$^{-/-}$ MEFs at 90% confluency. On the next day, transfected cells were split and seeded into 6 well plates (1:10 dilution) for continued growth. 48h after initial transection a second transfection was carried out with 20nM siRNA using the same procedure. Following re-transfection, cells were either lysed in RIPA buffer and subjected to immunoblotting for determination of knockdown efficiency or re-seeded into 6-well plates ($0.3x10^6$/2ml/6-well) followed by a switch and culture in a galactose-based medium for cell death assessment (procedure outlined in section 2.4).

Table 2. 6 siRNA transfection: reagents

Reagent	Manufacturer	Catalogue Number
SMARTpool: ON-TARGETplus mouse Ndufs3 siRNA	Dharmacon	L-047009-01-0005
SMARTpool: ON-TARGETplus mouse Sdha siRNA	Dharmacon	L-046818-01-0005
SMARTpool: ON-TARGETplus mouse Uqcrfs1 siRNA	Dharmacon	L-057582-01-0005
SMARTpool: ON-TARGETplus non-targeting siRNA	Dharmacon	D-001810-04
Lipofectamine® 2000	Fisher Scientific	10696153
OptiMEM	Invitrogen	11058021

2.3.3 Generation of knockout cell lines using CRISPR/Cas9 gene editing

Atg5$^{-/-}$, *Atg7*$^{-/-}$ and *Rb1cc1*$^{-/-}$ MEFs were generated using the clustered regularly interspaced short palindromic repeats (CRISPR)/Cas9 system. Ensembl, Aceview and CHOPCHOP databases were used to design CRISPR guide RNAs (gRNAs), 20 nucleotide sequences that determine the specificity of Cas9 nuclease to an exon present in all common splicing variants of a gene of interest. The gRNA oligomer was then annealed and ligated to a BbsI-linearized pspCas9(BB)-2A-GFP expression plasmid (Ran et al., 2013; a gift from Michael Lazarou). First, designed oligomers were diluted to a stock concentration of 100μM in RNase free H_2O (Fisher Scientific). Second, oligoduplexes were formed by oligomer annealing and 5' end phosphorylation in a PCR reaction as follows: 1μl of each of the pair of oligomers were mixed in a PCR

reaction tube with 1µl of 10x T4 DNA ligase buffer (New England BioLabs), 1µl of T4 polynucleotide kinase (New England BioLabs) and 6µl of sterile RNase free H_2O. PCR reactions were placed on a Veriti 96-Well Thermal Cycler (Applied Biosystems) and proceeded through cycles as follows: cycle 1 (37°C for 30min), cycle 2 (95°C for 5min) followed by cycle 3 (a ramp down to 25°C at -5°C/min) and a hold cycle (4°C).

Ligation of oligoduplexes with pspCas9(BB)-2A-GFP expression plasmid was preceded by plasmid digestion with BbsI (Fisher Scientific) for 15min at 37°C. 10ng of plasmid were mixed with 1ul of BbsI restriction enzyme and 2µl of 10x fast digest green buffer in a total volume of 20µl prepared in sterile RNase free H_2O. The linearized plasmid was then resolved on a 0.8% agarose gel and extracted from the gel using a Qiaquick gel extraction kit (Qiagen). Oligoduplex to plasmid ligation was achieved by mixing 6ul of oligoduplex reaction, 10ng of digested pspCas9(BB)-2A-GFP expression plasmid, 1µl of 10x T4 ligase buffer and 1µl of T4 DNA ligase (New England BioLabs) prepared to a total volume of 10µl in sterile RNase free H_2O. Ligation reaction was carried out at a constant temperature of 16°C overnight.

Bacterial transformation was then prepared using 10µl of NEB® 10-beta Competent E. coli (High Efficiency) (New England BioLabs), 4µl of ligation product. Transformation mixtures were incubated on ice for 30min, heat-pulsed at 42°C for 30sec, incubated on ice for 2 min, followed by the addition of 950µl of S.O.C. medium (Invitrogen) and 1h incubation at 37°C in a shaker set at 220rpm. Following 1h incubation, 300µl of each transformation reaction was plated on LB agar (Fisher Scientific) plates containing 100µgxml^{-1} ampicillin (Sigma) and incubated overnight at 37°C. Colonies were picked and grown in 5ml of LB broth (Fisher Scientific) overnight at 37°C in a shaker set to 220rpm. Plasmid DNA was extracted using the QIAprep Spin Miniprep Kit (Qiagen) to a final volume of 50µl in warm (60°C) sterile RNase free H_2O and sent for sequencing (Eurofins Genomics). *Npc1*$^{+/+}$ MEF cell line seeded into a 6-well plate was then transfected with the correct DNA ligation products. Cells were allowed to grow for 48h post seeding before transfection with Lipofectamine 2000 (Fisher Scientific) with 1.6µg DNA in OptiMEM (Invitrogen). Cells were trypsinised and re-suspended in FACS sorting medium (5% FBS (BioSera), 1mM ETDA (Sigma) in PBS) 24h post transfection. GFP-positive cells were individually sorted by FACS into 96-well cell culture plates. Immunoblotting was performed to screen for an autophagy defect in single cell colonies after expansion.

Table 2. 7 CRISPR guide RNA generation: primer design

Accession	Target Gene /Exon	Species	Primer Sequence
NM_053069 – isoform 1	Atg5/exon 6	mouse	5’ caccgACCAGTTTTGGGCCATCAAC 3’
			5’ aaacGTTGATGGCCCAAAACTGGTc 3’
NM_053069 – isoform 1	Atg5/exon 7	mouse	5’ caccgCTTTCATCCAGAAGCTGTTC 3’
			5’ aaacGAACAGCTTCTGGATGAAAGc 3’
NM_001253717	Atg7/exon 3	mouse	5’ caccgGAACGAGTACCGCCTGGACG 3’
			5’ aaacCGTCCAGGCGGTACTCGTTCc 3’
NM_001253717	Atg7/exon 4	mouse	5’ caccgCACTGAACTCCAACGTCAAG 3’
			5’ aaacCTTGACGTTGGAGTTCAGTGc 3’
NM_009826.4	Rb1cc1/exon 3	mouse	5’ caccgTATGTGTTTCTGGTTAACAC 3’
			5’ aaacGTGTTAACCAGAAACACATAc 3’
NM_009826.4	Rb1cc1/ exon 10	mouse	5’ caccgCTAACAGCTCTATTACAAGG 3’
			5’ aaacCCTTGTAATAGAGCTGTTAGc 3’

Table 2. 8 CRISPR guide RNA generation: equipment & reagents

Equipment/Reagent/Consumable	Manufacturer/Vendor	Catalogue Number
Veriti 96-Well Thermal Cycler	Applied Biosystems	
Burner Bunsen Natural Gas 13mm	SLS	BUR3000
Glass spreaders	Sigma	S4522-6EA
10x fast digest green buffer	Thermo Fisher Scientific	B72
α-select Gold Efficiency Competent Cells	Bioline	BIO-85027
Agarose	Thermo Fisher Scientific	BP1356-500
Ampicillin	Sigma	A5354
96-well plates	Fisher Scientific	11835275
CytoOne non-treated culture dish	Starlab	CC7672-3394
EDTA	Sigma	EDS
FastDigest BbsI (BpiI)	Fisher Scientific	FD1014
Invitrogen™ S.O.C. Ready-to-Use Medium	Fisher Scientific	11528896
LB Agar, Miller (powder)	Fisher Scientific	10734724
LB Broth, Miller	Fisher Scientific	10638013
Lipofectamine® 2000	Fisher Scientific	10696153
NEB® 10-beta Competent *E. coli*	New England BioLabs	BIO-85025
OptiMEM	Invitrogen	11058021
peqGREEN	Peqlab	37-5000
PfuUltra II Fusion HS DNA Polymerase	Agilent Technologies	600672
pspCas9(BB)-2A-GFP	Ran *et al*., 2013	x
QIAprep Spin Miniprep Kit	Qiagen	27104
QIAquick Gel Extraction Kit	Qiagen	28704
RNase free H_2O	GE Healthcare	B-003000-WB-100
Stable Competent E. coli (High Efficiency)	New England BioLabs	C3040

S.O.C. medium	Invitrogen	15544034
T4 DNA ligase	New England BioLabs	M0202S
T4 DNA ligase reaction buffer	New England BioLabs	B0202S
T4 polynucleotide kinase	New England BioLabs	M0201S
Tris-Acetate-EDTA 50x	Fisher Scientific	BP1332-1
XL10-Gold® Ultracompetent Cells	Agilent Technologies	200314

2.4 Experimental culture media and conditions

Two types of cell culture media were used in this study. First, a glucose-based medium prepared as high glucose DMEM (Sigma) supplemented with 10% FBS (BioSera), 100Uxml^{-1} penicillin/streptomycin (Sigma) and 2mM L-glutamine (Sigma). Second, to induce mitochondrial respiration, cells were cultured in a glucose-free Gibco™ DMEM (Fisher Scientific) supplemented with 10% FBS (BioSera), 100Uxml^{-1} penicillin/streptomycin (Sigma) and 4mM L-glutamine (Sigma), 10mM D-galactose (Sigma) 10mM HEPES (Sigma) and 1mM sodium pyruvate solution referred to as galactose-based medium.

Table 2. 9 Experimental culture media: composition

Reagent	Manufacturer/Vendor	Catalogue Number
DMEM	Sigma	D6546
Gibco™ DMEM	Fisher Scientific	12307263
Foetal Bovine Serum (FBS)	BioSera	FB1001H
L-glutamine solution	Sigma	G7513
Penicillin/Streptomycin	Sigma	P4333
HEPES	Sigma	H0887
Sodium Pyruvate Solution	Sigma	S8636
D-galactose	Sigma	G0750

For experimental purposes, *Atg5*$^{+/+}$ and *Atg5*$^{-/-}$ MEFs and *Npc1*$^{+/+}$ and *Npc1*$^{-/-}$ MEFs, and human control and NPC1 patient fibroblasts were always seeded into cell culture dishes in glucose-based medium 24h prior to treatment start. Cells were washed in sterile PBS 24h after seeding and fed glucose- or galactose-based media as indicated. Type of cell culture vessel, length of treatment and experimental conditions are summarized at the start of each experimental method.

2.5 Mitochondrial function assessment

2.5.1 Seahorse analysis

For all Seahorse-based analyses, *Atg5*$^{+/+}$ and *Atg5*$^{-/-}$ MEFs ($0.8x10^4$ cells/well) were seeded directly into Seahorse XF24 cell culture microplates (Agilent, 100777-004). Cells were re-fed a glucose-based medium 24h after seeding and cultured for a further 20h before the start of a Seahorse-based analysis. All Seahorse-based measurements were carried out in collaboration with Dr Satomi Miwa (Institute for Cell and Molecular Biology, Newcastle University, Newcastle upon Tyne, UK). Two-tailed unpaired Student's *t*-tests were carried out to determine the statistical differences between sample averages from three independent experiments.

Whole cell bioenergetics - OCR and ECAR measurements

Cellular oxygen consumption rates (OCR) and extracellular acidification rate (ECAR) in *Atg5*$^{+/+}$ and *Atg5*$^{-/-}$ MEFs were measured in parallel using a Seahorse XF24 analyser in unbuffered basic medium supplemented with 5mM glucose, 1mM sodium pyruvate, 2mM L-glutamine and 3% FBS or for galactose-based medium with 10mM galactose, 1mM sodium pyruvate, 4mM L-glutamate and 3% FBS. During analysis the following compounds were added to test mitochondrial activity and cellular bioenergetics flux: 0.5µM oligomycin to inhibit ATP synthase, 2.5µM FCCP to stimulate mitochondrial oxygen consumption to maximum capacity, 80mM 2-deoxyglucose (2-DG) to inhibit glycolytic flux and 0.5µM rotenone with 2.5µM antimycin A to inhibit complex I and III respectively. Calculation of ATP production was carried out as described in (Mookerjee *et al.*, 2015).

Permeabilised cell bioenergetics: Complex I- and II-linked respiration

To measure complex I- and II-linked respiration, cells were permeabilised using Seahorse XF Plasma Membrane Permeabilizer (Agilent Technologies) and OCR was measured in the assay buffer (115mM KCl, 10mM KH_2PO_4, 2mM $MgCl_2$, 3mM HEPES, 1mM EGTA and 0.2% fatty acid-free BSA, pH 7.2, at 37°C) with complex I substrates (10 mM pyruvate and 1 mM malate) or complex II substrate (4mM succinate and 0.5uM rotenone).. During analysis the following compounds were added to test mitochondrial activity and cellular bioenergetics flux: 4mM ADP, 0.5µM oligomycin, 2.5µM FCCP, and 2.5µM antimycin A.

Table 2. 10 Seahorse analysis: reagents

Reagent	Manufacturer/Vendor	Catalogue Number
2-deoxyglucose	Sigma	D8375
ADP	Sigma	A5285
Antimycin A	Sigma	A8674
D-galactose	Sigma	G0750
D-glucose	Sigma	G8270
FCCP	Sigma	C2920
Malate	Sigma	M6413
Oligomycin	Sigma	O4876
Pyruvate	Sigma	P5280
Rotenone	Sigma	R8875

2.5.2 High-resolution respirometry assay

For a respirometry-based assay, *Atg5*$^{+/+}$ and *Atg5*$^{-/-}$ MEFs (0.3x10^6 cells/well) were seeded into 6-well cell culture dishes. Cells were switched into glucose or galactose-based media 24h after seeding and cultured for a further 20h before the start of a respirometry-based analysis. All respirometry-based measurements were carried out in collaboration with Prof Alberto Sanz (Institute for Cell and Molecular Biology, Newcastle University, Newcastle upon Tyne, UK).

Respirometry measurements were performed in permeabilized cells using an OROBOROS Oxygraph-2k system. Following 20h culture in a galactose-based medium, cells were trypsinized, collected, counted and 1x10^6 cells were re-suspended in O2k media (0.5mM EGTA, 3mM $MgCl_2$, 60mM lactobionic acid, 20mM taurine, 10mM KH_2PO_4, 20mM HEPES, 110mM D-sucrose, 1g/L BSA, fatty acid free). Suspended cells were transferred into Oxygraph-2k chambers, permeabilized with digitonin (10 µgxµl^{-1}), and sequentially supplemented with pyruvate (5mM) and malate (2mM), ADP (4mM), and succinate (10mM). The Oxygraph-2k chambers were left to equilibrate after each compound addition for measurement of O_2 consumption. All measurements were carried out in 2ml volume at 37°C. Two-tailed unpaired Student's *t*-tests were carried out to determine the statistical differences between sample averages from three independent experiments.

Table 2. 11 High-resolution respirometry measurement: reagents

Reagent	Manufacturer/Vendor	Catalogue Number
ADP	Sigma	A2754-1G
Digitonin	Santa Cruz biotechnology	sc-280675
L-(−)-Malic acid	Sigma	02288-10G
Sodium pyruvate	Sigma	P-8574
Dimethyl succinate	Sigma	W239607

2.5.3 mMP measurements

For mMP measurements, *Atg5*$^{+/+}$ and *Atg5*$^{-/-}$ MEFs ($0.8x10^4$ cells/well) cells were seeded into 96-well-size CELLview cell culture slide (Greiner Bio-One). Following 40h culture in a galactose-based medium, and treatment with indicated compounds, cells were co-stained with 16.7nM tetramethylrhodamine, methyl ester (TMRM; Fisher Scientific) and 100nM mitotracker green (MTG; Fisher Scientific). 10x stock of each compound was prepared in conditioned galactose-based medium (24h culture on *Atg5*$^{-/-}$ MEFs, collected and filtered through a 0.22µm pore-size filter) and 100µl were added directly to PBS-washed culture wells. Following a 30min incubation in the dark at 37°C, the dye-containing medium was aspirated, cells were washed and re-fed non-dye containing conditioned medium. Live cell imaging was performed in a maintained atmosphere of 37°C and 5% CO_2 using and LSM700 microscope (Zeiss) with a C-Apochromat 40x/1.20 W Korr M27 water immersion lens equipped with photon-multiplier tubes. The excitation sources used were solid state laser lines 488nm and 561nm. Image analysis was performed in ImageJ (version 1.49) (National Institutes of Health) by outlining cells as regions of interest to determine a ratio of TMRM to MTG raw integrated density values per cell. Quantification was performed on 30–40 cells per condition in three independent experiments. Two-tailed unpaired Student's *t*-tests were carried out to determine the statistical differences between sample averages from three independent experiments.

Table 2. 12 mMP measurement: reagents

Consumable/Reagent	Manufacturer/Vendor	Catalogue Number
Nalgene™ 25mm Syringe Filters, 0.2µm pore size	Fisher Scientific	15352388
BD Discardit™ Eccentric Luer-Slip Two-Piece Syringe	Fisher Scientific	10345844
CELLview cell culture slide	Greiner Bio-One	543079
TMRM	Fisher Scientific	T668
MTG	Fisher Scientific	M7514

2.6 MS-based metabolomics

Atg5$^{+/+}$ and *Atg5*$^{-/-}$ MEFs (0.3x10^6/well), and *Npc1*$^{+/+}$ and *Npc1*$^{-/-}$ MEFs (0.2x10^6/well) were seeded in 6-well plates and cultured in the galactose-based medium for 16h and 48h, respectively. Two sets of wells were seeded in parallel, one for establishing cell number count and cell protein measurements, the second for metabolic processing. The first set of cells were trypsinized, counted to establish cell number/well and processed for immunoblotting (discussed in 2.13). The second set was processed at indicated time points by a rapid wash with cold PBS and addition of chilled lysis buffer (50% methanol (Sigma), 30% acetonitrile (Sigma), 20% dH_2O) at concentration of 2x10^6 cells/ml. Cell lysates were collected into chilled Eppendorf tubes, agitated 10x by triturating with a P1000 and stored at -20°C until all samples were collected. All samples were then vortexed for 45s and centrifuged at 13 000rpm. Sample supernatants were transferred into a fresh Eppendorf tube and subjected to liquid chromatography-MS analysis in collaboration with Dr Oliver D.K. Maddocks (Institute of Cancer Sciences, University of Glasgow, Glasgow, UK).

Output from MS-based analysis was subjected to statistical analysis by MetaboAnalyst 4.0. To determine the relatedness between *Atg5*$^{+/+}$ and *Atg5*$^{-/-}$ MEFs samples, I employed a principal component analysis (PCA), a form of multivariate statistical analysis applied to non-scaled and auto-scaled (mean-centred and divided by SD of each variable) data sets. Furthermore, a univariate statistical test coupled with *Atg5*$^{-/-}$/*Atg5*$^{+/+}$ fold change of each metabolite were plotted on a volcano plot. Statistical significance of differences was determined using the Student's *t*-test with *P* value corrected with false discovery rate (FDR) method of Benjamini and Hochberg, which does not assume a consistent standard deviation (SD).

Table 2. 13 MS-based cell collection: reagents

Consumable/Reagent	Manufacturer/Vendor	Catalogue Number
Methanol	Fisher Scientific	10675112
Acetonitrile	Sigma	271004

2.7 NAD$^+$/NADH assay

Isolated NAD$^+$/NADH measurements in human control and NPC1 patient fibroblasts were performed using a Promega detection NAD/NADH-Glo^{TM} assay as per manufacturer's instructions (Promega). Cells subcultured in the galactose-based

medium only or supplemented with NAM and NMN (varied concentrations) for 4 passages were seeded into cell culture 96-well plates ($0.8x10^4$ cells/well) and left to grow for an additional 48 hours. Cells were then equilibrated at RT for 5min, medium was discarded and 75µl of PBS and 75µl of lysis buffer containing dodecyltrimethylammonium bromide (DTAB, Sigma) (0.1% DTAB in 0.2N NaOH) were added to each well. 30µl of each sample was saved for a protein concentration measurement. 2x 50µl of total volume from each well were transferred to clean wells for separate NAD^+ and NADH measurements. 25µl of 0.4N HCl was added to wells of NAD^+ measurement and the plate was sealed prior to 15min incubation at 60°C. Following a 10min equilibration period at RT, NAD^+ measurement wells were topped up with 25µl of 0.5M Trizma® base solution (Sigma). 50µl of 0.5M Trizma® hydrochloride (Sigma) was added to wells of NADH measurement. β-NAD^+ (Sigma) and β-NADH (Sigma) standards were prepared at 500nM, 100nM, 50nM, 10nM and 5nM concentrations. 25µl of each standard and each sample were transferred to an opaque 96-well plate and topped up with 25µl of the NAD/NADH-Glo™ (Promega) reagent. Plates were then sealed and incubated at RT in the dark for 1h. Luminescence output was captured, normalized to NAD^+/NADH standards and protein levels. Statistical analysis was carried out on average values of quadruplicate measurements of 5x control cell lines and 5x NPC1 patient cell lines. Initially, one-way analysis and multiple comparisons were used to determine whether NAD^+ and NADH levels vary between three groups of cell lines based on an autophagy deficit (control, no autophagy impairment detected (NAI) and autophagy deficient (AI)). Later, linear regression analysis was carried out in Graphpad Prism 8 on log_2 transformed dose data and individual NAD^+ measurement values to determine whether increasing doses of NAM and NMN supplementation leads to a linear increase in NAD^+ levels.

Table 2. 14 NAD^+/NADH assay: reagents

Reagent	Manufacturer/Vendor	Catalogue Number
DC Protein Assay Kit	BioRad	500-0112
DTAB	Sigma	D8638
NAD/NADH-Glo™ Assay	Promega	G9072
Trizma® base	Sigma	T1503
Trizma® hydrochloride	Sigma	T5941
β-NAD^+	Sigma	N0632
β-NADH	Sigma	N8129

2.8 ROS measurements

ROS measurements were carried out and analysed by two different methods, flow cytometry (primary human fibroblast) and confocal imaging (MEFs). For the confocal imaging of fixed samples, *Atg5*$^{+/+}$ and *Atg5*$^{-/-}$ MEFs were seeded on 13mm coverglass (VWR) into a 6-well plate (0.3x10^6/well) to keep seeding densities consistent with other experiments. Superoxide formation was detected using a final concentration of 2.5µM MitoSOX (Invitrogen). A 10x stock of MitoSOX was prepared in conditioned culture medium and was added to cultured cells 20h after a switch to the galactose-based medium, followed by a 10min incubation at 37°C in the dark. Cells were then fixed in 3.7% formaldehyde (FA; Sigma) for 5min, washed thrice in 1xPBS and mounted on glass slides (VWR) using a non-DAPI fluoroshield mounting medium (abcam). Fluorescence images of fixed cells were compiled at RT on an inverted DMi8-CS microscope (Leica), with a Plan-Apochromat 40x/1.30 oil immersion objective, equipped with an ORCA-Flash4v2.0 camera (Hamamatsu). The excitation source used is a Sola365 light engine (Lumencor). Image analysis was performed in ImageJ (version 1.49) (National Institutes of Health). MitoSOX intensity per cell was quantified after thresholding was applied by using the region of interest (ROI) feature in ImageJ. The significance of observed differences in MitoSOX intensity was determined by a two-tailed unpaired Student's *t*-test on data from three independent experiments. Imaging and quantification of MitoSOX intensity was done in collaboration with Dr Filippo Scialo.

For flow cytometry-based ROS analysis, human fibroblasts were subcultured in a galactose-based medium for 4 passages. Cells were then seeded in 6-well dishes (0.15x10^6), left to grow for 48h and then stained with 10µM 5-(and-6)-2′,7′-dichlorodihydrofluorescein diacetate, acetyl ester (-H2DCFDA; Life Technologies) for 30min in the dark at 37°C. Stained cells were then trypsinized, spun and re-suspended in a FACS sorting medium (3% FBS (BioSera) in PBS). Flow cytometry data (10 000 hits) was acquired on BD FACSCanto™ benchtop analyser (BD Biosciences), and analysed using the FlowJo software. First, data was gated to exclude debris or doublet events. Second, geometric averages of the resulting populations were calculated. Statistical analysis was carried out on geometric averages of 3x control cell lines and 3x NPC1 (AI) patient cell lines.

Table 2. 15 ROS measurement: reagents

Consumable/Reagent	Manufacturer/Vendor	Catalogue Number
13mM Coverglass	VWR	631-0150
20x PBS	New England BioLabs	9808
Foetal Bovine Serum (FBS)	BioSera	FB1001H
Fluoroshield mounting medium	abcam	ab104135
Formaldehyde solution	Sigma	F8775
Microscope slides, SuperFrost®	VWR	631-0116
MitoSOX	Invitrogen	LSM36008

2.9 BN PAGE analysis

Blue Native polyacrylamide gel electrophoresis (BN-PAGE) was carried on *Atg5*$^{+/+}$ and *Atg5*$^{-/-}$ MEFs (1.5x10^6/dish), and *Npc1*$^{+/+}$ and *Npc1*$^{-/-}$ MEFs (1.2x10^6/dish). *Atg5 and Npc1* cells were seeded into 10cm dishes (1.5x10^6/10ml/dish) and switched to both, glucose and galactose-based media for 16h and 48h, respectively. Cells were collected for mitochondrial isolation and BN-PAGE analysis at the indicated time points. Dr Yoana Rabanal-Ruiz (current affiliation at Regional Center for Biomedical Research, University of Castilla-La Mancha, Spain) supervised and helped with optimization of the mitochondrial isolation protocols.

Table 2. 16 BN-PAGE solutions: composition

Homogenization solution	Solubilization base solution	Loading dye	3x gel buffer
20mM HEPES-KOH pH7.6	20mM BisTris pH7.4	100mM BisTris pH7.0	150mM BisTris pH7.1
220mM D-mannitol	50mM NaCl	50mM ε-amino n-caproic acid	200mM ε-amino n-caproic acid
70mM sucrose	10% glycerol		
1mM EDTA	*10mM DTT	5% Coomassie blue G	
*0.5mM PMSF			**20x Anode buffer**
*2mM DTT			1M BisTris pH7.0
*2x Halt inhibitors			
4% acrylamide gel	**13% acrylamide gel**	**Empty well buffer**	**10x Cathode buffer**
33.3% 3x gel buffer	33.3% 3x gel buffer	20mM BisTris pH7.0	500mM Tricine
43.8% of 30% acrylamide	12.93% of 30% acrylamide	50mM NaCl	150mM BisTris-unbuffered
20% glycerol	0% glycerol	10% glycerol	0.2% Coomassie blue G
2.9% MQH_2O	53.7% MQH_2O	0.5% Coomassie blue G	

* reagents to be added immediately before use

2.9.1 Sample Preparation – Mitochondrial Isolation.

Cell Homogenisation

Cells grown in 10cm dishes were scrapped in 5ml of ice-cold PBS and transferred into a 15ml falcon tube. Cells were pelleted at 2900rpm for 5min in a table top centrifuge pre-cooled to 4°C, resuspended in 3ml of homogenisation solution transferred into a homogeniser and processed with 60 strokes. Homogenised cells were transferred into pre-chilled 1.5ml Eppendorf tubes and centrifuged at 2900rpm for 5min in a table top centrifuge pre-cooled to 4°C to pellet cellular debris. Supernatant was transferred into a fresh pre-chilled 1.5ml Eppendorf tube immediately after centrifugation. A total of 5x subsequent washes were carried out until no pellet was observed. 3ml of cell homogenate were then pooled and 300µl of supernatant was collected and stored as a whole cell lysate for immunoblot analysis.

Mitochondrial isolation

Whole cell homogenates were further processed to isolate mitochondria. Approximately 2.5ml of homogenate was transferred into fresh pre-chilled 1.5ml Eppendorf tubes and centrifuged at 13,000rpm for 10min in a table top centrifuge pre-cooled to 4°C. Supernatant was removed and collected as cytoplasmic fraction. The pellet that consisted of isolated mitochondria was resuspended in homogenisation solution and washed twice by centrifugation at 13,000rpm for 10min. Mitochondrial pellet was then re-suspended in 70-100µL of homogenisation solution and protein concentration was determined using the DC Protein Assay Kit (BioRad) and a FLUOstar Omega plate reader (BMG Labtech). 25µl aliquots of isolated mitochondria were stored at -80°C.

2.9.2 BN-PAGE analysis

Isolated mitochondria were solubilised in presence of either digitonin (Santa Cruz Biotechnology) or triton X-100 (Sigma) detergents to study supercomplex and holocomplex assembly, respectively. Digitonin was first prepared as a 5% solution and boiled for 5min to achieve full solubilisation. 30µg of isolated mitochondria were pelleted and re-suspended by 20x trituration in 30µl of solubilisation base solution supplemented with 100mM dithiothreitol (DTT) (Fisher Scientific) and digitonin (0.8-1%) (Santa Cruz Biotechnology) or triton X-100 (0.8%-1%), as indicated in figure

legends. Following resuspension, samples were incubated on ice for 20min to achieve solubilisation. Mitochondrial debris and insoluble material were pelleted by centrifugation at 13 000rpm for 10min at 4°C. The supernatant was then mixed with 3µl BN-PAGE loading dye. 30µl of solubilised samples were separated on a 4%-13% gradient acrylamide (Severn Biotech) BN-PAGE gel. The gradient gel was mixed and poured using a set up comprising of a gradient maker (Fisher Scientific 11544424) and a peristaltic pump in the presence of 0.1% ammonium persulfate (Sigma) and 0.13% TEMED (Sigma). The protein ladder was prepared as a mixture of 10mg/mL thyroglobulin (669kDa; Sigma), 10mg/mL ferritin (440kDa; Sigma) and 10mg/mL bovine serum albumin (140kDa and 67kDa; Sigma) in ladder solution (20mM BisTris pH 7.0, 50mM NaCl, 10% glycerol and 0.5% Coomassie Blue G). Cathode and anode buffers were used for protein separation. Cathode buffer in the inside chamber and clear anode buffer in the outside chamber were used for separation until sample dye front reached ½ of the gel in running conditions of 100V, 10mA for 1h. The run was then paused and a Coomassie Blue G-free cathode buffer was used to replace Coomassie Blue-G-containing cathode buffer. Following cathode buffer switch, gel run conditions were adjusted to 300V, 15mA and gel was ran for a further 1h 20min. The gel run conditions were maintained at 4°C.

BN-PAGE transfer was performed using a wet transfer method in presence of pre-chilled Tris-Glycine buffer (25mM Trizma® base (Sigma), 0.192M glycine (Sigma), supplemented with 10%/20% methanol (Fisher Scientific) onto an Immobilon-P polyvinylidene difluoride membrane (PVDF, Merck Milipore IPVH00010). Transfer conditions of 100V for 1h were sufficient for transfer of high-molecular weight complexes. PVDF membranes with transferred protein complexes were then incubated in de-stain buffer (40% methanol (Fisher Scientific), 10% glacial acetic acid (Sigma)) to reveal and mark the molecular weight ladder, prior to incubation in blocking solution (5% skimmed dry milk (Marvel), 0.1% Tween20 (Sigma) in PBS) for 1 hour at RT. The blocking solution was drained and membranes were incubated with primary antibodies diluted in blocking solution at 4°C overnight. Following overnight incubation, draining of the primary antibody, membranes were washed thrice in PBS, PBS-0.1% Tween 20, and PBS for 5min each. Membranes were then incubated with the corresponding secondary antibodies conjugated to horseradish peroxidase (HRP) for 1 hour at RT. The following secondary antibodies were used: anti-rabbit HRP (1:5000, Sigma), anti-mouse HRP (1:5000, Sigma). Membranes were washed thrice in PBS, PBS-Tween 20

and PBS as before. Clarity western ECL substrate (BioRad) was used to visualise chemiluminescence on LAS4000 (Fujifilm). BN-PAGE is a qualitative method, nevertheless, conclusions drawn from chemiluminescence signal are based on three independent experiments.

Table 2. 17 BN-PAGE: reagents

Consumable/Reagent	Manufacturer/Vendor	Catalogue No.
20x PBS	New England BioLabs	9808
2x Halt complete phosphatase and protease inhibitor cocktail	Fisher Scientific	10311494
30% Acrylamide/Bis-acrylamide	Severn Biotech	20-2100-10
Ammonium persulphate (APS)	Sigma	A3678
BisTris	Santa Cruz Biotechnology	sc-216088A
Bovine Serum Albumin (BSA)	Sigma	5482
Clarity western ECL substrate	BioRad	170-5061
Coomassie blue G250	Sigma	B0770
DC Protein Assay Kit	BioRad	500-0112
Digitonin	Santa Cruz Biotechnology	sc-280675
D-Mannitol	Sigma	M4125
DTT	Fisher Scientific	R0861
EDTA	Sigma	EDS
Ferritin	Sigma	F4503
Glacial acetic acid	Sigma	537020
Glass homogeniser	Sigma	D8938
Glycerol	Sigma	G5516
Glycine	Sigma	G8898
Goat-α-mouse HRP	Sigma	A2554
Goat-α-rabbit HRP	Sigma	A0545
Gradient mixer	Fisher Scientific	11544424
HEPES	Sigma	H3375
Immobilon-P polyvinylidene difluoride (PVDF) membrane	Millipore	IPVH00010
Marvel non-fat dry milk powder	Asda	N/A
Methanol	Fisher Scientific	10675112
N,N,N',N'-Tetramethylethylenediamine (TEMED)	Sigma	T9281
NaCl	Sigma	S7653
PMSF	Sigma	93482
Rabbit-α-guinea pig HRP	Dako	P0141
Sucrose	Sigma	S0389
Thyroglobulin	Sigma	T9145
Tricine	Sigma	T0377
Triton X-100	Sigma	X100
Trizma® base (Tris)	Sigma	T1503
Tween 20	Sigma	P1379
ε-amino n-caproic acid	Calbiochem	1381

Table 2. 18 BN-PAGE: antibody list

ETC Complex	Protein name	Antibody Species	Dilution Rate	Vendor	Catalogue Number
CI	NDUFA9	ms	1:1000	abcam	ab14713
CII	SDHA	rb	1:1000	NEB	D6jgm
CIII	UQCRC2	ms	1:1000	abcam	ab14745
CIV	MT-CO1	rb	1:1000	abcam	ab14705
CV	ATP5A	ms	1:50 000	abcam	ab14748
	PDHA	ms	1:1000	abcam	MSP07

2.10 Cell viability measurements

2.10.1 MTT assay following H_2O_2 treatment

Cell viability upon H_2O_2 treatment was measured indirectly by a high-throughput methylthiazolyldiphenyl-tetrazolium bromide (MTT) assay. Human control and NPC1 patient fibroblasts were seeded into a 96-well plate ($0.1x10^4$ cells/well) following subculture of 4 passages in the galactose-based medium. Cell viability was challenged by H_2O_2 addition 48h after seeding. H_2O_2 concentrations are indicated in corresponding figure legends. Following a 2h incubation after H_2O_2 addition, 2.5µg/ml MTT (Sigma, M2128) was added to each well and cells were incubated in the dark at 37°C for additional two hours. After MTT incubation and prior to crystal solubilisation, formazan formation was captured by bright field EVOS xl core microscope (Invitrogen), with a Plan-Apochromat 20x/0.8 M27 air immersion objective, equipped with an Axiocam 503 camera. Formazan crystals were then solubilized by addition of 200µl of 40mM HCl in isopropanol (Sigma, 34863), followed by a 10min shaking incubation at room temperature. Absorbance was read at 570nm. All absorbance values were first corrected with protein concentration values obtained from a duplicate plate and then normalized to an internal control of non H_2O_2 treated cells. Statistical analysis in the form of non-linear regression analysis was carried out on averages of triplicate measurements of 3x control cell lines and 3x NPC1 patient cell lines challenged with several doses of H2O2 as indicated in the figure legend, and on triplicate measurements of a single CTRL and NPC1 cell subcultured in media supplemented with increasing doses of NAM and NMN and challenged with the highest dose of H_2O_2. Non-linear regression analyses were carried on log_2 transformed doses and normalized y-axis values (cell viability) to determine whether cells elicited a dose-response change in cell viability. Non-linear regression analysis was carried out in Graphpad Prism 8 using the log(agonist) vs. normalized response – variable slope

analysis on individual values. Analysis residuals were plotted on quantile-quantile plots to determine whether data meet the assumption of normal distribution and fit the model of dose-response.

2.10.2 Fluorescent dye based cell viability assay

Atg5$^{+/+}$ and *Atg5*$^{-/-}$ MEFs (0.06x10^6 cells/well) were seeded into a 12-well plate. Following a 23h culture in galactose medium, cell viability was assessed using Ready Probes Cell Viability Imaging kit (Fisher Scientific, #R37609) as per company instructions. Briefly, NucBlue Live reagent (Hoechst 33342) and NucGreen Dead reagent (FITC/GFP) were added to the media for 30 min to determine cell viability by counting total vs. dead cells. NucBlue Live reagent stains all cell nuclei, while NucGreen Dead reagent stains only the nuclei of cells with compromised plasma membrane. Cells were imaged on an inverted DM IL LED Leica microscope equipped with an Invenio 3SII digital camera (3.1 Mpix Colour CMOS; DeltaPix). Cell viability was not quantified in this experiment.

2.10.3 Immunoblotting-based cleaved caspase 3 detection

Cell viability was assayed in *Atg5*$^{+/+}$ and *Atg5*$^{-/-}$ MEFs (0.3x10^6 cells/well), *Npc1*$^{+/+}$ and *Npc1*$^{-/-}$ MEFs (0.2x10^6 cells/well), and all CRISPR/Cas9 autophagy-deficient cell lines (0.2x10^6 cells/well). Cells were seeded into 6-well plates and cultured in the galactose-based medium until morphology changes associated with apoptosis were detected (time points varied for different cell lines and are indicated in figure legends). Cells were then imaged on an inverted DM IL LED Leica microscope equipped with an Invenio 3SII digital camera (3.1 Mpix Colour CMOS; DeltaPix) and processed for immunoblotting-based detection of caspase 3 cleavage (discussed in section 2.13)

2.11 Compound treatment rescue of cell death

All cell death rescue treatments were optimized in 6-well culture dishes. *Atg5*$^{+/+}$ and *Atg5*$^{-/-}$ MEFs (0.3x10^6 cells/well), and *Npc1*$^{+/+}$ and *Npc1*$^{-/-}$ MEFs (0.2x10^6 cells/well) were seeded in 6-well plates and switched to the galactose-based medium at 24h post-seeding. Tested compounds (Table 2.19) were mixed into the galactose-based medium prior to the switch. Five to six concentrations were tried of each compound to establish, which concentration is the most effective. Treatment success was initially

confirmed by cell morphology at a 24h (*Atg5*$^{-/-}$) or a 72h (*Npc1*$^{-/-}$) time point and further confirmed by immunoblotting-based detection of lack of caspase 3 cleavage.

Table 2. 19 Compounds used to rescue cell death

Reagent	Manufacturer/ Vendor	Catalogue Number	Solvent	MW	Final Conc.
Z-VAD-fmk	Enzo life sciences	ALX-260-02-M001	DMSO	467.50	20μM
N-Acetyl-L-Cysteine	Sigma	A7250	H_2O	163.19	10mM
MitoQ10	Kindy gifted by Dr Michael Murphy		DMSO	678.81	100nM
S1QEL2.2	Life Chemicals Europe	F2068-0013	DMSO	470.00	500nM
Sodium Pyruvate	Sigma	P2256	H_2O	110.04	10mM
ML385	Sigma	SML1833	DMSO	511.59	5μM
FK866	Sigma	F8557	DMSO	427.97	10nM
Sirtinol	Cambridge Bioscience	CAY10523	DMSO	394.50	20μM
Olaparib		CAY10621-5	DMSO	434.50	10μM
78c	Merck	5.38763	DMSO	413.53	200nM
Nicotinamide	Sigma	72340	H_2O	122.12	varied
β-Nicotinamide Mononuncleotide	Sigma	N3502	H_2O	334.22	varied
Nicotinamide Riboside	Chromadex	14315	H_2O	290.70	5mM
Celecoxib	Kindly gifted by Dr Peter Banks		DMSO	381.37	10μM
Hydroxy celecoxib			DMSO	397.4	2.5μM
Rapamycin	Sigma	R8781	DMSO	915.17	100nM
Lithium Chloride	Sigma	L7026	DMSO	42/39	1mM
H_2O_2	Sigma	H1009	H_2O	34.01	varied

2.12 Immunoblotting

2.12.1 Sample preparation

Cells cultured in 6-well plates were washed in 1x ice-cold PBS and lysed in 50-100μl of RIPA buffer (Sigma) supplemented with 1x Halt complete phosphatase and protease inhibitor cocktail (Fisher Scientific). Following a 20min incubation on ice, cell lysates were centrifuged for 10min at 13 000rpm at 4˚C and the supernatant was transferred into a fresh pre-chilled microcentrifuge tube. Protein content in the supernatant of whole cell lysates was quantified using the DC Protein Assay Kit (BioRad) and a FLUOstar Omega plate reader (BMG Labtech). Samples were prepared to equal concentrations in 2x Laemmli sample buffer (BioRad) supplemented with 5% β-mercaptoethanol (Sigma), boiled at 100°C for 5min and cooled for 10min at RT prior to storage at -80°C.

2.12.2 Immunoblotting

30-40µg of protein from each sample was separated on 10%, 12% or 15% acrylamide Tris-Glycine gels (prepared as mixture of MQH_2O, acrylamide (Severn Biotech), Tris 1.5M pH8.0/Tris 1.0M pH6.8 (Sigma) TEMED (Sigma) and APS (Sigma). Gels were ran in a Tris-Glycine buffer (250mM Trizma® base (Sigma), 1.92M glycine (Sigma), 1% SDS (Fisher Scientific) and transferred onto an Immobilon-P polyvinylidene difluoride membrane (PVDF, Merck Milipore IPVH00010) membrane using Trans-Blot® Semi-Dry transfer set (BioRad) at 17V for 1h in Tris-Glycine buffer (Trizma® base (Sigma), 1.92M glycine (Sigma). Blotted membranes were incubated in a blocking solution (5% skimmed dry milk (Marvel), 0.1% Tween20 (Sigma) in PBS) for 1 hour at RT. The blocking solution was drained and membranes were incubated with primary antibodies (Table 2.21) diluted in blocking solution at 4°C overnight.

Following overnight incubation, the primary antibodies were recovered, and membranes were washed thrice in PBS, PBS-0.1% Tween 20, and PBS for 5min each. Membranes were incubated with the corresponding secondary antibodies conjugated to horseradish peroxidase (HRP) for 1 hour at RT. The following secondary antibodies were used: anti-rabbit HRP (1:5000 Sigma A0545), anti-mouse HRP (1:5000 Sigma A2554), anti-guinea pig (1:5000 Dako Denmark P0141). Membranes were washed thrice in PBS and PBS-0.1% Tween 20, and PBS for 5min each. Clarity western ECL substrate (BioRad) was used to visualise chemiluminescence on LAS4000 (Fujifilm). Quantification of immunoblots was carried out in the ImageJ software (version 1.49) (National Institutes of Health) by measuring raw integrated density of each protein band after background subtraction. Protein levels were normalized to loading controls. Two-tailed unpaired Student's t-test was carried out on the experimental data from at least three independent experiments to establish the significance of observed changes. One immunoblot in this study was generated by Dr Elsje G. Otten (current affiliation at MRC Laboratory for Molecular Biology, Cambridge, Francis Crick Avenue, Cambridge Biomedical Campus, Cambridge, UK).

Table 2. 20 Immunoblotting: reagents

Reagent/Consumable	Manufacturer/Vendor	Catalogue Number
20x PBS	New England Bio	9808
2x Laemmli buffer	BioRad	1610737
30% Acrylamide/Bis-acrylamide	Severn Biotech	20-2100-10
Ammonium persulphate (APS)	Sigma	A3678

Bovine Serum Albumin (BSA)	Sigma	A2153
Clarity western ECL substrate	BioRad	170-5061
DC Protein Assay Kit	BioRad	500-0112
DC Protein Assay Kit	BioRad	500-0112
Empty Gel Cassettes, mini, 1.0 mm	Life Sciences	NC2010
Empty Gel Cassettes, mini, 1.5 mm	Life Sciences	NC2015
Gel loading tips	Starlab	1022 0600
Glycine	Sigma	G8898
Goat-α-mouse HRP	Sigma	A2554
Goat-α-rabbit HRP	Sigma	A0545
Immobilon-P polyvinylidene difluoride (PVDF) membrane	Millipore	IPVH00010
Marvel non-fat dry milk powder	Asda	N/A
Methanol	Fisher Scientific	10284580
N,N,N',N'-Tetramethylethylenediamine (TEMED)	Sigma	T9281
Phosphatase inhibitor cocktail 100X	Fisher Scientific	1861280
Polyoxyethylene sorbitan (Tween-20)	Sigma	93774
Precision Plus Protein™ Dual Colour Standards	BioRad	610374
Rabbit-α-guinea pig HRP	Dako	P0141
RIPA	Sigma	R0278
SDS 20%	Fisher Scientific	10607443
Thick blotting paper	VWR	732-0594
Trizma® base (Tris)	Sigma	T1503
β-mercaptoethanol (β-mE)	Sigma	M3148

Table 2. 21 Immunoblotting: primary antibodies

Protein Identity	Protein name	Antibody Species	Size (kDa)	Dilution Rate	Vendor	Catalogue Number
ETC - CI	NDUFA9	ms	40	1:1000	abcam	ab14713
ETC - CI	NDUFB8	rb	22	1:1000	abcam	ab110242
ETC - CI	NDUFB9	rb	22	1:1000	abcam	ab106699
ETC - CI	NDUFS1	rb	75	1:1000	abcam	ab169540
ETC - CI	NDUFS3	ms	30	1:1000	abcam	ab110246
ETC - CI	NDUFV2	rb	27	1:1000	Proteintech	15301-1-AP
ETC- CII	SDHA	rb	70	1:1000	NEB	D6jgm
ETC- CIII	UQCRC2	ms	49.5	1:1000	abcam	ab14745
ETC- CIV	MT-CO1	rb	57	1:1000	abcam	ab14705
ETC- CV	ATP5A	ms	53	1:50 000	abcam	ab14748
OMM	VDAC	ms	39	1:1000	abcam	ab14734
OMM	TOMM20	ms	16	1:1000	abcam	ab56783
dynamics	OPA1	rb	110	1:1000	abcam	ab42364
dynamics	DRP1	ms	82	1:1000	abcam	ab56788
dynamics	Mfn2	ms	86	1:800	sigma	HPA030554

mito other	NDI1	rb	50	1:1000	Takao Yagi's lab (Scripps Institute, CA)	
oxidation	Prdxn-SO3	rb	26	1:2000	abcam	ab16830
autophagy	ATG5	rb	56	1:1000	Sigma	A0856
autophagy	FIP200 (Rb1cc1)	Rb	200	1:1000	NEB	12436S
autophagy	p62	gp	62	1:1000	Progen	GP62-C
autophagy	LC3B	rb	14-16	1:1000	CST	3868S
loading ctrl	actin	rb	42	1:1000	CST	4967

2.13 Autophagy flux assay

2.13.1 Immunoblot-based measurement

Autophagy flux in *Npc1*$^{+/+}$ and *Npc1*$^{-/-}$ MEFs and human control and NPC1 patient fibroblasts was established in both glucose and galactose-based culture conditions (and treatments) by immunoblotting for LC3-I and LC3-II levels to establish levels of both forms in steady-state, in state of induced autophagy, and state of autophagy block introduced by bafilomycin A1 (BAF A1,Enzo Life Sciences, BML-CM110-0100). First, autophagy flux was established in each cell line relative to its control by comparing basal state of LC3-II levels (upon culture in medium alone) to LC3-II levels upon inhibition of autophagosome degradation by BAF A1 treatment. In MEFs, BAF A1 was mixed with galactose medium to a final concentration of 100nM and added to cells upon medium switch. Cells were then collected and processed for immunoblotting 24h after treatment start. In human fibroblasts, autophagy impairment was first tested upon culture in a glucose-based medium. Control and NPC1 patient fibroblasts ($0.120x10^6$ cells/well) were seeded into 6-well plates, left to grow for 48h. BAF A1 was added directly to cell culture medium in each well to prevent confounding effect by cell re-feeding. Cell were collected and processed for immunoblotting 4h after BAF A1 addition. Autophagy flux upon culture in the galactose-based medium was established after subculture in the medium for 4 passages and following the same protocol as above. In addition, effect of autophagy enhancers and compounds that rescue cell death on autophagy flux was established by co-treatment with BAF A1 and the different compounds in galactose medium in the same conditions as above. All collected samples were processed by immunoblotting as described in section 1.13.

2.13.2 Immunofluorescence-based measurement

Human fibroblasts were seeded on sterile coverslips and cultured in glucose medium. Following 48h culture, cells were fixed and permeabilized in 100% methanol chilled at -20°C for 5min and blocked in normal goat serum/PBS–Tween for 1 h, all at room temperature and incubated with LC3 antibody (1:1000, Cell Signalling Technology, 3868S). Cells were washed and incubated with Alexa Fluor 488 goat anti-rabbit (H+L) antibody (1:1000; Fisher Scientific; A-11008) for 1 h at room temperature. Coverslips were mounted on slides with Prolong Gold antifade reagent with DAPI (Fisher Scientific). Fluorescence images were compiled at room temperature on an Axio observer Z1 microscope (Zeiss), with a Plan-Apochromat 20x/0.8 M27 air immersion objective, equipped with an Axiocam 503 camera. Analysis was performed in ImageJ (version 1.49) (National Institutes of Health) using thresholding and regions of interest to determine numbers of LC3 puncta per cell. Statistical analysis was carried out on triplicate measurements of 5x control cell lines and 2x NPC1 NAI patient cell lines and 3x NPC1 AI patient cell lines by as pair-wise two-tailed unpaired Student's *t*-tests.

Chapter 3. Autophagy deficiency leads to cell death by apoptosis in the context of obligatory mitochondrial respiration.

3.1 Introduction

Accumulation of dysfunctional protein aggregates and organelles is a characteristic feature of aged cells and tissues and is likely to occur as a result of decreased efficiency of cellular catabolism (see section 1.5.1) (Marino and Lopez-Otin, 2004; Cuervo *et al.*, 2005). Genetic autophagy impairment was shown to lead to neurodegeneration, premature ageing phenotypes, aberrations to mitochondrial structure and function, and increased cell death in multiple mouse models (Komatsu *et al.*, 2005; Qu *et al.*, 2007). Cells isolated from mouse models of autophagy deficiency provide an excellent model to study underlying molecular pathology of diseases presenting with an autophagy defect. They also provide a good platform for evaluating efficacy and toxicity of potential therapeutic compounds. However, the relatively brief survival, sensitivity, and the technical difficulty and expense of isolation and culture of primary cells limit their adaptability to high-throughput compound screening (Marroquin *et al.*, 2007). Therefore, tumour- and tissue-derived immortalized cells have become the staple of cell-based drug-discovery efforts (Marroquin *et al.*, 2007). However, most cell culture media have a high glucose content and cells in culture often adapt to this glucose abundance by generating the majority of their ATP via aerobic glycolysis even in the presence of healthy mitochondria and saturating O_2 levels (Ibsen, 1961). This glucose-addiction phenomenon can often disguise underlying mitochondrial defects, and in the context of drug-discovery, mask a compound's effect on mitochondrial bioenergetics and its potential toxicity *in vivo* (Marroquin *et al.*, 2007). Therefore, cell culture in galactose, an alternative carbon substrate that forces cells to respire via OXPHOS due to no net ATP gain from glycolysis, is recommended to circumvent the glucose-addiction phenomenon in cultured cells (Rossignol *et al.*, 2004; Marroquin *et al.*, 2007).

In the first set of experiments, I examined mitochondrial bioenergetics in the context of autophagy abolition in immortalized *Atg5*$^{-/-}$ MEFs cultured in the glucose-based medium. In addition, I focused on optimizing a galactose-based culture for the purpose of revealing potential mitochondrial defects masked by glucose addiction. Upon observations of rapid loss of viability of autophagy deficient cells in galactose media, I

sought to elucidate the underlying mechanism of pathology revealed by enforced mitochondrial respiration.

3.2 Metabolic re-wiring is present in glucose-addicted *Atg5*$^{-/-}$ MEFs

To determine whether a block in autophagy-mediated mitochondrial quality control affects mitochondrial function, I investigated the effect of a genetic autophagy knockout in *Atg5*$^{-/-}$ MEFs by assessing mitochondrial bioenergetics *in vitro*. Two main methods currently employed in intact mitochondria/cells/tissues for the measurement of mitochondrial metabolism are the high-throughput high-sensitivity Seahorse XF Extracellular Flux Analyzer (Seahorse XF, Seahorse Bioscience Inc./Agilent) and low-throughput high-sensitivity Oxygraph-2k respirometry (O2k, Oroboros Instruments) (Ballard, Horan and Pichaud, 2012).

The O2k system is based on real-time measurement of O_2 concentration and consumption as an indirect measurement of ETC function in isolated mitochondria or cells suspended in O_2-saturated medium (Oroboros Instruments, 2019). Manual injection of ETC substrates and inhibitors allows for flexibility in substrate titration assessment of the ETC complex function and mitochondrial membrane integrity (Oroboros Instruments, 2019). In addition to O_2 consumption, the Seahorse XF system is capable of an indirect measurement of metabolic re-wiring to aerobic glycolysis via changes in extracellular pH (Agilent, 2019). Seahorse XF is also advantageous due to lower cell numbers required for a stable measurement and is particularly useful for measurements in cells cultured in monolayers. However, the Seahorse XF system requires extensive optimization and each assay is limited to injection of only four pre-determined compounds. An important technical difference between the O2k and the Seahorse XF systems lies in the cell state during measurement. While in Seahorse XF, adherent cells are analysed in their native state, i.e. adhered to the bottom of a 24-well or 96-well plate, the O2k requires for cells to be analysed in suspension. Both methods were used in my study to determine mitochondrial bioenergetics in *Atg5*$^{+/+}$ and *Atg5*$^{-/-}$ MEFs cultured in glucose-based and galactose-based media.

3.2.1 ATP production via OXPHOS is decreased in Atg5$^{-/-}$ MEFs

Seahorse XF-based analysis of intact cells revealed a significant metabolic re-wiring to ATP generation via glycolysis in the *Atg5*$^{-/-}$ MEFs compared to control (Figure 3.1A). Initially, oxygen consumption rate (OCR) was measured in intact *Atg5*$^{+/+}$ and *Atg5*$^{-/-}$ MEFs by sequential injections of oligomycin (ATPase inhibition, measurement of proton leak), FCCP ((carbonyl cyanide-4-(trifluoromethoxy) phenylhydrazone), stimulates ETC due to IMM permeabilization) and antimycin A (CIII inhibition, induces complete block of oxygen consumption). Data gathered in this experimental set-up allows for identification of basal respiration, ATP production, proton leak, spare respiratory capacity and non-mitochondrial respiration levels (Fig 3.1A). Interestingly, basal respiration rate and the spare respiratory capacity are both reduced in *Atg5*$^{-/-}$ MEFs. Extracellular acidification rate (ECAR) measurement was carried out by sequential addition of oligomycin, FCCP, 2-DG (competitive glucose inhibition, functions to inhibit glycolysis) and antimycin A + rotenone (CIII and CI inhibitors) to establish the proportion of ATP generated via glycolysis based on a method published previously (Figure 3.1B) (Mookerjee *et al.*, 2015). I observed that a greater proportion of ATP was generated by aerobic glycolysis in *Atg5*$^{-/-}$ MEFs and total ATP generation potential seems to be reduced, though not significantly (Fig 3.1C). In addition, increased rate of pyruvate reduction to lactate in *Atg5*$^{-/-}$ MEFs was confirmed by metabolite profiling of cells cultured in glucose medium (Figure 3.1D). Altogether, Seahorse-based measurements in intact cells reveal that *Atg5*$^{-/-}$ MEFs generate less ATP via OXPHOS and rely on glycolytic ATP production to make up for the difference, which indicates an underlying defect in OXPHOS utilization.

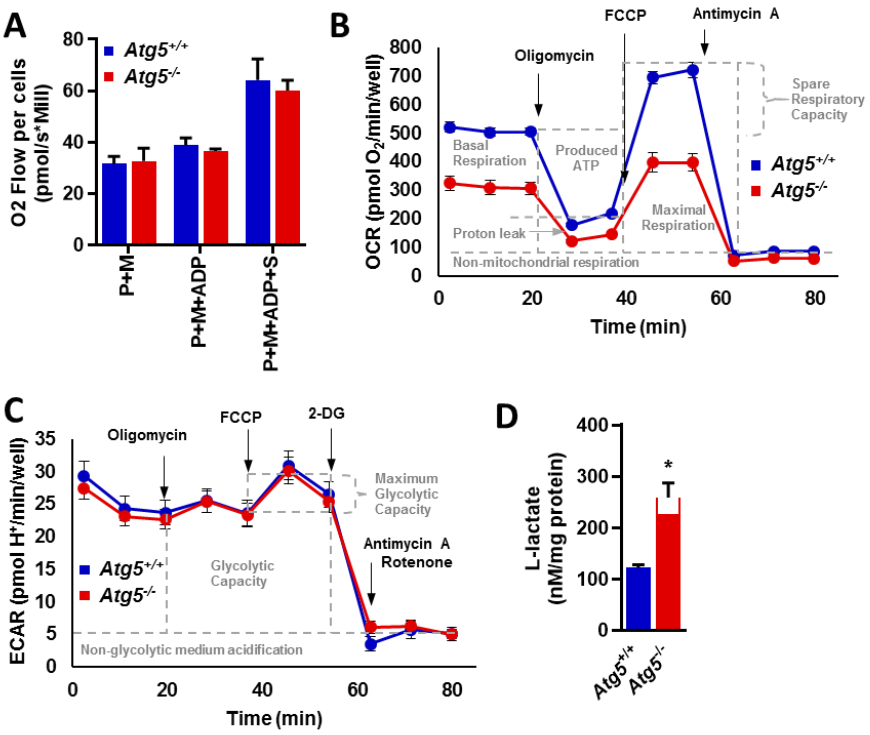

Figure 3. 1 *Atg5*$^{-/-}$ MEFs cultured in glucose-based medium undergo metabolic re-wiring

(A-D) Mitochondrial bioenergetics vary between *Atg5*$^{+/+}$ and *Atg5*$^{-/-}$ MEFs. (A,B) Seahorse analysis of OCR and ECAR were analysed in basal conditions or following additions of oligomycin, FCCP, 2-DG, antimycin A and rotenone as indicated. (C) ATP production calculation was based on Seahorse analysis in *Atg5*$^{+/+}$ and *Atg5*$^{-/-}$ MEFs pre-cultured in glucose-based medium for 20h. (D) Intracellular lactate levels were detected by LC-MS analysis in *Atg5*$^{+/+}$ and *Atg5*$^{-/-}$ MEFs pre-cultured in glucose medium for 20h. Error bars represent S.E.M. *p<0.05 (n=3). Seahorse analyses were carried out in collaboration with by Dr Satomi Miwa. Dr Oliver Maddocks carried out LC-MS sample processing.

3.2.2 ETC alterations in Atg5$^{-/-}$ MEFs cultured in a glucose-based medium

Further Seahorse analysis was performed on permeabilized cells to investigate the nature of mitochondrial dysfunction in *Atg5*$^{-/-}$ MEFs. Addition of CI and CII substrates (pyruvate+malate, and succinate, respectively) allows for distinction of electron flow via CI-CIII-CV SC chains, and CII-CIII-CIV SC chains (Fig 3.2A,B). Similarly to O2k respirometry, permeabilized cells are stimulated to respire by addition of ADP, a complex V substrate (state 3_{ADP}). Subsequent additions of oligomycin (state $4_{oligomycin}$), FCCP (state $3_{uncoupled}$) and antimycin (complete ETC inhibition) allow for mitochondrial CI-/CII-linked function assessment by the respiratory control ratio (RCR), a product of state 3 division by state 4. RCR indicates the coupling between respiration (O_2 consumption) and ADP phosphorylation to ATP (Brand and Nicholls, 2011). Coupling of CI-linked e^- flow to ATP production is significantly reduced in *Atg5*$^{-/-}$ MEFs. Thus, Seahorse XF analysis in permeabilized adherent cells uncovered an underlying defect of e^- flux through CI of the ETC and, perhaps, a compensatory increase in the CII-linked respiration in *Atg5*$^{-/-}$ MEFs (Fig 3.2C).

Additionally, *Atg5*$^{-/-}$ MEFs present with a significant downregulation of nuclear-encoded CI matrix subunits (Ndufb8, Ndufs3, Ndufa9 and Ndufv2) when cultured in glucose medium (Figure 3.2D,E). Levels of other mitochondrial ETC complex subunits and a control OMM protein (Mfn2) remain unchanged (Figure 3.2D). The Ndufv2 and Ndufs3 proteins are subunits of matrix CI N and Q modules, respectively, while the Ndufa9 protein acts as a supernumerary subunit of the Q module (Sánchez-Caballero, Guerrero-Castillo and Nijtmans, 2016; Zhu, Vinothkumar and Hirst, 2016) (Figure 3.2E).

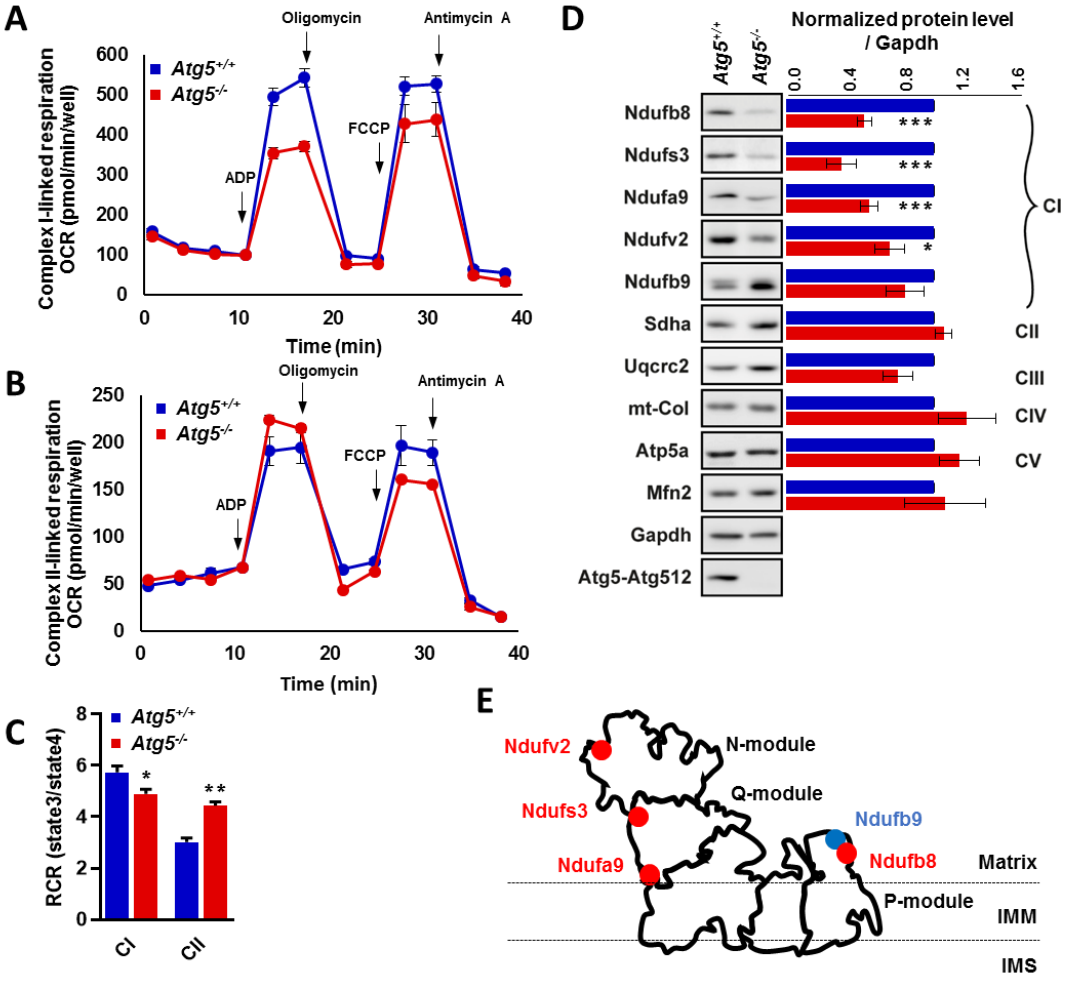

Figure 3. 2 Functional and structural CI deficiency is observed in *Atg5*$^{-/-}$ MEFs

(A-C) CI-linked mitochondrial bioenergetics are altered in *Atg5*$^{-/-}$ MEFs. Seahorse analysis of OCR was carried out in permeabilized cells cultured in CI (PM) (A) or CII (S) (B) based media. OCR measurements occurred in basal conditions or following additions of oligomycin, FCCP, 2-DG, antimycin A and rotenone as indicated. (D) Representative immunoblots and quantification of CI-CV complex subunits in *Atg5*$^{+/+}$ and *Atg5*$^{-/-}$ MEFs cultured in a glucose-based medium. (E) Graphic representation of CI of the ETC and the predicted location of probed significantly reduced (red) and non-reduced (blue) subunits. Error bars represent S.E.M. *p<0.05, **p<0.01 ***p<0.001 (n=3). Seahorse analyses were carried out in collaboration with Dr Satomi Miwa.

Importantly, all three subunits are located in the matrix region of CI involved in NADH oxidation and their downregulation in autophagy deficient cells could reflect a loss of the matrix arm. Little is known about the function and location of the most significantly affected subunit of CI, the Ndufb8 protein. It has been assigned as a supernumerary subunit of the membrane P module (Sánchez-Caballero, Guerrero-Castillo and Nijtmans, 2016; Zhu, Vinothkumar and Hirst, 2016), and some literature fails to mention the subunit altogether (Elurbe and Huynen, 2016). It is perhaps a loose association with the complex that hampers Ndufb8 assignment and detection of localisation in CI, as well as its pronounced loss in the autophagy deficient cells. The reason for stability of the Ndufb9 subunit levels, as opposed to other probed CI subunits remains unclear. Although the role of the accessory Ndufb9 subunit in CI is unknown, its involvement in CI Fe-S cluster assembly has been suggested and recent findings predict that due to its location at the distal end of the membrane arm, and its conservation across species, Ndufb9 may be involved in CI-CIII interaction and SC assembly (Gu *et al.*, 2016). Altogether, by studying mitochondrial bioenergetics, I uncovered lower capacity of CI-linked OCR and downregulation of some nDNA-encoded CI matrix subunits in *Atg5*$^{-/-}$ MEFs. Despite my observations, *Atg5*$^{-/-}$ MEFs retain their viability and proliferative capacity when cultured in glucose-based medium.

3.3 Mitochondrial dysfunction in *Atg5*$^{-/-}$ MEFs leads to apoptotic cell death

It was previously observed that galactose-based culture not only reveals drug toxicity (Marroquin *et al.*, 2007), but also leads to loss of cell viability in cells suffering from severe defects in oxidative phosphorylation (Robinson *et al.*, 1992). Based on the data obtained previously, I hypothesized that reduced mitochondrial quality control in autophagy deficiency would result in mitochondrial dysfunction, which may be masked by glucose addiction. To test this hypothesis, I cultured *Atg5*$^{+/+}$ and *Atg5*$^{-/-}$ MEFs in glucose- and galactose-based media and monitored the effect of autophagy impairment on cell viability. Furthermore, I assessed SC assembly, and ROS production in both media to examine whether CI-linked dysfunction is an artefact of glucose addiction, or persists upon cell culture in the galactose-based medium.

3.3.1 Cell culture in a galactose-based medium forces cells to rely on OXPHOS

The dependency of *Atg5*$^{+/+}$ and *Atg5*$^{-/-}$ MEFs respiration on OXPHOS in galactose medium was first confirmed by supplementation of glucose and galactose growth media with rotenone (CI inhibitor) and antimycin A (CIII inhibitor). Supplementation with either of the inhibitors resulted in rapid cell death in cells cultured in a galactose-based medium, but had no effect on cells in glucose culture (Figure 3.3A). Additionally, metabolite profiling revealed a significant reduction of lactate levels in both cell types when cultured in a galactose-based medium, when compared to culture in glucose-based medium (Figure 3.3B). Lastly, a switch of *Atg5*$^{+/+}$ and *Atg5*$^{-/-}$ MEFs to the galactose-based medium results in increased levels of electron transport chain (ETC) subunits (confirmed by increase of mRNA levels, data not shown) (Figure 3.3C). I have thus confirmed that cell culture in galactose-based media promotes cellular dependency on OXPHOS and time-dependent increase in ETC subunit expression.

3.3.2 ETC functional defects revealed upon culture of Atg5$^{-/-}$ *MEFs in galactose-based medium*

To examine whether increased ETC subunit expression affects ETC complex and SC structure I carried out qualitative BN-PAGE analysis on mitochondrial fractions isolated from *Atg5*$^{+/+}$ and *Atg5*$^{-/-}$ MEFs after 20h culture in glucose- and galactose-based media. Samples solubilised in digitonin (Dig; SC analysis) or triton X-100 (TX-100; individual complex analysis) were resolved on a gradient polyacrylamide gel and immunoblotted with an anti-Ndufa9 antibody to detect CI (Figure 3.4A) (Lazarou *et al.*, 2007). First, levels of CI holocomplex detected in TX-100 solubilized samples did not vary between *Atg5*$^{+/+}$ and *Atg5*$^{-/-}$ MEFs in either culture media. Second, assembly of CI into SCs was detected in dig-solubilised samples by the presence of a high molecular weight bands corresponding to CI-$CIII_2$-CIV_n SCs. In these conditions, all of CI species were detected in high-order SC assembly. This finding is not surprising as it was previously reported that functional CI assembly depends on its association with a $CIII_2$, and it is thus expected that in a healthy scenario, mitochondria will only contain functional CI within the SC structure (Schägger *et al.*, 2004; Moreno-Lastres *et al.*, 2012).

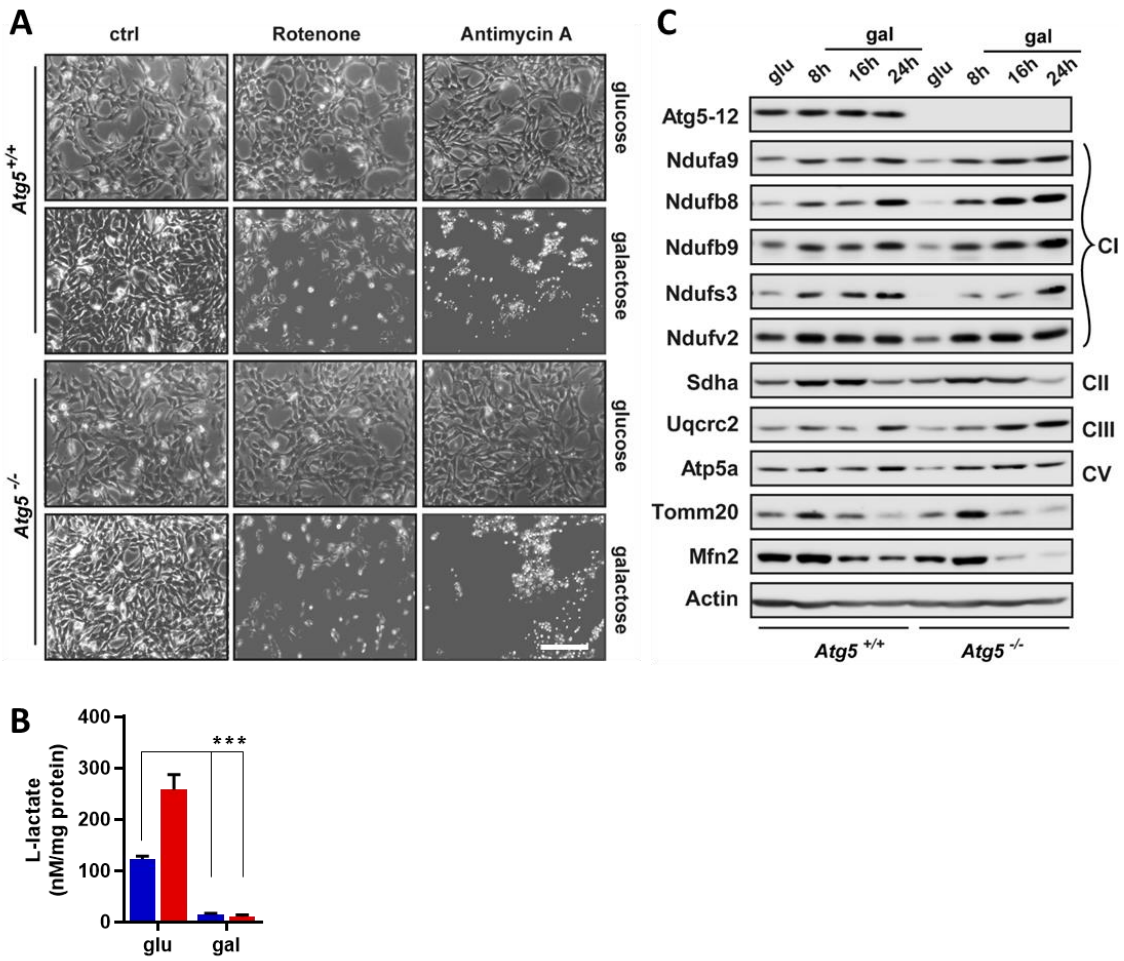

Figure 3. 3 Cell culture in galactose-based medium forces cells to rely on OXPHOS

(A) Bright field microscopy images of *Atg5*$^{+/+}$ and *Atg5*$^{-/-}$ MEFs cultured in glucose or galactose-based media only or supplemented with 1μM rotenone, or 40μM antimycin A were imaged after 3 hours of treatment. (n=1). (B) Intracellular lactate levels were detected by LC-MS analysis in *Atg5*$^{+/+}$ and *Atg5*$^{-/-}$ MEFs pre-cultured in glucose-based or galactose-based medium for 20h. (n=3). (C) Representative western blots of Atg5-Atg12 conjugate; CI subunits: Ndufa9, Ndufb8, Ndufb9, Ndufs3 and Ndufv2; CII subunit Sdha; CIII subunit Uqcrc2; ATP synthase subunit Atp5a and OMM membrane protein Mfn2 and Tomm20 in *Atg5*$^{+/+}$ and *Atg5*$^{-/-}$ MEFs switched to galactose-based medium. Scale bar represents 200μm. Error bars represent S.E.M. ***p<0.001 (n=3). Dr Oliver Maddocks carried out LC-MS sample processing. Western blot data was generated by Dr Elsje G. Otten.

In contrast, a subset of $CIII_2$ remained free of SC assembly (Figure 3.4B). Solubilisation of mitochondria by both, dig and TX-100, led to appearance of same size bands of CII in all four conditions, which indicates that CII does not to participate in SC assembly in galactose fed cells (3.4B). No gross differences between levels of individual complexes or SCs were detected between samples from *Atg5*$^{+/+}$ and *Atg5*$^{-/-}$ MEFs, from which I conclude that no aberrant SC assembly or complex structural defects are present. Interestingly, increased levels of high molecular weight species corresponding to $CI+CIII_2+CIV_n$ SCs were detected in cells upon culture in the galactose-based medium (Figure 3.4A).

Following analysis of ETC complex structure, I focused on analysis of its function. Cells cultured in galactose-based medium were analysed by Seahorse XF Analyser and O2k respirometry methods to assess ETC functionality linked to O_2 consumption and its coupling to ATP generation. In contrast to the respirometry measurement upon cell pre-culture in glucose-based medium, addition of CI substrates to oxygraph medium revealed a significantly lower rate of O_2 reduction in *Atg5*$^{-/-}$ MEFs compared to *Atg5*$^{+/+}$ MEFs (Figure 3.4C). This reduced capacity for O_2 reduction persisted upon addition of CII substrate. In addition, Seahorse-based analysis revealed a lower potential of non-permeabilized *Atg5*$^{-/-}$ MEFs to generate ATP via OXPHOS (Figure 3.4C). Altogether, these results confirm the presence of a mitochondrial defect, pertaining to the ETC, in *Atg5*$^{-/-}$ MEFs. Noteworthy is the lack of glycolysis-mediated ATP production in either cell line, further confirming that cell culture in the galactose-based medium provides a good model to study OXPHOS.

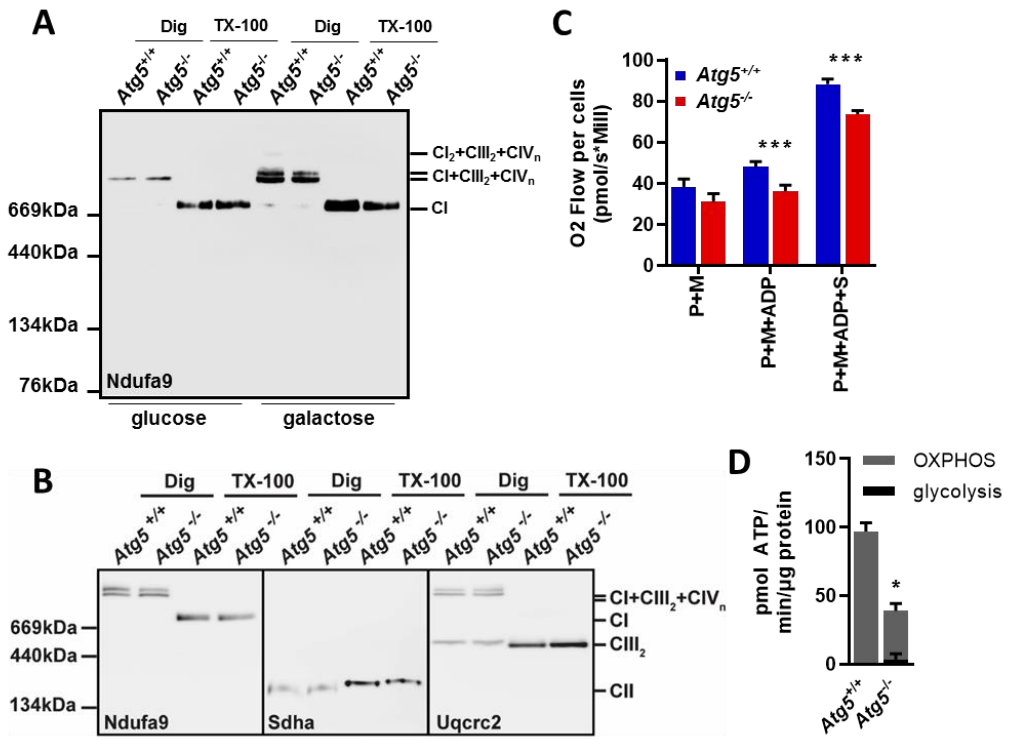

Figure 3. 4 Culture in galactose-based medium leads to changes in mitochondrial bioenergetics without affecting ETC complex assembly

(A-B) ETC holocomplex and SC levels and structure are not altered in *Atg5*$^{-/-}$ MEFs pre-cultured for 20h in glucose- or galactose-based media. (A) BN-PAGE immunoblots of CI (Ndufa9) holocomplexes solubilised in 1µM triton X-100 (TX-100), or SCs solubilised in 0.8µM digitonin (dig). (B) BN-PAGE immunoblots of CI (Ndufa9), CII (Sdha) and CIII (Uqcrc2) holocomplexes solubilised in 1µM triton X-100 (TX-100), or SCs solubilised in 0.8µM digitonin (dig). (C) Respirometry analysis was carried out by sequential additions of CI substrates pyruvate and malate (PM), ADP, and a CII substrate succinate (S) into suspension of 1 million cells permeabilized with digitonin and pre-cultured in galactose-based medium for 20h. (C) ATP production calculation was based on Seahorse analysis in *Atg5*$^{+/+}$ and *Atg5*$^{-/-}$ MEFs pre-cultured in glucose-based medium for 20h. Error bars represent S.E.M. *p<0.05, ***p<0.001 (n=3). Seahorse and respirometry analyses were carried out in collaboration with Dr. Satomi Miwa and Prof Alberto Sanz, respectively.

3.3.3 Galactose culture of MEFs results in increased ROS production and loss of mMP

I further hypothesised that loss of autophagic clearance of dysfunctional mitochondria would lead to high levels of electron leakage from the ETC and increased ROS generation. Release of ROS was examined by staining cells with MitoSOX Red, a mitochondria-targeted superoxide-sensitive dye. MitoSOX-based staining revealed higher levels of mitochondrial superoxide generation in autophagy deficient *Atg5*$^{-/-}$ MEFs cultured in glucose medium, which, increased further upon a switch and culture in galactose medium (Figure 3.5A,B). As expected by increased dependency of ATP generation on OXPHOS, superoxide levels increased in both cell lines upon culture in the galactose-based medium. Cellular oxidative damage load in *Atg5*$^{-/-}$ MEFs was examined by western blot analysis of hyperoxidized peroxiredoxin (peroxiredoxin-SO3 (Prdx-SO3)), an enzyme involved in the antioxidant system, subjected to an irreversible inactivation due to increased oxidative stress (Woo *et al.*, 2003). Compared to controls, *Atg5*$^{-/-}$ MEFs lysates contain significantly higher levels of the inactive peroxiredoxin form in glucose medium that, similarly to MitoSOX signal, increase in both cell lines upon culture in galactose medium (Figure 3.5C).

mMP maintenance relies on CI/CIII/CIV-dependent H^+ pumping across the IMM initiated by e^- flow through the complexes (Ramsay, 2019). I hypothesized that decreased reduction of O_2 (Figure 3.4B) combined with increased e^- leak (Figure 3.5A,B) in my model are likely to contribute to IMM depolarization. Measurement of mMP was carried out in live cells *in situ*. Tetramethylrhodamine methyl ester (TMRM), a slow cationic dye used for steady state mMP measurement, was co-loaded into cells with non-potential dependent MitoTracker green (MTG) (Dalle Pezze *et al.*, 2014). Confirming my hypothesis, analysis of the ratio of TMRM to MTG per cell revealed IMM depolarisation in *Atg5*$^{-/-}$ MEFs cultured in galactose-based medium. No significant difference was observed between the two cell lines when cultured in glucose-based medium (representative images not shown) (Figure 3.5E).

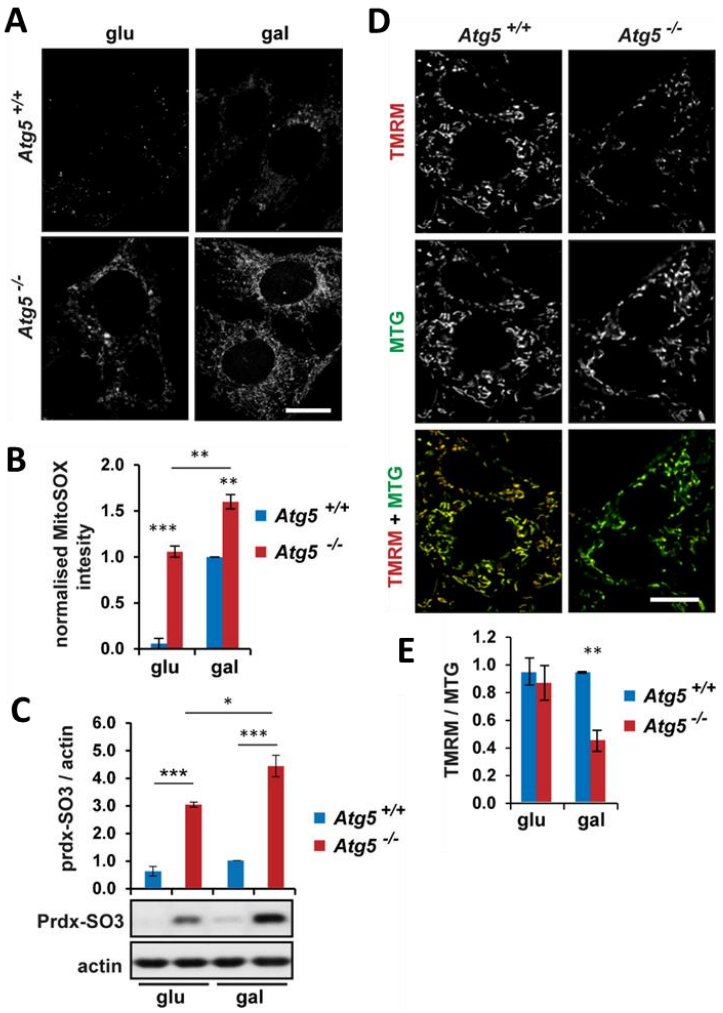

Figure 3. 5 Culture in galactose-based medium leads to increased ROS levels in *Atg5*$^{-/-}$ MEFs

(A-C) ROS load is increased in *Atg5*$^{-/-}$ MEFs. (A) Representative images of MitoSOX fluorescence of *Atg5*$^{+/+}$ and *Atg5*$^{-/-}$ MEFs cultured for 22h in glucose- and galactose-based media. (B) Quantitation of MitoSOX intensity in the same conditions as (A). (C) Representative western blots and quantitation of peroxiredoxin-SO3 (Prdx-SO3) levels of *Atg5*$^{+/+}$ and *Atg5*$^{-/-}$ MEFs cultured in glucose and galactose-based media. Prdx-SO3 levels were normalised to actin. (D) Representative immunofluorescence images of dual stained cells with TMRM and MTG upon culture in galactose-based medium. (E) Quantitation of TMRM:MTG ratio in the same conditions as (D). Scale bars represent 20μm. Error bars represent S.E.M., *p<0.05, **p<0.01, ***p < 0.001 (n=3).

3.3.4 Culture in galactose-based medium leads to apoptotic cell death of Atg5$^{-/-}$ MEFs.

Importantly, a switch to and subsequent culture of *Atg5*$^{-/-}$ MEFs in galactose led to increased levels of cell death, defined by morphological changes and cell detachment, and observed by bright field microscopy (Figure 3.6A). Higher level of cell death of *Atg5*$^{-/-}$ MEFs in galactose medium was further confirmed by a cell viability assay (Figure 3.6B). Levels of apoptosis and autophagy deficiency were probed by western blot analysis and significantly increased levels of caspase 3 cleavage, a marker of apoptosis, were observed in *Atg5*$^{-/-}$ MEFs compared to *Atg5*$^{+/+}$ MEFs (Figure 3.6C). In addition, *Atg5*$^{-/-}$ MEFs were transduced with a human GFP-ATG5 fusion construct to rule out the possibility that clonal differences are the cause of the difference of cell death levels between *Atg5*$^{+/+}$ and *Atg5*$^{-/-}$ MEFs. Reintroduction of ATG5 into *Atg5*$^{-/-}$ MEFs resulted in complete rescue of cell death upon culture in galactose medium (Figure 3.6C). Furthermore, an autophagy defect in *Atg5*$^{-/-}$ MEFs, and autophagy reconstitution in *Atg5*$^{-/-}$+GFP-ATG5 MEFs was confirmed by the absence of LC3-I to LC3-II processing; and by increased levels of an autophagy receptor and substrate p62 and rescue of LC3 processing, respectively (Figure 3.6C). Finally, Z-VAD-fluoromethylketone (Z-VAD-fmk) a cell membrane permeable pan-caspase inhibitor, is traditionally used to confirm the apoptotic mode of cell death via inhibition of caspase activity. Culture supplementation with Z-VAD-fmk added to media after 20h of culture led to increased *Atg5*$^{-/-}$ MEFs cell viability, as observed by bright field microscopy (Figure 3.6D), despite the detection of increased levels of caspase 3 cleavage (Figure 3.6E). In my model, Z-VAD-fmk does not prevent caspase 3 cleavage, but rather seems to prevent its downstream activity, thus preventing cell death signalling. Increased survival of cells *Atg5*$^{-/-}$ MEFs in medium supplemented with Z-VAD-fmk thus supports my hypothesis that cells cultured in galactose medium die via apoptosis.

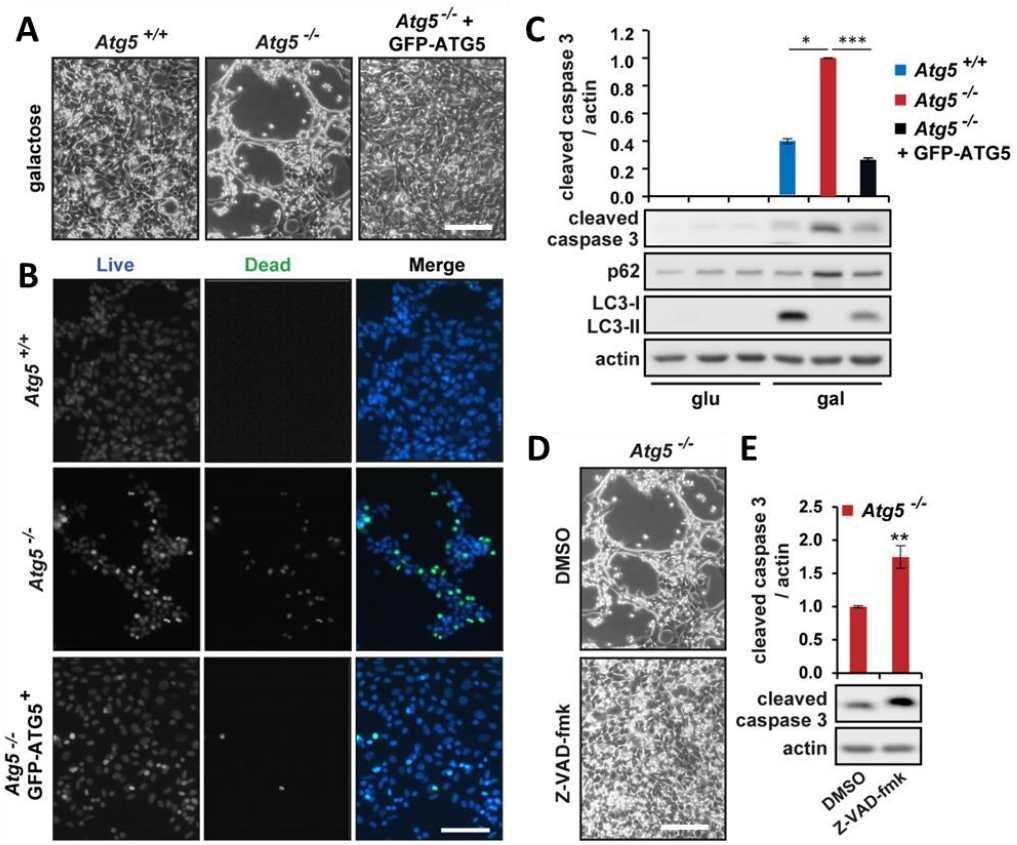

Figure 3. 6 Enforcing mitochondrial respiration in autophagy deficient cells leads to cell death

(A) Bright field microscopy images of *Atg5*$^{+/+}$ and *Atg5*$^{-/-}$ MEFs switched to galactose-based medium upon 24h of culture. (B) Cell death of *Atg5*$^{-/-}$ MEFs cultured in galactose medium was further confirmed by ReadyProbes fluorescent dyes in the same condition as (A). (C) Representative western blot and quantitation of cell death marker, cleaved caspase 3; and of autophagy markers p62 and LC3, in *Atg5*$^{+/+}$, *Atg5*$^{-/-}$, *Atg5*$^{-/-}$ stably expressing GFP-ATG5 MEFs cultured in glucose and galactose-based media for 24h. (D) Bright field microscopy images of *Atg5*$^{-/-}$ MEFs cultured in galactose-based medium only or supplemented with Z-VAD-fmk (20μM; added to culture medium at 20h). Cells were imaged after 24h in culture. (E) Quantitation of caspase 3 cleavage in the same conditions as (D) Cleaved caspase 3 levels were normalised to actin. Error bars represent S.E.M. Scale bar represents 200μm. ***p<0.001 (n=3).

3.3.5 Multiple model cell lines of autophagy-deficiency die an apoptotic cell death upon culture in a galactose-based medium.

To test whether apoptotic cell death in galactose medium is specific to the loss of the Atg5 protein I utilised the CRISPR/Cas9 system to generate multiple autophagy-deficient cell lines. Atg5, Atg7 and Rb1cc1 (FIP200) are proteins involved in early stages of the autophagy pathway (Figure 1.2) and their loss results in autophagy impairment and neurodegeneration (Komatsu *et al.*, 2005; Hara *et al.*, 2008; Liang *et al.*, 2010). The success of a gene knockout was confirmed upon single clone expansion by testing for an autophagy defect by western blot analysis of LC3 lipidation status and p62 protein levels (data not shown). Subsequent prolonged culture of *Atg5*$^{-/-}$, *Atg7*$^{-/-}$ and *Rb1cc1*$^{-/-}$ MEFs in galactose-based medium, but not in glucose-based medium, resulted in apoptotic cell death observed by bright field microscopy (Figure 3.7A) and confirmed by analysing cleaved caspase 3 levels by western blotting (Figure 3.7B). I conclude that apoptotic cell death in galactose media is a general phenotype of autophagy deficient cells.

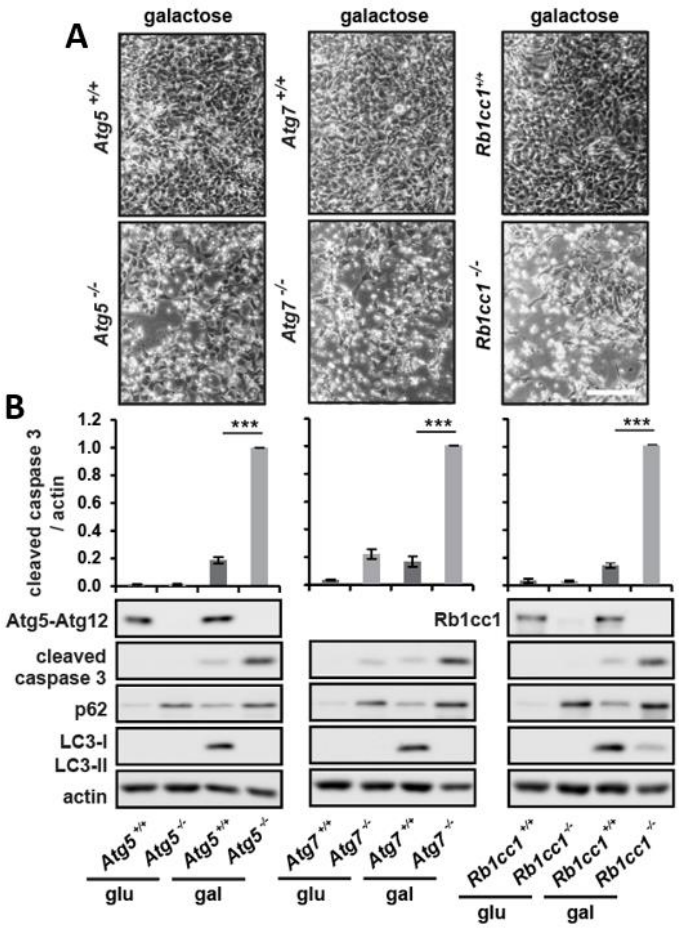

Figure 3. 7 Enforced OXPHOS leads to apoptotic cell death in multiple autophagy knockout models

(A) Bright field microscopy images of *Atg5*$^{-/-}$, *Atg7*$^{-/-}$ and *Rb1cc1*$^{-/-}$ MEFs and corresponding control cell lines cultured in galactose medium for 110h. (B) Representative western blot of targeted proteins Atg5-Atg12 conjugate and Rb1cc1, autophagy markers p62 and LC3, and an apoptosis marker, cleaved caspase 3, in *Atg5*$^{-/-}$, *Atg7*$^{-/-}$ and *Rb1cc1*$^{-/-}$ MEFs in the same conditions as (A). Scale bar represents 200μm. Error bars represent S.E.M. Cleaved caspase 3 levels were normalised to actin levels. ***p<0.001. (n=3).

3.4 Chapter Conclusions

Experimental results presented in this chapter characterize the degree to which mitochondrial bioenergetics depend on functional autophagy. I first observed that genetic interruption of autophagy leads to compromised mitochondrial bioenergetics (Figure 3.1A,B) accompanied by metabolic re-wiring towards aerobic glycolysis (Figure 3.1B,C). A more detailed assessment of mitochondrial ability to channel e^- via CI-$CIII_2$-CIV or CII- $CIII_2$-CIV routes revealed dysfunction in CI-linked respiration (Figure 3.2A-C) accompanied by a striking loss of CI core and accessory matrix-arm subunits encoded in nDNA (Figure 3.2D). CI modules that form the matrix arm, the N (NADH oxidation) and Q (ubiquinone reduction) modules, harbour the FMN cofactor and a series of Fe-S clusters necessary for e^- liberation from NADH, and e^- channelling along the Fe-S clusters to the ubiquinone binding site (Giachin *et al.*, 2016; Sánchez-Caballero, Guerrero-Castillo and Nijtmans, 2016). Current models of CI assembly propose that addition of the N-module constitutes the last step immediately prior to assembly factor removal and initiation of CI catalytic activity (Sánchez-Caballero, Guerrero-Castillo and Nijtmans, 2016). Thus, loss of CI matrix arm in dysfunctional mitochondria could lead to the loss of CI activity and a defect in mitochondrial energetics. However, structural analysis of CI assembly and incorporation into SCs did not reveal any gross aberrations (Figure 3.4A). Further information is required to characterize the true extent of ETC defect in glucose-cultured cells. A proteomics-based study of ETC complexes from isolated mitochondria would build on my findings of whole-cell CI subunit depletion, while a BN-PAGE based study of in-gel activity of ETC complexes would inform about CI and SC ability to reduce substrate *in situ*. Further study of the causes of subunit depletion, i.e. reduced expression or increased degradation, would improve my understanding of the underlying molecular mechanism of isolated CI deficiency in glucose-cultured autophagy deficient cells. However, the relevance of my findings to a physiological scenario, excluding cancer, is questionable. It is quite possible that my observations of isolated CI deficiency in *Atg5*$^{-/-}$ MEFs are artefacts of glucose addiction and merely reflect an adaptation to a larger mitochondrial defect, which is masked by cell culture in a glucose-based medium.

I therefore switched glucose-cultured *Atg5*$^{+/+}$ and *Atg5*$^{-/-}$ MEFs into a galactose-based medium to force cells to depend on mitochondria to maintain cellular bioenergetics and thus reflect a more physiologically relevant scenario. I first confirmed that galactose-based culture increased cellular dependency on OXPHOS-based ATP production by

testing cell sensitivity to mitochondrial toxins and by measuring cellular lactate levels (Figure 3.3 A,B). Remarkably, I observed rapid changes of cellular morphology 22h after media switch followed by apoptotic cell death of *Atg5*$^{-/-}$ MEFs at 24h (Figure 3.6). Studies of ETC structure upon cell culture medium switch revealed a time-dependent increase of all ETC subunits (Figure 3.3C) and increased SC formation (Figure 3.4A,B) in both cell lines. However, the lack of a structural defect in *Atg5*$^{-/-}$ MEFs was not indicative of ETC functionality. Study of mitochondrial bioenergetics revealed a decrease in what appears to be CI-linked respiration coupling to O_2 consumption (Figure 3.4C), lower potential for ATP generation (Figure 3.4D), and increased ROS production (Figure 3.5A,B) in *Atg5*$^{-/-}$ MEFs. Altogether, the ETC dysfunction and increased e^- leakage correlate with the loss of mMP prior to cell death (Figure 3.5D,E). In summary, cell culture in galactose-based media led to identification of a defect in mitochondrial bioenergetics and loss of cell viability. Results from the glucose- and galactose-based studies lead us to hypothesize that the defect is ETC specific, likely linked to increased CI expression upon-galactose culture and a result of loss coupling of CI-mediated e^- entry to O_2 reduction to H_2O at CIV. These results suggest that increased dependency on mitochondrial respiration (i.e. in neurons) can be damaging to cells deficient in autophagy and mitochondria might provide an exciting target for therapies downstream of autophagy dysfunction.

3.5 Chapter Discussion

3.5.1 Implications of increased ROS production on CI activity

CI is the largest and most intricate complex of the ETC composed of 44 discrete proteins. CI subunit expression, mitochondrial import, assembly and degradation are multifactorial and subject to multiple forms of quality control (Karunadharma *et al.*, 2015; Giachin *et al.*, 2016; Zhu, Vinothkumar and Hirst, 2016). Recent LC-MS based analysis of ETC subunit longevity revealed a difference in the half-lives of ETC complex subunits (Karunadharma *et al.*, 2015). The most persistent difference was identified between mtDNA and nDNA-encoded subunits, likely due to the fact that mtDNA encoded subunits are hydrophobic membrane proteins that encode the core of ETC complexes and largely rely on autophagy for their recycling (Vincow *et al.*, 2013; Johnston and Williams, 2016). Subunits encoded in the nucleus had a 14% shorter half-life irrespective of their localization to the membrane- or matrix-resident ETC modules. As expected, subunits docked to the IMM via their transmembrane helices

that form the membrane-bound modules of ETC complexes had, on average, lower turnover rates than their matrix-facing and matrix-resident counterparts (Karunadharma *et al.*, 2015). Of most interest to my study was the observation that subunits of the CI matrix arm and membrane-bound accessory subunits undergo faster turnover than the core CI members, perhaps due to their proximity to damaging ROS/RNS species. In fact, mitochondrial matrix proteases Lon and caseinolytic peptidase proteolytic subunit (ClpP) were found to associate with, and degrade the subunits of CI matrix arm and several membrane-bound peptides upon IMM depolarization and increased ROS release (Pryde, Taanman and Schapira, 2016). The subunits that had undergone degradation in this study (NDUFA9, NDUFB8, NDUFS1, NDUFS2 and NDUFV2) largely overlap with those tested in my study (NDUFA9, NDUFB8, NDUFS3, NDUFV2). The overlap between the two studies suggests that the loss of CI subunits upon culture of *Atg5*$^{-/-}$ MEFs in a glucose-based medium could be a reflection of an attempt to mitigate the potential harmful consequences of CI dysfunction. Interestingly, the loss of nDNA encoded CI subunits was not reflected as a loss of CI complex when analysed by BN-PAGE. This could reflect the lower sensitivity of the BN-PAGE method or the nature of CI assembly, whereby a selective loss of the CI matrix arm may not impede its incorporation in SCs (Schägger *et al.*, 2004; Moreno-Lastres *et al.*, 2012).

CI is one of the major sites of ROS release *in vivo* and is itself susceptible to ROS/RNS-induced inactivation (Clementi *et al.*, 1998; Brown and Borutaite, 2004; Hurd *et al.*, 2008; Ryan *et al.*, 2012). Although initially proposed as a system for CI dysfunction (reviewed in (Brown and Borutaite, 2004)), the FMN molecule and Fe-S co-factors in ETC complexes were reported to be resistant to modification by oxidative and nitrosative stresses (Pearce *et al.*, 2005). Instead, ROS/RNS-mediated inhibition is likely mediated by PTM of the individual complex subunits (Ryan *et al.*, 2012). Four ROS/RNS-associated PTMs of CI subunits were identified as S-glutathionylation, S-nitrosation, tyrosine nitration and carbonylation (Chithra and Bharath, 2019). Although several CI subunits are targets of the latter two PTMs, the impact of subunit carbonylation and nitration on CI function remains unknown (Chithra and Bharath, 2019). S-glutathionylation is a spontaneous and reversible adduct formation between a cysteine thiol group and oxidised glutathione (GSSG) (Fratelli *et al.*, 2002). Two CI subunits, NDUFS1 and NDUFV1, are susceptible to S-glutathionylation upon mitochondrial incubation with GSSG or oxidative and nitrosative species (Taylor *et al.*,

2003). Investigation of the effect of subunit S-glutathionylation revealed an increase in ROS production and inhibition of CI activity (Taylor *et al.*, 2003).

S-nitrosation was first reported to reversibly inhibit CI in macrophages (Clementi *et al.*, 1998). Further study of CI S-nitrosation identified a single CI subunit, ND3, that is modified by this PTM (Galkin and Moncada, 2007; Galkin *et al.*, 2008). ND3 is a core CI mtDNA-encoded subunit that contains a cysteine-39 residue in an unstructured loop that is only exposed to the matrix when CI adopts a de-active state (Galkin *et al.*, 2008). Interestingly, it was previously described that only the de-active state of CI, adopted due to loss of substrate or O_2, is susceptible to functional inhibition by S-nitrosation (Galkin and Moncada, 2007). Interestingly, CI conformation changes and activity state do not affect its association with SCs and therefore cannot be detected by a BN-PAGE analysis (Babot *et al.*, 2014). Altogether, these studies led to the identification of a potential mechanism of CI inactivation and a therapeutic target that has been further explored in models of ischaemia-reperfusion (I/R) injury, and in the design of pathogenesis-activated therapeutics (Chouchani *et al.*, 2013; Methner *et al.*, 2014; Galkin and Moncada, 2017). Furthermore, although regulated enzyme-assisted S-nitrosation is reversible upon challenge by the cellular detoxification enzymes, CI is also susceptible to irreversible modifications by $ONOO^-$ species (Galkin and Moncada, 2007). Implications of this research highlight that the perfect storm of shortage of mitochondrial substrate and increased load of ROS/RNS can lead to an irreversible CI inactivation and pathology. Having identified a CI-linked dysfunction and increased release of ·O2 in my models, it would be interesting to explore the range of ROS/RNS-mediated PTMs of CI to establish whether the reduced CI activity I observed is linked to increased ROS load and pathological CI deactivation.

3.5.2 CI-linked dysfunction in autophagy deficiency – relevance to the ageing field

Accumulation of dysfunctional mitochondria and harmful increase in ROS have long been assumed to contribute to the general ageing phenotype and to the pathogenesis of age-related, particularly neurodegenerative disorders. Some of these assumptions stem from reports of the pathology of mitochondrial disease (MD), otherwise known as mitochondrial energy generation disorders (Frazier, Thorburn and Compton, 2019). MD is clinically diverse, and heterogeneous in terms of mode of inheritance, disease onset and tissue specificity (Frazier, Thorburn and Compton, 2019). Mutations in a

total of almost 300 mtDNA and nDNA genes have been linked to MD, ranging from genes that have a direct impact on mitochondrial energetics to those with a wider impact on mitochondrial homeostasis and general cellular metabolism (Frazier, Thorburn and Compton, 2019).

CI deficiency is the most commonly observed cause of MD (Smeitink, van den Heuvel and DiMauro, 2001; Scheffler, 2015). To date, pathogenic mutations were identified in genes encoding the core subunits of the complex (14/14), accessory subunits (13/30) and CI assembly factors (11/15) (Frazier, Thorburn and Compton, 2019). Of utmost importance is a finding that despite the intense progress in identification of pathogenic mutations that result in CI deficiency, the disease-causing mutation of over 50% of patients presenting with a CI defect has not been identified (Scheffler, 2015). Apart from genetic mutations, it is worth considering that oxidative and non-oxidative PTM-mediated modulation of CI activity could be at play (Chithra and Bharath, 2019; Gowthami *et al.*, 2019). Decreased levels and activity of CI have, amongst other mitochondrial defects, been reported from models of healthy ageing (Bowling *et al.*, 1993; Petrosillo *et al.*, 2008), disease-relevant models and patient tissues suffering from cardiovascular disease (Cabré *et al.*, 2017; Forte *et al.*, 2019), PD (Greenamyre *et al.*, 2001), and AD (Fukuyama *et al.*, 1996; Aksenov *et al.*, 1999; Rhein *et al.*, 2009). It has long been assumed that loss of CI activity in these tissues underlie some, if not all, of the pathology. However, recent findings from fly (Scialò *et al.*, 2016), fish (Baumgart *et al.*, 2016) and mouse models (Zhang *et al.*, 2015) challenge these assumptions, for long-term mild CI-inhibition leads to increased lifespan in the fly and fish models and improved cognition in an AD mouse model. Moreover a recent detailed characterization of brain pathology in a PD patient cohort confirmed that CI-deficiency occurs in all regions of the PD brain and does not correlate with mtDNA-damage, or α-synuclein aggregation in the substantia nigra (Flønes *et al.*, 2018). In fact, less α-synuclein aggregation was observed in neurons with the most prominent CI-deficiency. These ground-breaking studies reflect my results from glucose-cultured cells where CI levels and activity are reduced in autophagy-deficiency. In addition, I have shown that forcing mitochondrial respiration in these conditions promotes ROS release and cell death. Together, these results suggest that a decline in CI levels and activity may be deliberate, protective and merely a consequence of age-related mitochondrial or autophagy dysfunction.

3.5.3 Study limitation

One major limitation of this study is the lack of information about cellular mitochondrial mass. Logically, loss of autophagy-mediated whole-organelle clearance could result in accumulation of dysfunctional mitochondria that would alter cellular bioenergetics and release excessive amount of ROS species. Alternatively, increased mitochondrial recycling via non-autophagy dependent MDV budding could maintain a stable pool of organelles. However, the experimental evidence to support either of these assumptions is lacking and inconsistent, mainly due to the variability of mitochondrial markers utilized to measure mitochondrial content (addressed below). Establishment of mitochondrial mass in my model cell lines would help us ascertain the true extent of mitochondrial dysfunction and answer the underlying question of whether dysfunction in *Atg5*$^{-/-}$ MEFs arises as a consequence of an accumulation of a small population of damaging non-recycled dysfunctional mitochondria (if mitochondrial mass increases), or a more widespread dysfunction of the majority of organelles (if no increase is detected). Measurement of mitochondrial mass could also alter my interpretation of results obtained by respiratory analyses and ROS measurement. Finally, the underlying cause of mitochondrial dysfunction, ROS release, mMP dissipation, their correlation/causation relationships to cell death, and their potential as therapeutic targets are further explored in Chapter 4.

Chapter 4. Autophagy deficiency promotes NAD(H) nucleotide imbalance

4.1 Introduction

Two functions of autophagy are crucial for cellular physiology. Firstly, maintenance of a healthy pool of cellular organelles and proteins protects cells from dysfunction and developing disease-related pathologies (Labbadia and Morimoto, 2015). Secondly, liberated pools of carbohydrates, lipids, nucleotides and amino acids act as anabolic substrates for biosynthesis and cellular growth or undergo catabolic processing for energy generation or gluconeogenesis. Thus they directly impact upon cellular energy generation and glucose oxidation pathways (Rabinowitz and White, 2010).

Several directions of study have focused on the role of autophagy-mediated nutrient liberation in sustaining cellular metabolism. Recent studies from the White laboratory reveal a substantial metabolic re-wiring in autophagy deficient cancer cells, which likely occurs to support nucleotide synthesis and sustain oxidative metabolism for maintenance of growth. First, pulse-chase studies with isotope-labelled carbon and nitrogen atoms in amino acids and in glucose identified autophagy as a pathway central to glucose and energy metabolism in starved tumour cells (Guo *et al.*, 2016). Second, the group identified that supplementation of starved *BRaf V600E/+* tumour-derived cells with TCA cycle precursors (sodium pyruvate or glutamine) prevent starvation induced loss of viability (Strohecker *et al.*, 2013). Further supporting their findings from a cellular model, the critical role of autophagy in cancer promotion comes from a study of a conditional whole-body *Atg7* knockout in a mouse model of KRas-driven lung cancer (Karsli-Uzunbas *et al.*, 2014) . Despite an observation that the mice suffered from a shortened lifespan due to increased susceptibility to infection and early-onset neurodegeneration, the growth and development of pre-existing tumours was severely stunted and authors detected appearance of cells positive for caspase 3 activation, suggesting an altered tumour cell fate when substrates provided by autophagy-mediated recycling are no longer available.

Outside the realm of cancer biology, the role of autophagy in cellular metabolism was recently explored in the control of immune cell differentiation and activation (reviewed in (O'Neill, Kishton and Rathmell, 2016; Riffelmacher, Richter and Simon, 2018).

Briefly, the multiple roles of autophagy in differentiation and activation of immune cells include mitochondrial depletion to promote aerobic glycolysis and thus push cells into a state of high proliferation prior to differentiation; breakdown of lipid droplets to release free fatty acids to sustain fatty acid oxidation; and degradation of cargo destined for externalization on the plasma membrane. In addition, autophagy seems to be critical for the maintenance of a quiescent state of hematopoietic stem cells (HSCs) and 'stemness' in old HSCs by the clearance of active mitochondria (Ho *et al.*, 2017), though the mechanism of clearance was not explored in this study.

Although it is now clear that autophagy is necessary for rapid metabolic reprogramming during periods of starvation, activation of immune cells or prolonged proliferation in cancer, it is unclear how autophagy impairment affects cellular homeostasis in non-starvation conditions, and cellular function upon the change of an energy substrate. I focused the experiments outlined in this chapter on exploring how autophagy impairment influences cellular metabolism in my model with a specific interest in the spatial interaction of the two aspects of autophagy function, the functional and metabolic, and how they converge on cell survival.

4.2 Autophagy deficiency leads to NADH and NAD+ depletion

4.2.1 Identification of NAD(H) nucleotide imbalance in Atg5$^{-/-}$ MEFs

To elucidate the upstream mechanism of mitochondrial bioenergetic dysfunction and cell death in *Atg5*$^{-/-}$ MEFs, I carried out targeted metabolic profiling, focusing on investigations of pathways involved in glucose metabolism and OXPHOS, namely glycolysis, the PPP and the TCA cycle. Additionally, amino acid and nucleotide levels were probed to determine the impact of autophagy deficiency on the levels of metabolic substrates and the cellular energy charge (Rabinowitz and White, 2010; De la Fuente *et al.*, 2014; Guo *et al.*, 2016). Cells cultured in the galactose-based medium were subjected to metabolite extraction 16h after medium switch, consistent with mitochondrial bioenergetics measurement timeframe and well before any apoptosis-related morphological changes can be observed by bright-field microscopy and while no caspase 3 cleavage can be detected by western blotting (not shown).

Mass peak data output of the metabolomics study was first corrected to cellular protein levels and then subjected to statistical analysis by MetaboAnalyst 4.0. To determine

the relatedness, or lack thereof, between *Atg5*$^{+/+}$ and *Atg5*$^{-/-}$ MEFs I employed a principal component analysis (PCA), a form of multivariate statistical analysis. The nature of PCA predisposes the result to bias towards highly abundant variables (H. Yamamoto *et al.*, 2014), and indeed, analysis of data that did not undergo any degree of normalization led to separation of the most abundant metabolites (Figure 4.1A,B). Thus, the variables were first normalized by auto-scaling (mean-centred and divided by SD of each variable) by the MetaboAnalyst platform (Appendix 1) and then subjected to the PCA analysis. A scatter plot of PC score vectors (observations plot) revealed separate clusters of autophagy-efficient and autophagy-deficient MEFs thus strongly suggesting that autophagy deficiency promotes a distinguishable change in a cell's metabolic profile (Fig 4.1C). I then evaluated a scatter plot of the corresponding factor loading to discern which metabolites contribute to the separation of the two groups (Fig 4.1D), identifying a group of metabolites consisting mostly of nucleotides and a separate group of pentose phosphate pathway intermediates.

Furthermore, I carried out univariate statistical testing to determine which metabolites varied significantly between the two cell lines. A volcano plot was assembled to demonstrate the most significantly changing metabolites determined by the Student's *t*-test with *p* value corrected with false discovery rate (FDR), coupled with *Atg5*$^{-/-}$ / *Atg5*$^{+/+}$ fold change of each metabolite (Figure 4.2A). By plotting the magnitude of change against the measure of statistical significance, I identified NADH as the most significantly depleted metabolite in *Atg5*$^{-/-}$ MEFs. In contrast, glucose-6-phosphate was the only significantly enriched metabolite that met the cut-off criteria of the volcano plot. A full list of 'discovered' metabolites, i.e. those with adjusted *p* values low enough to ensure that no more than 1% of these discoveries are false positives (Q=1%) was determined using the original FDR method of Benjamini and Hochberg (Figure 4.2B). The method analyses each metabolite individually without assuming a consistent SD (Fig 4.2B).

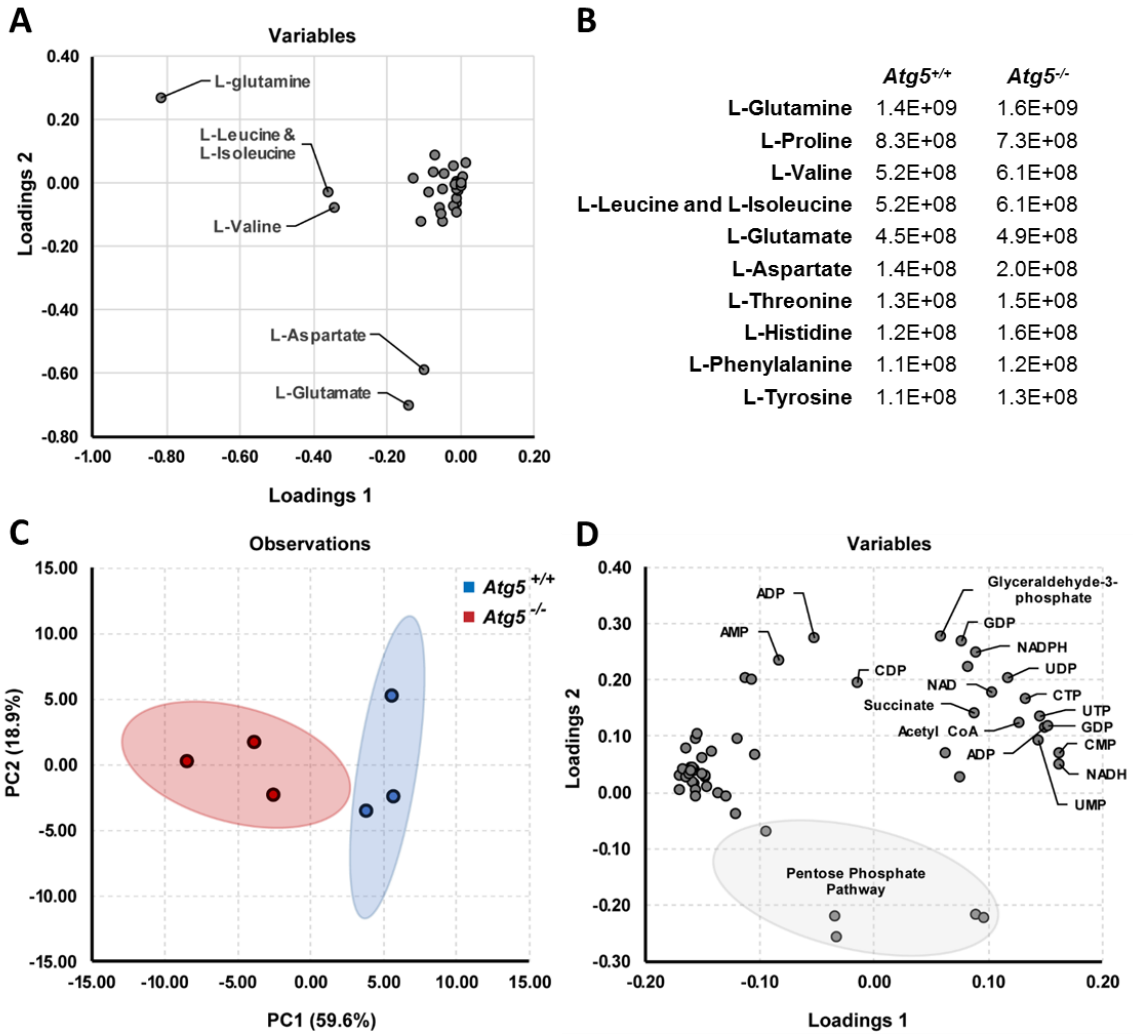

	Atg5$^{+/+}$	*Atg5*$^{-/-}$
L-Glutamine	1.4E+09	1.6E+09
L-Proline	8.3E+08	7.3E+08
L-Valine	5.2E+08	6.1E+08
L-Leucine and L-Isoleucine	5.2E+08	6.1E+08
L-Glutamate	4.5E+08	4.9E+08
L-Aspartate	1.4E+08	2.0E+08
L-Threonine	1.3E+08	1.5E+08
L-Histidine	1.2E+08	1.6E+08
L-Phenylalanine	1.1E+08	1.2E+08
L-Tyrosine	1.1E+08	1.3E+08

Figure 4. 1 Multivariate analysis of metabolic data from *Atg5*$^{+/+}$ and *Atg5*$^{-/-}$ MEFs

(A) PCA loadings plot of non-scaled data. (B) List of top 10 most abundant metabolites in *Atg5*$^{+/+}$ *and Atg5*$^{-/-}$ MEFs. (C) PCA scores plot based on auto-scaled data. (D) PCA loadings plot based on auto-scaled data.

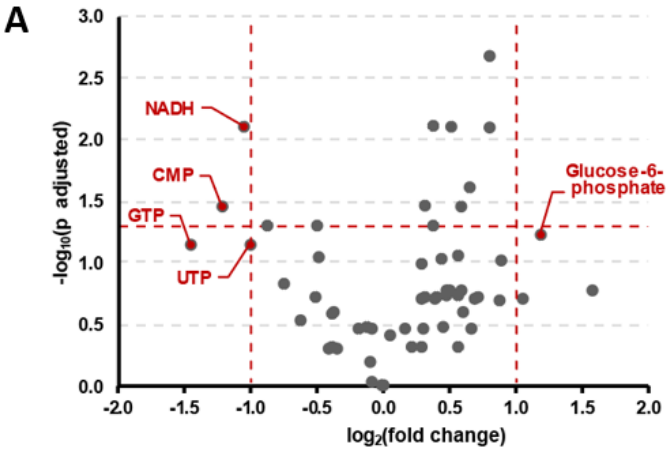

B

	FC	p.ajusted
NADH	0.4792	0.0077
CMP	0.4293	0.0336
Glucose 6-phosphate	2.2699	0.0572
GTP	0.3656	0.0691
UTP	0.4958	0.0691

Figure 4. 2 Univariate analysis of metabolic data from *Atg5*$^{+/+}$ and *Atg5*$^{-/-}$ MEFs

(A) Volcano plot representation of all analysed metabolites in a pairwise comparison of *Atg5*$^{+/+}$ *and Atg5*$^{-/-}$ MEFs. The data were plotted as log2 fold change versus –log10 of the FDR adjusted p-value. The significance cut-off was set to an FDR adjusted p-value of 0.05 (-log10 (adjusted p value) > 1,3). Fold change significance cut-off was set at a two-fold change (-1 ≥ log2 (fold change) ≥ 1). Thresholds are shown as dashed red lines. 'Discovered' metabolites identified by univariate analysis are labelled in red. (B) A full list of 'discovered' metabolites. FC – fold change.

Log2 conversion of metabolite concentration averages was performed and compared between the *Atg5*$^{+/+}$ and *Atg5*$^{-/-}$ MEFs to visualise the fold change and statistical significance change of each metabolite in a heatmap (Figure 4.3). This type of visualisation corroborates the findings of the unbiased and unsupervised analysis performed in the MetaboAnalyst, but in addition informs about the overall state of all intermediates of a given pathway. Many intermediates of glucose oxidation pathways of glycolysis and the TCA cycle vary significantly between the two cell lines (Figure 4.3A). However, there is a lack of an overall change in one direction, thus the pathways look largely unperturbed. In contrast, the intermediates of the PPP and levels of many amino acids are significantly increased in *Atg5*$^{-/-}$ MEFs (Figure 4.3A,B). Nonetheless, it is difficult to infer the biological significance of this finding without a time course data. The lack of depletion in amino acid levels in my model is likely due to the fact that only macroautophagy is expected to be impaired in *Atg5*$^{-/-}$ MEFs and CMA or microautophagy could contribute to amino acid replenishment (Tasset and Cuervo, 2016).

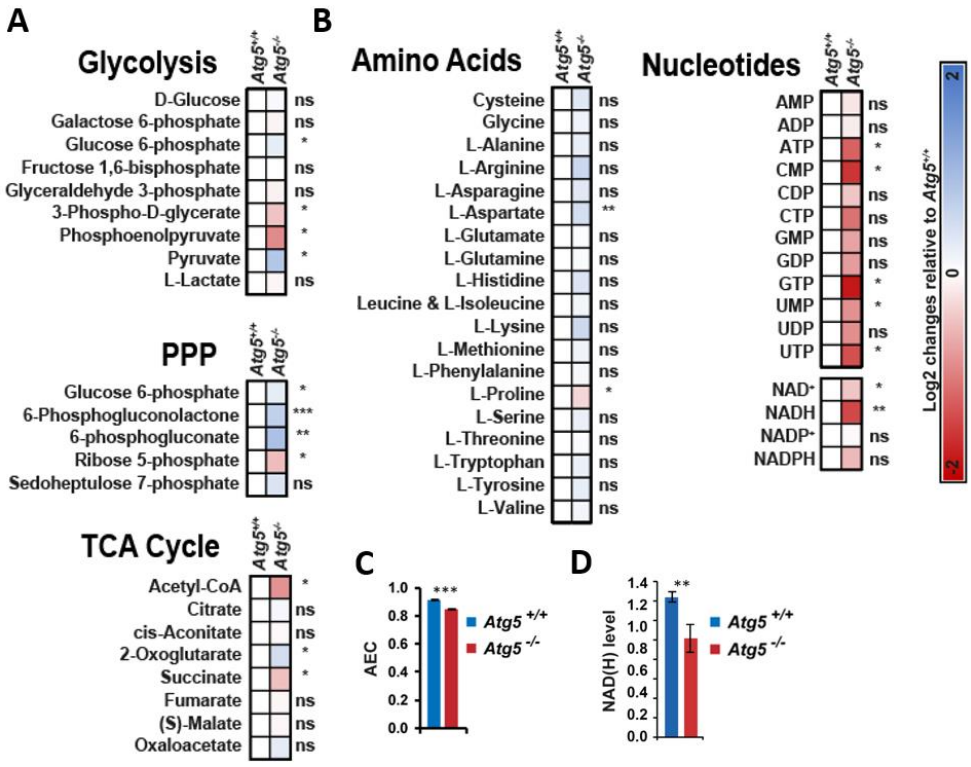

Figure 4. 3 Pathway-identity-based depiction of metabolomics data from *Atg5*$^{+/+}$ and *Atg5*$^{-/-}$ MEFs

(A,B) Metabolite profiling in *Atg5*$^{+/+}$ and *Atg5*$^{-/-}$ MEFs. Metabolites are depicted as a heatmap of log2(FC) of *Atg5*$^{-/-}$ MEFs to *Atg5*$^{+/+}$. (A) Metabolite organization is based on their association to glucose oxidation pathways of glycolysis, pentose phosphate pathway (PPP) and tricarboxylic acid (TCA) cycle. (B) Amino acids are organized alphabetically. Nucleotide order is first alphabetical and depends on the energy charge they carry. (C) Pooled NAD^+ and NADH levels. (D) Adenylate energy charge (AEC) AEC=(ATP + 0.5 ADP)/(ATP + ADP + AMP). Error bars represent S.E.M. *** $p < 0.001$. Dr Oliver Maddocks carried out LC-MS sample processing.

In addition, cells are cultured in an excess of amino acids, thus a lack of recycling might not have a significant impact on intracellular amino acid levels. It does not appear as if the flux through the PPP is impaired. In contrast, the relative increase of 6-phosphogluconolactone and 6-phosphogluconate suggest an increased re-direction of glucose-6-phosphate from glycolysis to the oxidative phase of PPP, which serves to reduce $NADP^+$ to NADPH and promote ROS detoxification and anabolism (Hanschmann *et al.*, 2013). The lack of increase in ribose-5-phosphate relative to the other PPP intermediates could be relevant. Ribose-5-phosphate is the bridge between the oxidative and non-oxidative phases of the PPP and serves as a precursor for the nucleotide and amino acid synthesis (Hove-Jensen *et al.*, 2017). Following that train of thought, the most negatively affected cluster of metabolites in *Atg5*$^{-/-}$ MEFs is the nucleotide pool (Figure 4.3B). Perhaps unsurprisingly, I observed a significant decrease in ATP levels and a corresponding, though not significant, increases in ADP and AMP. Interestingly, adenylate energy charge (AEC) calculated as a proxy to cellular metabolic energy status first described by Atkinson and Walton (Atkinson and Walton, 1967) although significantly different between the two cell lines, did not deviate from what is considered the normal interval (0.7 and 0.95) (Fig 4.3C) (De la Fuente *et al.*, 2014).

Unexpectedly, both NAD^+ and NADH, were significantly reduced. Total NAD levels, expressed as a sum of NAD^+ and NADH (expressed as (NAD(H)), is also reduced (Figure 4.3D). A limitation of my approach is that the metabolic profiling analysis was carried out on whole cell lysates, so NADH depletion could occur in any cellular compartment. However, if considered in the context with my membrane potential measurement in *Atg5*$^{-/-}$ MEFs (Figure 3.5), it is likely that at least a portion of the NADH depletion occurs in mitochondria. Due to the relevance of NADH to mitochondrial function and the recently described relevance of NAD^+ depletion to ageing, I selected NAD^+ metabolism the corresponding pathways for further study.

4.2.2 Causal role of NAD metabolism in galactose-induced cell death

Identification of NAD(H) as the most significantly depleted metabolite in *Atg5*$^{-/-}$ MEFs focused my research on the role of NAD^+ and its reduced form, NADH in the cell. Redox imbalance and the decrease of total NAD levels led us to question whether

NAD^+ depletion plays a role in cell death. To interrogate this hypothesis, I focused on the main pathway of NAD^+ synthesis in cells, the NAD^+ salvage pathway. As discussed previously (section 1.4.4), NAMPT is the rate-limiting enzyme of the NAM branch of NAD^+ salvage pathway (Fig 4.4A). A potent inhibitor of NAMPT, an FK866 compound, identified in an anti-tumour drug screen, was found to decrease levels of NAM conversion by approximately 97% compared to control (Hasmann and Schemainda, 2003; Khan, Tao and Tong, 2006). Furthermore, a respirometry study on pre-treated permeabilized cells showed FK866 reduced CI-linked O_2 consumption but did not have an effect on activity of other ETC complexes. In this study, FK866 treatment slowed down cellular proliferation and metabolism and led to apoptotic cell death (Hasmann and Schemainda, 2003). Although multiple pathways lead to NAD^+ biosynthesis in cells, I tested whether inhibition of NAMPT by FK866 and the resulting depletion of NAD^+ would be sufficient to initiate cell death in wild type MEFs cultured in galactose-based medium and thus phenocopy the defect in *Atg5*$^{-/-}$ MEFs. Indeed, supplementation of galactose medium with FK866 led to exacerbation of caspase 3 cleavage in *Atg5*$^{+/+}$ MEFs upon prolonged (48h) culture, thus confirming that NAD^+ depletion may play a role in the cell death of *Atg5*$^{-/-}$ MEFs cultured in a galactose-based medium (Figure 4.4B,C). It is also worthwhile to note that NAMPT inhibition was not detrimental to the survival of *Atg5*$^{+/+}$ MEFs cultured in a glucose-based medium and thus seems to affect only cells which are actively respiring.

I further focused on the role of mitochondria-specific NADH depletion. By transiently transfecting *Atg5*$^{-/-}$ MEFs with a non-proton translocating single-subunit NADH–ubiquinone reductase from *Saccharomyces cerevisiae* (Ndi1) I expected to see amelioration of the cell death phenotype (Seo *et al.*, 2000). *NDI1* expression in a *Drosophila* model was previously shown to rescue of CI KD lethality by effectively by-passing CI and donating e^- directly to the ubiquinone pool (Sanz *et al.*, 2010). Based on my findings of decreased CI function (Figure 3.1A,B) I hypothesized that increased e^- flow to the ETC would lead to increased cell survival. To my surprise, Ndi1 expression in my model led to further cell death exacerbation (Figure 4.4D,E). A logical, but initially overlooked, explanation of this unexpected result springs to mind. The presence of Ndi1 in my system is likely to contribute to faster mitochondrial NADH turnover to NAD^+. However, due to the lack of proton-pumping associated with Ndi1 function, lower $\Delta\Psi$ per molecule of NADH would be expected, thus further contributing to loss of mMP.

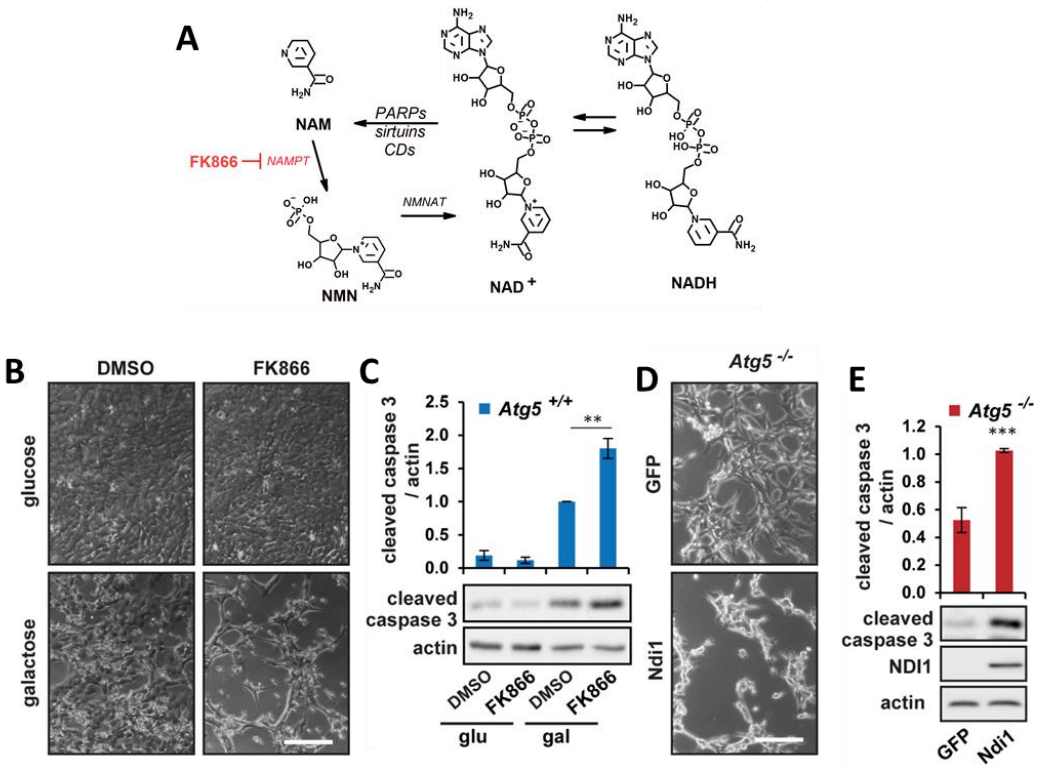

Figure 4. 4 Exploration of NADH depletion causality in apoptosis

(A) Graphic representation of the NAM branch of NAD salvage pathway. In red: the rate-limiting enzyme of the NAM branch NAMPT and its inhibitor, FK866. (B) Bright field microscopy images of *Atg5*$^{+/+}$ MEFs cultured in glucose or galactose-based media supplemented with 10nM FK866 or vehicle (DMSO). Cells were imaged 48h after medium switch and treatment start when we observed morphological changes associated with apoptosis. (C) Representative western blot and quantification of cleaved caspase 3 levels in the same conditions. (D) Bright field microscopy images of *Atg5*$^{-/-}$ MEFs transiently expressing GFP-NDI1 (NDI1) or GFP after 18h culture in a galactose-based medium. (E) Representative western blot and quantification of cleaved caspase 3 and NDI1 levels in the same conditions as (D). Scale bar represents 200µm. Error bars represent S.E.M. Cleaved caspase 3 levels were normalised to actin. **p<0.01, ***p<0.001, (n=3).

4.3 NAD nucleotide-boosting strategies promote *Atg5*$^{-/-}$ MEFs survival

4.3.1 Inhibition of NADases

Having established the role of NAD(H) depletion in cell death causation, I next aimed to confirm that boosting NAD^+ levels is sufficient to rescue cell death in my models. Current exploration into pharmacologically boosting NAD^+ levels in the field of aging focuses on three approaches – NAD^+ precursor supplementation, inhibition of NADases and activation of NAD^+ biosynthesis by targeting the activity of a rate-limiting NAMPT enzyme (Rajman, Chwalek and Sinclair, 2018). Of the three approaches, I chose to explore supplementing cell culture medium with NAD^+ precursors and inhibiting NAD^+ consuming enzymes.

To investigate whether NAD depletion occurs as a result of increased activity of cellular NADases, I treated *Atg5*$^{-/-}$ MEFs with inhibitors against the major classes of NADases, SIRTs, PARPs, and CD38 (Fig 4.5A) (Rajman, Chwalek and Sinclair, 2018). I based the selection of inhibitors used in this study on their described efficiency and ability to inhibit the largest number of family members (Murai *et al.*, 2012; Villalba and Alcaín, 2012). Supplementation of galactose-based medium with olaparib (PARPs), sirtinol (SIRTs) or 78c (CD38) led to the rescue of cell death of *Atg5*$^{-/-}$ MEFs (Figure 4.5B,C). These results have several implications to consider. Firstly, I hypothesize that all of these interventions would result in a boost of NAD^+ levels due to its reduced cleavage as a co-substrate, but cannot rule out off-target effects without a direct NAD^+ measurement and/or directly measuring levels of enzyme activity. Secondly, I can conclude that the function of any of these enzymes is likely not necessary for cellular survival in these conditions.

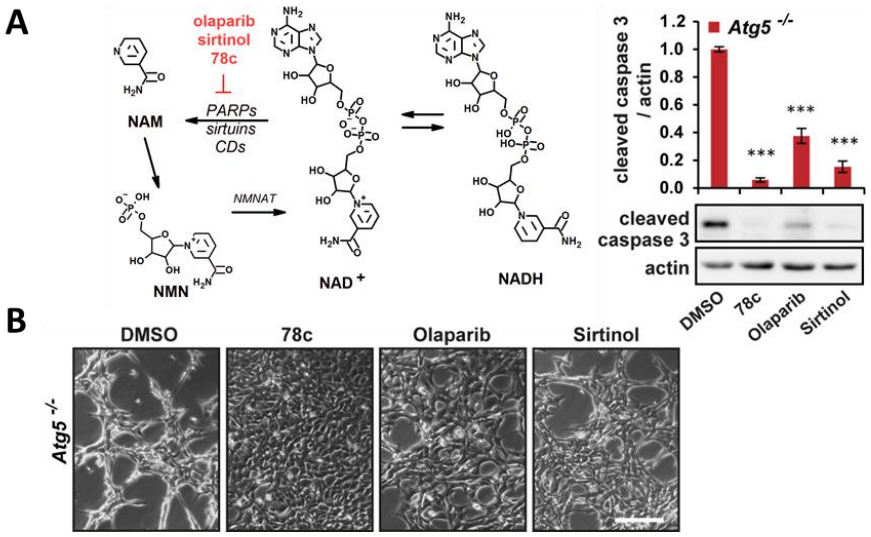

Figure 4. 5 NADase inhibition rescues viability of *Atg5*$^{-/-}$ MEFs

(A) Graphical representation of the NAM branch of NAD$^+$ salvage pathway. In red: inhibitors of PARPs, SIRTs and CD38 used in this study. (B) Bright field microscopy images of *Atg5*$^{-/-}$ MEFs cultured in a galactose-based medium supplemented with 100µM 78c, 10µM olaparib, 20µM sirtinol or vehicle (DMSO). Cells were imaged 24h after medium switch and start of the treatment. (C) Representative western blot and quantification of cleaved caspase 3 levels in the same conditions as (B) Scale bar represents 200µm. Error bars represent S.E.M. Cleaved caspase 3 levels were normalised to actin levels. ***p<0.001. (n=3).

4.3.2 Supplementation of NAD$^+$-salvage pathway precursors

In the second line of investigation, I chose to supplement galactose-based medium with two NAD$^+$ precursors NAM and NR, which enter the NAD$^+$ salvage pathway through two separate branches and are converted into NMN (Fig 4.6A). NAM and NR supplementation have the highest potential of translational application for age-related chronic diseases and are both currently explored in over 50 clinical trials (https://clinicaltrials.gov/). Medium supplementation with each of the two precursors led to a robust rescue of cell survival and proliferation of *Atg5*$^{-/-}$ MEFs (Fig 4.6B,C).

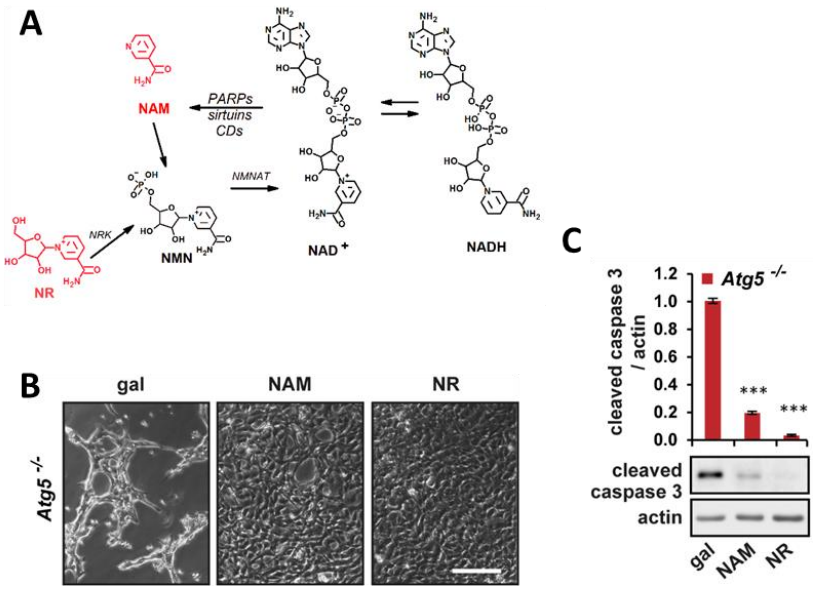

Figure 4. 6 NAD precursor supplementation rescues viability of *Atg5*$^{-/-}$ MEFs

(A) Graphical representation of the NAM and NR branches of NAD^+ salvage pathway. In red: NAM and NR precursor molecules. (B) Bright field microscopy images of *Atg5*$^{-/-}$ MEFs cultured in a galactose-based medium supplemented with 5mM NAM or 5mM NR. Cells were imaged 24h after medium switch and start of the treatment. (C) Representative western blot and quantification of cleaved caspase 3 levels in the same conditions as (B) Scale bar represents 200µm. Error bars represent S.E.M. Cleaved caspase 3 levels were normalised to actin. ***p<0.001. (n=3).

To confirm that cell death rescue occurs as a result of increased NAD(H) levels and not as an indirect result of increased NAM levels in the cells, I tried a reversibility study by co-treating cells with NAM and FK866 to prevent NAM conversion to NAD^+. However, consistent with the original study (Hasmann and Schemainda, 2003), this strategy did not prove effective and no reversibility was achieved, likely due to the previously described antidote effect of NAM on FK866 activity (data not shown). I can thus only conclude that decline in cellular NAD(H) levels is responsible for cell commitment to apoptosis and interventions aimed at recovery of NAD(H) levels improve cell viability.

4.4 Mitochondrial dysfunction and apoptosis are linked to the depletion of NADH levels.

4.4.1 Increased availability of CI substrates exacerbates cell death

NADH:ubiquinone oxidoreductase, or complex I, is the entry point of electrons delivered by NADH into the ETC. CI is the largest of the four complexes of the ETC and has been shown to be the major site of mitochondrial superoxide production (Hirst, King and Pryde, 2008). Since I observed decreased CI-linked O_2 consumption in *Atg5*$^{-/-}$ MEFs (Figure 3.4C), I endeavoured to characterise the role of CI and ETC in galactose-induced cell death. Low CI-linked O_2 consumption could be linked to several phenomena. First, decreased CI holocomplex assembly or supercomplex assembly would lead to the lack of sites for NADH oxidation, but my BN-PAGE gels have shown no gross defects in CI assembly (Fig 3.4A). An alternative mechanism could centre on low availability of NADH, either due to the lack of TCA substrate or due to increased e^- leak from semiubiquinone, thus potentially uncoupling NADH consumption from mMP generation and O_2 reduction. I sought to identify the potential role of each branch.

First, I explored the potential benefits of supplementing cells with additional pyruvate. I hypothesized that increased pyruvate availability as a TCA substrate, in contrast to galactose, which requires processing to enter into glycolysis (Rogers and Segal, 1981), would provide a more accessible substrate for oxidation and help bridge any potential period of energy stress upon first introduction of galactose. In addition, pyruvate is an established antioxidant for cells cultured in a glucose-based medium. I therefore cultured *Atg5*$^{-/-}$ MEFs in a galactose-based medium supplemented with SP a cell-permeable form of pyruvate (in addition to galactose). Surprisingly, increased availability of a mitochondrial TCA cycle substrate, which I hypothesized would boost mitochondrial function, led to significantly higher levels of cell death in *Atg5*$^{-/-}$ MEFs (Fig 4.7A,B). To show that the effect of pyruvate supplementation on cell death its due to its role as a TCA substrate, I treated cells with UK-5099, an inhibitor of mitochondrial pyruvate carrier (MPC) (Zhong *et al.*, 2015). Interestingly, cell treatment with UK-5099 had a moderate cell death rescue effect (Fig 4.7A,B). More importantly, co-treatment with SP and UK-5099 led to a complete reversal of SP-mediated cell death exacerbation, suggesting that pyruvate presence within the mitochondria as a substrate for the TCA cycle has a negative effect on cell survival. Metabolic profiling of cells supplemented with SP revealed a shift in NAD redox state by increased NADH

re-oxidation to NAD^+ in *Atg5*$^{-/-}$ MEFs (Fig 4.7C). Increased pyruvate and lactate levels in *Atg5*$^{-/-}$ MEFs cells supplemented with pyruvate indicate that a portion of NADH is utilized for cytoplasmic pyruvate oxidation to lactate by the enzyme lactate dehydrogenase to re-generate cellular NAD^+ levels to support glycolytic flux and activity of NAD^+-consuming enzymes. However, intermediates of the TCA cycle are also enriched in *Atg5*$^{-/-}$ MEFs supplemented with pyruvate and improved cell viability in cells treated with UK-5099, which I hypothesize led to decreased pyruvate availability in mitochondria, also support my hypothesis that increased mitochondrial respiration in the absence of MQC is detrimental and can lead to the loss of cell viability.

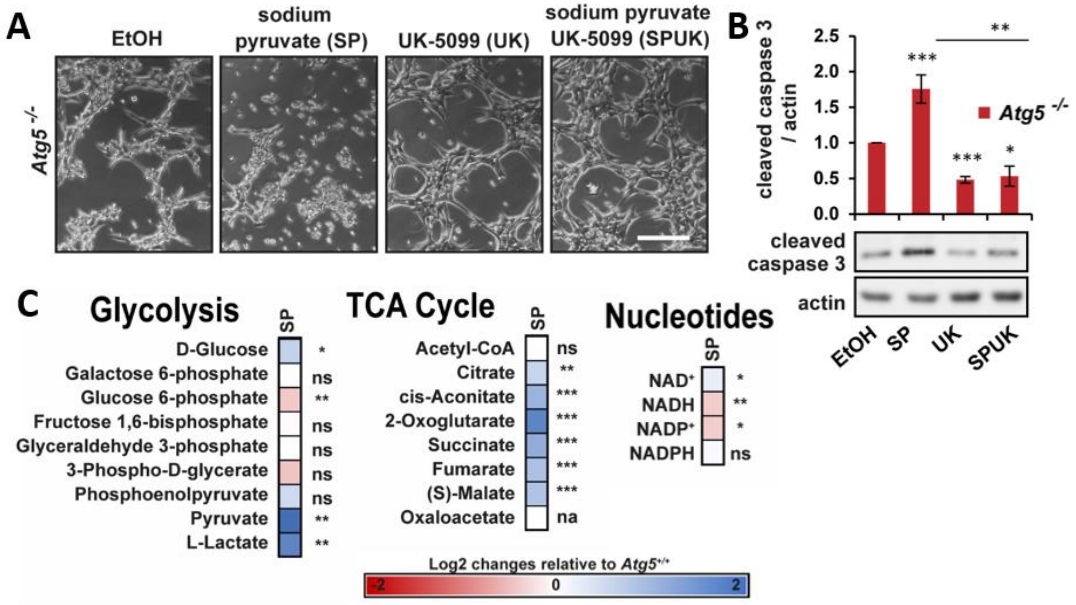

Figure 4. 7 Exposure of *Atg5*$^{-/-}$ MEFs to increased levels of OXPHOS substrate exacerbates cell death

(A) Bright field microscopy images of *Atg5*$^{-/-}$ MEFs cultured in the galactose-based medium for 22 hours, supplemented with 10mM sodium pyruvate (SP), 50μM UK-5099 (UK), or both (SPUK), at 0h. (B) Representative western blot and quantification of caspase 3 cleavage in the same conditions as (A). (C) Intermediates of glycolysis and PPP, and nucleotides depicted as a heatmap of log2(FC) of *Atg5*$^{-/-}$ MEFs supplemented with SP to *Atg5*$^{-/-}$ MEFs cultured in the galactose-based medium. Scale bar represents 200μm. Error bars represent S.E.M. Cleaved caspase 3 levels were normalised to actin. *p<0.05, **p<0.01***p<0.001. (n=3).

4.4.2 Role of ETC in cell death of Atg5$^{-/-}$ MEFs

Next, I employed culture condition changes and pharmacological and genetic approaches to further explore whether manipulation of entry and flow of e^- through the ETC can modulate cellular viability. I first cultured cells in either atmospheric levels of oxygen (21% O_2) or a hypoxic (1% O_2) environment. Hypoxic culture was employed to restrict OXPHOS by reducing oxygen tension (Papandreou *et al.*, 2006; Solaini *et al.*, 2010). Among the many unknowns, which accompany hypoxic culture of cells growing in a galactose-based medium, the most prominent one is the ability of cells to cope with metabolic re-wiring towards aerobic glycolysis in the absence of glucose. In spite of my expectations, control cells were capable of growth in hypoxic conditions, potentially by re-wiring TCA metabolism to support life on glutamine (Metallo *et al.*, 2011) (data not shown). Hypoxic cell culture of *Atg5*$^{-/-}$ MEFs in the galactose-based medium resulted in a complete rescue of apoptotic cell death and increased cell proliferation (Figure 4.8A,B).

To investigate whether decreased e^- flow through the ETC can alleviate cell death in my model, I tested genetic manipulation of ETC function by siRNA knockdown (KD) of nuclear-encoded subunits of the ETC. A single subunit of each of the complexes was selected for genetic targeting based on their role within the complex itself. The NADH:ubiquinone oxidoreductase core subunit S3 (Ndufs3) of the CI hydrogenase module is one of the iron-sulphur protein components and features early in CI subcomplex and holocomplex assembly (Vogel *et al.*, 2007). Mutations in *NDUFS3* are linked to Leigh syndrome (Bénit *et al.*, 2004; Lou *et al.*, 2018), a child-onset neurological disorder resulting from a severe CI deficiency. Knockdown of NDUFS3 was previously shown to result in a loss of CI incorporation in SCs tracked by the NDUFA9 CI subunit (Lapuente-Brun *et al.*, 2013). Succinate dehydrogenase complex flavoprotein subunit A (Sdha) of CII was targeted because it is the major catalytic subunit of CII, a site of succinate oxidation and it was shown to produce a bioenergetics defect, without excessive ROS release or increased proliferation (Guzy *et al.*, 2008).

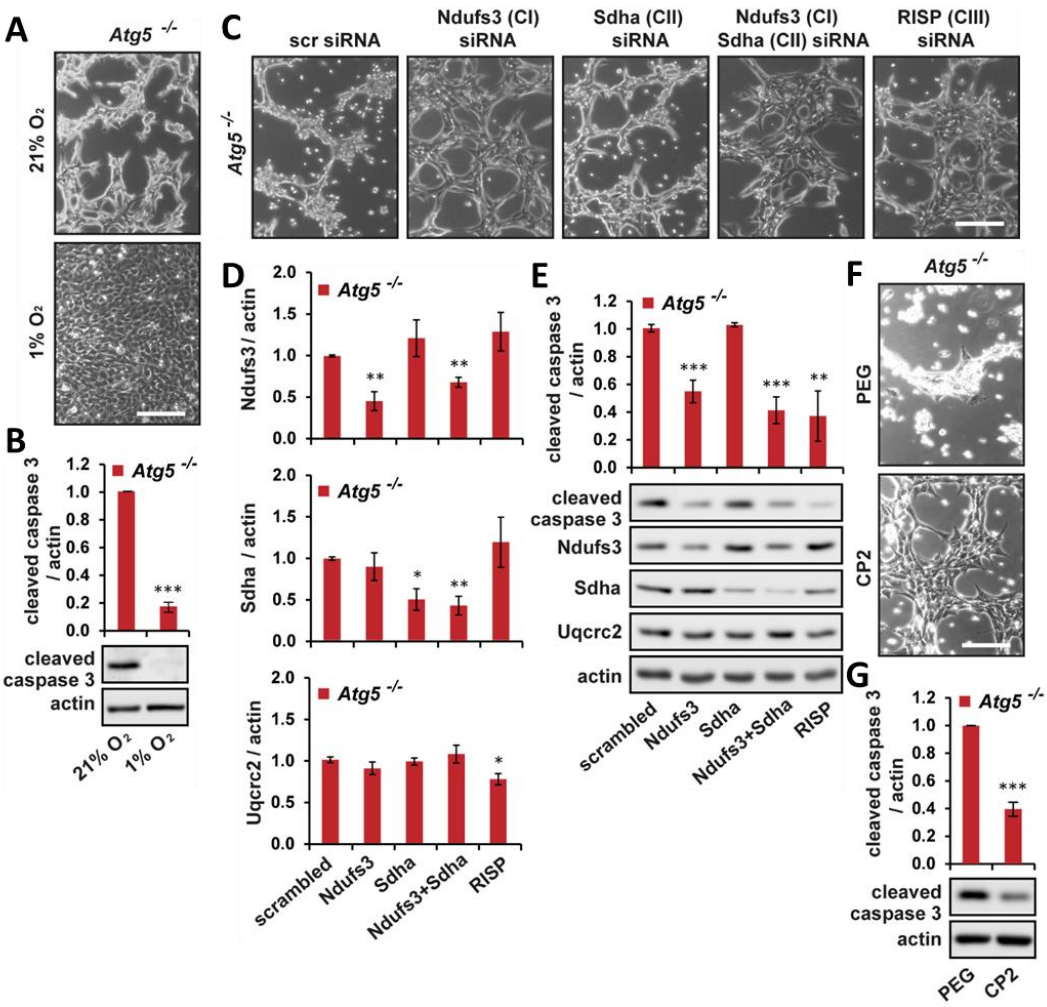

Figure 4. 8 Decreased e$^-$ flux through the ETC ameliorates cell death of *Atg5*$^{-/-}$ MEFs

(A) Bright field microscopy images of *Atg5*$^{-/-}$ MEFs cultured in a galactose-based medium in atmospheric oxygen (21% O2) or hypoxia (1% O2). (B) Representative western blot and quantification of caspase 3 cleavage in the same conditions as (A). (C) Bright field microscopy images of *Atg5*$^{-/-}$ MEFs transfected with scrambled, ETC complex I (Ndufs3), ETC complex II (Sdha) and ETC complex III (Uqcrfs1) subunit-specific siRNA. (D) Quantitation of siRNA-mediated knockdown efficiency. (E) Representative western blot and quantification of caspase 3 cleavage and levels of Ndufs3, Sdha and Uqcrc2 subunits of ETC complexes. (F) Bright field microscopy images of *Atg5*$^{-/-}$MEFs cultured in a galactose-based medium for 24hs, supplemented with 10μM CP2, a mild Complex I inhibitor, or vehicle (PEG) at 0h. (G) Representative western blot and quantitation of caspase 3 cleavage in the same conditions as (F). Scale bar represents 200μm. Error bars represent S.E.M. Cleaved caspase 3, Ndufs3, Sdha and Uqcrc2 levels were normalised to actin. *p<0.05, **p<0.01***p<0.001. (n=3).

And finally, the ubiquinol-cytochrome c reductase iron-sulphur subunit (Uqcrfs1, Rieske Iron-Sulphur Polypeptide (RISP)) is a member of a three-subunit catalytic complex of CIII necessary for e^- transport (Diaz, Enríquez and Moraes, 2012). Uqcrfs1 is also the last CIII subunit incorporated into the complex immediately following Fe-S cluster addition to its C-terminal region (Fernandez-Vizarra and Zeviani, 2018). Although reports do not agree on whether Uqcrfs1 knockdown leads to a reduction or production of ROS, all studies agree that Uqcrfs1 silencing decreases mitochondrial respiration due to a loss of CIII catalytic activity even in absence of an assembly defect (Owens *et al.*, 2011; Diaz, Enríquez and Moraes, 2012; Rabinovitch *et al.*, 2017).

Figure 4.8D shows the knockdown efficiency of the targeted subunits (Uqcrc2, a structural CIII subunit, was used as a proxy for Uqcrfs1/RISP) compared to control cells transfected with scrambled siRNA. The relatively low levels of suppression, I hypothesize, is driven by the potential of cells to tolerate reduction of OXPHOS-linked respiration (CI and CIII) and TCA cycle (CII) while their ability to redirect their metabolism towards aerobic glycolysis is severely limited. I have previously observed that CI and CIII participate in SC assembly in MEFs cultured in galactose-based medium and thus CI likely constitutes the major route of e^- entry and flow within the ETC (Fig 3.4B). It was therefore not surprising that Ndufs3 and Uqcrfs1 silencing led to a significant delay of cell death (Fig 4.C,E). In contrast, KD of Sdha, a CII subunit, had no obvious effect on cell viability and a combination of Ndufs3 and Sdha silencing did not provide any additional benefit compared to Ndufs3 silencing alone.

To then explore a pharmacological CI-targeted intervention I chose to test CP2, a recently discovered tricyclic pyrone compound. CP2 was first shown to lead to amelioration of pathological phenotypes in Alzheimer's mice by the promotion of mitochondrial trafficking in neurons, and by decreasing the load of amyloid-β aggregation (Hong *et al.*, 2009). Upon further study in mouse neurons by Trushina group (Zhang *et al.*, 2015), CP2 was shown to accumulate in mitochondria, increase ETC coupling, and mildly inhibit CI activity by occupying a CI redox centre, the flavin mononucleotide (FMN). Similarly to CI KD, CP2 treatment in *Atg5*$^{-/-}$ MEFs led to increased cell viability upon culture in galactose medium (Fig 4.8F,G). Thus, although the presence of a CI defect in autophagy deficiency is yet to be unequivocally confirmed, I have shown in these proof-of-concept experiments that strategies

decreasing e^- flow through the ETC delay cell death induced in my model of autophagy-deficient cells forced to rely on OXPHOS.

4.4.3 Strategies targeted at the reduction of ROS delay cell death

To investigate the role of ROS in the initiation of apoptotic cell death upon *Atg5*$^{-/-}$ MEF culture in the galactose-based medium, I supplemented culture medium with N-acetylcysteine (NAC), the acetylated form of cysteine that acts as a precursor for the synthesis of glutathione of the antioxidant system (Dodd *et al.*, 2008), and a mitochondria-targeted ubiquinone antioxidant, $MitoQ_{10,}$ (James *et al.*, 2005). Although both treatment strategies led to improvements in cell viability (Fig 4.9A,B), $MitoQ_{10}$ only led to a partial rescue and it is possible that a higher concentration might have a more beneficial effect. However, I did confirm that $MitoQ_{10}$ supplementation led to a decrease of superoxide load in *Atg5*$^{-/-}$ MEF (Fig 4.9C). Although effective, neither NAC nor $MitoQ_{10}$ scavenge ROS released from CI specifically. For this purpose I cultured *Atg5*$^{-/-}$ MEFs in a galactose-based medium supplemented with a suppressor of e^- leak from the CI Iq site (S1QEL2.2) (Brand *et al.*, 2016). S1QELs are novel compounds previously shown to diminish ROS originating from reverse electron transport at CI ubiquinone binding site, yet not affect OXPHOS or cell growth (Brand *et al.*, 2016; Banba *et al.*, 2019). A targeted suppression of superoxide generation at CI by the S1QEL2.2 treatment significantly reduced cell death of *Atg5*$^{-/-}$ MEFs (Fig. 4.9C,D). The significance of S1QEL2.2-mediated cell death rescue is yet to be explored further, but if S1QELs are truly confirmed to prevent RET it could suggest the CI ROS leak occurs due to over-reduction of the ubiquinone pool. Together these data confirm that ROS in *Atg5*$^{-/-}$ MEFs are likely to be of mitochondrial origin and cell death can be rescued by increasing the capacity of the antioxidant system, or by preventing ROS release.

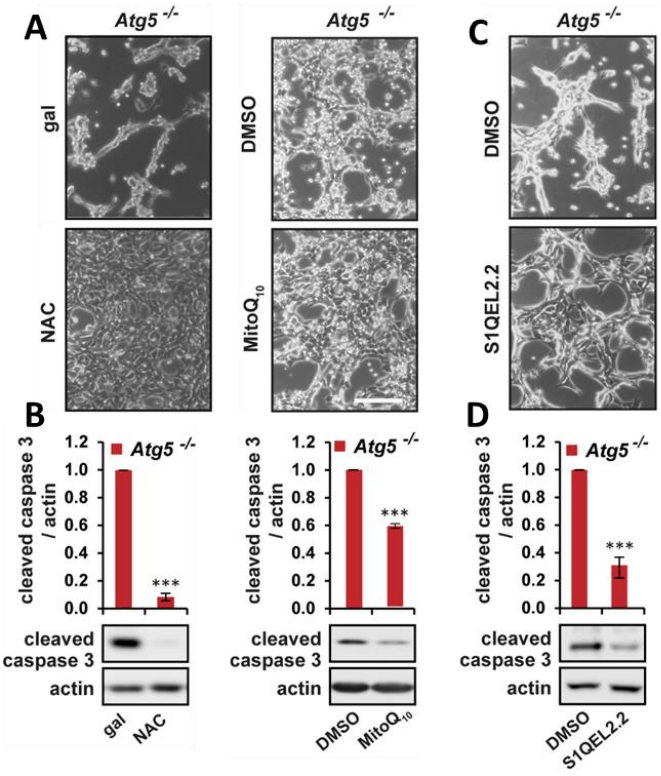

Figure 4. 9 ROS scavenging strategies rescue cell death of *Atg5*$^{-/-}$ MEFs

(A) Bright field microscopy images of *Atg5*$^{-/-}$ MEFs cultured in a galactose-based medium for 24h, supplemented with 2.5mM NAC, 20nM $MitoQ_{10}$ or vehicles at 0h. (B) Representative western blot and quantification of caspase 3 cleavage in the same conditions as (C). Bright field microscopy images of *Atg5*$^{-/-}$ MEFs cultured in a galactose-based medium for 24h, supplemented with 500nM S1QEL2.2 or vehicle (DMSO) at 0h. Scale bar represents 200µm. Error bars represent S.E.M. Cleaved caspase 3, Ndufs3, Sdha and Uqcrc2 levels were normalised to actin levels. ***p<0.001. (n=3).

4.5 Recovery of NADH levels coincides with the restoration of mMP

Thus far, I have explored the two branches of enquiry, NADH depletion and mitochondrial dysfunction, in isolation. Multiple strategies targeted at either branch were successful in promoting cell viability (Fig 4.10A). Both, supplementation with NAM/NR, and ROS scavenging had an effect on their respective target, i.e. boosting NAD levels and decreasing ROS levels. However, the impact of interventions aimed at either branch could result in unintended effects.

Increased levels of NAD^+ could lead to a boost in the antioxidant system and increased ETC coupling via activation and the concerted action of SIRT1 and SIRT3 (Ansari *et al.*, 2017; Singh *et al.*, 2017). Similarly, predicted lower respiration rates due to silencing or inhibition of ETC components might result in lower rates of ROS release. To investigate which of these phenomena best correlates with cell death rescue, I singled out a treatment from each of the employed strategies and carried out MitoSOX-based staining to evaluate ROS production and metabolic profiling to quantify levels of NAD^+/NADH. As predicted, levels of superoxide production were mildly, but significantly reduced in $MitoQ_{10}$ treated cells (Fig 4.10A,B). Surprisingly, NAM supplementation did not have any effect on superoxide formation and a previously unreported increase of superoxide release was detected in CP2 treated cells. Thus, reduction in mitochondrial ROS release is not achieved in all conditions that prevent cell death. In contrast, all tested treatments led to the recovery of NADH levels and a corresponding recovery in mMP (Fig. 4.10C,D,E). It is worth to note that neither of the selected treatments, which rescue cell viability, improve cellular ATP levels. In fact, of all the tested nucleotides, recovery of NADH levels is the most predictive of cell viability.

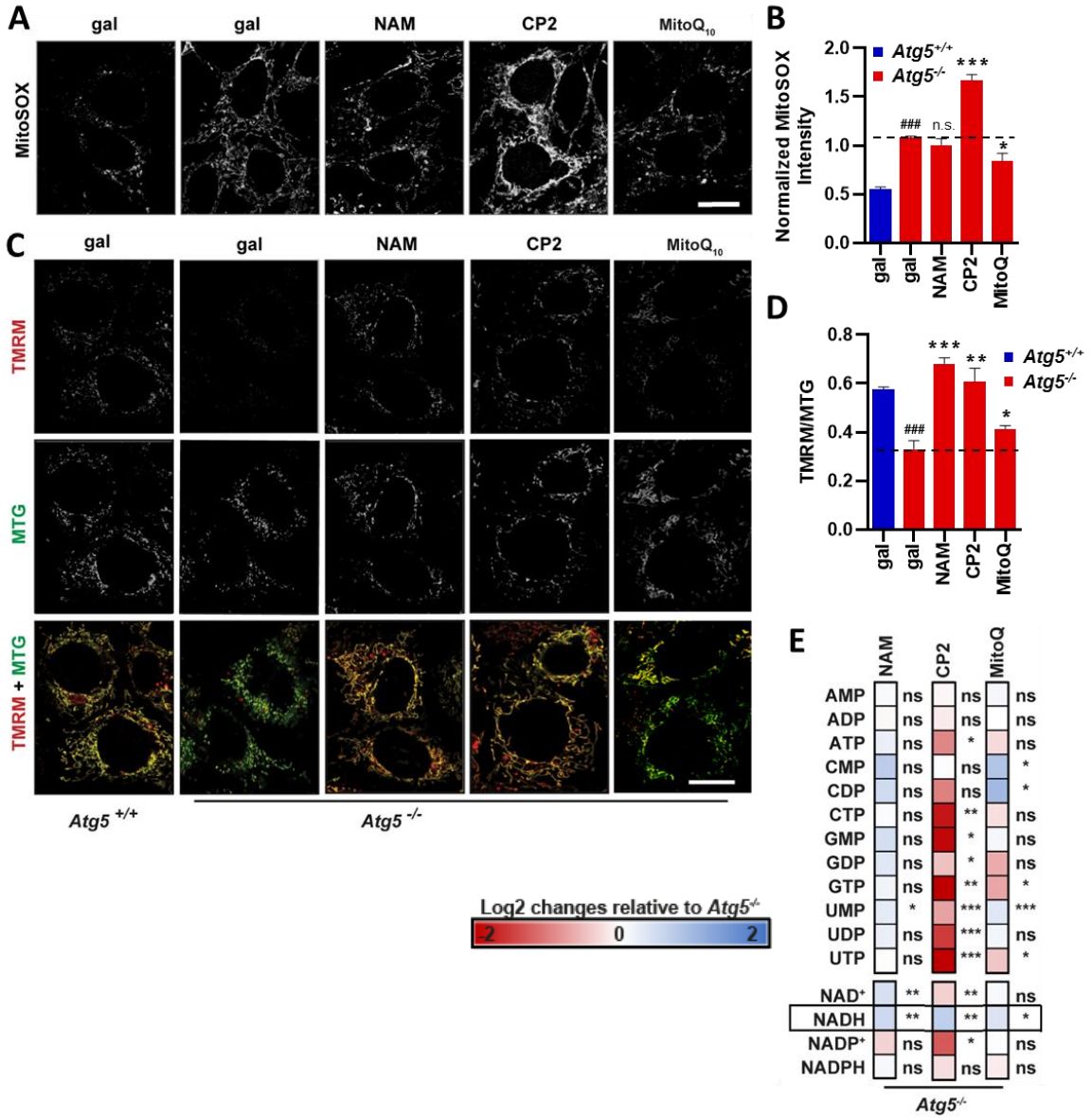

Figure 4. 10 NADH-linked maintenance of mMP is critical for cell survival of *Atg5*$^{-/-}$ MEFs

(A,B) Superoxide levels, quantified by MitoSOX staining, do not correlate with cellular survival. (A) Representative images of MitoSOX fluorescence of *Atg*$^{+/+}$ and *Atg5*$^{-/-}$ MEFs cultured in a galactose-based medium alone or supplemented with 5mM NAM, 10μM CP2 or 20nM $MitoQ_{10}$ for 24h. (B) Quantitation of MitoSOX intensity in the same conditions as (A). (C,D) Treatments that improve cell viability increase mMP in *Atg5*$^{-/-}$ MEFs. (C) Representative immunofluorescence images of cells stained with TMRM and MTG. (D) Quantitation of TMRM:MTG ratio in the same conditions as (C). (E) Metabolite profiling is depicted as a heatmap of log2(FC) change of *Atg5*$^{-/-}$ MEFs treatment with the corresponding compound to *Atg5*$^{-/-}$ MEFs in galactose alone. Scale bars represent 20μm. Error bars represent S.E.M., *p<0.05, **p<0.01, ***p < 0.001. (n=3).

To investigate whether the recovery of mMP is necessary and sufficient to prevent cell death in my model, I carried out a dose-variable supplementation with oligomycin, an ATP synthase inhibitor. ATP synthase consumes mMP by channelling protons pumped into the IMS by the ETC. Standard dose of oligomycin (10μM), traditionally used to induce mitophagy (in co-treatment with a CIII inhibitor, antimycin A) in glucose-cultured cells, led to a cell death reminiscent of that in response to antimycin and rotenone treatment in cells cultured in a galactose-based medium (Fig 3.3A). However, employing a simple bright field microscopy-based observation of cell death morphology, I identified a dose of oligomycin, which prevented cell death (Fig 4.11A). I further confirmed my finding by an immunoblot-based investigation of caspase 3 cleavage (Fig 4.11B). Finally, mMP measurement revealed that addition of 1nM oligomycin at the time of the culture medium switch helps cells maintain a healthy $\Delta\Psi$ (Fig 4.11C).

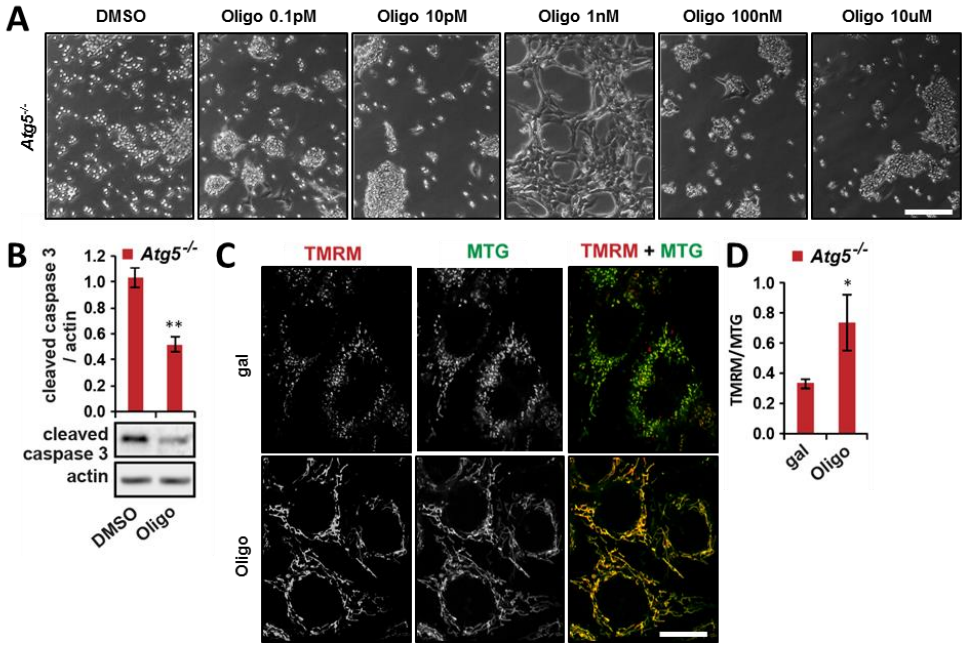

Figure 4. 11 Increasing mMP alone is sufficient to prevent cell death of *Atg5*$^{-/-}$ MEFs

(A) Bright field microscopy images of *Atg5*$^{-/-}$ MEFs cultured in a galactose-based medium supplemented with increasing doses of oligomycin (0.1pM - 10μM) or vehicle (DMSO). Cells were imaged at 44h to estimate the true cell death rescue potential of the treatment. (B) Representative western blot and quantification of caspase 3 cleavage in cells supplemented with 1nM oligomycin or vehicle (DMSO). Scale bar represents 20μm (C) Representative immunofluorescence images of TMRM and MTG stained cells cultured in the same condition as in (B). (D) Quantitation of TMRM:MTG ratio in the same conditions as (C). Scale bar represents 200μm. Error bars represent S.E.M. Cleaved caspase 3 levels were normalised to actin levels. *p<0.05, **p<0.01. (n=3).

4.6 Chapter conclusions

In Chapter 3, I characterized the changes in ETC complex composition and bioenergetics and discussed how autophagy impairment drives mitochondrial dysfunction, ROS release, loss of mMP and apoptotic cell death. In chapter 4, I have shown that autophagy abolition is sufficient to drive disruption of nucleotide and NAD(H) metabolism (Figure 4.1/4.2/4.3B). By interfering with the NAD^+ salvage pathway in *Atg5*$^{+/+}$ MEFs, I have demonstrated that depletion of the NAD pool is sufficient to drive apoptosis in wild type cells that rely on mitochondrial OXPHOS for ATP generation (Figure 4.4B,C). I have further demonstrated that low levels of NADH negatively correlate with mMP and cell survival in *Atg5*$^{-/-}$ MEFs (Figure 4.4D,E; Figure

4.7C; Figure 4.10E). My results also indicate that, at the timepoint I chose for my investigation, levels of superoxide release are increased, but do not always correlate with cellular survival and thus cannot be the sole cause of all of the observed pathology (Figure 4.10A,B). Therefore, I have identified two separate branches of molecular pathology which arise as a result of autophagy abolition, firstly, mitochondrial ROS release and secondly, NAD(H) depletion.

Mitochondrial dysfunction in my system resembles a runaway system. Several lines of my investigation show that mild impairment of mitochondrial OXPHOS by genetic or pharmacological interference with e^- entry and the flow through the ETC promotes cellular viability (Figure 4.7 A,B; Figure 4.8C-G, Figure 4.11A-D). In contrast, increased e^- entry into the ETC or increased levels of accessible substrate promote cell death (Figure 4.4D,E; Figure 4.7A,B). The negative impact of mitochondrial OXPHOS in a system that lacks a major portion of its quality control relates to elevated release of ROS. ROS detoxification by three distinct routes of action, i.e. supplementation with NAC, $MitoQ_{10}$ and S1QEL2.2, promotes cellular viability and supports my hypothesis that mitochondrial dysfunction contributes to cell death in my model (Figure 4.9A-D). I have also identified two potential targets of therapeutic potential at the mitochondrial route of dysfunction relating to mild ETC complex inhibition and ROS scavenging. I discuss the translational potential of ROS scavenging and pyruvate entry modulation in section 1.7.2.

Depletion of nucleotides, and specifically of the NAD(H) pool, could arise by multiple mechanisms and lead to a variety of downstream dysfunctions. Due to the complexity of NAD^+ synthesis, subcellular localization and consumption, it would be difficult to pinpoint the exact cause of depletion and thus identify a specific pathway or enzyme to target by either inhibition or activation strategies. Nevertheless, two results of my metabolic profiling suggest that some of the total NAD^+ depletion I observe could be due to lower flux through the synthesis pathways. Specifically, two metabolites that are required for NAD^+ salvage and *de novo* synthesis, ATP and ribose-5-phosphate, are both significantly decreased in *Atg5*$^{-/-}$ MEFs compared to *Atg5*$^{+/+}$ MEFs (Figure 4.3A,B; Figure 1.5 (Hove-Jensen *et al.*, 2017). Increased NAD^+ consumption by NADases in my system is supported by my study of SIRT1/2, PARP1/2 and CD38 inhibition, all of which lead to cell death rescue (Figure 4.5). Measurement of the total NAD(H) levels upon NADase inhibition, or the activity of individual enzymes might be required to

pinpoint the direct cause of NAD(H) depletion. From the current results, I can conclude that inhibition of each group of enzymes should lead to a greater total pool of NAD^+ and that activity of none of the targeted enzymes is essential for cell survival. On a similar note, boosting NAD^+ levels by NAM and NR supplementation led to a complete rescue of cell death in *Atg5*$^{+/+}$ MEFs (Figure 4.6). By metabolic profiling of *Atg5*$^{-/-}$ MEFs supplemented with NAM, I confirmed that NAM is readily converted to NAD^+ and NADH (Figure 4.10E).

Although I initially studied the two branches of mitochondrial dysfunction and NAD^+ metabolism aberration in isolation, the spatial-temporal relatedness of the two could not be overlooked. Mitochondrial metabolism and function requires sufficient levels of NAD^+ to promote carbon oxidation by acting as an e^- donor to the TCA cycle and, in the form of NADH, shuttle e^- to CI of the ETC (Balaban, Nemoto and Finkel, 2005). In addition, mitochondrial SIRTs and PARPs require NAD^+ as a substrate to maintain the fidelity of mitochondrial ETC and DNA repair (Cantó, Menzies and Auwerx, 2015). Taking all of the above into account, I suggest that the major underlying pathology of autophagy deficiency is NAD(H) depletion, which in turn affects mitochondrial function and ultimately leads to mitochondrial depolarization and apoptosis.

4.7 Chapter discussion

4.7.1 The chicken and egg of NADH depletion and mitochondrial dysfunction in autophagy-deficiency

Metabolomic profiling in my study supports the idea that autophagy deficiency leads to depletion of cellular NAD(H) pool and NADH availability for mitochondrial respiration. In contrast to other studies, which suggest that NAD^+ promotes cell viability due to its interaction as a co-substrate to longevity-promoting SIRTs (Mouchiroud *et al.*, 2013; Camacho-Pereira *et al.*, 2016), my model shows the underlying mechanism of improved mitochondrial function might be of a different nature. my approach to boosting NAD^+/NADH levels not only by supplementing precursors of NAD^+ via its salvage pathway, but also by inhibition of NAD^+ consuming enzymes shows that cell death in my model can likely be rescued by simply increasing the availability of the NAD^+ nucleotide as a co-factor for mitochondrial metabolism and maintenance of mMP.

However, autophagy impairment also leads to compromised mitochondrial recycling and thus leads to accumulation dysfunctional organelles (Lazarou *et al.*, 2015). Within mitochondria, NADH links carbon oxidation to ETC by donating e^- to CI of the ETC. If e^- are liberated from NADH, donated to the ETC, but leak before they fully contribute to proton pumping at CIII and CIV, the loop would be broken and indiscriminate NADH oxidation by CI could occur, thus leading to NADH depletion, and ROS-mediated damage. ROS levels and damage to cellular macromolecules lead to increased activity of NAD-consuming enzymes (SIRTs and PARPs) and depletion of NAD^+ (Merksamer *et al.*, 2013; Hegedűs and Virág, 2014). I have so far not been able to establish the cause of NAD(H) depletion in autophagy deficiency, but it seems likely that both, mitochondrial dysfunction-linked increased consumption of NADH, and depletion of the cytoplasmic NAD^+ pool by SIRTs and PARPs both contribute to loss of cellular viability.

4.7.2 Limitations and translational potential

The main limitation of this study was the lack of information about where NAD^+/NADH depletion occurs. I carried out my metabolomics profiling on whole cell lysates to capture the largest possible amount of metabolomics data relating to autophagy deficiency and mitochondrial dysfunction, which allowed us to study the levels of macromolecules recycled by autophagy including the intermediates of carbon metabolism. From my study, I was able to conclude that whole-cell levels of amino acids and the majority of metabolic pathways remain unperturbed in my model and it is specifically nucleotides, which are negatively affected. Further study of subcellular NAD pools and their oxidation states would benefit from the recent development of NAD/(P)/H sensor and reporter molecules that can be targeted to any subcellular compartment (Hung *et al.*, 2011; Bilan *et al.*, 2014; Y. Zhao *et al.*, 2015; Cambronne *et al.*, 2016). Specifically, mitochondrial targeting of such sensors could provide further insight into real-time changes in NAD oxidation states in my model. Furthermore, such probes could also validate the results of my current and future therapeutic strategies, including NADase inhibition, NAD^+-precursor supplementation and ETC modulation.

Another limitation of this study is the lack of understanding of the main contributors to the NAD(H) depletion in my system. A proteomics- and metabolomics- approaches could help elucidate the involvement of NAD^+ synthesis enzymes and intermediates, respectively, to identify a potential bottleneck. Additionally, optimization of immunoblot assays of PARP and SIRT activity, and fluorescence-based NAD(H) detection assays

is currently underway within the group and should lead to the identification of the main NAD^+-consumption pathways in these cells. Preliminary data point to an excessive PARP activation upon *Atg5*$^{-/-}$ MEFs culture in the galactose-based medium, which precedes cell death. In fact, my preliminary study indicates that both PARP and SIRT activity diminish in the last two hours prior to caspase 3 cleavage (data not shown), further supporting my finding that NAD^+ levels are depleted in my model.

Within this study, I explored several paths of dysfunction that occur downstream of autophagy abolition and identified multiple therapeutic targets within mitochondria to protect them from runaway NADH consumption and excessive ROS release. I also established that antioxidant supplementation may be beneficial in this system. Although, ROS have long been associated with the pathogenesis of age-related disease and neurodegeneration, the majority of clinical trials testing the efficacy of general antioxidant and vitamin supplementation failed to show improved outcomes and reported an increase in all-cause mortality upon chronic- or high-dose supplementation (reviewed in (Schmidt *et al.*, 2015). Thus, the therapeutic potential of mitochondria-targeted antioxidants including Coenzyme Q10 and $MitoQ_{10}$ was evaluated. However, neither of these antioxidants stopped PD progression (NCT00740714) (Snow *et al.*, 2010; Beal *et al.*, 2014). Similarly, vitamin E/C and coenzyme Q supplementation efficacy were tested in an AD clinical trial (NCT00117403), with no success in ameliorating amyloid β or Tau pathology in cerebrospinal fluid (Galasko *et al.*, 2012). Worryingly, vitamin supplementation instead led to faster cognitive decline. Lastly, one further phase 2 clinical trial is currently planned, though not yet recruiting. This trial is aimed at short-term effects of $MitoQ_{10}$ supplementation on the vasodilation in AD patients (NCT03514875). These studies show that although successful in ameliorating cell death in my model, antioxidant supplementation in the form of vitamins or $MitoQ_{10}$ is currently not successful in the clinic.

In addition, my findings corroborate a new line of PD research based on an observation reported from a retrospective study of patients with diabetes mellitus type 2 (DMT2) who were treated with glitazone (GTZ), a member of a class of insulin sensitizing compounds otherwise known as thiazolidinediones (TZD) (Brauer *et al.*, 2015). TZDs were previously described as PPARγ activators and mild CI inhibitors (Scatena *et al.*, 2004). However, upon discovery of the mitochondrial pyruvate carrier (MPC), TZDs

were reported to specifically inhibit MPC-mediated pyruvate transport into mitochondria (Scatena *et al.*, 2004; Divakaruni *et al.*, 2013). Interestingly, DMT2 patients on glitazone were 28% less likely to develop PD, when compared to DMT2 patients on other anti-diabetic medication (Brauer *et al.*, 2015). Although the effect was quite mild in real terms (6.4 individuals compared to 8.8 individuals per 10 000), and limited to patients with diabetes, it did prompt further study of pyruvate metabolism and mitochondrial function in animal models of PD (Ghosh *et al.*, 2016). In this study, use of MSDC-0160, a specific MPC inhibitor, prevents neurodegeneration and motor deficits in genetic- and MPTP-induced PD mice. These results mirror my use of UK-5099 in *Atg5*$^{-/-}$ MEFs, whereby the inhibition of pyruvate entry into mitochondria promoted cell viability in cells that lack autophagy.

However, the effect of a TZD pioglitazone compound was tested in a phase 2 clinical trial in PD (NCT01280123) and the trial outcomes were not found to be sufficient to support a larger trial (Investigators, 2015). Furthermore, two MPC inhibitors, pioglitazne (NCT00760578) and MSDC-0160 (NCT01374438, NCT00760578) were tested in phase 2 clinical trials. Published results of the MSDC-0160 study indicate that cerebellar glucose metabolism is maintained in patients in the treatment group, compared to its decline in the placebo group (Shah *et al.*, 2014). However, two phase 3 trials were terminated due to the lack of drug efficacy (NCT01931566; NCT02284906) and no further trials in AD are currently underway. Thus, mitochondria-targeted strategies of antioxidant treatment and modulation of pyruvate entry to mitochondria supported by the findings in this study proved ineffective for the treatment of neurodegeneration in the clinical setting. In contrast, multiple clinical trials of NAD(H)-supplementation strategies to treat neurodegenerative and age-related disorders are currently underway and show early success (discussed in section 6.2).

Chapter 5. NAD(H) deficiency is identified in a disease-relevant model presenting with autophagy impairment.

5.1 Introduction

Physiological deficiency of autophagic flux is not limited to defects in pathway initiation, but can occur at any stage of cargo recognition, autophagosome formation, vesicle trafficking and lysosome-autophagosome fusion (Menzies, Fleming and Rubinsztein, 2015). Autophagic stress was previously reported from multiple models of NPC disease, including neurons from *Npc1*$^{-/-}$ mice (Liao *et al.*, 2007; Meske *et al.*, 2014), in NPC patient fibroblasts (Pacheco, Kunkel and Lieberman, 2007) and in human embryonic stem cell-derived neurons (Ordonez *et al.*, 2012; Sarkar *et al.*, 2013). One consistent observation between all studies is the accumulation of autophagosomes, though authors diverge on their hypotheses of the underlying cause and best course of treatment. One group argues that autophagosome accumulation is a result of increased autophagy induction (Pacheco, Kunkel and Lieberman, 2007), others advocate defective clearance as the underlying cause (Sarkar *et al.*, 2013; Meske *et al.*, 2014). Moreover, the Ordonez study supports both views (Ordonez *et al.*, 2012). Furthermore, treatment with HPβCD that mobilizes cholesterol from endosomes and lysosomes and rescues what is considered the underlying pathology of the disease, was reported to both increase (Meske *et al.*, 2014) and block (Sarkar *et al.*, 2013) autophagic flux. Studies from neuronal cultures derived from patient fibroblasts suggest that accumulation of autophagic vesicles leads to mitochondrial fragmentation and can itself contribute to toxicity in neurons with high levels of spontaneous autophagy (Ordonez *et al.*, 2012). In these neurons, inhibition of autophagy initiation by 3-MA treatment prevented mitochondrial fragmentation, and interestingly also led to reduction of p62 puncta (Ordonez *et al.*, 2012). The lack of understanding of the underlying cause of NPC disease and differences between models and tissue presentation of the disease complicate translation of any potential therapeutic treatment into the clinic (discussed in more detail in section 1.5.4).

I have so far explored the effects of autophagy interruption at the stages of initiation and characterized the resulting changes in mitochondrial function and NAD(H) homeostasis. I next sought to test whether a late-stage block in autophagy flux would lead to a similar cellular phenotype. For my study, I first chose a knockout model of

NPC disease, the *Npc1*$^{+/+}$ and *Npc1*$^{-/-}$ MEFs, that were previously characterized with impaired autophagy flux and autophagosome accumulation (Sarkar *et al.*, 2013) and explored the state of mitochondrial bioenergetics and NAD(H) metabolism. I then aimed to explore the translational potential of my findings using a patient fibroblast model of NPC.

5.2 *Npc1*$^{-/-}$ MEFs display phenotypes similar to *Atg5*$^{-/-}$ MEFs

Current knowledge of NAD(H) metabolism in NPC is quite limited. As of yet, no published study has focused on the levels and metabolism of NAD(H) in NPC patient cells or mouse/cell models. Evidence of the potential benefit of nicotinamide supplementation arises from a single small study of mice with infantile NPC disease. Authors of this observational study hypothesize that nicotinamide may act as a histone deacetylase inhibitor or by modulation of oxidative stress (Marshall, Borbon and Erickson, 2017).

In contrast, several studies characterized mitochondrial dysfunction in NPC to date. In a mouse study of NPC disease, authors reported increased levels of cholesterol associated with both the outer and inner mitochondrial membranes (Yu *et al.*, 2005). Further characterization of mitochondrial function revealed inefficient respiration, loss of ATP and mitochondrial depolarization in NPC mouse brains, which improved upon incubation of isolated mitochondria with HPβCD (Yu *et al.*, 2005). Mitochondria were later reported to adopt a fragmented morphology in human embryonic stem cell-derived neurons, but no further effort was made to characterize mitochondrial bioenergetics (Ordonez *et al.*, 2012). A recent characterization of mitochondrial mass and function in cells derived from NPC1 patients shows increased cholesterol content in mitochondrial membrane, mitochondrial accumulation and a corresponding increased respiration, but surprisingly, with no changes in mMP, and decreased ROS and ATP levels (Woś *et al.*, 2016). It is interesting to note that although reports from NPC models agree that mitochondrial dysfunction is present, its exact nature in terms of bioenergetics, morphology and metabolism seems to vary between the multiple mouse and human models.

5.2.1 ETC alterations in Npc1$^{-/-}$ *MEFs cultured in a glucose-based medium*

In an approach similar to my study of *Atg5*$^{+/+}$ and *Atg5*$^{-/-}$ MEFs, I first cultured *Npc1*$^{+/+}$ and *Npc1*$^{-/-}$ MEFs in a glucose based-medium and characterized the state of

mitochondrial bioenergetics. First, Seahorse XF-based analysis of non-permeabilized cells revealed a lower basal respiration rate (prior to oligomycin addition) and lower spare respiratory capacity (following addition of FCCP) in *Npc1*$^{-/-}$ MEFs (Figure 5.1A). OCR and ECAR measurements were then used to calculate total ATP level production and the proportion of ATP produces by OXPHOS or by glycolysis (Figure 5.1A,B) (Mookerjee and Brand, 2015). *Npc1*$^{-/-}$ MEFs have the same potential for ATP generation as *Npc1*$^{+/+}$ MEFs, although a significantly greater proportion of ATP is generated by aerobic glycolysis (Figure 5.1C). Thus, although the mitochondrial bioenergetics are compromised in *Npc1*$^{-/-}$ MEFs, they are capable of cellular metabolic rewiring to supplement any depletion of cellular energy charge.

I then performed Seahorse XF analysis of mitochondrial respiration on permeabilized cells in the presence of either CI substrates (pyruvate+ malate) or a CII substrate (succinate). CI-linked state 3_{ADP} respiration (following ADP addition) was reduced in *Npc1*$^{-/-}$ MEFs (Figure 5.2A), while no dysfunction was found in CII-linked analysis (5.2B). State 3_{ADP} was then expressed as a ratio to state $4_{oligomycin}$ to indicate the coupling between O_2 consumption and ADP phosphorylation (Figure 5.2C). CI-linked RCR was significantly lower in *Npc1*$^{-/-}$ MEFs when compared to *Npc1*$^{+/+}$ MEFs. In contrast, the coupling between O_2 consumption and ADP phosphorylation upon CII substrate feed was significantly increased in *Npc1*$^{-/-}$ MEFs (Figure 5.2C).

Immunoblot-based analysis of ETC subunit levels revealed a significant depletion of CI core (Ndufs3 and Ndufv2) and accessory (Ndufa9) subunits from the matrix arm, and a relatively short-lived membrane arm subunit (Ndufb8) (Karunadharma *et al.*, 2015; Zhu, Vinothkumar and Hirst, 2016). In contrast the Ndufb9 membrane arm subunit remained unaffected. In addition, levels of CIII (Uqcrc2) and CV (Atp5a) subunits were decreased, though not significantly. Uqcrc2 is an accessory subunit of CIII and might not reflect CIII catalytic activity. Furthermore, the CII-$CIII_2$-CIV linked respiration (state 3_{ADP}) and RCR, as measured by Seahorse XF, are not altered in *Npc1*$^{-/-}$ MEFs and thus suggest that $CIII_2$, CIV and ATP synthase activities are not affected in *Npc1*$^{-/-}$ MEFs.

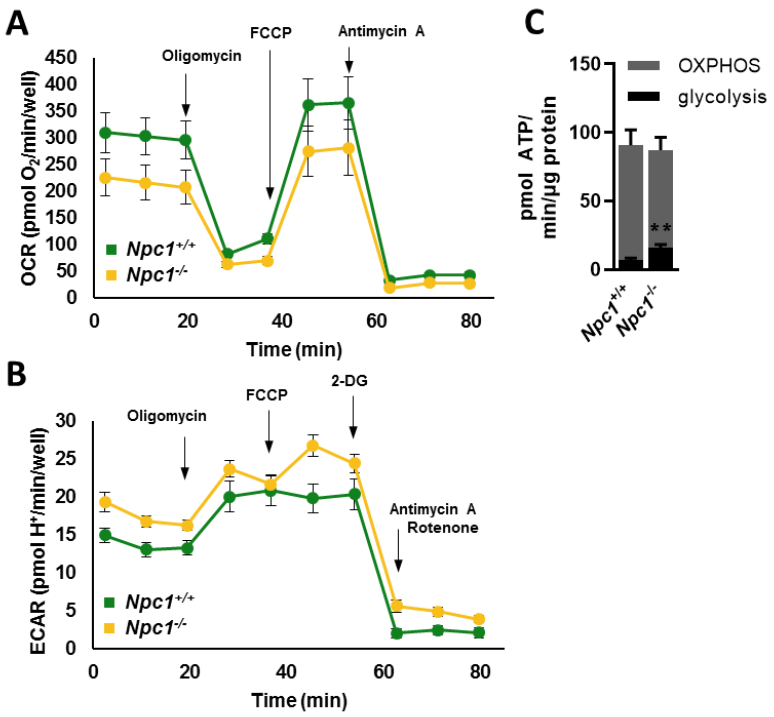

Figure 5. 1 *Npc1*$^{-/-}$ MEFs cultured in glucose-based medium undergo metabolic re-wiring

(A-C) Mitochondrial bioenergetics vary between *Npc1*$^{+/+}$ and *Npc1*$^{-/-}$ MEFs. (A,B) Seahorse analysis of OCR and ECAR were analysed in basal conditions or following additions of oligomycin, FCCP, 2-DG, antimycin A and rotenone as indicated. (C) ATP production calculation was based on Seahorse analysis in *Npc1*$^{+/+}$ and *Npc1*$^{-/-}$ MEFs pre-cultured in glucose-based medium for 48h. Error bars represent S.E.M. *p<0.05. (n=3). Seahorse analyses were carried out in collaboration with Dr Satomi Miwa.

5.2.2 Npc1$^{-/-}$ MEFs die upon prolonged culture in a galactose-based medium

A switch of *Npc1*$^{+/+}$ and *Npc1*$^{-/-}$ MEFs into a galactose-based medium led to a time-dependent increase of all mitochondrial ETC subunit levels, but not OMM proteins, in both cell lines (Figure 5.3A). This result suggests that the upregulation of mitochondrial ETC subunit expression upon galactose-based culture is autophagy-independent. More importantly, *Npc1*$^{-/-}$ cells recover the downregulated CI subunits to the levels comparable to wild-type cells, indicating that CI subunit downregulation observed upon culture in a glucose-based medium is an active, reversible process. Similarly, increased presence of SCs in mitochondria from both cell lines was detected by BN-PAGE analysis upon the switch to and culture in a galactose-based medium (Figure 5.3B). Interestingly, levels of CI holocomplex, detected after mitochondrial membrane solubilisation with TX-100 were comparable between both conditions and cell lines (Figure 5.3B). Culture in glucose-based medium revealed a drastically lower amount of SCs in *Npc1*$^{-/-}$ MEFs, which improved and recovered to *Npc1*$^{+/+}$ levels upon a switch to galactose. The one difference that was maintained between cell lines was the lack of a very high molecular weight species in extracts from *Npc1*$^{-/-}$ MEFs detected upon membrane solubilisation with digitonin (Figure 5.3B). I hypothesize that this species corresponds to a structure consisting of a CI dimer (CI_2), a CIII dimer ($CIII_2$) (Jha, Wang and Auwerx, 2016). Although the lack of the CI_2CIII_2 band was consistent between multiple replicates, the physiological significance of the CI_2CIII_2 assembly remains unknown. Due to technical difficulties were not able to measure mitochondrial bioenergetics in cell lines cultured in a galactose-based medium. I did, however, obtain cellular measurement of mitochondrial ROS levels and found an increased e^- leak in *Npc1*$^{-/-}$ MEFs cultured in both media (Figure 5.3C).

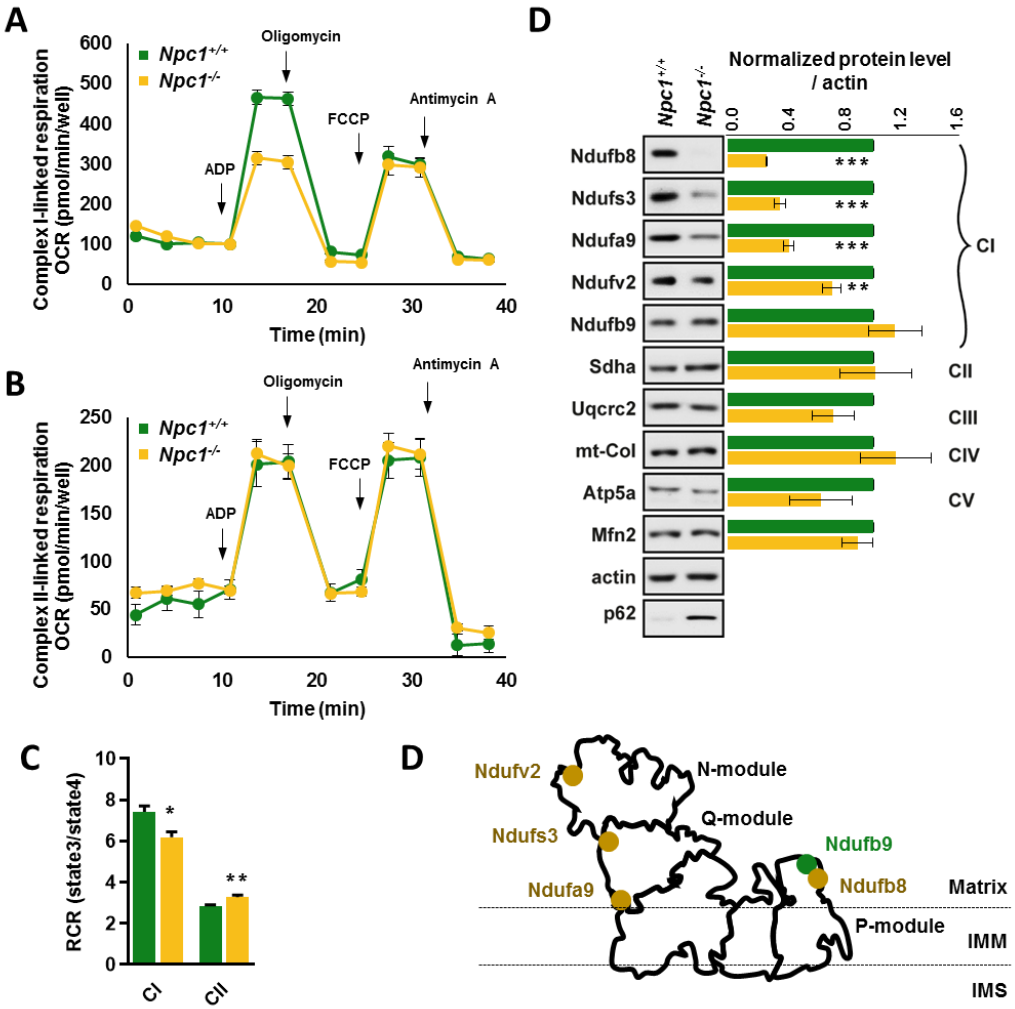

Figure 5. 2 Functional and structural CI deficiency is observed in *Npc1*$^{-/-}$ MEFs

(A-C) CI-linked mitochondrial bioenergetics is altered in *Npc1*$^{-/-}$ MEFs. Seahorse analysis of OCR was carried out in permeabilized cells fed with CI (PM) (A) or CII (S) (B) substrates. OCR measurements occurred in basal conditions or following additions of oligomycin, FCCP, 2-DG, antimycin A and rotenone as indicated. (C) Respiratory control ratio (RCR) was calculated in both conditions. (D) Representative immunoblots and quantification of CI-CV complex subunits in *Npc1*$^{+/+}$ and *Npc1*$^{-/-}$ MEFs cultured in a glucose-based medium. (E) Graphic representation of CI of the ETC and the predicted location of probed significantly reduced (yellow) and unaffected (green) subunits. Cells were pre-cultured in a glucose-based medium for 48h prior to all experiments. Error bars represent S.E.M. *p<0.05, **p<0.01 ***p<0.001. (n=3). Seahorse XF analyses were carried out in collaboration with Dr Satomi Miwa.

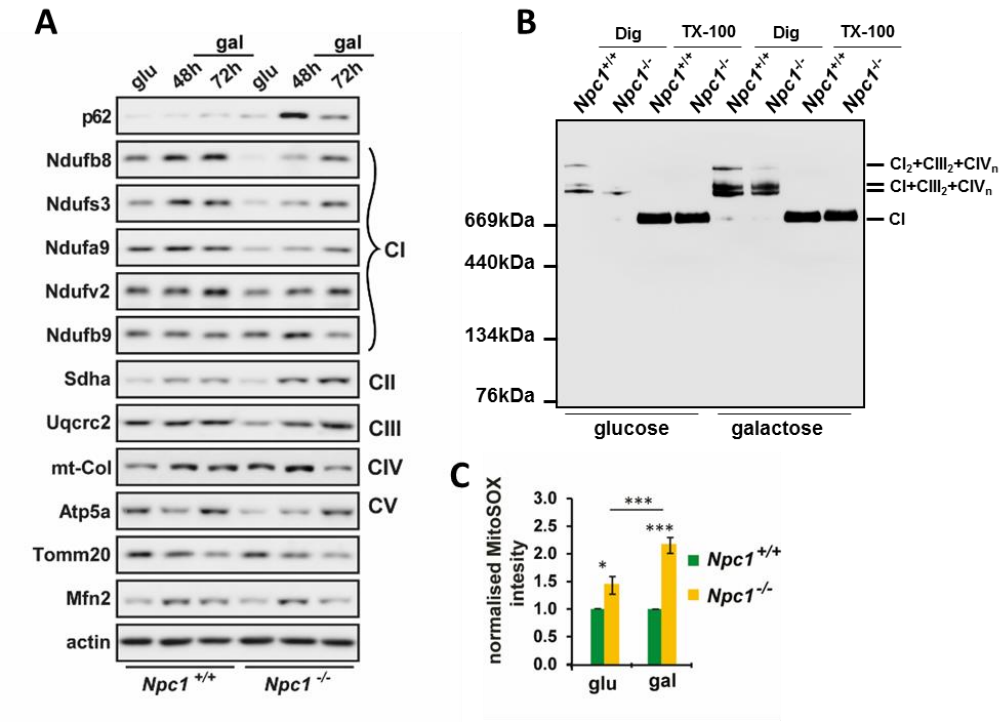

Figure 5. 3 Cell culture in galactose-based medium increases ETC levels and ROS release

(A) Representative western blots of p62, an autophagy receptor; CI subunits: Ndufa9, Ndufb8, Ndufb9, Ndufs3 and Ndufv2; CII subunit Sdha; CIII subunit Uqcrc2; CIV subunit mt-CoI; ATP synthase subunit Atp5a; and OMM membrane protein Mfn2 and Tomm20 in *Npc1*$^{+/+}$ and *Npc1*$^{-/-}$ MEFs switched to galactose-based medium for 48h. (B) BN-PAGE immunoblots of CI (Ndufa9) holocomplexes solubilised in 1μM triton X-100 (TX-100), or SCs solubilised in 0.8μM digitonin (dig). (C) Quantitation of MitoSOX intensity measured by FACS upon 60h culture in galactose-based medium. Error bars represent S.E.M. *p<0.05, ***p<0.001. (n=3).

Finally, prolonged culture of *Npc1*$^{-/-}$ MEFs in galactose medium led to increased levels of apoptotic cell death observed by bright field microscopy as cell detachment and confirmed by caspase 3 cleavage immunoblotting (Figure 5.4A,B). By bright field microscopy, I confirmed that stable expression of the NPC1 protein and culture medium supplementation with Z-VAD-fmk were both sufficient to rescue cell death (Figure 5.4A). By immunoblotting analysis of autophagy markers, p62 and LC3, I was also able to observe that LC3-II levels increase in all cell lines upon culture in a galactose-based medium and that higher levels of both markers, p62 and LC3-II indicative of a block in autophagy flux, were detected in *Npc1*$^{-/-}$ MEFs (Figure 5.4B).

In summary, the described sets of experiments suggest that the mitochondrial dysfunction I characterized in *Atg5*$^{-/-}$ MEFs occurs in a model of late-stage autophagy block, the *Npc1*$^{-/-}$ MEFs. To ascertain that *Npc1*$^{-/-}$ MEFs respond to the modulation of ETC, mitochondrial metabolism and ROS scavenging in a similar fashion to *Atg5*$^{-/-}$ MEFs I repeated several key experiments. First, cell transduction with an alternative NADH oxidoreductase, Ndi1, further reduced cellular survival (Figure 5.5A). Second, supplementation of extra substrate in the form of cell-permeable pyruvate significantly increased the rate of cell death in *Npc1*$^{-/-}$ MEFs (Figure 5.5B). Finally, mitochondria- and CI- specific ROS scavenging by $MitoQ_{10}$ and S1QEL2.2, led to a moderate, but significant increase in cell viability (Figure 5.4C,D). I have thus demonstrated that *Npc1*$^{-/-}$ MEFs not only display the key signs of mitochondrial dysfunction found in *Atg5*$^{-/-}$ MEFs, but that their response to metabolic and ETC modulation is analogous to that of *Atg5*$^{-/-}$ MEFs. Lastly, I have demonstrated that mitochondrial ROS contributes to the loss of cell viability in both models of autophagy deficiency.

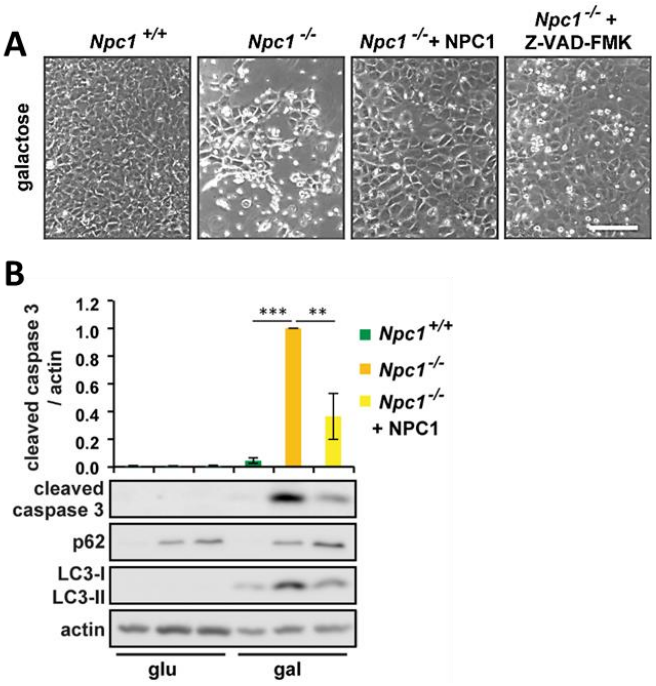

Figure 5. 4 *Npc1*$^{-/-}$ MEFs lose viability upon culture in galactose-based medium

(A) Bright field microscopy images of *Npc1*$^{+/+}$ and *Npc1*$^{-/-}$ MEFs cultured in galactose-based medium only (72h) or supplemented with Z-VAD-fmk (20μM; added to culture medium at 66h). (B) Representative western blot and quantitation of cell death marker, cleaved caspase 3; and of autophagy markers p62 and LC3, in *Npc1*$^{+/+}$, *Npc1*$^{-/-}$, *Npc1*$^{-/-}$ stably expressing NPC1 MEFs cultured in glucose or galactose-based media for 72h. Cleaved caspase 3 levels were normalised to actin. Error bars represent S.E.M. Scale bar represents 200μm. **p<0.01, ***p<0.001. (n=3).

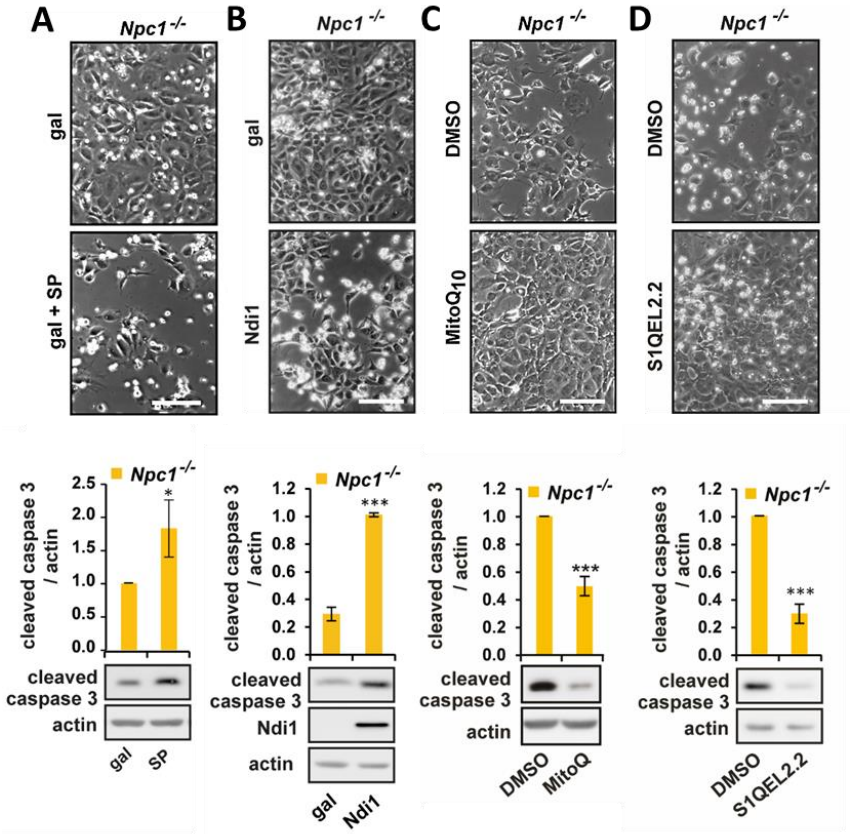

Figure 5. 5 *Npc1*$^{-/-}$ MEFs phenocopy key findings from *Atg5*$^{-/-}$ MEFs upon culture in galactose-based medium

(A-D) Bright field microscopy images; representative western blots and quantitation of caspase 3 cleavage in *Npc1*$^{-/-}$ MEFs transiently transfected with Ndi1 (A); or in *Npc1*$^{-/-}$ MEFs cultured galactose-based medium supplemented with 10mM sodium pyruvate (SP) (B); 20nM $MitoQ_{10;}$ or 500nM S1QEL2.2 all supplemented and re-fed at 0h and at each 24h interval (C,D). Cleaved caspase 3 levels were normalised to actin. Error bars represent S.E.M. Scale bar represents 200µm. *p<0.05, ***p<0.001. (n=3).

5.2.3 Npc1 KO leads to aberrant glucose metabolism and NADH depletion

I have so far established that *Npc1*$^{-/-}$ MEFs show the signs of mitochondrial, and specifically CI dysfunction similar to *Atg5*$^{-/-}$ MEFs. The next logical step was to establish whether NADH depletion underlies the dysfunction I observed. I therefore carried out metabolic profiling of nucleotide and amino acid levels, and intermediates of the glycolysis, PPP and TCA cycle in both cell lines. *Npc1*$^{+/+}$ and *Npc1*$^{-/-}$ MEFs were subjected to metabolite extraction after 48h culture in a galactose-based medium, consistent with the timeframe of mitochondrial bioenergetics measurements. Mass peak data output of the metabolomics study was first corrected to cellular protein levels and then subjected to statistical analysis by MetaboAnalyst 4.0. Log2 conversion of metabolite concentration averages and statistical analysis (the Student's *t*-test with *p* value corrected with false discovery rate (FDR)) of metabolite averages between the *Npc1*$^{+/+}$ and *Npc1*$^{-/-}$ MEFs were plotted in the form of a heatmap (Figure 5.6).

Loss of Npc1 had a variable effect on the levels of amino acids (Figure 5.6). Many amino acids were highly enriched in *Npc1*$^{-/-}$ MEFs, which includes all of the essential amino acids (*in italics*), cysteine, proline and asparagine. In contrast, the three most negatively affected amino acids are aspartate, glutamate and glutamine, which are also among the most abundant, and their depletion could be a result of a loss of protein recycling, impaired biosynthesis/uptake or increased usage. Importantly, glutamine and aspartate are necessary for purine and pyrimidine *de novo* synthesis and their loss could be an indication of a wider dysfunction (Tong, Zhao and Thompson, 2009). In contrast, the first three intermediates of glycolysis, galactose, glucose-6-phosphate, and fructose-1,6-bisphosphate are depleted. Glucose-6-phosphate is an intermediate of both glycolysis and the PPP. Increased utilization of glucose-6-phosphate by the PPP could explain both the relative decrease of an upstream intermediate, galactose-6-phosphate, and the depletion of a downstream glycolysis intermediate, fructose-1,6-bisphosphate. Increased levels of all detected PPP intermediates further support this hypothesis. Importantly, regardless of the changes upstream, the levels of glycolytic metabolites downstream of fructose-1,6-bisphosphate appear to be unperturbed (Figure 5.6).

The relative loss of pyruvate in *Npc1*$^{-/-}$ MEFs could, similarly to glucose-6-phosphate, be rationalized by its increased flux to acetyl coenzyme A (acetyl-CoA) that feeds into the TCA cycle. In fact, the progression of the TCA cycle in the forward direction (from

acetyl-CoA to oxaloacetate) seems to be stalled, suggesting that the whole cycle and NADH/$FADH_2$ generation could be compromised in these cells. In fact, the two most significantly depleted intermediates, 2-oxogluterate (also known as α-ketoglutarate) and malate, together with isocitrate (not detected) are subject to oxidation, and e^- donation to NAD^+. Surprisingly, what could be described as an impairment of mitochondrial bioenergetics, does not seem to have an effect on the levels and charge of the adenine nucleotide. In fact, the only nucleotide that is compromised in both, abundance and charge, is the uridine nucleotide.

Most importantly, I detected a significant depletion of NADH in *Npc1*$^{-/-}$ MEFs, and thus validated the result from *Atg5*$^{-/-}$ MEFs (Figure 4.3). Altogether, metabolite profiling in *Npc1*$^{-/-}$ MEFs revealed signs of dysregulation of all the investigated pathways and depletion of selected amino acids and nucleotides. These results suggest that the central cellular metabolism is perturbed in *Npc1*$^{-/-}$ MEFs to a much higher degree than in *Atg5*$^{-/-}$ MEFs. These findings were not unexpected, considering the different nature of autophagy perturbation in the two models and, in the case of NPC1, the downstream effect of lipid metabolism dysregulation. However, it is possible that the different nature of dysfunction could also lead to a different mechanism of cell death.

In the NPC1 model, I did not explore the underlying mechanism of NADH depletion, but rather focused the study to elucidate whether NAD^+ precursor supplementation can alleviate the dysregulation of cellular metabolism and prevent the observed loss of cell viability upon culture in a galactose-based medium. First, I established that a single dose of NAD^+ precursor, NAM, added to the galactose-based medium prior to culture medium switch, was sufficient to rescue caspase 3 cleavage and cell death in *Npc1*$^{-/-}$ MEFs (Figure 5.7A). Metabolite profiling at 48h confirmed that NAM supplementation boosted levels of NAD^+ and corrected a defect in NADH levels in *Npc1*$^{-/-}$ MEFs (Figure 5.7B). Unexpectedly, NAM supplementation corrected levels of glycolysis and TCA intermediates, and also led to a steady state increase in the levels of all amino acids. These findings reveal a link between NAD(H) levels and/or its function as a co-factor in the cellular metabolism, amino acid import or maintenance. Altogether, NAM supplementation led to a significant improvement in cellular viability and correction of metabolic dysfunction in *Npc1*$^{-/-}$ MEFs.

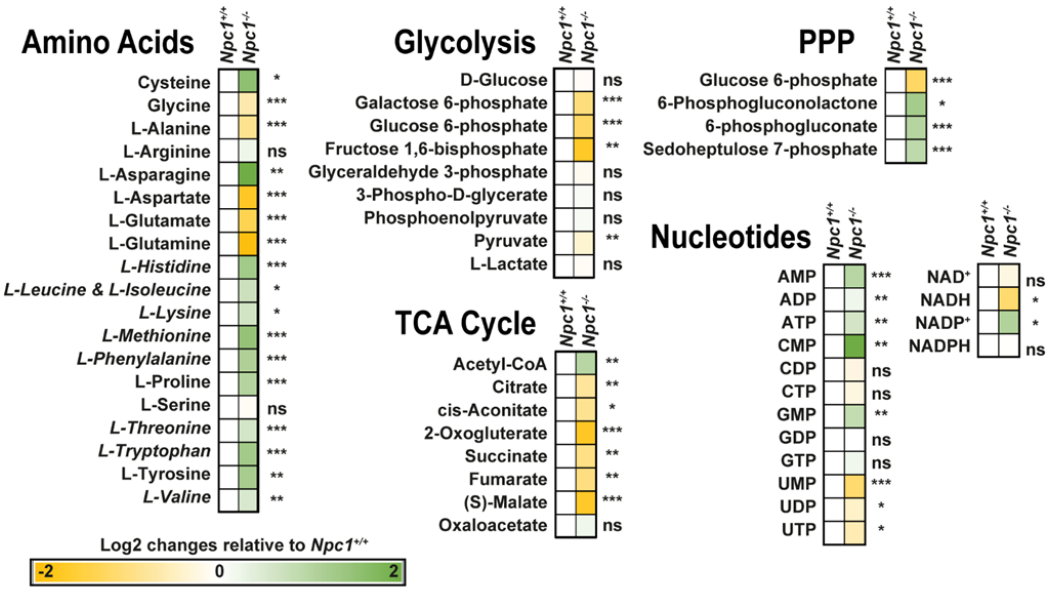

Figure 5. 6 Pathway-identity-based depiction of metabolic data from *Npc1*$^{+/+}$ and *Npc1*$^{-/-}$ MEFs

Metabolites are depicted as a heatmap of Log2(FC) of *Npc1*$^{-/-}$ MEFs to *Npc1*$^{+/+}$ MEFs. Metabolite organization is based on their association to glucose oxidation pathways of glycolysis, pentose phosphate pathway (PPP) and tricarboxylic acid (TCA) cycle. Amino acids are organized alphabetically. Nucleotide order is first alphabetical and depends on the energy charge they carry. Dr Oliver Maddocks carried out LC-MS sample processing.

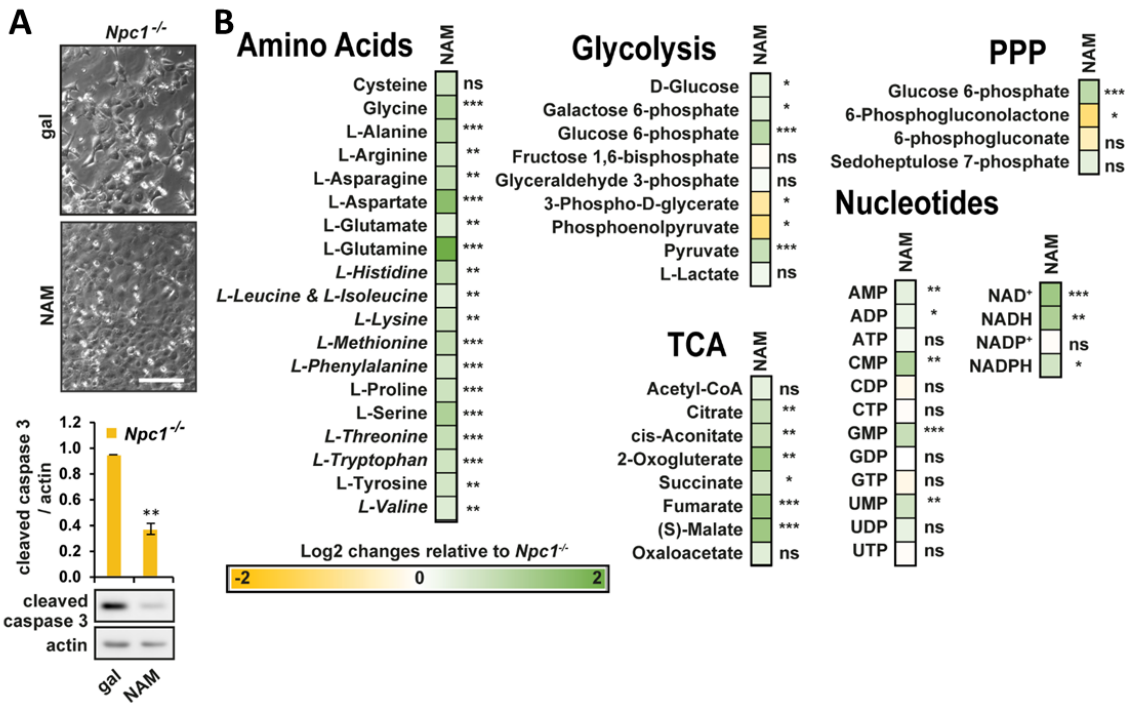

Figure 5. 7 NAM supplementation restores TCA metabolite and nucleotide levels in *Npc1*$^{-/-}$ MEFs

(A) Bright field microscopy images and representative western blots of cleaved caspase 3 in *Npc1*$^{-/-}$ MEFs cultured in a galactose-based medium only or supplemented with NAM. Cells were imaged 72h after medium switch and treatment start when we observed morphological changes associated with apoptosis. Scale bar represents 200µm. Error bars represent S.E.M. Cleaved caspase 3 levels were normalised to actin levels. **p<0.01. (n=3). (B) Metabolites are depicted as a heatmap of log2(FC) of *Npc1*$^{-/-}$ MEFs supplemented with NAM to *Npc1*$^{-/-}$ MEFs cultured in galactose-based medium only. Metabolite extraction was carried out after 48h of culture in a galactose-based medium. Metabolite organization is based on their association with glucose oxidation pathways of glycolysis, pentose phosphate pathway (PPP) or tricarboxylic acid (TCA) cycle. Nucleotide order is first alphabetical and depends on the energy charge they carry. Dr Oliver Maddocks carried out LC-MS sample processing.

5.2.4 Impaired autophagy flux in Npc1$^{-/-}$ MEFs can be restored by small molecule supplementation

Our initial hypothesis states that it is the block in autophagy that stands at the root of dysregulated mitochondrial and NAD(H) metabolism. I have thus far confirmed that mitochondrial and NAD(H) dysfunction does occur in *Npc1*$^{-/-}$ MEFs and that cell death in this model can be attenuated by either ROS scavenging or NAM supplementation. To establish that autophagy impairment is ultimately responsible for the observed molecular phenotypes and loss of cell viability, I sought to examine whether reconstitution of autophagy flux in *Npc1*$^{-/-}$ MEFs protects these cells from apoptotic cell death.

Previous studies demonstrated that autophagic flux can be restored in *Npc1*$^{-/-}$ MEFs (Sarkar *et al.*, 2013; Maetzel *et al.*, 2014). Two lines of inquiry identified three interventions to induce autophagy flux in these cells: starvation and rapamycin (which trigger mTOR-dependent autophagy induction (Maetzel *et al.*, 2014)), and lithium chloride (mTOR-independent autophagy induction (Sarkar *et al.*, 2013)). I chose rapamycin and lithium chloride as positive controls for this experiment. Further choice of tested compounds was based on a recent screening study carried out in the lab in collaboration with Dr Peter Banks (High Throughput Facility, Newcastle University), which aimed to identify compounds capable of restoring autophagy flux in *Npc1*$^{-/-}$ MEFs cultured in a glucose-based medium (unpublished data). The two hits of interest in the screen were rofecoxib and celecoxib.

I chose to initially test celecoxib, an FDA approved compound that inhibits cyclooxygenase-2, an enzyme involved in pro-inflammatory signalling (Davies *et al.*, 2000). Celecoxib was first approved for treatment of osteoarthritis and rheumatoid pain, but is currently the subject of over 16 active and recruiting, and over 40 completed phase 4 clinical trials due to observations of its multiple cellular targets and an anti-proliferative effect in cancer models (https://clinicaltrials.gov/) (Gong *et al.*, 2012). Published studies disagree on the effect of celecoxib on autophagy. It was first shown to induce autophagy in cancer cell lines (Huang and Sinicrope, 2010; Liu *et al.*, 2014) and later reported to inhibit autophagy due to increased lysosomal pH in a leukaemia cell line (Lu *et al.*, 2016). Altogether, I selected rapamycin (as a positive control), lithium chloride, celecoxib and hydroxycelecoxib (an inactive metabolite of celecoxib as a negative control) for testing.

I first established the dosage for each compound based on previous literature and their toxicity in cells cultured in the galactose-based medium. I then supplemented the galactose-based medium with each compound and observed LC3-II levels, as a direct readout of steady-state autophagosome number, and p62 levels as a readout of autophagosome turnover (Klionsky *et al.*, 2012). To determine autophagic flux, I carried out all experiments in the presence or absence of bafilomycin A1 (BAF A1) at a saturating concentration. BAF A1 is an inhibitor of lysosomal V-ATPase, that leads to lysosomal pH neutralization and thereby loss of autophagosome degradation (Klionsky *et al.*, 2012). LC3-II and p62 levels were then compared between untreated (steady state) and BAF A1 treated conditions (flux).

I first observed that levels of both, LC3-II and p62 increase in all BAF A1 supplemented conditions in *Npc1*$^{+/+}$ MEFs, suggesting that galactose-based culture alone induces autophagy in wild type cells (Figure 5.8A). Increase of LC3-II and p62 levels in BAF A1 supplemented conditions seems less prominent in *Npc1*$^{-/-}$ MEFs (Figure 5.8B). I further detected a decrease in steady state levels of p62 in both cell lines upon the treatment with rapamycin (Rap) and celecoxib (Figure 5.8A,B). By BAF A1 supplementation I confirmed that p62 degradation in these conditions is mediated by autophagy (Figure 5.8A-D). Similarly, I detected an increased LC3-II ratio in BAF A1 treated cells cultured in the presence of rapamycin and celecoxib relative to steady-state levels, a result that is indicative of increased autophagy flux (Figure 5.8C,D). Cell supplementation with hydroxycelecoxib had no effect on any of the examined readouts and does not seem to be involved in autophagy regulation. Interestingly, lithium chloride (LiCl) that was previously shown to induce autophagy in *Npc1*$^{-/-}$ MEFs (Sarkar, 2013) had no effect on autophagy flux in cells cultured in a galactose-based medium. In summary, I confirmed that rapamycin treatment improves autophagic flux in both cell lines and discovered that celecoxib supplementation mimics the effect of rapamycin, though the mechanism of autophagy induction by celecoxib remains unknown.

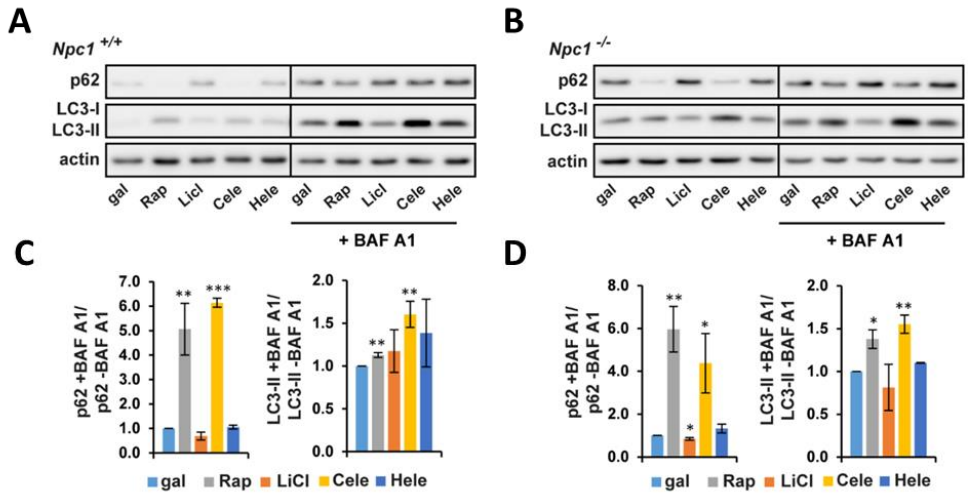

Figure 5. 8 Autophagy can be restored in *NPC1*$^{-/-}$ MEFs

(A-D) Rapamycin and celecoxib boost autophagy flux in *Npc1*$^{+/+}$ and *Npc1*$^{-/-}$ MEFs. Representative western blots of autophagy markers, p62 and LC3, in *Npc1*$^{+/+}$ MEFs (A) and *Npc1*$^{-/-}$ MEFs (B), cultured in the galactose medium only, or supplemented with 100nM rapamycin (Rap), 10mM lithium chloride (LiCl), 10μM celecoxib (Cele) or 2.5μM hydroxycelecoxib (Hele) in the presence or absence of 100nM bafilomycin A1 (BAF A1) for 24h. Quantitation of p62 and LC3-II levels in *Npc1*$^{+/+}$ MEFs (C) and *Npc1*$^{-/-}$ MEFs (D) in the same conditions as (A,B). Error bars represent S.E.M. Levels of autophagy markers were first normalised to actin and later expressed as a ratio between +BAF A1 and steady state conditions. *p<0.05, **p<0.01, ***p<0.001. (n=3).

5.2.5 Autophagy restoration promotes cell viability in Npc1$^{-/-}$ *MEFs*

Having established that rapamycin and celecoxib induce autophagy flux in *Npc1*$^{-/-}$ MEFs, I examined their effect on cellular viability. As predicted, a single dose of rapamycin and celecoxib at 0h that were shown to increase autophagic flux were also sufficient to prevent caspase 3 cleavage and cell death (Figure 5.9A,B). Supplementation with hydroxycelecoxib had no effect on cell survival. Unexpectedly, lithium chloride, despite not having restored autophagy flux in this model, led to cell death rescue. I did not examine this result in any more detail, but it might be worth a further investigation as it might provide an alternative route to rescue dysfunction in this cell line. Many studies report the beneficial effect of lithium supplementation on mitochondrial respiration and mMP (Bachmann *et al.*, 2009), CI activity (de Sousa *et al.*, 2015) and mitochondrial mobility (Chen *et al.*, 2010), some or all of which could be a result of increased autophagy-mediated clearance of dysfunctional mitochondria.

However, studies also suggest that lithium treatment induces increased expression of anti-apoptotic Bcl-2 protein and decreased expression of pro-apoptotic BAX protein (Chen and Chuang, 1999; Chen *et al.*, 1999; Youdim and Arraf, 2004), which might be worth following up as it could lead to cell death prevention downstream of autophagy impairment, mitochondrial dysfunction and NADH depletion by opposing apoptosis.

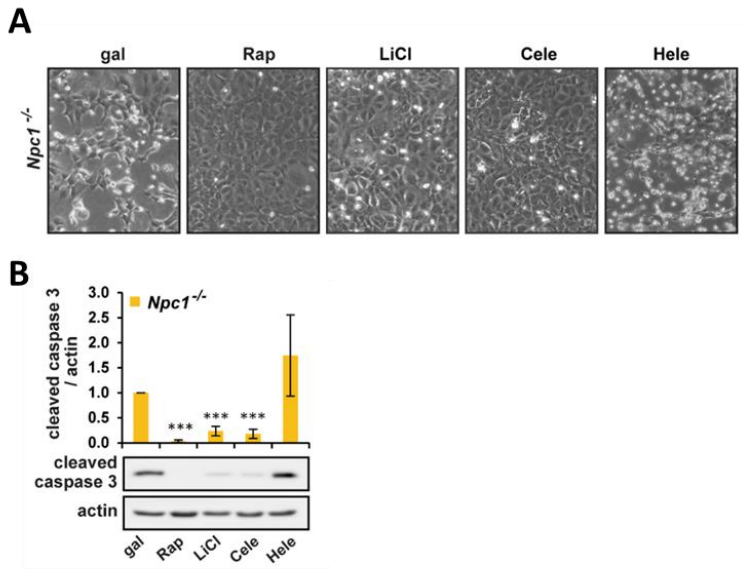

Figure 5. 9 Multiple tested compounds rescue cell death in *Npc1*$^{-/-}$ MEFs

(A) Representative bright field microscopy images of *Npc1*$^{-/-}$ MEFs cultured in the galactose medium only, or supplemented with 100nM rapamycin (Rap), 10mM lithium chloride (LiCl), 10μM celecoxib (Cele) or 2.5μM hydroxycelecoxib (Hele) for 72h. (B) Quantitation of caspase 3 cleavage in the same conditions as (A). Cleaved caspase 3 levels were normalised to actin. Error bars represent S.E.M. ***p<0.001. (n=3).

5.3 Investigation of NPC1 human patient fibroblasts

Human NPC1 patient fibroblasts and age-matched controls were used to investigate the translational potential of my results from the studies using mouse models of autophagy deficiency, the *Atg5* KO and *Npc1* KO MEFs. Five female cell lines were selected per group with the aim of achieving the best possible age-match. All selected NPC1 patient cell lines were previously shown to have a defect in cholesterol esterification and positive filipin staining, which are the staple laboratory procedures utilized in NPC1 diagnosis (Park *et al.*, 2003). Cell line selection was aimed to achieve a coverage of juvenile and adult-onset of disease and to include a wide range of common and rare, non-sense, mis-sense and frameshift NPC1 mutations (Table 5.1) (Park *et al.*, 2003; Geberhiwot *et al.*, 2018). Four patients (NPC1 1-4) carry two different *NPC1* mutations, most of which occur in the lysosomal lumen (L) I region of loop I (D874V, Y890X, P1007A, T1036M, (and also I1061T). Other mutations occur in lumen A region (c.451_452delAG), lumen M region (F1221), a transmembrane (TM) V region (D700N) and in a cytoplasm (C) H region (T825C) (Davies and Ioannou, 2000; Park *et al.*, 2003). The fifth patient was homozygous for the most prevalent NPC1 mutation, the I1061T missense that results in an increased targeting of the mutated, but functional NPC1 protein for degradation by the proteasome (Gelsthorpe *et al.*, 2008). Interestingly, each patient carried at least one allele with a mutation on the vesicle lumen-facing region of NPC1. Patients 1, 3 and 5 all carried both mutations in the loop I region, while patients 2 and 4 carried their lumen-facing mutations in loop A and an unstructured C-terminus-proximal lumen region, respectively (Davies and Ioannou, 2000). To the best of my knowledge, none of these cell lines had been previously profiled with respect to an autophagy defect.

Table 5. 1 Primary human fibroblasts used in this study

Study Label	Catalogue ID	Gender	Age	Disease Affected	Allele 1 Mutation Allele 2 Mutation
CTRL (1)	10176	Female	24	no	none
CTRL (2)	10263	Female	21	no	none
CTRL (3)	10632	Female	22	no	none
CTRL (4)	10705	Female	26	no	none
CTRL (5)	10763	Female	21	no	none
NPC1 (1)	GM17912	Female	11	yes	[P1007A]^{L};[T1036M)]^{L}
NPC1 (2)	GM17924	Female	21	yes	c.451_452delAG^{L};[Y825C]^{C}
NPC1 (3)	GM18387	Female	33	yes	[D874V]^{L};[Y890X]^{L}
NPC1 (4)	GM18402	Female	10	yes	[D700N]^{TM};[F1221fsX]^{L}
NPC1 (5)	GM18417	Female	25	yes	[I1061T]^{L}; [I1061T]^{L}

5.3.1 *Identification of autophagy deficiency in NPC1 patient fibroblasts*

Autophagy impairment in CTRL and NPC1 patient fibroblasts was monitored in glucose-based medium by steady state number of LC3 puncta, which correlate with autophagosome formation and degradation (Klionsky and Emr, 2000; Sarkar *et al.*, 2013). The number of steady-state LC3 puncta in all control human fibroblasts was low (less than 10 per cell) (Figure 5.10A,B). Intriguingly, the variability of LC3 puncta numbers was high in NPC1 patient fibroblasts (Figure 5.10A) and led to identification of two cell lines with no apparent autophagy impairment (NAI), and three cell lines with a potential autophagy impairment (AI) (Fig 5.1A,B). To confirm the absence and presence of an autophagy defect in NPC1 cells, whole cell lysate levels of LC3-II were monitored under conditions of inhibition of autophagosome fusion with the lysosome by treating cells with BAF A1 at a saturating concentration. CTRL cells displayed low levels of LC3-II in steady state conditions, which increased upon a four hour treatment with BAF A1 (Figure 5.10C). Analysis of NPC1 cells revealed variable LC3-II levels at steady state and an irregular effect of LC3-II accumulation upon the treatment with BAF A1 (Figure 5.10C). Patient cell lines 1 and 2 (NPC1 (1) and NPC1 (2)), which had low numbers of LC3 puncta also displayed lower steady state levels of LC3-II (Figure 5.10C). NPC1 samples re-run in a shuffled order to dispel the possibility of a gel edge-effect confirmed that NPC1 cell lines 1 and 2 are autophagy efficient (Appendix 2). In contrast, western blot analysis of NPC1 cell lines 3-5 corroborated results from immunofluorescence and confirmed that these cells are autophagy deficient, though autophagy flux does not appear to be blocked completely (Figure 5.10D). Three CTRL cell lines (2, 3 and 5) were then selected, based primarily on their growth rate, to

complement analysis of the three autophagy-deficient NPC1(3-5) cell lines. A repeated western blot run that contains the six selected cell lines further reveals the true extent of LC3-II accumulation in NPC1 cell lines as loaded next to CTRLs (Figure 5.10E).

I have previously established that NADH levels decrease in models of autophagy deficiency (Figures 4.3 and 5.7) and sought to examine whether this relationship persists in patient-derived cells presenting with a partial block in autophagy. To replicate the culture conditions from my MEF-based study, I cultured CTRL and NPC1 patient fibroblasts in the galactose-based medium. All cells were able to tolerate sub-culture in the galactose-based media with no apparent signs of cell death. I thus cultured cells for 14 days and characterized cellular NAD(H) and ROS levels as well as collecting cells for metabolic profiling. A kit-based measurement of NAD(H) levels was not sensitive enough to detect the levels of NADH in either CTRL or NPC1 cell lines (data not shown). Instead, I detected a significant depletion of whole-cell NAD^+ levels in NPC1 (AI) cell lines relative to the CTRL cells (Figure 5.11A). NAD^+ levels were not affected in NPC1 patient fibroblasts that do not have a defect in autophagy (NAI) (Figure 5.11A). Metabolic profiling of the three CTRL (2,3,5) and three NPC1 (3-5) cell lines further verified the kit-based measurement by detecting a significant reduction in NAD^+ levels (Figure 5.11B). This method also detected a large and highly significant depletion of NADH, and corroborated my findings from genetic autophagy-deficient models. In addition, although glycolysis and nucleotide levels do seem to be affected in NPC1 patient cells, the perturbations do not mirror those identified in *Npc1*$^{-/-}$ MEFs and the TCA cycle in NPC1 patient fibroblasts is not perturbed. Lastly, I performed a flow cytometry-based analysis of cellular ROS levels by a H2DCFDA stain and detected a significantly higher levels of ROS in all three NPC1 (AI) cell lines when compared to CTRLs (Figure 5.11C,D; Appendix 3).

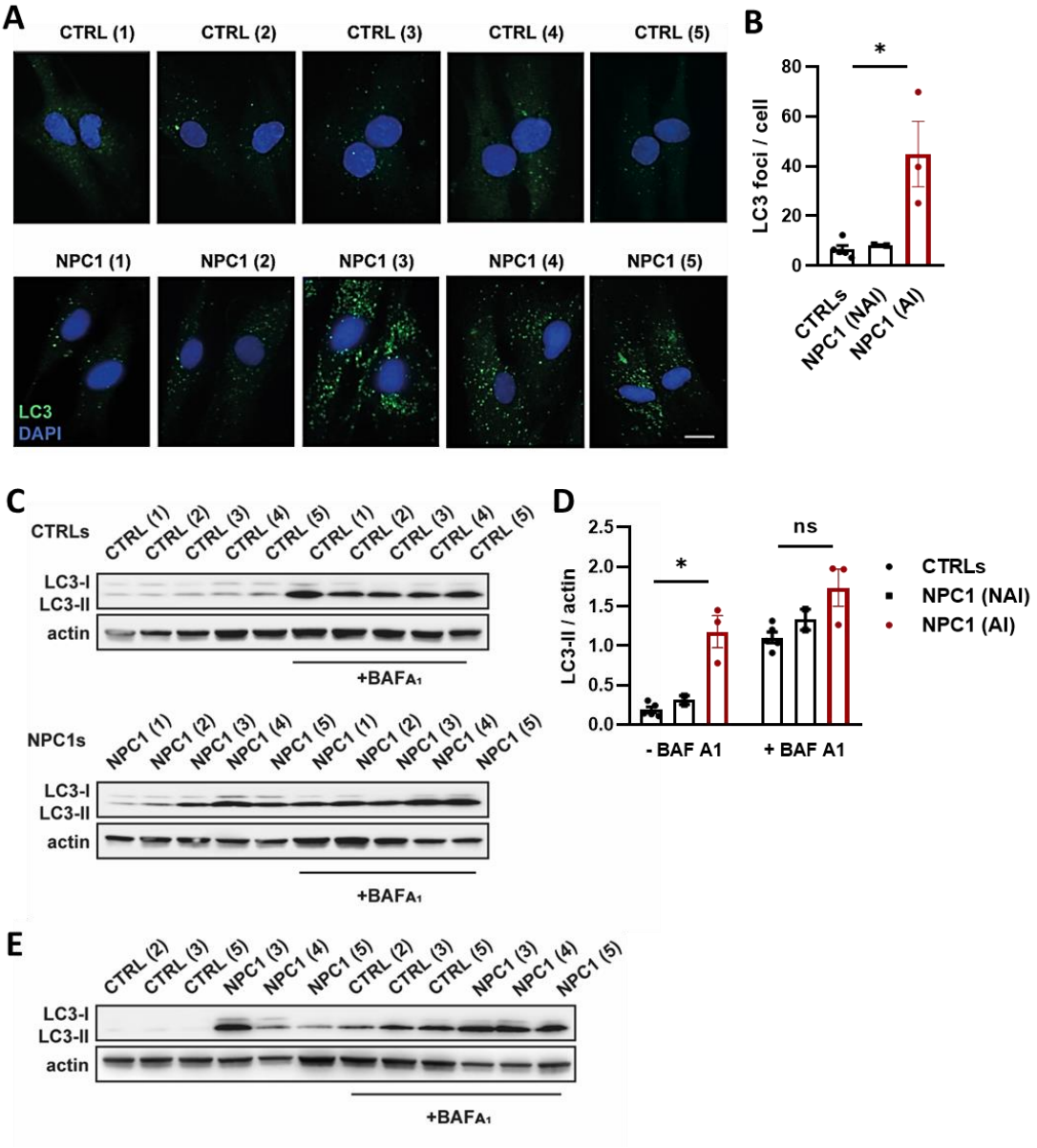

Figure 5. 10 Autophagy deficiency is present in some NPC1 patient fibroblasts

(A) Immunofluorescence staining with anti-LC3 antibody in CTRL and NPC1 patient fibroblasts. (B) LC3 puncta quantification in the same conditions as (A) following patient cell line classification into cells displaying no autophagy impairment (NAI) or autophagy impairment (AI). Scale bar represents 20µm. (C-D) Representative immunoblots and combined analysis of cellular autophagy levels in control and NPC1 patient fibroblasts treated with 100nM bafilomycin A1 (BAF A1) or vehicle (DMSO) for 24h. Error bars represent S.E.M. LC3 levels were normalised to actin. *p<0.05.

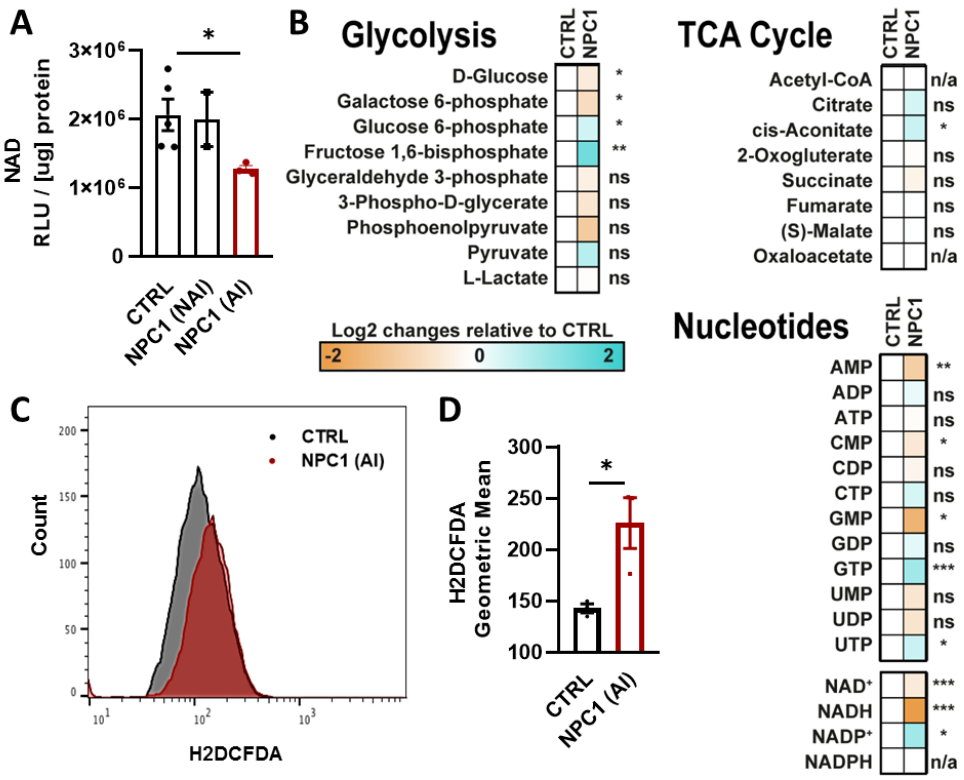

Figure 5. 11 Reduced NAD(H) levels and increased ROS are detected in NPC1 patient fibroblasts

(A) NAD level measurement by Promega's NAD/NADH-GloTM assay corrected for cellular protein levels in CTRL and NPC1 patient fibroblasts after sub-culture in the galactose-based medium. Data from NPC1 cell lines was split based on cell classification of displaying no autophagy impairment (NAI) or autophagy impairment (AI). (B) Metabolite profiling in CTRL and NPC1 (AI) cells. Metabolites are depicted as a heatmap of log2(FC) of NPC1s to CTRLs. Metabolite organization is based on their association with glucose oxidation pathways of glycolysis and tricarboxylic acid (TCA). Nucleotide order is first alphabetical and depends on the energy charge they carry. (C) Representative flow cytometry peaks of CTRL and NPC1 cellular ROS levels detected by H2DCFDA fluorescence intensity after sub-culture in the galactose-based medium (same conditions and length as (A) and (B). (D) Quantitation of H2DCFDA fluorescence intensity differences between CTRL and NPC1 (AI) cells. Error bars represent S.E.M. * $p < 0.05$. Dr Oliver Maddocks carried out LC-MS sample processing.

5.3.2 Autophagy deficiency in patient fibroblasts correlates with NAD depletion and increased sensitivity to ROS

Despite increased cellular ROS load and a significant depletion in both NAD^+ and NADH, NPC1 human fibroblasts do not die upon prolonged culture in a galactose-based medium. Increased susceptibility of NPC1 patient fibroblasts to exogenous stress was previously reported in glucose-based culture (Zampieri *et al.*, 2009). To determine whether depletion of NAD(H) in NPC1 patient fibroblasts increases their sensitivity to a short burst of oxidative stress, fibroblasts sub-cultured in a galactose-based medium for 14 days were exposed to increasing concentrations of H_2O_2. The percentage of viable cells was determined in NPC1 (AI) and CTRL human cell lines immediately after exposure to H_2O_2 by the MTT assay, in which 3-(4,5-Dimethyl-2-thiazolyl)-2,5-diphenyl-2H-tetrazolium bromide, a yellow water-soluble compound gets converted to a water-insoluble purple formazan crystals by mitochondrial dehydrogenases (Riss *et al.*, 2016). Cell viability response to increasing H_2O_2 supplementation was non-linear in CTRL and NPC1 cell lines. CTRL fibroblasts tolerate H_2O_2-induced oxidative stress at low H_2O_2 doses (Figure 5.12A). In fact, low doses of H_2O_2 seem to initiate a hormetic effect in CTRL cell lines by increasing their metabolic activity and redox potential, as measured by an increased conversion of MTT to formazan to the levels above baseline (Figure 5.12B). The two highest H_2O_2 doses I tested, 700μM and 1000μM respectively led to an approximately 50% and 100% decrease in cellular viability (Figure 5.12A,B).

In contrast, all tested H_2O_2 concentrations had a negative impact on the viability of NPC1 patient fibroblasts (Figure 5.12A). % viability of NPC1 cells as a function of H_2O_2 dose followed a common non-linear sigmoidal shape often observed in dose-response relationships. To test this relationship, I carried out a non-linear regression analysis of cell viability as a function of H_2O_2 dose dependency on cell viability data collected from NPC1 and CTRL cell lines using a log(H_2O_2) vs normalized response (0%-100%)-variable slope equation. Goodness of model fit analysis indicates that CTRL cell line response to H_2O_2 challenge does not fit the shape of a dose response curve, most likely due to the initial hormetic effect. In contrast, viability of NPC1 cells challenged with H_2O_2 is dose dependent, and my analysis indicates a good fit to the model, despite the non-Gaussian distribution of NPC1 data residuals (Figure 5.12C).

To explore the causative relationship between NAD(H) depletion and increased sensitivity to oxidative stress, one NPC1 (AI) human fibroblast cell line was selected for supplementation with increasing concentrations of two substrates of the NAD^+ salvage pathway, NMN and NAM. Both, NAM (1.0mM, 2.5mM, 5.0mM) and NMN (0.1mM, 0.25mM, 1.00mM) supplementation led to a linear increase in cellular NAD^+ levels (Figure 5.13A,B). NAM and NMN supplementation led to a dose-dependent rescue of cell viability, with the highest doses leading to cell viability recovery to approximately 100% (Figure 5.13C,D). In addition, the distribution of residuals of non-linear regression analysis did fit a Gaussian distribution (Figure 5.13C,D) and correlation analysis revealed a very strong positive correlation between NAD^+ levels and viability in NAM ($r=0.9522$, $R^2=0.9068$, $p=0.0478$) and NMN ($r=0.9941$, $R^2=0.9882$, $p=0.0059$) supplemented cells. Of note is that although lower doses of NMN were used for practical reasons, 1mM dose of NMN achieved a similar recovery of NAD^+ levels as a 1mM dose of NAM (0.0 data point on both x-axes) and seems to be as potent as 5mM dose of NAM in preventing loss of cell viability (Figure 5.13A,B). This observation could be a result of the NAM-mediated inhibition of cellular NADases, whereas no adverse effects of NMN supplementation have been described (Watson, Askew and Benson, 1995; Westphal, Dipp and Guarente, 2007; Marshall, Borbon and Erickson, 2017). Altogether, I conclude that NAD depletion in NPC1 patient fibroblasts directly leads to increased sensitivity to oxidative stress, which can be alleviated by supplementation of NAD^+ precursors and NAD^+ level recovery.

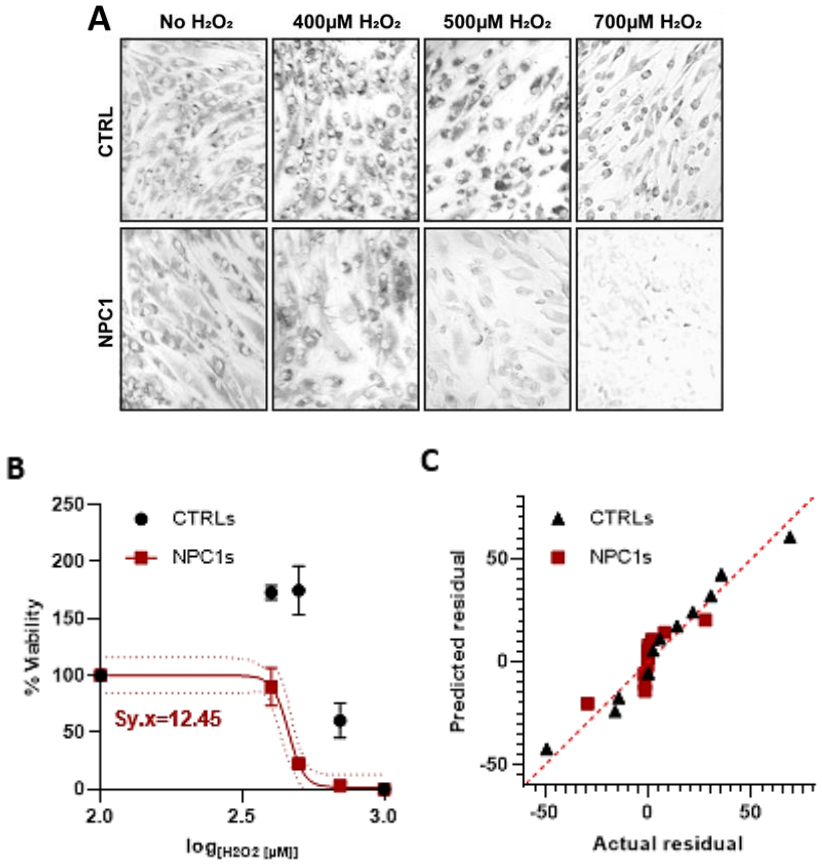

Figure 5. 12 NPC1 fibroblasts display increased sensitivity to exogenous oxidative stress

(A) Representative bright field microscopy images CTRL and NPC1 cell lines sub-cultured in the galactose-based medium, challenged with H_2O_2 treatment for 2h and processed by the MTT assay. (B) Modelled dose-response relationship of cell viability in the same conditions as (A). Dotted line represents a 95% confidence interval. Sy.x represents the standard deviation of regression residuals. (C) Quantile-Quantile plot of non-linear regression analysis residuals.

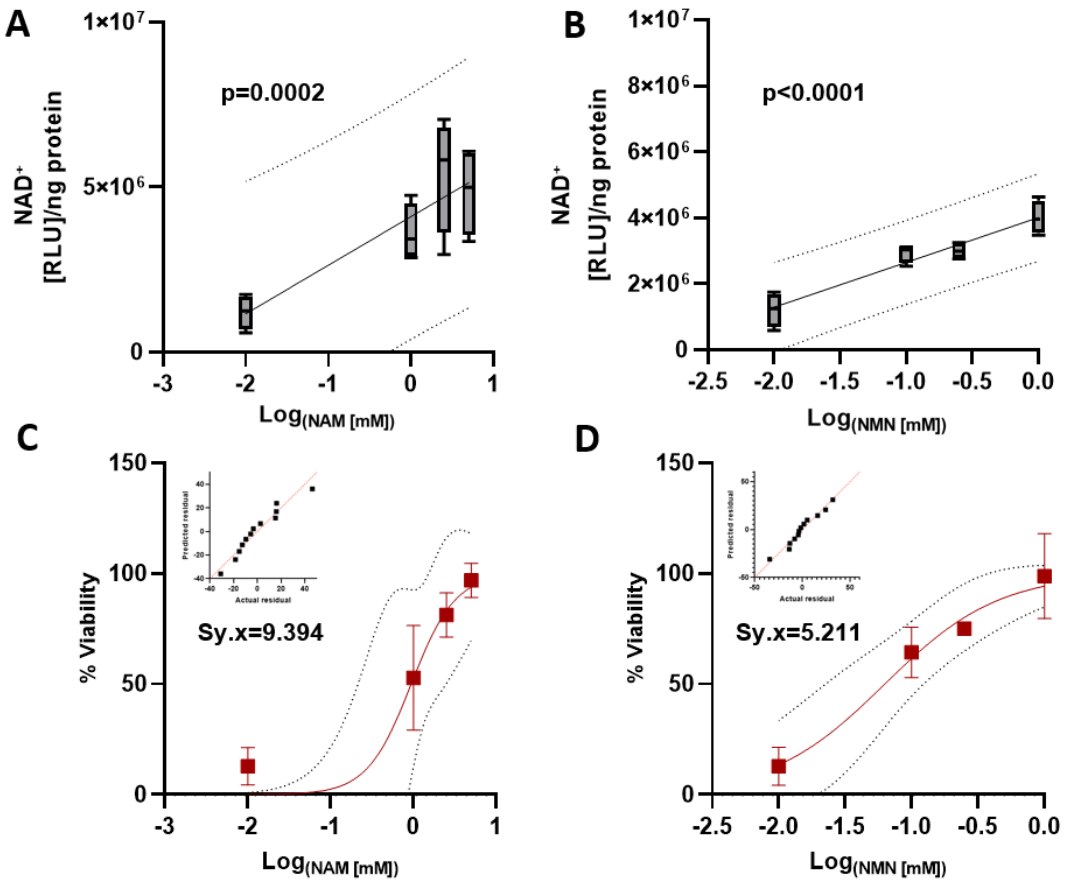

Figure 5. 13 NAD^+ recovery correlates with cell viability in NPC1 fibroblasts challenged with H_2O_2

(A,B) Long-term supplementation of NAD^+ precursors leads to recovery of cellular NAD^+ levels. NAD level measurement by Promega's NAD^+/NADH-Glo™ assay corrected for cellular protein in NPC1 (AI) cell line sub-cultured in the galactose-based medium supplemented with (A) 1mM, 2.5mM and 5mM NAM and (B) 0.1mM, 0.5mM and1mM NMN. (C-D) NAD^+ level recovery protects cells from H_2O_2-induced cell death. Modelled dose-response relationship of cell viability in the same conditions of NAM (C) and NMN (D) supplementation as (A,B). Miniaturized plots represent the Quantile-Quantile plots of non-linear regression analysis residuals. p values were calculated by linear regression analysis. Dotted lines represent a 95% confidence interval. Sy.x represents the standard deviation of regression residuals.

5.4 Chapter Conclusions

The aim of this chapter was to explore whether the cellular dysfunction characterized as a result of autophagy impairment in a genetic model translates to a model relevant to human disease. First, I characterized the bioenergetics dysfunction in immortalized *Npc1*$^{-/-}$ MEFs glucose- and galactose-based culture conditions. I detected an increased dependency of glucose-addicted *Npc1*$^{-/-}$ MEFs on ATP production via glycolysis (Figure 5.1A,B), but no apparent loss of ATP production potential (Figure 5.2C). Further analysis of ETC function and structure uncovered a CI-linked respiration defect (Figure 5.2A-C) and an isolated loss of CI subunits (Figurer 5.3.D). A switch of *Npc1*$^{+/+}$ and *Npc1*$^{-/-}$ MEFs to a galactose-based medium led to an increased dependency of energy generation on OXPHOS, evidenced by increased levels of ETC subunits and SC assembly, and mitochondrial ROS generation (Figure 5.3). Prolonged galactose-based culture also led to apoptotic cell death in *Npc1*$^{-/-}$ MEFs (Figure 5.4). Metabolic profiling of *Npc1*$^{+/+}$ and *Npc1*$^{-/-}$ MEFs revealed disruption in glucose oxidation pathways in *Npc1*$^{-/-}$ MEFs and, most importantly, confirmed my findings from *Atg5*$^{-/-}$ MEFs by detecting a depletion in NADH levels (Figure 5.4). Cell death of *Npc1*$^{-/-}$ MEFs upon culture in a galactose-based medium can be alleviated at all three stages of dysfunction. A continuous supplementation of culture media with ROS scavengers (Figure 5.5), or single doses of NAM (Figure 5.7) and autophagy inducers, rapamycin and celecoxib (Figure 5.9), were all capable of preserving cell viability.

Female NPC1 patient fibroblasts and age-matched CTRL primary cell lines were utilized to study the effect of autophagy-deficiency in a patient-relevant model. Autophagy flux and autophagosome number of two NPC1 cell lines resembled those of CTRL cell lines (Figure 5.10). Of the two cell lines, NPC1 (1) carries mutations in protein regions that face the vesicle lumen (Davies and Ioannou, 2000) and are also the 2nd and 3rd most prevalent (Park *et al.*, 2003). NPC1 (2) carries mutations that face both, the cytoplasm and the vesicle lumen, but are not common (Park *et al.*, 2003) and also do not seem to interfere with autophagy flux. However, I did identify three NPC1 cell lines with a clear autophagy impairment (Figure 5.10). The autophagy defect was strongest in the NPC1 (3) fibroblasts (Figure 5.10) that carry one common mutation, the D874V substitution in the loop I region (Davies and Ioannou, 2000; Park *et al.*, 2003). NPC1 (4) carries an uncommon D700N substitution in a transmembrane domain and a frameshift mutation at the C-terminal lumen-facing region of NPC1.

Importantly, NPC1 (5) patient is homozygous for the most prevalent I1061T mutation and presents with an autophagy dysfunction. It would be interesting to see whether the I1061T mutation would have a similar effect in a heterozygous scenario and thus increase the relevance of my findings to a wider circle of NPC1 patients. I have also established that autophagy deficiency in NPC disease correlates with NAD(H) depletion and increased sensitivity to oxidative stress which leads to cell death when challenged with H_2O_2 (Figures 5.11 and 5.12). Finally, NAD^+-boosting strategies in the form of NAM and NMN supplementation improve cell resistance to exogenous oxidative stress in a dose-dependent manner and could thus be considered as therapeutics in treating NPC disease presenting with an autophagy impairment. Crucially, not all *NPC1*-disease causing mutations lead to autophagy impairment and only testing more patient cell lines would lead to a proper estimate of the therapeutic potential of NAD precursor supplementation, if proven to have a benefit in preventing NPC disease progression.

5.5 Chapter Discussion

5.5.1 Npc1$^{-/-}$ MEF study relevance to neurodegeneration and NPC1 biomarkers

In this study, I first employed a genetic model of NPC1 disease, the *Npc1*$^{-/-}$ MEFs as an intermediate step between studies of a complete genetic interruption of autophagy (*Atg5*$^{-/-}$ MEFs) and study of human patient fibroblasts. Bioenergetics analysis of both immortalized MEF cell lines showed a small, but significant re-wiring of cellular ATP production to glycolysis (Figures 3.1 and 5.1). It is also worth keeping in mind that while total loss of the Npc1 protein in MEFs led to the disruption of glucose oxidation pathways, this was not observed in either *Atg5*$^{-/-}$ MEFs or NPC1 fibroblasts. Evidence from NPC1 mouse models and human NPC1 tissue suggests that metabolic re-wiring towards glycolysis does occur in disease-relevant tissues. First, study of NPC patient cerebrospinal fluid and post-mortem brain tissue revealed increased presence of neuroinflammation markers and glial activation, respectively (Cologna *et al.*, 2014). Chronic glial activation promotes an inflammatory response and ROS release that are thought to be central to brain pathology (Thameem Dheen, Kaur and Ling, 2007). Cellular re-wiring towards glycolysis was recently observed in activated microglia from *Npc1*$^{-/-}$ mouse model (*Npc1*^{nih}) that best recapitulates the human neurodegenerative phenotype (Cougnoux *et al.*, 2016). Microglia activation was mechanistically linked to increased stabilization of the hypoxia-inducible factor 1-alpha (HIF1α) expression.

Importantly, mouse treatment with HPβCD prevented HIF1α stabilization and glial activation in *Npc1*$^{-/-}$ mice, thus showing that the molecular trigger for glial re-programming could be cholesterol accumulation. Also in this study, increased levels of HIF1α were found in post-mortem cerebellar tissue from NPC patients. Results of these studies collectively show that *Npc1*$^{-/-}$ cells that are capable of metabolic re-wiring, i.e. microglia, do likely depend on increased glucose uptake, glycolytic ATP production, and PPP activation to produce NADPH and induce the activity of NADPH oxidase to produce ROS (Orihuela, McPherson and Harry, 2016). Chronic microglial activation could contribute to the neurodegenerative phenotype by releasing ROS species that can challenge nearby neurons.

Furthermore, metabolic profiling of *Npc1*$^{-/-}$ MEFs revealed that levels of several amino acids were disrupted, a phenomenon not observed in *Atg5*$^{-/-}$ MEFs. Due to a limited sample size collected for LC-MS analysis, I was not able to probe amino acid levels in NPC patient fibroblasts. It is therefore difficult to establish whether these aberrant findings are relevant to NPC1 disease or simply artefacts of genetic Npc1 depletion and cell culture. Results of two studies from a single group support my finding of amino acid aberrations in NPC1 disease (Ruiz-Rodado *et al.*, 2014; Probert *et al.*, 2017). The authors of these two studies set out to identify biomarkers of NPC disease by proton nuclear magnetic resonance (^{1}H NMR) profiling. First, urinary metabolic profiling of NPC1 patients and their heterozygous parent identified elevated levels of primarily branched-chain amino acids (leucine, isoleucine and valine) in NPC patients (Ruiz-Rodado *et al.*, 2014). A further study was carried out by blood sample profiling of NPC patients, untreated and treated with Miglustat, NPC heterozygous parents, and healthy control individuals (Probert *et al.*, 2017). Multivariate analysis of collected data suggested that, in addition to the expected disturbances in the levels of lipids, circulating lactate levels strongly contributed to the variation observed between NPC1 patient and healthy control samples. Furthermore, isoleucine, enriched in *Npc1*$^{-/-}$ MEFs in my study, was also increased in circulation of NPC patients compared to healthy control. Similarly, enrichment of histidine was identified as a discriminatory variable between NPC patients and heterozygous individuals (Probert *et al.*, 2017). Although these studies of metabolite levels originate from a single group, their results together suggest that NPC1 patients do in fact present with altered amino acid equilibrium, though the relevance of this observation to NPC disease pathology is unknown.

Interestingly, the urinary metabolic analysis of NPC patients and their heterozygous parents also parallels my profiling of *Npc1*$^{-/-}$ MEFs in another aspect, namely the pathway of nicotinic acid/nicotinamide metabolism that seemed to be disproportionately affected in NPC patients (Ruiz-Rodado *et al.*, 2014). Specifically, nicotinic acid (NA), nicotinamide mononucleotide (NMN) amide and degradation products of NAM generated in the liver (2PY, 4PY) were all low in urine samples from NPC patients. In contrast, levels of nicotinamide riboside (NR) and quinolinic acid (QA) were increased. Authors of this study hypothesized that the changes in NAD^+ precursors and degradation products could be a sign of niacin deficiency, though the causes and consequences of disrupted NA and NAM metabolism are not known. Lastly, except for a single small-scale juvenile-onset NPC1 mouse study, in which NAD+ supplementation improved some cognition phenotypes, (Marshall, Borbon and Erickson, 2017) the extent of dysfunction in NAD(H) metabolism and the potential of NAD(H) boosting therapies has not yet been explored.

5.5.2 NPC1 patient fibroblast study relevance to published research

Isolation of patient fibroblasts and study of cholesterol esterification and filipin levels is commonly used in NPC diagnosis (Park *et al.*, 2003). However, the relevance of a study carried out in fibroblasts to cells and tissues affected by the disease, i.e. spleen, liver and brain, remains to be established. In patient fibroblasts cultured in a galactose based medium I detected signs of increased ROS generation, some perturbations in the glycolysis pathway, NAD(H) depletion, and increased susceptibility to ROS-induced cell death.

To my knowledge no previous studies attempted NPC patient fibroblast culture in a galactose-based medium. Results of previous studies carried out in glucose-based culture of NPC patient fibroblasts vary greatly. First, a study of mitochondrial structure and function reports increased mitochondrial mass, a concurrent increase in the rate of O_2 consumption but reduced ATP content and ROS levels (Woś *et al.*, 2016) and thus do not correlate with my findings. In contrast, increased ROS and lipid peroxidation were found in NPC patient fibroblasts and NPC deficient human fibroblasts and a neuroblastoma cell model (Zampieri *et al.*, 2009). In addition, authors of this study also observed an increased susceptibility of NPC1 patient fibroblasts to H_2O_2 challenge, which led to increased cellular apoptosis (Zampieri *et al.*, 2009). A recent study also reported increased mitochondrial mass despite significantly lower

transcription levels of nDNA and mtDNA encoded ETC subunits, lower O_2 consumption rate and higher basal ROS levels in NPC1 patient cells (Yambire *et al.*, 2019). Together, these results suggest that NPC1 fibroblasts present with dysfunctional mitochondria potentially due to impaired mitochondrial quality control.

Increased oxidative stress was reported from multiple models of NPC disease and a plasma study of NPC patients (Smith *et al.*, 2009; Zampieri *et al.*, 2009). In the context of the NPC disease, *in vivo* biomarkers of increased oxidative stress and lower antioxidant defences were detected in plasma-, erythrocyte- and fibroblast-based screens of NPC patients (Fu *et al.*, 2010; Ribas *et al.*, 2012). In addition, oxidised cholesterol products in patient plasma were identified as specific biomarkers of NPC disease, that are modulated by Miglustat treatment (Jiang *et al.*, 2011; Hammerschmidt *et al.*, 2018). However, the pathological relevance of increased ROS to disease progression *in vivo* is unknown and mouse antioxidant (vitamin E and vitamin C) supplementation, when attempted, had no beneficial effect on mouse lifespan (Smith *et al.*, 2009) or rotarod performance, used as a proxy measurement of coordination (ataxia) (Bascunan-Castillo, 2004). Nevertheless, it would be interesting to test whether more targeted ROS scavenging strategies, such as use of MitoQ10 or S1QEl2.2 could be beneficial in alleviating mitochondrial dysfunction in NPC1 disease.

5.5.3 Study limitations

As discussed above, culture and study of patient fibroblasts is sufficient for NPC diagnosis (Vanier and Latour, 2015). Patient fibroblasts that carry specific mutations causing disease are also a more relevant model to study NPC1-mutant protein structure, dynamics and degradation, than animal models, including fruit flies, zebrafish, mouse and cat models that are currently used to study the disease (reviewed in (Fog and Kirkegaard, 2019)). In this study, I have demonstrated that study of patient fibroblasts is sufficient to also identify an autophagy and cell viability defect; and potential successful treatments. However, human fibroblasts might not be truly representative of the cells and tissues affected by disease pathology. An exciting method that could be employed to increase the relevance of fibroblasts isolated from patients would be to re-program patient fibroblasts into induced pluripotent stem cells and then differentiate into disease-relevant cell lines to observe cell line-specific functional defects (Karagiannis, 2019). Although these cells are still very much removed from an *in vivo* scenario, such approach could inform about the role of *NPC1*

mutation and absence or presence of an autophagy defect in disease progression and serve as a platform for disease modelling and drug testing.

Reprogramming of NPC patient fibroblasts into a disease-relevant cell line was already successfully attempted by multiple groups (Bergamin *et al.*, 2013; Sung *et al.*, 2017). In one of the earlier studies, the authors isolated multipotent adult stem cells from NPC patients and induced these cells to differentiate into neurons which recapitulated the phenotypes of NPC disease (Bergamin *et al.*, 2013). The major limitation of this study, i.e. the lack of sufficient cell quantity generated by their method, was addressed in multiple studies of induced pluripotent stem cells (iPSCs)-derived neuronal models. The authors of these studies established successful cultures and tested the effect of compounds with a potential clinical benefit (Sarkar *et al.*, 2013; Lee *et al.*, 2014; Maetzel *et al.*, 2014; Yu *et al.*, 2014; Cougnoux *et al.*, 2016). However, the method used to generate iPSCs is considered time-consuming, and labour intensive and thus may not be appropriate for larger-scale patient tests (Montserrat *et al.*, 2011). In addition, the iPSC approach requires cell re-programming to an embryonic-like state, which might abolish their relevance to the study of age-related diseases (Hermann and Storch, 2013). In the most recent study, authors attempted generation of induced neural stem cells (iNSCs) from isolated patient fibroblasts (Sung *et al.*, 2017). The authors applied a relatively simple method of cell reprogramming with two factors and succeeded in generating cells capable of differentiation into neurons, astrocytes and oligodendrocytes (Sung *et al.*, 2017). This study had also demonstrated the usefulness of such a model as a platform for neurodegenerative disease modelling and drug testing. However, since this study has not yet been validated by a different research group in NPC disease, caution should be exercised in interpreting these results. Altogether, advances in somatic cell re-programming could soon provide the platform for NPC and other disease modelling that could initially serve to validate findings from fibroblast models and thus establish the suitability of fibroblasts for further study. Additionally, somatic cell re-programming could provide a novel platform for personalized diagnosis and therapeutics.

Chapter 6. Discussion

It is increasingly recognized that age-related cellular dysfunction cannot be explained by a single cause and effect relationship and is instead underpinned by a complex network of pathway dysfunction, macromolecular damage and loss of metabolic homeostasis. The interrelatedness of these hallmarks of ageing is not fully understood and is often overlooked. To highlight one hallmark in particular, macroautophagy, a cellular pathway that contributes to cellular proteostasis, organelle health and nutrient recycling, is a known cytoprotective and pro-survival pathway that is a downstream target of multiple interventions that prolong healthspan and/or lifespan (Madeo *et al.*, 2015). Autophagy is restricted in conditions of nutrient excess (glucose, insulin, cellular lipids, ATP, NADH) (Pierzynowska *et al.*, 2018) and in aged tissue due to decreased levels of ATG proteins (Lipinski *et al.*, 2010), but can be stimulated genetically, pharmacologically and nutritionally. Studies from animal models of age-related disease show that autophagy stimulation is beneficial for the treatment of metabolic syndrome (Lim *et al.*, 2018), cardiovascular disease (Lavandero *et al.*, 2015), memory loss (Glatigny *et al.*, 2019) and neurodegeneration (Menzies *et al.*, 2017). However, open questions remain regarding the translational potential of autophagy stimulation to human ageing and age-related disease (Maiuri and Kroemer, 2019). Due to the multifaceted role of autophagy in supporting cellular health, function and viability, and the multitude of upstream regulators and their stimuli, it is difficult to tease out what is the upstream cause of autophagy decline in ageing and thus which 'druggable' proteins to target (Levine and Kroemer, 2019). The nature of autophagy dysfunction also varies in aged individuals and patients suffering from either sporadic disease or an inherited mutation. Conversely, stimulated autophagy sustains the accelerated growth of transformed cells (Nazio *et al.*, 2019) and resistance to starvation in senescence (Carroll *et al.*, 2017). Identification of an all-purpose autophagy-targeting therapy is thus unlikely and success in any therapeutic approach will likely be achieved by tailored approach to a specific disease.

6.1 Lessons learned from cellular KO models

To address this issue, I aimed to establish downstream effects of autophagy deficiency and identify potential targets, and small compound therapeutics that would form the basis of a holistic therapy approach. I undertook two branches of study to investigate whether autophagy deficiency alone is sufficient to lead to mitochondrial dysfunction

and deregulation of cellular metabolism that were identified as two hallmarks of ageing and age-related pathology (López-Otín *et al.*, 2016). To mimic the physiological metabolic state in cultured cells, I optimized culture in a galactose-based medium and established that it not only leads to loss of cell viability in MEF models of autophagy impairment (*Atg5*$^{-/-}$, *Npc1*$^{-/-}$, and CRISPR/Cas9-generated *Atg5*$^{-/-}$, A*tg7*$^{-/-}$ and *Rb1cc1*$^{-/-}$ MEFs) (Figures 3.6, 3.7, 5.4), but also uncovers a bioenergetic defect in mitochondria and a whole-cell reduction in NAD(H) levels (*Atg5*$^{-/-}$ and *Npc1*$^{-/-}$ MEFs) (Figures 3.2, 3.4, 3.5, 4.2, 4.3, 5.1, 5.2, 5.6). I hypothesize that while both phenotypes contribute to cellular dysfunction, and existence of an interdependent relationship is likely, it is the cellular depletion of NAD(H) levels that leads to the loss of mitochondrial membrane potential and ultimately apoptosis.

Within the scope of this study, I have not been able to uncover the underlying cause of NAD(H) depletion. Cellular NAD^+ levels are maintained by a dynamic balance between *de novo* NAD^+ synthesis, NAD^+ salvage and depleted by PARP-, sirtuin- and CD38-mediated cleavage (Cantó, Menzies and Auwerx, 2015). The success of NAM (and NR) -mediated recovery of NAD(H) levels in *Atg5*$^{-/-}$ and *Npc1*$^{-/-}$ MEFs leads us to conclude that the NAD(H) depletion I observe is not due to a bottleneck in the NAD^+ salvage pathway (Figure 1.4D; Figures 4.10, 5.7). Although I cannot comment on the activity, or lack thereof, of the NAD^+ *de novo* synthesis, I are currently focusing my efforts on measuring activity of the PARP, SIRT and CD38 enzymes in culture and their direct impact on NAD(H) level modulation. PARP and CD38 are both capable of severely depleting cellular NAD^+ pools (Pacher and Szabo, 2008; Camacho-Pereira *et al.*, 2016) and activity of both enzymes increases with ageing (Massudi *et al.*, 2012; Camacho-Pereira *et al.*, 2016).

Also in this study, mitochondrial respirometry assays revealed a dysfunction in CI-linked O_2 reduction to H_2O that I originally explored via mitochondria-based assays of BN-PAGE and immunoblotting to explore a mechanistic cause. However, I could not confirm gross aberrations in the levels or assembly of the ETC SCs that would explain an underlying structural cause for the dysfunction I detected (Figures 3.4, 5.3). As discussed above, targeted cellular metabolic profiling revealed a depletion in CI substrate and e^- carrier, NADH, in both immortalized models, *Atg5*$^{-/-}$ and *Npc1*$^{-/-}$ MEFs. I hypothesize that lower levels of NADH might affect the measured fitness of the CI-CIII-CIV-linked O_2 reduction even in the absence of an ETC structural aberration. I

believe that this observation highlights the interconnectedness of cellular pathways and functions. However, due to plasma membrane non-permeability to NAD(H), verifying causation relationships could be particularly challenging. It is therefore worth considering whether mitochondria respirometry assays would benefit from complementary studies, for example feeding permeabilized mitochondria NADH directly to identify whether the CI-CIII-CIV-linked O_2 reduction defect can be ameliorated.

Cellular NADH depletion can arise from either increased NADH consumption by cellular/mitochondrial NADH oxidases or lower activity/substrate availability of cellular/mitochondrial dehydrogenases. My data suggests that at least some of the NADH depletion occurs in mitochondria. As changes in the levels of the mitochondrial TCA cycle intermediates in *Atg5*$^{-/-}$ and *Npc1*$^{-/-}$ MEFs compared to their respective controls do not follow a common pattern (Figures 4.3, 5.6), it is unlikely that the NADH loss is potentiated by the loss of NAD^+ reduction to NADH. Instead I propose a mechanism, by which other mitochondrial phenotypes observed in *Atg5*$^{-/-}$ MEFs, increased $\bullet O_2$ production and loss of mMP (Figure 3.5), lead to indiscriminate NADH consumption by CI that is not coupled to H^+ pumping due to increased e^- leakage from the ETC/CI. Interestingly, cell supplementation with $MitoQ_{10}$ and the corresponding small, yet significant, recovery of NADH levels suggests that mitochondrial $\bullet O_2$ release contributes to NADH depletion and thus contributes to a vicious cycle that leads to the loss of cell viability (Figure 4.10). The underlying cause of increased mitochondrial ROS load, either as a result of increased e^- leakage or overwhelmed and insufficient detoxification remains unknown. However, it can be hypothesised that it may result from an insufficient mitochondrial recycling by autophagy.

6.2 Autophagy-NAD(H)-mitochondria axis: therapeutic relevance to age-related disease

Pharmacological stimulation of autophagy, mitochondrial ROS detoxification and NAD^+ levels elevation all rescue cell viability in the cell-based models. I have demonstrated that cell treatment with rapamycin and celecoxib induces autophagy in both, *Npc1*$^{+/+}$ and *Npc1*$^{-/-}$ MEFs and rescue cell death of *Npc1*$^{-/-}$ MEFs (Figures 5.8, 5.9). Downstream of autophagy impairment, mitochondrial $\bullet O_2$ and whole-cell H_2O_2 scavenging with S1QEL2.2, $MitoQ_{10}$ and NAC promote cell viability in *Atg5*$^{-/-}$ and *Npc1*$^{-/-}$ MEFs (Figures 4.9, 5.5). Finally, elevating NAD^+ levels by a single NAD^+ precursor

supplementation corrects metabolic deregulation and prevents cell death in both cell lines (Figures 4.6, 4.10, 5.7) (Figure 6.1).

Each of the three main interventions that were successful in this study are currently explored as potential therapeutics. As discussed above and in section 1.7.2, the translational potential of autophagy stimulation and ROS detoxification into the clinic are currently being explored. Of the possible targets for therapeutic exploration, NAD^+ precursor supplementation has the potential to become the most clinically relevant and universal intervention aimed at alleviating cellular pathology in diseases presenting with autophagy impairment. Deregulated enzymes involved in NAD^+ metabolism and low NAD^+ levels have been detected in human healthy aged tissue, in patients suffering from progeria syndromes, and a plethora of metabolic, cardiovascular, neurodegenerative and age-related diseases (Parsons *et al.*, 2002; Salek *et al.*, 2007; Borradaile and Pickering, 2009; Gomes *et al.*, 2013; Scheibye-Knudsen *et al.*, 2014; Wakade *et al.*, 2014; Zhu *et al.*, 2015; Ali *et al.*, 2016; Chini *et al.*, 2019; Okabe *et al.*, 2019). These studies highlight NAD^+ depletion, similarly to autophagy dysfunction, as a fairly universal hallmark of age- and disease-related pathology and the potential of NAD^+ supplementation as a strategy to alleviate pathology. On a molecular level, NAD^+ precursor supplementation showed variable levels of success in ameliorating the burdens of many of the hallmarks of ageing, including genomic instability, epigenetic alterations, stem cell exhaustion, loss of proteostasis, mitochondrial dysfunction, deregulated nutrient sensing and cellular senescence (reviewed in (Fang *et al.*, 2017)).

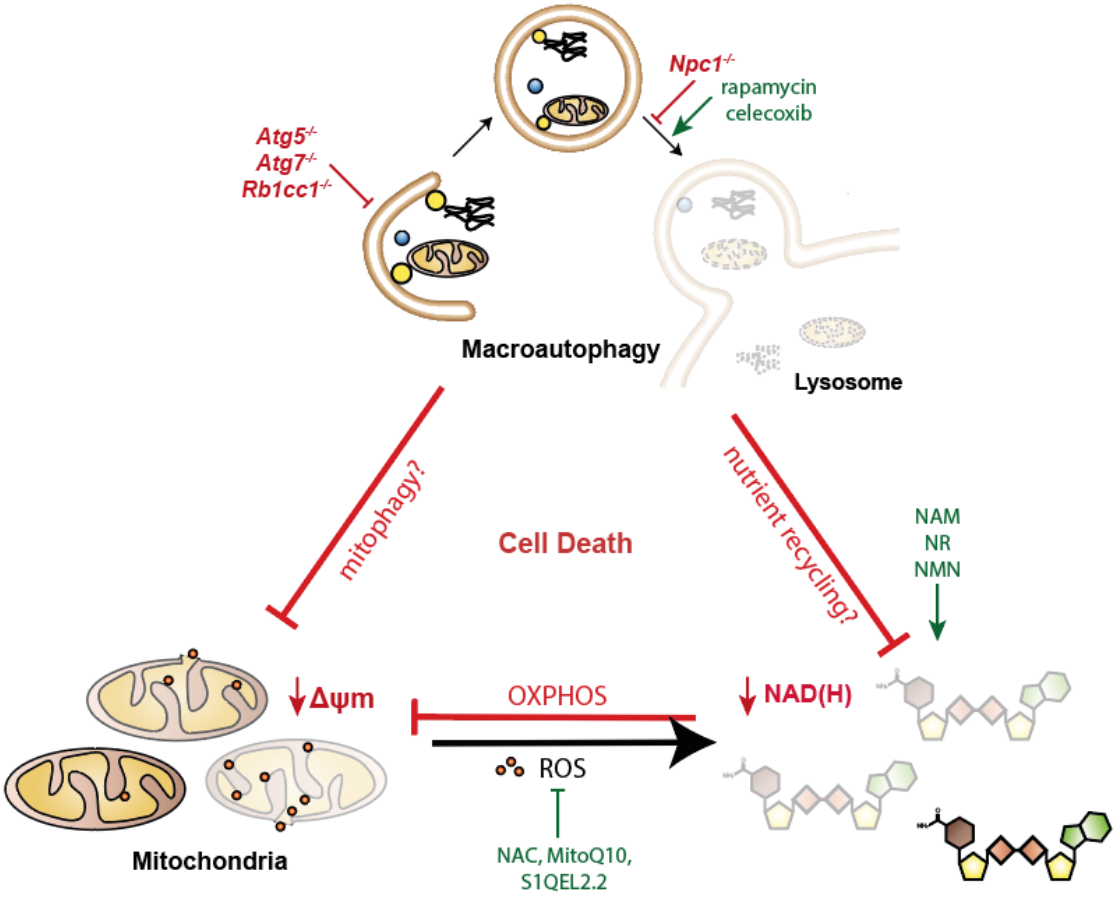

Figure 6. 1 Proposed mechanism of cell death caused by autophagy deficiency

We hypothesize that autophagy impairment at the stage of initiation (*Atg5*$^{-/-}$, *Atg7*$^{-/-}$ and *Rb1cc1*$^{-/-}$, or autophagosome fusion with lysosome (*Npc1*$^{-/-}$) leads to loss of organelle quality control (mitophagy) and nutrient recycling (NAD(H)). Loss of NADH affects mitochondrial e^- flow and contributes to loss of mMP (ΔΨm). In addition, dysfunctional mitochondria release ROS that further deplete cellular NADH stores and affect mitochondrial function. The vicious cycle of mitochondrial dysfunction and NADH depletion ultimately lead to loss of mMP and cell death. Interventions that induce autophagy (rapamycin, celecoxib), boost cellular NAD(H) levels (NAM, NR, NMN) and scavenge ROS (NAC, $MitoQ_{10}$ and S1QEL2.2) promote cell viability and combat the effects of autophagy deficiency.

In animal models of ageing and age-related disease, boosting NAD^+ levels by supplementation with its precursors NMN, NAM and NR successfully corrected many disease phenotypes (reviewed in (Aman *et al.*, 2018)). To highlight a few, NMN treatment at the start of reperfusion and continued supplementation thereafter reduces the extent of tissue damage following cerebral and cardiac ischaemia (Yamamoto *et al.*, 2014; Park *et al.*, 2016). NMN, NR and NAM supplementation alleviate the onset and progression of amyloid-β and tau pathology, and improve cognition in AD (Gong *et al.*, 2013; Liu *et al.*, 2013; Wang *et al.*, 2016; Hou *et al.*, 2018). Finally, moderate NAM supplementation improves glucose metabolism and reduces inflammation in mice fed on a high-fat diet, that serve as a model for impaired glucose tolerance and diabetes mellitus type 2 (DMT2) (Mitchell *et al.*, 2018).

Organismal NAD^+ precursor supplementation presents with two potential drawbacks. First, elevated levels of NAM could potentiate increased activity of NNMT-mediated formation of a degradation metabolite, *N*-methyl-NAM that was hypothesized to act as a CI toxin (Parsons *et al.*, 2002; Williams and Ramsden, 2005). Importantly, elevated NNMT levels were in post-mortem brain tissue of PD patients, and in white adipose tissue and the liver of diabetic humans and mice (Williams and Ramsden, 2005; Pissios, 2017). Second, elevation of NAMPT, the rate-limiting enzyme of NAD^+ salvage pathway from NAM, was observed in a range of malignant cancers and its inhibition by FK866 is explored as a therapeutic in cancer therapy (Yaku *et al.*, 2018). Thus, elevation of NAD^+ levels as a result of a therapy may need to be monitored to prevent the potentiation of neurodegeneration and tumorigenesis.

Nevertheless, the success of NAD^+-boosting strategies in animal models is currently followed up in a series of clinical trials (Table 6.1). Studies of NMN and NAM are relatively limited, and the majority of clinical trials have chosen to study the effect of NR. Although no results have yet been published from any of the completed phase 1 and phase 2 studies, further trials are planned or started recruiting individuals for NR-based study of a range of healthy-ageing and age-related disease including AD, PD, DMT2 and chronic kidney disease (CKD). It will thus be interesting to wait for the results of these trials and other pre-clinical studies and see whether NAD^+-boosting strategies truly have as general a therapeutic potential as is indicated by the studies to date.

Table 6. 1 Clinical trials: NAD+ boosting in age-related pathology

Identifier	Status	Phase	NAD+ precursor	Examined Outcomes
NCT03151707	Recruiting	4	NR	NAD^+/NADH ratio and bioenergetics in the brain of healthy individuals
NCT03743636	Recruiting	3	NR	walking performance in patient suffering from peripheral artery disease
NCT02258074	Not yet recruiting	2	NAM	serum phosphate and fibroblast growth factor 23 in patients suffering from CKD
NCT03061474	Recruiting	2	NAM	early tau-phosphorylation in AD
NCT03850886	Recruiting	2	NAM	safety and efficacy of NAM supplementation on NAFLD in patients with DMT2
NCT00580931	Completed	1/2	NAM	safety and efficacy of NAM supplementation in AD
NCT04040959	Not yet recruiting	2	NR	arterial stiffness in patients suffering from CKD
NCT04044131	Not yet recruiting	2	NR	safety and efficacy of mixture of NR and other supplements in AD and PD patients
NCT02942888	Not yet recruiting	N/A	NR	memory and blood flow in individuals presenting with MCI
NCT02950441	Recruiting	2	NR	skeletal muscle metabolic phenotype in elderly male individuals (70-80 years of age)
NCT03821623	Recruiting	2	NR	arterial stiffness and elevated systolic blood pressure in middle aged and older adults
NCT03579693	Recruiting	2	NR	skeletal muscle function in patients suffering from CKD
NCT03565328	Recruiting	2	NR	effect on skeletal muscle function in individuals with heart failure
NCT03482167	Recruiting	2	NR	memory and blood flow in individuals presenting with MCI
NCT03962114	Enrolling	2	NR	treatment of children suffering from Ataxia Telangiectasia
NCT02812238	Completed	2	NR	comparison of NR and fasting on the immune system of healthy volunteers
NCT03685253	Recruiting	1/2	NR	clinical and physiological outcomes of diabetic neuropathy in patients with DMT2
NCT02921659	Completed	1/2	NR	safety and efficacy of NR supplementation in healthy middle aged and older adults
NCT03423342	Completed	1/2	NR	safety and tolerability of NR supplementation in participant with systolic heart failure
NCT02689882	Completed	1	NR	pharmacokinetic study in healthy individuals

NCT02191462	Completed	1	NR	pharmacokinetic study of three different dosages in healthy individuals
NCT03568968	Not yet recruiting	N/A	NR	correction of NAD and metabolism deficiency in PD patients
NCT03808961	Not yet recruiting	N/A	NR	inflammation, motor and non-motor symptoms in PD patients
NCT03754842	Recruiting	N/A	NR	muscle regeneration in elderly individuals (55-80 years of age)
NCT03816020	Recruiting	N/A	NR	neuro-metabolic profile, motor symptoms and NAD levels in PD patients
NCT03818802	Recruiting	N/A	NR	bone, skeletal muscle and metabolic function in aged individuals (65-80 years of age)
NCT02835664	Completed	N/A	NR	metabolic health of pre-obese individuals
NCT02303483	Completed	N/A	NR	substrate metabolism, insulin sensitivity and body composition in obese men
NCT03562468	Completed	N/A	NR	cognitive function, mood and sleep in individuals over 55 years of age
NCT03151239	Not yet recruiting	N/A	NMN	insulin levels/sensitivity and vasodilation in female participants (55-75 years of age)

AD: Alzheimer's disease, CKD: chronic kidney disease, DMT2: diabetes mellitus type 2, NAFLD: non-alcoholic fatty liver disease, MCI: mild cognitive impairment, N/A: not applicable, NAM: nicotinamide, NR: nicotinamide riboside, NMN: nicotinamide mononucleotide, PD: Parkinson's disease
Data was collated from https://clinicaltrials.gov/.

6.3 Modelling NPC disease

Profiling of NPC1 patient fibroblasts was carried out to see whether my findings from MEF-based genetic models of autophagy blockage translate to a patient scenario where autophagy impairment could be complete, moderate, quite mild or non-existent. By selecting available fibroblast cells from patients who carry various mutations in the *NPC1* gene, I discovered that two patient cell lines presented with no autophagy impairment (Figure 5.10). In contrast, I have demonstrated that, in the context of NPC disease, autophagy impairment in the remaining three patient cell lines correlates with reduction in NAD^+ levels upon cell culture in a galactose-based medium (Figure 5.10, Figure 5.11). Further investigation by metabolic profiling revealed that NPC1 patient fibroblasts that present with an autophagy impairment are characterised by severely depleted levels of NAD^+ and NADH. Although patient fibroblast culture in a galactose-based medium does not lead to a loss in cell viability, the NPC1 cells contain a higher

load of cellular H_2O_2 and die rapidly when challenged with exogenous oxidative stress (Figure 5.12). Most importantly, I have demonstrated that a two-week long cell pre-treatment with NAD^+ precursors NAM and NMN raises NAD^+ levels in NPC patient cell lines and prevents loss of cell viability when challenged with exogenous H_2O_2 (Figure 5.13). These studies provide the basis for a continuing and future studies in mouse models of NPC disease, in patient cell-derived neuronal cell cultures and potentially a translation into the clinic.

6.4 Relevance of NPC disease to neurodegeneration

NPC is a rare autosomal-recessive progressive disorder that can clinically manifest as a visceral-neurodegenerative disease (early-infantile,<2 years), neurodegenerative disease (late-infantile, 2-6 year; and juvenile 6-15 years) and psychiatric-neurodegenerative disease (adult onset, 15+ years) (Geberhiwot *et al.*, 2018). The age of onset and the severity of the neurodegeneration typically predict the speed of disease progression and life expectancy (Geberhiwot *et al.*, 2018). NPC patients with adult onset of disease represent approximately 20%-27% of all sufferers and typically present with cognitive impairment and psychiatric disease manifestations including psychosis and depression (Geberhiwot *et al.*, 2018). Pathologically, NPC disease mostly affects liver and spleen (infant and juvenile onset), and brain tissues (mostly present in adolescent and adult onset) (Geberhiwot *et al.*, 2018; Fog and Kirkegaard, 2019). NPC patients with infantile and juvenile disease onset often develop hepatomegaly (abnormal liver enlargement) and splenomegaly (abnormal spleen enlargement) due to an accumulation of sphingolipids and unesterified cholesterol. Liver and spleen disease rarely lead to mortality in NPC disease and clinical interventions aimed at lowering liver disease have no effect on ameliorating the neurodegenerative phenotypes (Vanier, 2010). The main focus in the treatment and drug development is dedicated to the neurological disease. Cholesterol trafficking in the brain is unique due to the lack of permeability of BBB to lipoprotein, thus all cholesterol within the brain is synthesized locally and undergoes low rates of turnover (Zhang and Liu, 2015). Astrocytes in the brain produce cholesterol and its carrier, apolipoprotein E (ApoE) that delivers cholesterol to neurons to support neuronal synaptic function (Mauch *et al.*, 2001; Zhang and Liu, 2015). To utilize the exogenous cholesterol, neurons need to liberate the ApoE bound form to free cholesterol within the late endosomes and lysosomes and traffic such cholesterol by the action of NPC1 and NPC2 proteins (Mauch *et al.*, 2001; Zhang and Liu, 2015). It remains unknown

whether it is cholesterol-mediated organellar dysfunction, i.e. disruption of mitochondrial function or lysosome-mediated autophagy, or depleted levels of available cholesterol to maintain neuronal function that underlie the pathogenesis of the NPC1/2 loss of function mutations. Ultimately, NPC1/2 dysfunction leads to hypomyelination, neuroaxonal dystrophy and neurodegeneration (Walkley and Suzuki, 2004; Yu and Lieberman, 2013).

6.4.1 NPC: similarities to AD

Parallels have been observed and described between the clinical and molecular manifestations of NPC and AD. AD neuropathology was defined by the presence of extracellular amyloid plaques and intra-cellular hyper-phosphorylated neurofibrillary tangles (NFT) in post-mortem brain tissue from AD patients (Kumar, Singh and Ekavali, 2015). The structural basis of NFTs consists of tau protein aggregates paired helices. Current hypotheses of AD postulate that aberrant amyloid processing and deposition, or tau mutations lead to tau hyper-phosphorylation and NFT formation (Kumar, Singh and Ekavali, 2015). The interest of AD researchers in NPC disease originates from a study, in which post-mortem examination of NPC patient brain tissue identified the presence of NFTs with a strong presence of the tau protein (Love, Bridges and Case, 1995). The tangles in NPC brain tissue were structurally identical to those that define the pathology of AD disease, but intriguingly occurred in the absence of tau mutations or amyloidal plaques (Auer *et al.*, 1995; Love, Bridges and Case, 1995). NFTs in AD and adult-onset NPC were also strongly associated with neurodegeneration and strangely absent in the cerebellum of patients suffering from either disease (reviewed in (Bergeron, Poulin and Laforce, 2018)). Additionally, two studies of NPC neurons and AD neurons from the same laboratory report that the load of NFTs correlates with the levels of neuronal free cholesterol (Distl, Meske and Ohm, 2001; Distl *et al.*, 2003).

The most common genetic risk factor in AD is the epsilon-4 allele of ApoE (ApoE-ε4) (Strittmatter and Roses, 1996). ApoE is an enzyme expressed mostly in the liver and the brain and is, in the central nervous system, responsible for cholesterol and lipid homeostasis (Mahley, 2016). ApoE-ε4 encodes a form of the ApoE enzyme that has a lower binding affinity to its plasma membrane receptor, the lipoprotein receptor-related protein 1 (LRP1), when compared to an ε3 allele that in culture leads to lower levels of cholesterol release from cultured astrocytes (Gong *et al.*, 2002). Thus, at least the

ApoE-ε4 form of AD shares a common feature of cholesterol trafficking de-regulation with NPC that seems to correlate with NFT formation and neurodegeneration in both disorders.

6.4.2 NPC: similarities to PD

Connections were also observed between NPC and PD pathology. PD is a neurodegenerative disorder characterized by the loss of dopaminergic neurons within the substantia nigra region of the brain and Lewy body pathology (Fearnley and Lees, 1991; Rocha, De Miranda and Sanders, 2018). Lewy bodies are intracellular protein aggregates, the main protein component of which was identified as α-synuclein. It is believed that genetic mutations, PTMs, oxidation and deficient clearance of α-synuclein underlie its aggregation (Rocha, De Miranda and Sanders, 2018). The nature of involvement of α-synuclein in PD pathology has not yet been elucidated, but its ATP-dependent aggregation and sequestration into large inclusion bodies is thought to prevent its toxicity (Rocha, De Miranda and Sanders, 2018). The pathological link between NPC and PD was reported from heterozygote carriers of *NPC1* mutations that presented with parkinsonism (Kluenemann *et al.*, 2013) and rare aberrant α-synuclein phosphorylation pattern and Lewy body formation (2/10 cases) (Saito *et al.*, 2004). It is unclear however, whether a PD diagnosis is more prevalent in heterozygote *NPC1* carriers than in the general population. Authors of an earlier *in vitro* PD study reported that oxidised cholesterol metabolites promote α-synuclein fibril formation (Bosco *et al.*, 2006). Similarly, heterozygous mutation in *GBA1* gene encoding a lysosomal hydrolase glucocerebrosidase 1, a lysosomal hydrolase, is a genetic risk-factor for PD (Aharon-Peretz, Rosenbaum and Gershoni-Baruch, 2004; Crosiers *et al.*, 2016; Arkadir *et al.*, 2018). Individuals who carry two mutated *GBA1* alleles suffer from Gaucher's disease, the most prevalent lysosomal storage disorder characterised by the loss of GCase1 activity and disrupted lysosomal function and macroautophagy (Sun and Grabowski, 2010). A study of fibroblasts isolated from four PD patients who carry a heterozygous *GBA1* mutation revealed an autophagy impairment, increased cholesterol levels and cell sensitivity to exogenous oxidative stress (García-Sanz *et al.*, 2017). Moreover, genetic variants associated with a variety of lysosomal storage disorders were also found to associate with PD (Robak *et al.*, 2017). These studies together provide the evidence that lysosomal dysfunction, cholesterol accumulation and macroautophagy interruption alone or in combination promote α-synuclein

aggregation, may underlie PD pathology, and could provide therapeutic targets for PD patients who carry *GBA1* mutations and/or present with stalled autophagy or high cholesterol.

6.4.3 NAD(H): the common link?

Studies of LSDs, NPC, AD and PD identify the interrelatedness between the underlying pathology in LSDs, i.e. the impairment of lysosomal function, cholesterol accumulation and autophagy impairment, and its role in the potentiation of proteinopathy including tau and α-synuclein fibrilization. Another common feature between AD and PD is the de-regulation of NAD(H) metabolism (Wakade *et al.*, 2014; De Jesús-Cortés *et al.*, 2015; Ali *et al.*, 2016), that I also observed in NPC1 patient fibroblasts in this study. Following the success of NAD^+-boosting strategies in animal models of AD and PD, clinical trials have been set up to study the effect of NR supplementation in AD and PD patients (Table 6.1). Conversely, following the results of these clinical trials and outcomes on observed amyloid, tau and α-synuclein aberration in AD and PD, and NAD studies in NPC animal models, it will be interesting to see whether NPC patients will be able to also benefit from such interventions strategies and an improved understanding of the pathologies and their interrelatedness.

6.5 Concluding Remarks

This study has highlighted the interconnectedness of the pathways involved in the ageing process. I hypothesized that two functions of macroautophagy, the qualitative turnover of mitochondria and bulk recycling of amino acids and nucleotides, stand at the root of age-related pathology. I confirmed my hypothesis by identifying a novel link between autophagy impairment and de-regulation of NAD(H) metabolism that sensitises mitochondria and cells to metabolic and oxidative stresses that can induce loss of cellular viability (Figure 1.6). My study established that autophagy stimulation, ROS detoxification and NAD(H) level elevation are all relevant strategies to combat phenotypes arising from autophagy impairment. Furthermore, for the first time, I report that depletion of NAD(H) levels in NPC could underlie disease pathology in cells/tissues that suffer from dysfunctional autophagy. I believe that these exciting findings can have a wider impact on the study of the NPC disease, on diseases that present with autophagy impairment and on general age-related pathology, and could form the basis of future therapeutic strategies.

Appendices

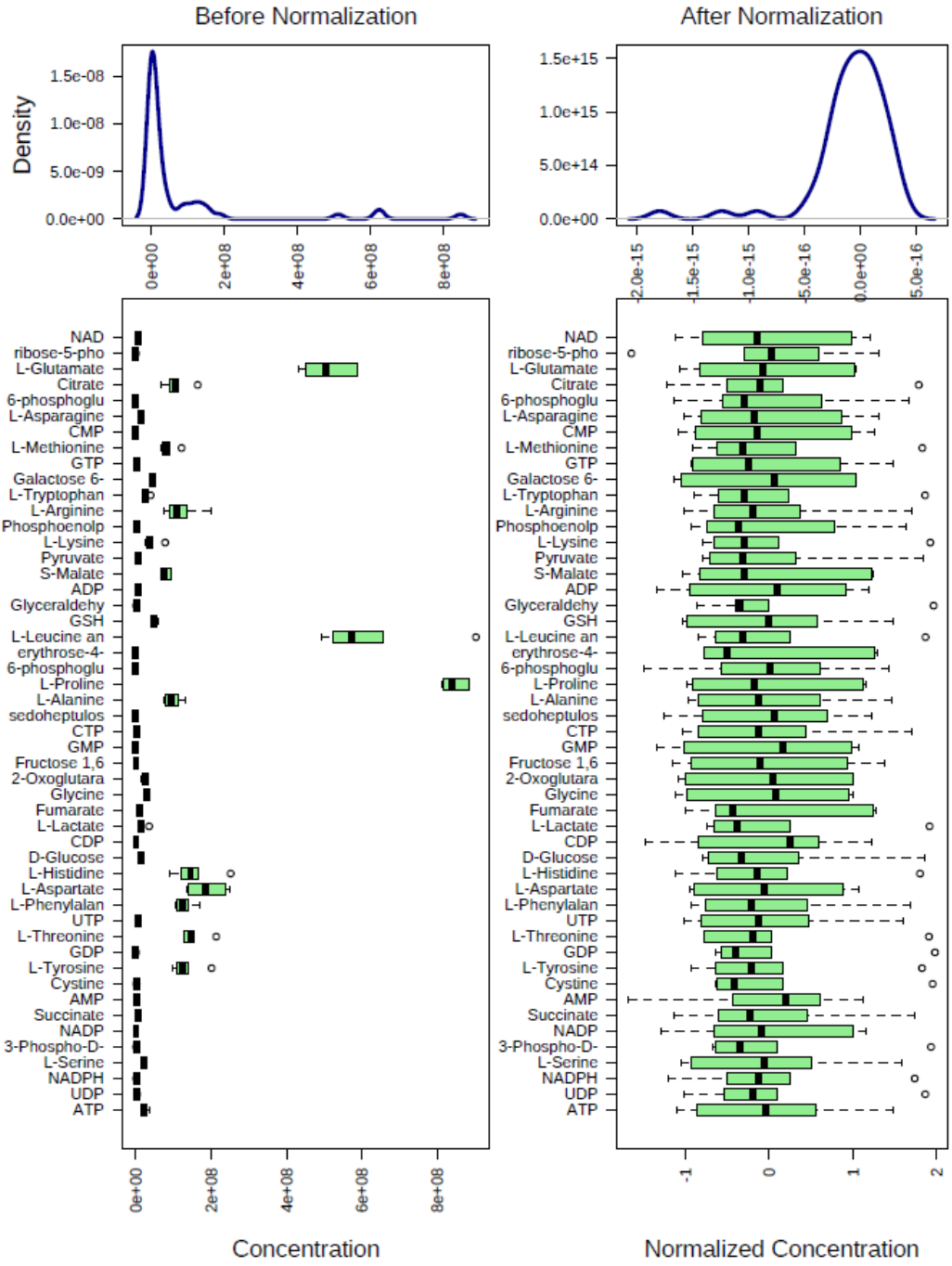

Appendix 1. Metabolomic data scaling for statistical analysis

Box plots and kernel density plots before and after normalization. The box plots show 50 features due to space limit. The density plots are based on all samples. Selected methods: Row-wise normalization (N/A); Data transformation: (N/A); Data scaling: Autoscaling.

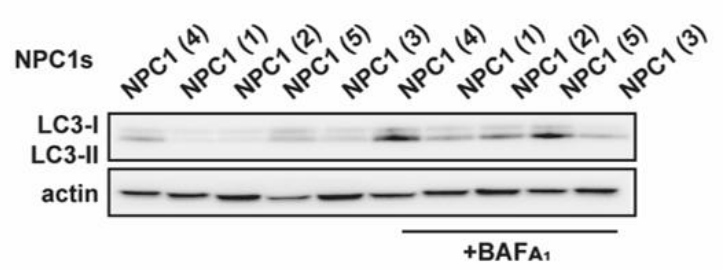

Appendix 2. Re-arranged loading and LC3-II detection in CTRL and NPC1 cell lines

Immunoblot of re-arranged sample loading of NPC1 patient fibroblast cell lines treated with 100nM bafilomycin A1 (BAF A1) or vehicle (DMSO) for 24h.

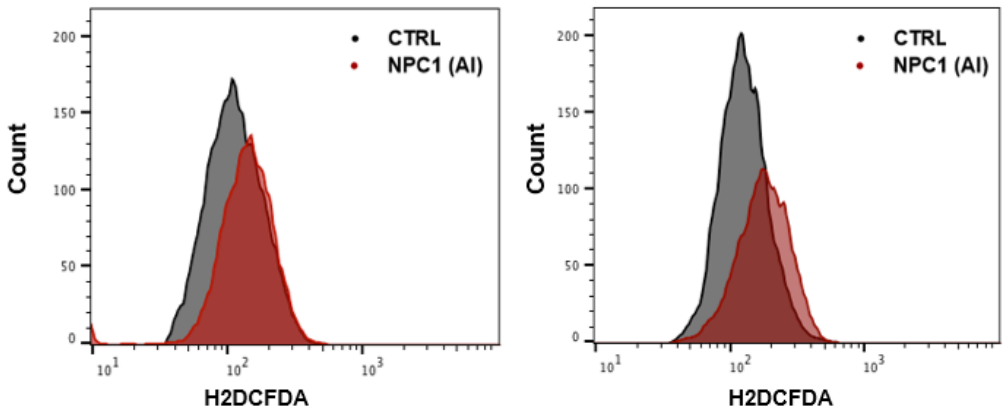

Appendix 3. Additional ROS data for CTRL and NPC1 patient cell lines

Flow cytometry peaks of CTRL and NPC1 cellular ROS levels detected by H2DCFDA fluorescence intensity after sub-culture in the galactose-based medium.

References

Agilent (2019) *Seahorse XF Analyzers*. Available at: https://www.agilent.com/en/products/cell-analysis/seahorse-analyzers (Accessed: 19 August 2019).

Aharon-Peretz, J., Rosenbaum, H. and Gershoni-Baruch, R. (2004) 'Mutations in the glucocerebrosidase gene and Parkinson's disease in Ashkenazi Jews', *New England Journal of Medicine*. Mass Medical Soc, 351(19), pp. 1972–1977.

Aksenov, M. Y. *et al.* (1999) 'The Expression of Several Mitochondrial and Nuclear Genes Encoding the Subunits of Electron Transport Chain Enzyme Complexes, Cytochrome c Oxidase, and NADH Dehydrogenase, in Different Brain Regions in Alzheimer's Disease', *Neurochemical Research*, 24(6), pp. 767–774. doi: 10.1023/A:1020783614031.

Aksoy, P. *et al.* (2006) 'Regulation of intracellular levels of NAD: a novel role for CD38', *Biochemical and biophysical research communications*. Elsevier, 345(4), pp. 1386–1392.

Ali, Y. O. *et al.* (2016) 'NMNAT2:HSP90 Complex Mediates Proteostasis in Proteinopathies', *PLoS biology*. Public Library of Science, 14(6), pp. e1002472–e1002472. doi: 10.1371/journal.pbio.1002472.

Allen, G. F. G. *et al.* (2013) 'Loss of iron triggers PINK1/Parkin-independent mitophagy', *EMBO reports*. 2013/11/01. John Wiley & Sons, Ltd, 14(12), pp. 1127–1135. doi: 10.1038/embor.2013.168.

Aman, Y. *et al.* (2018) 'Therapeutic potential of boosting NAD+ in aging and age-related diseases', *Translational Medicine of Aging*, 2, pp. 30–37. doi: https://doi.org/10.1016/j.tma.2018.08.003.

Anand, R. *et al.* (2014) 'The i-AAA protease YME1L and OMA1 cleave OPA1 to balance mitochondrial fusion and fission', *The Journal of Cell Biology*, 204(6), pp. 919 LP – 929. doi: 10.1083/jcb.201308006.

Anderson, K. A. *et al.* (2017) 'Metabolic control by sirtuins and other enzymes that sense NAD+, NADH, or their ratio', *Biochimica et Biophysica Acta (BBA) - Bioenergetics*, 1858(12), pp. 991–998. doi: https://doi.org/10.1016/j.bbabio.2017.09.005.

Ansari, A. *et al.* (2017) 'Function of the SIRT3 mitochondrial deacetylase in cellular physiology, cancer, and neurodegenerative disease', *Aging cell*. 2016/09/29. John Wiley and Sons Inc., 16(1), pp. 4–16. doi: 10.1111/acel.12538.

Arkadir, D. *et al.* (2018) 'Trio approach reveals higher risk of PD in carriers of severe vs. mild GBA mutations', *Blood Cells, Molecules, and Diseases*, 68, pp. 115–116. doi: https://doi.org/10.1016/j.bcmd.2016.11.007.

Arndt, V., Rogon, C. and Höhfeld, J. (2007) 'To be, or not to be — molecular chaperones in protein degradation', *Cellular and Molecular Life Sciences*, 64(19–20), pp. 2525–2541. doi: 10.1007/s00018-007-7188-6.

Arnoult, D. (2007) 'Mitochondrial fragmentation in apoptosis', *Trends in Cell Biology*, 17(1), pp. 6–12. doi: https://doi.org/10.1016/j.tcb.2006.11.001.

Atkinson, D. E. and Walton, G. M. (1967) 'Adenosine triphosphate conservation in metabolic regulation rat liver citrate cleavage enzyme', *Journal of Biological Chemistry*. ASBMB, 242(13), pp. 3239–3241.

Auer, I. A. *et al.* (1995) 'Paired helical filament tau (PHFtau) in Niemann-Pick type C disease is similar to PHFtau in Alzheimer's disease', *Acta neuropathologica*. Springer, 90(6), pp. 547–551.

Avalos, J. L., Bever, K. M. and Wolberger, C. (2005) 'Mechanism of Sirtuin Inhibition by Nicotinamide: Altering the NAD+ Cosubstrate Specificity of a Sir2 Enzyme', *Molecular Cell*, 17(6), pp. 855–868. doi: https://doi.org/10.1016/j.molcel.2005.02.022.

Axe, E. L. *et al.* (2008) 'Autophagosome formation from membrane compartments enriched in phosphatidylinositol 3-phosphate and dynamically connected to the endoplasmic reticulum', *The Journal of cell biology*. The Rockefeller University Press, 182(4), pp. 685–701. doi: 10.1083/jcb.200803137.

Babot, M. *et al.* (2014) 'ND3, ND1 and 39kDa subunits are more exposed in the de-active form of bovine mitochondrial complex I', *Biochimica et Biophysica Acta (BBA) - Bioenergetics*, 1837(6), pp. 929–939. doi: https://doi.org/10.1016/j.bbabio.2014.02.013.

Bachmann, R. F. *et al.* (2009) 'Common effects of lithium and valproate on mitochondrial functions: protection against methamphetamine-induced mitochondrial damage', *International Journal of Neuropsychopharmacology*, 12(6), pp. 805–822. doi: 10.1017/S1461145708009802.

Balaban, R. S., Nemoto, S. and Finkel, T. (2005) 'Mitochondria, Oxidants, and Aging', *Cell*, 120(4), pp. 483–495. doi: https://doi.org/10.1016/j.cell.2005.02.001.

Balch, W. E. *et al.* (2008) 'Adapting Proteostasis for Disease Intervention', *Science*, 319(5865), pp. 916 LP – 919. doi: 10.1126/science.1141448.

Balchin, D., Hayer-Hartl, M. and Hartl, F. U. (2016) 'In vivo aspects of protein folding and quality control', *Science*, 353(6294), p. aac4354. doi: 10.1126/science.aac4354.

Ballard, J. W. O., Horan, M. P. and Pichaud, N. (2012) 'Review: Quantifying Mitochondrial Dysfunction in Complex Diseases of Aging', *The Journals of Gerontology: Series A*, 67(10), pp. 1022–1035. doi: 10.1093/gerona/glr263.

Ban, T. *et al.* (2017) 'Molecular basis of selective mitochondrial fusion by heterotypic action between OPA1 and cardiolipin', *Nature Cell Biology*. Nature Publishing Group, 19, p. 856. Available at: https://doi.org/10.1038/ncb3560.

Banba, A. *et al.* (2019) 'Defining the mechanism of action of S1QELs, specific suppressors of superoxide production in the quinone-reaction site in mitochondrial complex I', *Journal of Biological Chemistry*. ASBMB, p. jbc-RA119.

Barbosa, M. T. P. *et al.* (2007) 'The enzyme CD38 (a NAD glycohydrolase, EC 3.2.2.5) is necessary for the development of diet-induced obesity', *The FASEB Journal*. Federation of American Societies for Experimental Biology, 21(13), pp. 3629–3639. doi: 10.1096/fj.07-8290com.

Bascunan-Castillo, E. C. (2004) 'Tamoxifen and vitamin E treatments delay symptoms in the mouse model of Niemann-Pick C', *Journal of applied genetics.* Poznań, Poland :, p. 461.

Baughman, J. M. *et al.* (2011) 'Integrative genomics identifies MCU as an essential component of the mitochondrial calcium uniporter', *Nature*. Nature Publishing Group, 476(7360), p. 341.

Baumgart, M. *et al.* (2016) 'Longitudinal RNA-Seq Analysis of Vertebrate Aging Identifies Mitochondrial Complex I as a Small-Molecule-Sensitive Modifier of Lifespan', *Cell Systems*, 2(2), pp. 122–132. doi: https://doi.org/10.1016/j.cels.2016.01.014.

Bazil, J. N. *et al.* (2013) 'Analysis of the Kinetics and Bistability of Ubiquinol:Cytochrome c Oxidoreductase', *Biophysical Journal*, 105(2), pp. 343–355. doi: https://doi.org/10.1016/j.bpj.2013.05.033.

Beal, M. F. *et al.* (2014) 'A randomized clinical trial of high-dosage coenzyme Q10 in early Parkinson disease: no evidence of benefit', *JAMA neurology*. American Medical Association, 71(5), pp. 543–552.

Bénit, P. *et al.* (2004) 'Mutant NDUFS3 subunit of mitochondrial complex I causes Leigh syndrome', *Journal of medical genetics*. BMJ Group, 41(1), pp. 14–17. doi: 10.1136/jmg.2003.014316.

Bento, C. F. *et al.* (2016) 'Mammalian Autophagy: How Does It Work?', *Annual Review of Biochemistry*. Annual Reviews, 85(1), pp. 685–713. doi: 10.1146/annurev-biochem-060815-014556.

Bergamin, N. *et al.* (2013) 'A human neuronal model of Niemann Pick C disease developed from stem cells isolated from patient's skin', *Orphanet journal of rare diseases*. BioMed Central, 8(1), p. 34.

Berger, F. *et al.* (2005) 'Subcellular compartmentation and differential catalytic properties of the three human nicotinamide mononucleotide adenylyltransferase isoforms', *Journal of Biological Chemistry*. ASBMB, 280(43), pp. 36334–36341.

Bergeron, D., Poulin, S. and Laforce, R. (2018) 'Cognition and anatomy of adult Niemann–Pick disease type C: Insights for the Alzheimer field', *Cognitive Neuropsychology*. Routledge, 35(3–4), pp. 209–222. doi: 10.1080/02643294.2017.1340264.

Berghe, T. Vanden *et al.* (2014) 'Regulated necrosis: the expanding network of non-apoptotic cell death pathways', *Nature reviews Molecular cell biology*. Nature Publishing Group, 15(2), p. 135.

Bernardi, R. *et al.* (1997) 'Analysis of poly (ADP-ribose) glycohydrolase activity in nuclear extracts from mammalian cells', *Biochimica et Biophysica Acta (BBA)-Protein Structure and Molecular Enzymology*. Elsevier, 1338(1), pp. 60–68.

Berry-Kravis, E. *et al.* (2018) 'Long-Term Treatment of Niemann-Pick Type C1 Disease With Intrathecal 2-Hydroxypropyl-β-Cyclodextrin', *Pediatric Neurology*, 80, pp. 24–34. doi: https://doi.org/10.1016/j.pediatrneurol.2017.12.014.

Bilan, D. S. *et al.* (2014) 'Genetically encoded fluorescent indicator for imaging NAD+/NADH ratio changes in different cellular compartments', *Biochimica et Biophysica Acta (BBA) - General Subjects*, 1840(3), pp. 951–957. doi: https://doi.org/10.1016/j.bbagen.2013.11.018.

Bingol, B. *et al.* (2014) 'The mitochondrial deubiquitinase USP30 opposes parkin-mediated mitophagy', *Nature*. Nature Publishing Group, a division of Macmillan Publishers Limited. All Rights Reserved., 510, p. 370. Available at: https://doi.org/10.1038/nature13418.

Bonkowski, M. S. and Sinclair, D. A. (2016) 'Slowing ageing by design: the rise of NAD(+) and sirtuin-activating compounds', *Nature reviews. Molecular cell biology*. 2016/08/24, 17(11), pp. 679–690. doi: 10.1038/nrm.2016.93.

Borradaile, N. M. and Pickering, J. G. (2009) 'Nicotinamide phosphoribosyltransferase imparts human endothelial cells with extended replicative lifespan and enhanced angiogenic capacity in a high glucose environment', *Aging Cell*. John Wiley & Sons, Ltd (10.1111), 8(2), pp. 100–112. doi: 10.1111/j.1474-9726.2009.00453.x.

Bosco, D. A. *et al.* (2006) 'Elevated levels of oxidized cholesterol metabolites in Lewy body disease brains accelerate α-synuclein fibrilization', *Nature Chemical Biology*, 2(5), pp. 249–253. doi: 10.1038/nchembio782.

Boswell-Casteel, R. C. and Hays, F. A. (2017) 'Equilibrative nucleoside transporters-A review', *Nucleosides, nucleotides & nucleic acids*. 2016/10/19, 36(1), pp. 7–30. doi: 10.1080/15257770.2016.1210805.

Böttinger, L. *et al.* (2012) 'Phosphatidylethanolamine and cardiolipin differentially affect the stability of mitochondrial respiratory chain supercomplexes', *Journal of molecular biology*. Elsevier, 423(5), pp. 677–686.

Boutant, M. and Cantó, C. (2014) 'SIRT1 metabolic actions: Integrating recent advances from mouse models', *Molecular Metabolism*, 3(1), pp. 5–18. doi: https://doi.org/10.1016/j.molmet.2013.10.006.

Bowling, A. C. *et al.* (1993) 'Age-dependent impairment of mitochondrial function in primate brain', *Journal of neurochemistry*. Wiley Online Library, 60(5), pp. 1964–1967.

Brand, M. D. *et al.* (2016) 'Suppressors of Superoxide-H2O2 Production at Site IQ of Mitochondrial Complex I Protect against Stem Cell Hyperplasia and Ischemia-Reperfusion Injury', *Cell Metabolism*, 24(4), pp. 582–592. doi: https://doi.org/10.1016/j.cmet.2016.08.012.

Brand, M. D. and Nicholls, D. G. (2011) 'Assessing mitochondrial dysfunction in cells',

Biochemical Journal, 437(3), pp. 575 LP – 575. doi: 10.1042/BJ4370575u.

Brauer, R. *et al.* (2015) 'Glitazone treatment and incidence of Parkinson's disease among people with diabetes: a retrospective cohort study', *PLoS medicine*. Public Library of Science, 12(7), p. e1001854.

Brown, G. C. and Borutaite, V. (2004) 'Inhibition of mitochondrial respiratory complex I by nitric oxide, peroxynitrite and S-nitrosothiols', *Biochimica et Biophysica Acta (BBA)-Bioenergetics*. Elsevier, 1658(1–2), pp. 44–49.

Bruick, R. K. (2000) 'Expression of the gene encoding the proapoptotic Nip3 protein is induced by hypoxia', *Proceedings of the National Academy of Sciences*. National Acad Sciences, 97(16), pp. 9082–9087.

Cabré, R. *et al.* (2017) 'Sixty years old is the breakpoint of human frontal cortex aging', *Free Radical Biology and Medicine*, 103, pp. 14–22. doi: https://doi.org/10.1016/j.freeradbiomed.2016.12.010.

Camacho-Pereira, J. *et al.* (2016) 'CD38 Dictates Age-Related NAD Decline and Mitochondrial Dysfunction through an SIRT3-Dependent Mechanism', *Cell Metabolism*, 23(6), pp. 1127–1139. doi: https://doi.org/10.1016/j.cmet.2016.05.006.

Cambronne, X. A. *et al.* (2016) 'Biosensor reveals multiple sources for mitochondrial NAD⁺', *Science*, 352(6292), pp. 1474 LP – 1477. doi: 10.1126/science.aad5168.

Campisi, J. *et al.* (2019) 'From discoveries in ageing research to therapeutics for healthy ageing', *Nature*, 571(7764), pp. 183–192. doi: 10.1038/s41586-019-1365-2.

Cantó, C., Menzies, K. J. and Auwerx, J. (2015) 'NAD+ Metabolism and the Control of Energy Homeostasis: A Balancing Act between Mitochondria and the Nucleus', *Cell Metabolism*, 22(1), pp. 31–53. doi: https://doi.org/10.1016/j.cmet.2015.05.023.

Caro, P. *et al.* (2010) 'Mitochondrial DNA sequences are present inside nuclear DNA in rat tissues and increase with age', *Mitochondrion*, 10(5), pp. 479–486. doi: https://doi.org/10.1016/j.mito.2010.05.004.

Carroll, B. *et al.* (2017) 'Persistent mTORC1 signaling in cell senescence results from defects in amino acid and growth factor sensing', *J Cell Biol*. Rockefeller University Press, 216(7), pp. 1949–1957.

Carroll, B. *et al.* (2018) 'Oxidation of SQSTM1/p62 mediates the link between redox state and protein homeostasis', *Nature Communications*, 9(1), p. 256. doi: 10.1038/s41467-017-02746-z.

Chaitanya, G. V., Steven, A. J. and Babu, P. P. (2010) 'PARP-1 cleavage fragments: signatures of cell-death proteases in neurodegeneration', *Cell communication and signaling : CCS*. BioMed Central, 8, p. 31. doi: 10.1186/1478-811X-8-31.

Chan, E. Y. W. *et al.* (2009) 'Kinase-inactivated ULK proteins inhibit autophagy via their conserved C-terminal domains using an Atg13-independent mechanism', *Molecular and cellular biology*. Am Soc Microbiol, 29(1), pp. 157–171.

Chau, V. *et al.* (1989) 'A multiubiquitin chain is confined to specific lysine in a targeted short-lived protein', *Science*, 243(4898), pp. 1576 LP – 1583. doi: 10.1126/science.2538923.

Chen, G. *et al.* (1999) 'The Mood-Stabilizing Agents Lithium and Valproate RobustIIncrease the Levels of the Neuroprotective Protein bcl-2 in the CNS', *Journal of neurochemistry*. Wiley Online Library, 72(2), pp. 879–882.

Chen, R.-W. and Chuang, D.-M. (1999) 'Long term lithium treatment suppresses p53 and Bax expression but increases Bcl-2 expression A prominent role in neuroprotection against excitotoxicity', *Journal of Biological Chemistry*. ASBMB, 274(10), pp. 6039–6042.

Chen, S. *et al.* (2010) 'HDAC6 regulates mitochondrial transport in hippocampal neurons', *PloS one*. Public Library of Science, 5(5), p. e10848.

Chen, Z. *et al.* (2015) 'PARP-1 promotes autophagy via the AMPK/mTOR pathway in CNE-2 human nasopharyngeal carcinoma cells following ionizing radiation, while inhibition of autophagy contributes to the radiation sensitization of CNE-2 cells', *Molecular medicine reports*. Spandidos Publications, 12(2), pp. 1868–1876.

Chicco, A. J. and Sparagna, G. C. (2007) 'Role of cardiolipin alterations in mitochondrial dysfunction and disease', *American Journal of Physiology-Cell Physiology*. American Physiological Society, 292(1), pp. C33–C44. doi: 10.1152/ajpcell.00243.2006.

Childs, B. G. *et al.* (2015) 'Cellular senescence in aging and age-related disease: from mechanisms to therapy', *Nature Medicine*. Nature Publishing Group, a division of Macmillan Publishers Limited. All Rights Reserved., 21, p. 1424. Available at: https://doi.org/10.1038/nm.4000.

Chini, C. *et al.* (2019) 'The NADase CD38 is induced by factors secreted from senescent cells providing a potential link between senescence and age-related cellular NAD+ decline', *Biochemical and Biophysical Research Communications*, 513(2), pp. 486–493. doi: https://doi.org/10.1016/j.bbrc.2019.03.199.

Chithra, Y. and Bharath, M. M. S. (2019) '17 Role of Post-Translational Modifications of Mitochondrial Complex I in Mitochondrial Dysfunction and Human Brain Pathologies', *Handbook of Mitochondrial Dysfunction*. CRC Press, p. 1947.

Chouchani, E. T. *et al.* (2013) 'Cardioprotection by S-nitrosation of a cysteine switch on mitochondrial complex I', *Nature medicine*. Nature Publishing Group, 19(6), p. 753.

Christian, F. (2017) 'Mitochondrial metabolites: undercover signalling molecules', *Interface Focus*. Royal Society, 7(2), p. 20160100. doi: 10.1098/rsfs.2016.0100.

Chu, C. T. *et al.* (2013) 'Cardiolipin externalization to the outer mitochondrial membrane acts as an elimination signal for mitophagy in neuronal cells', *Nature cell biology*. Nature Publishing Group, 15(10), p. 1197.

Clementi, E. *et al.* (1998) 'Persistent inhibition of cell respiration by nitric oxide: crucial role of S-nitrosylation of mitochondrial complex I and protective action of glutathione', *Proceedings of the National Academy of Sciences*. National Acad Sciences, 95(13), pp. 7631–7636.

Cogliati, S. *et al.* (2018) 'Regulation of Mitochondrial Electron Transport Chain Assembly', *Journal of Molecular Biology*, 430(24), pp. 4849–4873. doi: https://doi.org/10.1016/j.jmb.2018.09.016.

Cogliati, S., Enriquez, J. A. and Scorrano, L. (2016) 'Mitochondrial Cristae: Where Beauty Meets Functionality', *Trends in Biochemical Sciences*, 41(3), pp. 261–273. doi: https://doi.org/10.1016/j.tibs.2016.01.001.

Collins, G. A. and Goldberg, A. L. (2017) 'The Logic of the 26S Proteasome', *Cell*, 169(5), pp. 792–806. doi: https://doi.org/10.1016/j.cell.2017.04.023.

Cologna, S. M. *et al.* (2014) 'Human and mouse neuroinflammation markers in Niemann-Pick disease, type C1', *Journal of Inherited Metabolic Disease*, 37(1), pp. 83–92. doi: 10.1007/s10545-013-9610-6.

Coppé, J.-P. *et al.* (2008) 'Senescence-associated secretory phenotypes reveal cell-nonautonomous functions of oncogenic RAS and the p53 tumor suppressor', *PLoS biology*. Public Library of Science, 6(12), p. e301.

Correia-Melo, C. *et al.* (2016) 'Mitochondria are required for pro-ageing features of the senescent phenotype', *The EMBO Journal*. John Wiley & Sons, Ltd, 35(7), pp. 724–742. doi: 10.15252/embj.201592862.

Cougnoux, A. *et al.* (2016) 'Necroptosis in Niemann–Pick disease, type C1: a potential therapeutic target', *Cell death & disease*. Nature Publishing Group, 7(3), p. e2147.

Crosiers, D. *et al.* (2016) 'Mutations in glucocerebrosidase are a major genetic risk factor for Parkinson's disease and increase susceptibility to dementia in a Flanders-Belgian cohort',

Neuroscience Letters, 629, pp. 160–164. doi: https://doi.org/10.1016/j.neulet.2016.07.008.

Cuervo, A. M. *et al.* (2005) 'Autophagy and aging: the importance of maintaining" clean" cells', *Autophagy*. Taylor & Francis, 1(3), pp. 131–140.

Cuervo, A. M. (2010) 'Chaperone-mediated autophagy: selectivity pays off', *Trends in Endocrinology & Metabolism*, 21(3), pp. 142–150. doi: https://doi.org/10.1016/j.tem.2009.10.003.

Cummings, J. (2018) 'Lessons Learned from Alzheimer Disease: Clinical Trials with Negative Outcomes', *Clinical and translational science*. 2017/08/02. John Wiley and Sons Inc., 11(2), pp. 147–152. doi: 10.1111/cts.12491.

Dalle Pezze, P. *et al.* (2014) 'Dynamic modelling of pathways to cellular senescence reveals strategies for targeted interventions', *PLoS computational biology*. Public Library of Science, 10(8), p. e1003728.

Davies, J. P. and Ioannou, Y. A. (2000) 'Topological analysis of Niemann-Pick C1 protein reveals that the membrane orientation of the putative sterol-sensing domain is identical to those of 3-hydroxy-3-methylglutaryl-CoA reductase and sterol regulatory element binding protein cleavage-activating', *Journal of Biological Chemistry*. ASBMB, 275(32), pp. 24367–24374.

Davies, N. M. *et al.* (2000) 'Clinical Pharmacokinetics and Pharmacodynamics of Celecoxib', *Clinical Pharmacokinetics*, 38(3), pp. 225–242. doi: 10.2165/00003088-200038030-00003.

Davila, A. *et al.* (2018) 'Nicotinamide adenine dinucleotide is transported into mammalian mitochondria', *eLife*. Edited by A. Dillin. eLife Sciences Publications, Ltd, 7, p. e33246. doi: 10.7554/eLife.33246.

DBGET Search Result: REACTION NAD (no date). Available at: https://www.genome.jp/dbget-bin/www_bfind_sub?mode=bfind&max_hit=1000&locale=en&serv=gn&dbkey=reaction&keywords=NAD&page=3 (Accessed: 30 January 2019).

Denton, R. M. (2009) 'Regulation of mitochondrial dehydrogenases by calcium ions', *Biochimica et Biophysica Acta (BBA)-Bioenergetics*. Elsevier, 1787(11), pp. 1309–1316.

Detmer, S. A. and Chan, D. C. (2007) 'Functions and dysfunctions of mitochondrial dynamics', *Nature Reviews Molecular Cell Biology*. Nature Publishing Group, 8, p. 870. Available at: https://doi.org/10.1038/nrm2275.

Diaz, F., Enríquez, J. A. and Moraes, C. T. (2012) 'Cells Lacking Rieske Iron-Sulfur Protein Have a Reactive Oxygen Species-Associated Decrease in Respiratory Complexes I and IV', *Molecular and Cellular Biology*, 32(2), pp. 415 LP – 429. doi: 10.1128/MCB.06051-11.

Distl, R. *et al.* (2003) 'Cholesterol storage and tau pathology in Niemann–Pick type C disease in the brain', *The Journal of Pathology*. John Wiley & Sons, Ltd, 200(1), pp. 104–111. doi: 10.1002/path.1320.

Distl, R., Meske, V. and Ohm, T. G. (2001) 'Tangle-bearing neurons contain more free cholesterol than adjacent tangle-free neurons', *Acta neuropathologica*. Springer, 101(6), pp. 547–554.

Divakaruni, A. S. *et al.* (2013) 'Thiazolidinediones are acute, specific inhibitors of the mitochondrial pyruvate carrier', *Proceedings of the national academy of sciences*. National Acad Sciences, 110(14), pp. 5422–5427.

Dodd, S. *et al.* (2008) 'N-acetylcysteine for antioxidant therapy: pharmacology and clinical utility', *Expert Opinion on Biological Therapy*. Taylor & Francis, 8(12), pp. 1955–1962. doi: 10.1517/14728220802517901.

Dooley, H. C. *et al.* (2014) 'WIPI2 Links LC3 Conjugation with PI3P, Autophagosome Formation, and Pathogen Clearance by Recruiting Atg12–5-16L1', *Molecular Cell*, 55(2), pp. 238–252. doi: https://doi.org/10.1016/j.molcel.2014.05.021.

Dorn, G. W. (2010) 'Mitochondrial pruning by Nix and BNip3: an essential function for cardiac-expressed death factors', *Journal of cardiovascular translational research*. Springer, 3(4), pp. 374–383.

Dunn William A., J. *et al.* (2005) 'Pexophagy: The Selective Autophagy of Peroxisomes', *Autophagy*. Taylor & Francis, 1(2), pp. 75–83. doi: 10.4161/auto.1.2.1737.

Elhassan, Y. S., Philp, A. A. and Lavery, G. G. (2017) 'Targeting NAD+ in metabolic disease: new insights into an old molecule', *Journal of the Endocrine Society*. Oxford University Press, 1(7), pp. 816–835.

Elurbe, D. M. and Huynen, M. A. (2016) 'The origin of the supernumerary subunits and assembly factors of complex I: A treasure trove of pathway evolution', *Biochimica et Biophysica Acta (BBA) - Bioenergetics*, 1857(7), pp. 971–979. doi: https://doi.org/10.1016/j.bbabio.2016.03.027.

Fang, E. F. *et al.* (2014) *Defective mitophagy in XPA via PARP-1 hyperactivation and NAD+/SIRT1 reduction*, *Cell*. doi: 10.1016/j.cell.2014.03.026.

Fang, E. F. *et al.* (2017) 'NAD+ in Aging: Molecular Mechanisms and Translational Implications', *Trends in Molecular Medicine*, 23(10), pp. 899–916. doi: https://doi.org/10.1016/j.molmed.2017.08.001.

Fang, J. *et al.* (2013) 'Dihydro-orotate dehydrogenase is physically associated with the respiratory complex and its loss leads to mitochondrial dysfunction', *Bioscience reports*. Portland Press Limited, 33(2), p. e00021.

Fearnley, J. M. and Lees, A. J. (1991) 'Ageing and Parkinson's disease: substantia nigra regional selectivity', *Brain*. Oxford University Press, 114(5), pp. 2283–2301.

Fei, P. *et al.* (2004) 'Bnip3L is induced by p53 under hypoxia, and its knockdown promotes tumor growth', *Cancer cell*. Elsevier, 6(6), pp. 597–609.

Fernandez-Vizarra, E. and Zeviani, M. (2018) 'Mitochondrial complex III Rieske Fe-S protein processing and assembly', *Cell Cycle*. Taylor & Francis, 17(6), pp. 681–687. doi: 10.1080/15384101.2017.1417707.

Ferrucci, L. *et al.* (2015) 'Reconsidering the Role of Mitochondria in Aging', *The Journals of Gerontology: Series A*, 70(11), pp. 1334–1342. doi: 10.1093/gerona/glv070.

Finley, D. *et al.* (1994) 'Inhibition of proteolysis and cell cycle progression in a multiubiquitination-deficient yeast mutant.', *Molecular and Cellular Biology*, 14(8), pp. 5501 LP – 5509. doi: 10.1128/MCB.14.8.5501.

Finley, D. (2009) 'Recognition and Processing of Ubiquitin-Protein Conjugates by the Proteasome', *Annual Review of Biochemistry*. Annual Reviews, 78(1), pp. 477–513. doi: 10.1146/annurev.biochem.78.081507.101607.

Finley, D., Chen, X. and Walters, K. J. (2016) 'Gates, Channels, and Switches: Elements of the Proteasome Machine', *Trends in Biochemical Sciences*, 41(1), pp. 77–93. doi: https://doi.org/10.1016/j.tibs.2015.10.009.

Fløynes, I. H. *et al.* (2018) 'Neuronal complex I deficiency occurs throughout the Parkinson's disease brain, but is not associated with neurodegeneration or mitochondrial DNA damage', *Acta Neuropathologica*, 135(3), pp. 409–425. doi: 10.1007/s00401-017-1794-7.

Fog, C. K. and Kirkegaard, T. (2019) 'Animal models for Niemann-Pick type C: implications for drug discovery & development', *Expert Opinion on Drug Discovery*. Taylor & Francis, 14(5), pp. 499–509. doi: 10.1080/17460441.2019.1588882.

Formosa, L. E. *et al.* (2018) 'Building a complex complex: Assembly of mitochondrial respiratory chain complex I', *Seminars in Cell & Developmental Biology*, 76, pp. 154–162. doi: https://doi.org/10.1016/j.semcdb.2017.08.011.

Forte, M. *et al.* (2019) 'Mitochondrial complex I deficiency and cardiovascular diseases: current evidence and future directions', *Journal of Molecular Medicine*, 97(5), pp. 579–591. doi:

10.1007/s00109-019-01771-3.

Fouquerel, E. *et al.* (2014) 'ARTD1/PARP1 Negatively Regulates Glycolysis by Inhibiting Hexokinase 1 Independent of NAD+ Depletion', *Cell Reports*, 8(6), pp. 1819–1831. doi: https://doi.org/10.1016/j.celrep.2014.08.036.

Fratelli, M. *et al.* (2002) 'Identification by redox proteomics of glutathionylated proteins in oxidatively stressed human T lymphocytes', *Proceedings of the National Academy of Sciences*, 99(6), pp. 3505 LP – 3510. doi: 10.1073/pnas.052592699.

Frazier, A. E., Thorburn, D. R. and Compton, A. G. (2019) 'Mitochondrial energy generation disorders: genes, mechanisms, and clues to pathology', *Journal of Biological Chemistry*. ASBMB, 294(14), pp. 5386–5395.

Fu, R. *et al.* (2010) 'Oxidative stress in Niemann–Pick disease, type C', *Molecular Genetics and Metabolism*, 101(2), pp. 214–218. doi: https://doi.org/10.1016/j.ymgme.2010.06.018.

Fukuyama, R. *et al.* (1996) 'Gene expression of ND4, a subunit of complex I of oxidative phosphorylation in mitochondria, is decreased in temporal cortex of brains of Alzheimer's disease patients', *Brain research*. Elsevier, 713(1–2), pp. 290–293.

Galasko, D. R. *et al.* (2012) 'Antioxidants for Alzheimer disease: a randomized clinical trial with cerebrospinal fluid biomarker measures', *Archives of neurology*, 69(7), pp. 836–841. doi: 10.1001/archneurol.2012.85.

Galkin, A. *et al.* (2008) 'Identification of the mitochondrial ND3 subunit as a structural component involved in the active/deactive enzyme transition of respiratory complex I', *Journal of Biological Chemistry*. ASBMB, 283(30), pp. 20907–20913.

Galkin, A. and Moncada, S. (2007) 'S-nitrosation of mitochondrial complex I depends on its structural conformation', *Journal of Biological Chemistry*. ASBMB, 282(52), pp. 37448–37453.

Galkin, A. and Moncada, S. (2017) 'Modulation of the conformational state of mitochondrial complex I as a target for therapeutic intervention', *Interface Focus*. The Royal Society, 7(2), p. 20160104.

Galluzzi, L. *et al.* (2018) 'Molecular mechanisms of cell death: recommendations of the Nomenclature Committee on Cell Death 2018', *Cell Death & Differentiation*, 25(3), pp. 486–541. doi: 10.1038/s41418-017-0012-4.

Ganley, I. G. *et al.* (2009) 'ULK1· ATG13· FIP200 complex mediates mTOR signaling and is essential for autophagy', *Journal of Biological Chemistry*. ASBMB, 284(18), pp. 12297–12305.

García-Sanz, P. *et al.* (2017) 'N370S-GBA1 mutation causes lysosomal cholesterol accumulation in Parkinson's disease', *Movement Disorders*. John Wiley & Sons, Ltd, 32(10), pp. 1409–1422. doi: 10.1002/mds.27119.

Gattermann, N. *et al.* (2004) 'Severe impairment of nucleotide synthesis through inhibition of mitochondrial respiration', *Nucleosides, Nucleotides and Nucleic Acids*. Taylor & Francis, 23(8–9), pp. 1275–1279.

Geberhiwot, T. *et al.* (2018) 'Consensus clinical management guidelines for Niemann-Pick disease type C', *Orphanet journal of rare diseases*. BioMed Central, 13(1), p. 50. doi: 10.1186/s13023-018-0785-7.

Gelsthorpe, M. E. *et al.* (2008) 'Niemann-Pick type C1 I1061T mutant encodes a functional protein that is selected for endoplasmic reticulum-associated degradation due to protein misfolding', *The Journal of biological chemistry*. 2008/01/23. American Society for Biochemistry and Molecular Biology, 283(13), pp. 8229–8236. doi: 10.1074/jbc.M708735200.

Ghio, S. *et al.* (2016) 'Interaction of α-synuclein with biomembranes in Parkinson's disease—role of cardiolipin', *Progress in lipid research*. Elsevier, 61, pp. 73–82.

Ghosh, A. *et al.* (2016) 'Mitochondrial pyruvate carrier regulates autophagy, inflammation, and neurodegeneration in experimental models of Parkinson's disease', *Science Translational Medicine*, 8(368), pp. 368ra174 LP-368ra174. doi: 10.1126/scitranslmed.aag2210.

Giachin, G. *et al.* (2016) 'Dynamics of human mitochondrial complex I assembly: implications for neurodegenerative diseases', *Frontiers in molecular biosciences*. Frontiers, 3, p. 43.

Gincel, D., Zaid, H. and Shoshan-Barmatz, V. (2000) 'Calcium Binding and Translocation by VDAC: a possible regulatory mechanism in mitochondrial function', *Biochemical Society Transactions*. Portland Press Limited, 28(5), p. A390.3-A390. doi: 10.1042/bst028a390b.

Glatigny, M. *et al.* (2019) 'Autophagy Is Required for Memory Formation and Reverses Age-Related Memory Decline', *Current Biology*, 29(3), pp. 435-448.e8. doi: https://doi.org/10.1016/j.cub.2018.12.021.

Gomes, A. P. *et al.* (2013) 'Declining NAD+ Induces a Pseudohypoxic State Disrupting Nuclear-Mitochondrial Communication during Aging', *Cell*, 155(7), pp. 1624–1638. doi: https://doi.org/10.1016/j.cell.2013.11.037.

Gómez-Sánchez, R. *et al.* (2018) 'Atg9 establishes Atg2-dependent contact sites between the endoplasmic reticulum and phagophores', *The Journal of Cell Biology*, 217(8), pp. 2743 LP – 2763. doi: 10.1083/jcb.201710116.

Gong, B. *et al.* (2013) 'Nicotinamide riboside restores cognition through an upregulation of proliferator-activated receptor-γ coactivator 1α regulated β-secretase 1 degradation and mitochondrial gene expression in Alzheimer's mouse models', *Neurobiology of Aging*, 34(6), pp. 1581–1588. doi: https://doi.org/10.1016/j.neurobiolaging.2012.12.005.

Gong, J.-S. *et al.* (2002) 'Apolipoprotein E (ApoE) isoform-dependent lipid release from astrocytes prepared from human ApoE3 and ApoE4 knock-in mice', *Journal of Biological Chemistry*. ASBMB, 277(33), pp. 29919–29926.

Gong, L. *et al.* (2012) 'Celecoxib pathways: pharmacokinetics and pharmacodynamics', *Pharmacogenetics and genomics*, 22(4), pp. 310–318. doi: 10.1097/FPC.0b013e32834f94cb.

Goodwin, P. M. *et al.* (1978) 'The effect of gamma radiation and neocarzinostatin of NAD and ATP levels in mouse leukaemia cells', *Biochimica et Biophysica Acta (BBA)-General Subjects*. Elsevier, 543(4), pp. 576–582.

Gowthami, N. *et al.* (2019) 'Mapping the protein phosphorylation sites in human mitochondrial complex I (NADH: Ubiquinone oxidoreductase): A bioinformatics study with implications for brain aging and neurodegeneration', *Journal of Chemical Neuroanatomy*, 95, pp. 13–28. doi: https://doi.org/10.1016/j.jchemneu.2018.02.004.

Grant, R. S., Coggan, S. E. and Smythe, G. A. (2009) 'The physiological action of picolinic Acid in the human brain', *International journal of tryptophan research : IJTR*. Libertas Academica, 2, pp. 71–79. Available at: https://www.ncbi.nlm.nih.gov/pubmed/22084583.

Greaves, L. C. *et al.* (2014) 'Clonal expansion of early to mid-life mitochondrial DNA point mutations drives mitochondrial dysfunction during human ageing', *PLoS genetics*. Public Library of Science, 10(9), p. e1004620.

Greenamyre, J. T. *et al.* (2001) 'Complex I and Parkinson's disease', *IUBMB life*. Wiley Online Library, 52(3-5), pp. 135–141.

Gross, C. J. and Henderson, L. M. (1983) 'Digestion and absorption of NAD by the small intestine of the rat', *The journal of nutrition*. Oxford University Press, 113(2), pp. 412–420.

Grozio, A. *et al.* (2013) 'CD73 protein as a source of extracellular precursors for sustained NAD+ biosynthesis in FK866-treated tumor cells', *Journal of Biological Chemistry*. ASBMB, 288(36), pp. 25938–25949.

Gu, J. *et al.* (2016) 'The architecture of the mammalian respirasome', *Nature*. Macmillan Publishers Limited, part of Springer Nature. All rights reserved., 537, p. 639. Available at: https://doi.org/10.1038/nature19359.

Guarente, L. (2014) 'Aging Research—Where Do We Stand and Where Are We Going?', *Cell*, 159(1), pp. 15–19. doi: https://doi.org/10.1016/j.cell.2014.08.041.

Guo, F. *et al.* (2018) 'Autophagy in neurodegenerative diseases: pathogenesis and therapy',

Brain Pathology. Wiley Online Library, 28(1), pp. 3–13.

Guo, J. Y. *et al.* (2016) 'Autophagy provides metabolic substrates to maintain energy charge and nucleotide pools in Ras-driven lung cancer cells', *Genes & development*. Cold Spring Harbor Laboratory Press, 30(15), pp. 1704–1717. doi: 10.1101/gad.283416.116.

Gupte, R., Liu, Z. and Kraus, W. L. (2017) 'PARPs and ADP-ribosylation: recent advances linking molecular functions to biological outcomes', *Genes & Development*. Cold Spring Harbor Lab, 31(2), pp. 101–126.

Guzy, R. D. *et al.* (2008) 'Loss of the SdhB, but Not the SdhA, Subunit of Complex II Triggers Reactive Oxygen Species-Dependent Hypoxia-Inducible Factor Activation and Tumorigenesis', *Molecular and Cellular Biology*, 28(2), pp. 718 LP – 731. doi: 10.1128/MCB.01338-07.

Hammerschmidt, T. G. *et al.* (2018) 'Molecular and biochemical biomarkers for diagnosis and therapy monitorization of Niemann-Pick type C patients', *International Journal of Developmental Neuroscience*, 66, pp. 18–23. doi: https://doi.org/10.1016/j.ijdevneu.2017.11.007.

Hanschmann, E.-M. *et al.* (2013) 'Thioredoxins, glutaredoxins, and peroxiredoxins—molecular mechanisms and health significance: from cofactors to antioxidants to redox signaling', *Antioxidants & redox signaling*. Mary Ann Liebert, Inc. 140 Huguenot Street, 3rd Floor New Rochelle, NY 10801 USA, 19(13), pp. 1539–1605.

Hara, T. *et al.* (2006) 'Suppression of basal autophagy in neural cells causes neurodegenerative disease in mice', *Nature*. Nature Publishing Group, 441, p. 885. Available at: https://doi.org/10.1038/nature04724.

Hara, T. *et al.* (2008) *FIP200, a ULK-interacting protein, is required for autophagosome formation in mammalian cells*, *The Journal of cell biology*. doi: 10.1083/jcb.200712064.

Harbauer, A. B. *et al.* (2014) 'The Protein Import Machinery of Mitochondria—A Regulatory Hub in Metabolism, Stress, and Disease', *Cell Metabolism*, 19(3), pp. 357–372. doi: https://doi.org/10.1016/j.cmet.2014.01.010.

Harman, D. (1972) 'The biologic clock: the mitochondria?', *Journal of the American Geriatrics Society*. Wiley Online Library, 20(4), pp. 145–147.

Harper, J. W. and Bennett, E. J. (2016) 'Proteome complexity and the forces that drive proteome imbalance', *Nature*. Nature Publishing Group, a division of Macmillan Publishers Limited. All Rights Reserved., 537, p. 328. Available at: https://doi.org/10.1038/nature19947.

Harper, J. W., Ordureau, A. and Heo, J.-M. (2018) 'Building and decoding ubiquitin chains for mitophagy', *Nature Reviews Molecular Cell Biology*. Nature Publishing Group, a division of Macmillan Publishers Limited. All Rights Reserved., 19, p. 93. Available at: https://doi.org/10.1038/nrm.2017.129.

Hasmann, M. and Schemainda, I. (2003) 'FK866, a Highly Specific Noncompetitive Inhibitor of Nicotinamide Phosphoribosyltransferase, Represents a Novel Mechanism for Induction of Tumor Cell Apoptosis', *Cancer Research*, 63(21), pp. 7436 LP – 7442. Available at: http://cancerres.aacrjournals.org/content/63/21/7436.abstract.

Hayashi-Nishino, M. *et al.* (2009) 'A subdomain of the endoplasmic reticulum forms a cradle for autophagosome formation', *Nature cell biology*. Nature Publishing Group, 11(12), p. 1433.

Hegedűs, C. and Virág, L. (2014) 'Inputs and outputs of poly(ADP-ribosyl)ation: Relevance to oxidative stress', *Redox Biology*, 2, pp. 978–982. doi: https://doi.org/10.1016/j.redox.2014.08.003.

Henderson, M. X. *et al.* (2017) 'Unbiased proteomics of early Lewy body formation model implicates active microtubule affinity-regulating kinases (MARKs) in synucleinopathies', *Journal of Neuroscience*. Soc Neuroscience, 37(24), pp. 5870–5884.

Henning, R. J., Bourgeois, M. and Harbison, R. D. (2018) 'Poly (ADP-ribose) Polymerase

(PARP) and PARP Inhibitors: Mechanisms of Action and Role in Cardiovascular Disorders', *Cardiovascular toxicology*. Springer, 18(6), pp. 493–506.

Hermann, A. and Storch, A. (2013) 'Induced neural stem cells (iNSCs) in neurodegenerative diseases', *Journal of Neural Transmission*, 120(1), pp. 19–25. doi: 10.1007/s00702-013-1042-9.

Hipp, M. S., Kasturi, P. and Hartl, F. U. (2019) 'The proteostasis network and its decline in ageing', *Nature Reviews Molecular Cell Biology*. Nature Publishing Group, p. 1.

Hirst, J., King, M. S. and Pryde, K. R. (2008) 'The production of reactive oxygen species by complex I', *Biochemical Society Transactions*, 36(5), pp. 976 LP – 980. doi: 10.1042/BST0360976.

Ho, T. T. *et al.* (2017) 'Autophagy maintains the metabolism and function of young and old stem cells', *Nature*. Macmillan Publishers Limited, part of Springer Nature. All rights reserved., 543, p. 205. Available at: https://doi.org/10.1038/nature21388.

Hong, H.-S. *et al.* (2009) 'Inhibition of Alzheimer's amyloid toxicity with a tricyclic pyrone molecule in vitro and in vivo', *Journal of neurochemistry*, 108(4), pp. 1097–1108. doi: 10.1111/j.1471-4159.2008.05866.x.

Hosokawa, N. *et al.* (2009) 'Nutrient-dependent mTORC1 association with the ULK1–Atg13–FIP200 complex required for autophagy', *Molecular biology of the cell*. Am Soc Cell Biol, 20(7), pp. 1981–1991.

Hou, Y. *et al.* (2018) 'NAD⁺ supplementation normalizes key Alzheimer's features and DNA damage responses in a new AD mouse model with introduced DNA repair deficiency', *Proceedings of the National Academy of Sciences*, 115(8), p. E1876 LP-E1885. doi: 10.1073/pnas.1718819115.

Houtkooper, R. H., Pirinen, E. and Auwerx, J. (2012) 'Sirtuins as regulators of metabolism and healthspan', *Nature reviews. Molecular cell biology*, 13(4), pp. 225–238. doi: 10.1038/nrm3293.

Hove-Jensen, B. *et al.* (2017) 'Phosphoribosyl Diphosphate (PRPP): Biosynthesis, Enzymology, Utilization, and Metabolic Significance', *Microbiology and Molecular Biology Reviews*, 81(1), pp. e00040-16. doi: 10.1128/MMBR.00040-16.

Huang, D. *et al.* (2015) 'Spatial and temporal dynamics of the cardiac mitochondrial proteome AU - Lau, Edward', *Expert Review of Proteomics*. Taylor & Francis, 12(2), pp. 133–146. doi: 10.1586/14789450.2015.1024227.

Huang, R. *et al.* (2015) 'Deacetylation of Nuclear LC3 Drives Autophagy Initiation under Starvation', *Molecular Cell*, 57(3), pp. 456–466. doi: https://doi.org/10.1016/j.molcel.2014.12.013.

Huang, S. and Sinicrope, F. (2010) 'Celecoxib-induced apoptosis is enhanced by ABT-737 and by inhibition of autophagy in human colorectal cancer cells', *Autophagy*. Taylor & Francis, 6(2), pp. 256–269. doi: 10.4161/auto.6.2.11124.

Huang, X. and Dixit, V. M. (2016) 'Drugging the undruggables: exploring the ubiquitin system for drug development', *Cell Research*. The Author(s), 26, p. 484. Available at: https://doi.org/10.1038/cr.2016.31.

Van Humbeeck, C. *et al.* (2011) 'Parkin Interacts with Ambra1 to Induce Mitophagy', *The Journal of Neuroscience*, 31(28), pp. 10249 LP – 10261. doi: 10.1523/JNEUROSCI.1917-11.2011.

Van Humbeeck, C. *et al.* (2014) 'The deubiquitinase USP15 antagonizes Parkin-mediated mitochondrial ubiquitination and mitophagy', *Human Molecular Genetics*, 23(19), pp. 5227–5242. doi: 10.1093/hmg/ddu244.

Hung, Y. P. *et al.* (2011) 'Imaging cytosolic NADH-NAD+ redox state with a genetically encoded fluorescent biosensor', *Cell metabolism*. Elsevier, 14(4), pp. 545–554.

Hurd, T. R. *et al.* (2008) 'Complex I within Oxidatively Stressed Bovine Heart Mitochondria Is Glutathionylated on Cys-531 and Cys-704 of the 75-kDa Subunit POTENTIAL ROLE OF CYS RESIDUES IN DECREASING OXIDATIVE DAMAGE', *Journal of Biological Chemistry*. ASBMB, 283(36), pp. 24801–24815.

Hwang, E. S. and Song, S. B. (2017) 'Nicotinamide is an inhibitor of SIRT1 in vitro, but can be a stimulator in cells', *Cellular and Molecular Life Sciences*. Springer, 74(18), pp. 3347–3362.

Ibsen, K. H. (1961) 'The Crabtree effect: a review', *Cancer research*. American Association for Cancer Research, 21(7), pp. 829–841.

Ichas, F. and Mazat, J.-P. (1998) 'From calcium signaling to cell death: two conformations for the mitochondrial permeability transition pore. Switching from low-to high-conductance state', *Biochimica et Biophysica Acta (BBA)-Bioenergetics*. Elsevier, 1366(1–2), pp. 33–50.

Investigators, N. E. T. in P. D. (NET-P. F.-Z. (2015) 'Pioglitazone in early Parkinson's disease: a phase 2, multicentre, double-blind, randomised trial', *The Lancet. Neurology*. 2015/06/23, 14(8), pp. 795–803. doi: 10.1016/S1474-4422(15)00144-1.

Ishihara, N. *et al.* (2006) 'Regulation of mitochondrial morphology through proteolytic cleavage of OPA1', *The EMBO Journal*, 25(13), pp. 2966 LP – 2977. doi: 10.1038/sj.emboj.7601184.

James, A. M. *et al.* (2005) 'Interactions of Mitochondria-targeted and Untargeted Ubiquinones with the Mitochondrial Respiratory Chain and Reactive Oxygen Species: IMPLICATIONS FOR THE USE OF EXOGENOUS UBIQUINONES AS THERAPIES AND EXPERIMENTAL TOOLS ', *Journal of Biological Chemistry* , 280(22), pp. 21295–21312. doi: 10.1074/jbc.M501527200.

Jaquenod De Giusti, C., Roman, B. and Das, S. (2018) 'The influence of microRNAs on Mitochondrial Calcium', *Frontiers in physiology*. Frontiers, 9, p. 1291.

De Jesús-Cortés, H. *et al.* (2015) 'Protective efficacy of P7C3-S243 in the 6-hydroxydopamine model of Parkinson's disease', *Npj Parkinson'S Disease*. The Author(s), 1, p. 15010. Available at: https://doi.org/10.1038/npjparkd.2015.10.

Jha, P., Wang, X. and Auwerx, J. (2016) 'Analysis of Mitochondrial Respiratory Chain Supercomplexes Using Blue Native Polyacrylamide Gel Electrophoresis (BN-PAGE)', *Curr Protoc Mouse Biol.*, 6, pp. 1–14. doi: 10.1002/9780470942390.mo150182.

Jiang, X. *et al.* (2011) 'A sensitive and specific LC-MS/MS method for rapid diagnosis of Niemann-Pick C1 disease from human plasma', *Journal of lipid research*. ASBMB, 52(7), pp. 1435–1445.

Jin, S. M. *et al.* (2010) 'Mitochondrial membrane potential regulates PINK1 import and proteolytic destabilization by PARL', *The Journal of Cell Biology*, 191(5), pp. 933 LP – 942. doi: 10.1083/jcb.201008084.

Johansen, T. and Lamark, T. (2011) 'Selective autophagy mediated by autophagic adapter proteins', *autophagy*. Taylor & Francis, 7(3), pp. 279–296.

Johnston, I. G. and Williams, B. P. (2016) 'Evolutionary Inference across Eukaryotes Identifies Specific Pressures Favoring Mitochondrial Gene Retention', *Cell Systems*, 2(2), pp. 101–111. doi: https://doi.org/10.1016/j.cels.2016.01.013.

Jones, A. J. Y. *et al.* (2017) 'Respiratory complex I in Bos taurus and Paracoccus denitrificans pumps four protons across the membrane for every NADH oxidized', *Journal of Biological Chemistry*. ASBMB, 292(12), pp. 4987–4995.

Jung, C. H. *et al.* (2009) 'ULK-Atg13-FIP200 complexes mediate mTOR signaling to the autophagy machinery', *Molecular biology of the cell*. Am Soc Cell Biol, 20(7), pp. 1992–2003.

Kagan, V. E. *et al.* (2004) 'Oxidative lipidomics of apoptosis: redox catalytic interactions of cytochrome c with cardiolipin and phosphatidylserine', *Free Radical Biology and Medicine*. Elsevier, 37(12), pp. 1963–1985.

Kanai, M. *et al.* (2007) 'Inhibition of Crm1–p53 interaction and nuclear export of p53 by poly (ADP-ribosyl) ation', *Nature cell biology*. Nature Publishing Group, 9(10), p. 1175.

Karagiannis, P. (2019) ‘Clinical Potential of Induced Pluripotent Stem Cells’, in *Medical Applications of iPS Cells*. Springer, pp. 3–12.

Karsli-Uzunbas, G. *et al.* (2014) ‘Autophagy Is Required for Glucose Homeostasis and Lung Tumor Maintenance’, *Cancer Discovery*, 4(8), pp. 914 LP – 927. doi: 10.1158/2159-8290.CD-14-0363.

Karunadharma, P. P. *et al.* (2015) ‘Respiratory chain protein turnover rates in mice are highly heterogeneous but strikingly conserved across tissues, ages, and treatments’, *The FASEB Journal*. Federation of American Societies for Experimental Biology, 29(8), pp. 3582–3592. doi: 10.1096/fj.15-272666.

Katsyuba, E. *et al.* (2018) ‘De novo NAD(+) synthesis enhances mitochondrial function and improves health’, *Nature*. 2018/10/24, 563(7731), pp. 354–359. doi: 10.1038/s41586-018-0645-6.

Kennedy, B. E. *et al.* (2014) ‘Adaptations of energy metabolism associated with increased levels of mitochondrial cholesterol in Niemann-Pick type C1-deficient cells’, *Journal of Biological Chemistry*. ASBMB, 289(23), pp. 16278–16289.

Khan, J. A., Tao, X. and Tong, L. (2006) ‘Molecular basis for the inhibition of human NMPRTase, a novel target for anticancer agents’, *Nature Structural & Molecular Biology*, 13(7), pp. 582–588. doi: 10.1038/nsmb1105.

Kihara, A. *et al.* (2001) ‘Beclin–phosphatidylinositol 3-kinase complex functions at the trans-Golgi network’, *EMBO reports*. John Wiley & Sons, Ltd, 2(4), pp. 330–335.

Kim, Y. E. *et al.* (2013) ‘Molecular Chaperone Functions in Protein Folding and Proteostasis’, *Annual Review of Biochemistry*. Annual Reviews, 82(1), pp. 323–355. doi: 10.1146/annurev-biochem-060208-092442.

Kirchner, P. *et al.* (2019) ‘Proteome-wide analysis of chaperone-mediated autophagy targeting motifs’, *PLoS biology*. Public Library of Science, 17(5), p. e3000301.

Klionsky, D. J. *et al.* (2012) ‘Guidelines for the use and interpretation of assays for monitoring autophagy’, *Autophagy*. Taylor & Francis, 8(4), pp. 445–544. doi: 10.4161/auto.19496.

Klionsky, D. J. and Emr, S. D. (2000) ‘Autophagy as a Regulated Pathway of Cellular Degradation’, *Science*, 290(5497), pp. 1717 LP – 1721. doi: 10.1126/science.290.5497.1717.

Kluenemann, H. H. *et al.* (2013) ‘Parkinsonism syndrome in heterozygotes for Niemann–Pick C1’, *Journal of the Neurological Sciences*, 335(1), pp. 219–220. doi: https://doi.org/10.1016/j.jns.2013.08.033.

Komatsu, M. *et al.* (2005) ‘Impairment of starvation-induced and constitutive autophagy in Atg7-deficient mice’, *The Journal of Cell Biology*, 169(3), pp. 425 LP – 434. doi: 10.1083/jcb.200412022.

Kopito, R. R. (2000) ‘Aggresomes, inclusion bodies and protein aggregation’, *Trends in Cell Biology*, 10(12), pp. 524–530. doi: https://doi.org/10.1016/S0962-8924(00)01852-3.

Koshiba, T. *et al.* (2004) ‘Structural Basis of Mitochondrial Tethering by Mitofusin Complexes’, *Science*, 305(5685), pp. 858 LP – 862. doi: 10.1126/science.1099793.

Kotani, T. *et al.* (2018) ‘The Atg2-Atg18 complex tethers pre-autophagosomal membranes to the endoplasmic reticulum for autophagosome formation’, *Proceedings of the National Academy of Sciences*. National Acad Sciences, 115(41), pp. 10363–10368.

Koyano, F. *et al.* (2014) ‘Ubiquitin is phosphorylated by PINK1 to activate parkin’, *Nature*. Nature Publishing Group, a division of Macmillan Publishers Limited. All Rights Reserved., 510, p. 162. Available at: https://doi.org/10.1038/nature13392.

Kuma, A. *et al.* (2004) ‘The role of autophagy during the early neonatal starvation period’, *Nature*. Macmillan Magazines Ltd., 432, p. 1032. Available at: https://doi.org/10.1038/nature03029.

Kuma, A., Komatsu, M. and Mizushima, N. (2017) 'Autophagy-monitoring and autophagy-deficient mice', *Autophagy*. 2017/08/18. Taylor & Francis, 13(10), pp. 1619–1628. doi: 10.1080/15548627.2017.1343770.

Kumar, A., Singh, A. and Ekavali (2015) 'A review on Alzheimer's disease pathophysiology and its management: an update', *Pharmacological Reports*, 67(2), pp. 195–203. doi: https://doi.org/10.1016/j.pharep.2014.09.004.

Kwon, Y. T. and Ciechanover, A. (2017) 'The Ubiquitin Code in the Ubiquitin-Proteasome System and Autophagy', *Trends in Biochemical Sciences*, 42(11), pp. 873–886. doi: https://doi.org/10.1016/j.tibs.2017.09.002.

De la Fuente, I. M. *et al.* (2014) 'On the dynamics of the adenylate energy system: homeorhesis vs homeostasis', *PloS one*. Public Library of Science, 9(10), pp. e108676–e108676. doi: 10.1371/journal.pone.0108676.

Labbadia, J. and Morimoto, R. I. (2015) 'The Biology of Proteostasis in Aging and Disease', *Annual Review of Biochemistry*. Annual Reviews, 84(1), pp. 435–464. doi: 10.1146/annurev-biochem-060614-033955.

Lachmann, R. H. *et al.* (2004) 'Treatment with miglustat reverses the lipid-trafficking defect in Niemann–Pick disease type C', *Neurobiology of disease*. Elsevier, 16(3), pp. 654–658.

Lackner, L. L. (2019) 'The Expanding and Unexpected Functions of Mitochondria Contact Sites', *Trends in Cell Biology*, 29(7), pp. 580–590. doi: https://doi.org/10.1016/j.tcb.2019.02.009.

Lapuente-Brun, E. *et al.* (2013) 'Supercomplex Assembly Determines Electron Flux in the Mitochondrial Electron Transport Chain', *Science*, 340(6140), pp. 1567 LP – 1570. doi: 10.1126/science.1230381.

Lavandero, S. *et al.* (2015) 'Autophagy in cardiovascular biology', *The Journal of Clinical Investigation*. The American Society for Clinical Investigation, 125(1), pp. 55–64. doi: 10.1172/JCI73943.

Lazarou, M. *et al.* (2007) 'Analysis of the Assembly Profiles for Mitochondrial- and Nuclear-DNA-Encoded Subunits into Complex I', *Molecular and Cellular Biology*, 27(12), pp. 4228 LP – 4237. doi: 10.1128/MCB.00074-07.

Lazarou, M. *et al.* (2015) 'The ubiquitin kinase PINK1 recruits autophagy receptors to induce mitophagy', *Nature*. 2015/08/12, 524(7565), pp. 309–314. doi: 10.1038/nature14893.

Lee, H. *et al.* (2014) 'Pathological roles of the VEGF/SphK pathway in Niemann–Pick type C neurons', *Nature communications*. Nature Publishing Group, 5, p. 5514.

Lee, I. H. *et al.* (2008) 'A role for the NAD-dependent deacetylase Sirt1 in the regulation of autophagy', *Proceedings of the National Academy of Sciences*, 105(9), pp. 3374 LP – 3379. doi: 10.1073/pnas.0712145105.

Lee, J. J. *et al.* (2018) 'Basal mitophagy is widespread in Drosophila but minimally affected by loss of Pink1 or parkin', *The Journal of Cell Biology*, 217(5), pp. 1613 LP – 1622. doi: 10.1083/jcb.201801044.

Lee, Y.-K. and Lee, J.-A. (2016) 'Role of the mammalian ATG8/LC3 family in autophagy: differential and compensatory roles in the spatiotemporal regulation of autophagy', *BMB reports*. Korean Society for Biochemistry and Molecular Biology, 49(8), pp. 424–430. doi: 10.5483/BMBRep.2016.49.8.081.

Levine, B. and Kroemer, G. (2019) 'Biological Functions of Autophagy Genes: A Disease Perspective', *Cell*, 176(1), pp. 11–42. doi: https://doi.org/10.1016/j.cell.2018.09.048.

Levine, B. and Yuan, J. (2005) 'Autophagy in cell death: an innocent convict?', *The Journal of Clinical Investigation*. The American Society for Clinical Investigation, 115(10), pp. 2679–2688. doi: 10.1172/JCI26390.

Li, W. *et al.* (2014) 'MicroRNA-137 is a novel hypoxia-responsive microRNA that inhibits

mitophagy via regulation of two mitophagy receptors FUNDC1 and NIX', *Journal of Biological Chemistry*. ASBMB, 289(15), pp. 10691–10701.

Li, Z. *et al.* (2011) 'Mitochondrial ROS generation for regulation of autophagic pathways in cancer', *Biochemical and Biophysical Research Communications*, 414(1), pp. 5–8. doi: https://doi.org/10.1016/j.bbrc.2011.09.046.

Liang, C.-C. *et al.* (2010) 'Neural-specific deletion of FIP200 leads to cerebellar degeneration caused by increased neuronal death and axon degeneration', *Journal of Biological Chemistry*. ASBMB, 285(5), pp. 3499–3509.

Liao, G. *et al.* (2007) 'Cholesterol accumulation is associated with lysosomal dysfunction and autophagic stress in Npc1−/− mouse brain', *The American journal of pathology*. Elsevier, 171(3), pp. 962–975.

Lill, R. and Kispal, G. (2000) 'Maturation of cellular Fe–S proteins: an essential function of mitochondria', *Trends in Biochemical Sciences*, 25(8), pp. 352–356. doi: https://doi.org/10.1016/S0968-0004(00)01589-9.

Lim, H. *et al.* (2018) 'A novel autophagy enhancer as a therapeutic agent against metabolic syndrome and diabetes', *Nature Communications*, 9(1), p. 1438. doi: 10.1038/s41467-018-03939-w.

Lin, M.-Y. *et al.* (2017) 'Releasing Syntaphilin Removes Stressed Mitochondria from Axons Independent of Mitophagy under Pathophysiological Conditions', *Neuron*, 94(3), pp. 595-610.e6. doi: https://doi.org/10.1016/j.neuron.2017.04.004.

Lin, M. T. and Beal, M. F. (2006) 'Mitochondrial dysfunction and oxidative stress in neurodegenerative diseases', *Nature*. Nature Publishing Group, 443, p. 787. Available at: https://doi.org/10.1038/nature05292.

Lin, S.-J. and Guarente, L. (2003) 'Nicotinamide adenine dinucleotide, a metabolic regulator of transcription, longevity and disease', *Current Opinion in Cell Biology*, 15(2), pp. 241–246. doi: https://doi.org/10.1016/S0955-0674(03)00006-1.

Lionaki, E. *et al.* (2015) 'Mitochondria, autophagy and age-associated neurodegenerative diseases: New insights into a complex interplay', *Biochimica et Biophysica Acta (BBA) - Bioenergetics*, 1847(11), pp. 1412–1423. doi: https://doi.org/10.1016/j.bbabio.2015.04.010.

Lipinski, M. M. *et al.* (2010) 'Genome-wide analysis reveals mechanisms modulating autophagy in normal brain aging and in Alzheimer's disease', *Proceedings of the National Academy of Sciences*. National Acad Sciences, 107(32), pp. 14164–14169.

Liu, D. *et al.* (2013) 'Nicotinamide forestalls pathology and cognitive decline in Alzheimer mice: evidence for improved neuronal bioenergetics and autophagy procession', *Neurobiology of aging*. Elsevier, 34(6), pp. 1564–1580.

Liu, J. *et al.* (2003) 'Phospholipid Scramblase 3 Controls Mitochondrial Structure, Function, and Apoptotic Response11NIH grants K08CA795093 (RML) and K08AR48618 (DG); Huntsman Cancer Foundation.', *Molecular cancer research*. AACR, 1(12), pp. 892–902.

Liu, L. *et al.* (2012) 'Mitochondrial outer-membrane protein FUNDC1 mediates hypoxia-induced mitophagy in mammalian cells', *Nature cell biology*. Nature Publishing Group, 14(2), p. 177.

Liu, M. *et al.* (2014) 'Celecoxib regulates apoptosis and autophagy via the PI3K/Akt signaling pathway in SGC-7901 gastric cancer cells', *International journal of molecular medicine*. Spandidos Publications, 33(6), pp. 1451–1458.

Lloyd-Evans, E. and Platt, F. M. (2010) 'Lipids on Trial: The Search for the Offending Metabolite in Niemann-Pick type C Disease', *Traffic*. John Wiley & Sons, Ltd (10.1111), 11(4), pp. 419–428. doi: 10.1111/j.1600-0854.2010.01032.x.

López-Otín, C. *et al.* (2013) 'The Hallmarks of Aging', *Cell*, 153(6), pp. 1194–1217. doi: https://doi.org/10.1016/j.cell.2013.05.039.

López-Otín, C. *et al.* (2016) 'Metabolic Control of Longevity', *Cell*, 166(4), pp. 802–821. doi: https://doi.org/10.1016/j.cell.2016.07.031.

Losón, O. C. *et al.* (2013) 'Fis1, Mff, MiD49, and MiD51 mediate Drp1 recruitment in mitochondrial fission', *Molecular Biology of the Cell*. American Society for Cell Biology (mboc), 24(5), pp. 659–667. doi: 10.1091/mbc.e12-10-0721.

Lou, X. *et al.* (2018) 'A Novel NDUFS3 mutation in a Chinese patient with severe Leigh syndrome', *Journal of Human Genetics*, 63(12), pp. 1269–1272. doi: 10.1038/s10038-018-0505-0.

Love, S., Bridges, L. R. and Case, C. P. (1995) 'Neurofibrillary tangles in Niemann—Pick disease type C', *Brain*. Oxford University Press, 118(1), pp. 119–129.

Lu, Y. *et al.* (2016) 'Celecoxib exerts antitumor effects in HL-60 acute leukemia cells and inhibits autophagy by affecting lysosome function', *Biomedicine & Pharmacotherapy*, 84, pp. 1551–1557. doi: https://doi.org/10.1016/j.biopha.2016.11.026.

Madeo, F. *et al.* (2015) 'Essential role for autophagy in life span extension', *The Journal of Clinical Investigation*. The American Society for Clinical Investigation, 125(1), pp. 85–93. doi: 10.1172/JCI73946.

Maetzel, D. *et al.* (2014) 'Genetic and Chemical Correction of Cholesterol Accumulation and Impaired Autophagy in Hepatic and Neural Cells Derived from Niemann-Pick Type C Patient-Specific iPS Cells', *Stem Cell Reports*, 2(6), pp. 866–880. doi: https://doi.org/10.1016/j.stemcr.2014.03.014.

Mahley, R. W. (2016) 'Central nervous system lipoproteins: ApoE and regulation of cholesterol metabolism', *Arteriosclerosis, thrombosis, and vascular biology*. Am Heart Assoc, 36(7), pp. 1305–1315.

Maiuri, M. C. and Kroemer, G. (2019) 'Therapeutic modulation of autophagy: Which disease comes first', *Cell Death Differ*, 26, pp. 680–689.

Malavasi, F. *et al.* (2008) 'Evolution and function of the ADP ribosyl cyclase/CD38 gene family in physiology and pathology', *Physiological Reviews*, 88(3), pp. 841–886. doi: 10.1152/physrev.00035.2007.

Mancias, J. D. and Kimmelman, A. C. (2016) 'Mechanisms of Selective Autophagy in Normal Physiology and Cancer', *Journal of molecular biology*. 2016/03/04, 428(9 Pt A), pp. 1659–1680. doi: 10.1016/j.jmb.2016.02.027.

De Marchi, U. *et al.* (2014) 'NCLX protein, but not LETM1, mediates mitochondrial Ca2+ extrusion, thereby limiting Ca2+-induced NAD (P) H production and modulating matrix redox state', *Journal of Biological Chemistry*. ASBMB, 289(29), pp. 20377–20385.

Marino, G. and Lopez-Otin, C. (2004) 'Autophagy: molecular mechanisms, physiological functions and relevance in human pathology', *Cellular and Molecular Life Sciences CMLS*. Springer, 61(12), pp. 1439–1454.

Marroquin, L. D. *et al.* (2007) 'Circumventing the Crabtree Effect: Replacing Media Glucose with Galactose Increases Susceptibility of HepG2 Cells to Mitochondrial Toxicants', *Toxicological Sciences*, 97(2), pp. 539–547. doi: 10.1093/toxsci/kfm052.

Marshall, C. A., Borbon, I. A. and Erickson, R. P. (2017) 'Relative efficacy of nicotinamide treatment of a mouse model of infantile Niemann-Pick C1 disease', *Journal of applied genetics*. Springer, 58(1), pp. 99–102.

Martin, J., Mahlke, K. and Pfanner, N. (1991) *Role of an energized inner membrane in mitochondrial protein import. Delta psi drives the movement of presequences*, *The Journal of biological chemistry*.

Martinus, R. D. *et al.* (1996) 'Selective Induction of Mitochondrial Chaperones in Response to Loss of the Mitochondrial Genome', *European Journal of Biochemistry*. John Wiley & Sons, Ltd (10.1111), 240(1), pp. 98–103. doi: 10.1111/j.1432-1033.1996.0098h.x.

Massudi, H. *et al.* (2012) 'Age-associated changes in oxidative stress and NAD+ metabolism in human tissue', *PloS one*. Public Library of Science, 7(7), p. e42357.

Matalonga, J. *et al.* (2017) 'The Nuclear Receptor LXR Limits Bacterial Infection of Host Macrophages through a Mechanism that Impacts Cellular NAD Metabolism', *Cell Reports*, 18(5), pp. 1241–1255. doi: https://doi.org/10.1016/j.celrep.2017.01.007.

Matheoud, D. *et al.* (2016) 'Parkinson's disease-related proteins PINK1 and Parkin repress mitochondrial antigen presentation', *Cell*. Elsevier, 166(2), pp. 314–327.

Matsuda, N. *et al.* (2010) 'PINK1 stabilized by mitochondrial depolarization recruits Parkin to damaged mitochondria and activates latent Parkin for mitophagy', *The Journal of cell biology*. Rockefeller University Press, 189(2), pp. 211–221.

Mauch, D. H. *et al.* (2001) 'CNS Synaptogenesis Promoted by Glia-Derived Cholesterol', *Science*, 294(5545), pp. 1354 LP – 1357. doi: 10.1126/science.294.5545.1354.

McLelland, G.-L. and Fon, E. A. (2018) 'Principles of mitochondrial vesicle transport', *Current Opinion in Physiology*, 3, pp. 25–33. doi: https://doi.org/10.1016/j.cophys.2018.02.005.

McLelland, G. *et al.* (2014) 'Parkin and PINK1 function in a vesicular trafficking pathway regulating mitochondrial quality control', *The EMBO Journal*, p. e201385902. doi: 10.1002/embj.201385902.

McWilliams, T. G. *et al.* (2016) 'mito-QC illuminates mitophagy and mitochondrial architecture in vivo', *The Journal of Cell Biology*, 214(3), pp. 333 LP – 345. doi: 10.1083/jcb.201603039.

McWilliams, T. G. *et al.* (2018) 'Basal Mitophagy Occurs Independently of PINK1 in Mouse Tissues of High Metabolic Demand', *Cell Metabolism*, 27(2), pp. 439-449.e5. doi: https://doi.org/10.1016/j.cmet.2017.12.008.

McWilliams, T. G. and Ganley, I. G. (2016) 'Life in lights: Tracking mitochondrial delivery to lysosomes in vivo', *Autophagy*. Taylor & Francis, 12(12), pp. 2506–2507. doi: 10.1080/15548627.2016.1234567.

Mears, J. A. *et al.* (2011) 'Conformational changes in Dnm1 support a contractile mechanism for mitochondrial fission', *Nature structural & molecular biology*. 2010/12/19, 18(1), pp. 20–26. doi: 10.1038/nsmb.1949.

Menzies, F. M. *et al.* (2017) 'Autophagy and Neurodegeneration: Pathogenic Mechanisms and Therapeutic Opportunities', *Neuron*, 93(5), pp. 1015–1034. doi: https://doi.org/10.1016/j.neuron.2017.01.022.

Menzies, F. M., Fleming, A. and Rubinsztein, D. C. (2015) 'Compromised autophagy and neurodegenerative diseases', *Nature Reviews Neuroscience*. Nature Publishing Group, a division of Macmillan Publishers Limited. All Rights Reserved., 16, p. 345. Available at: https://doi.org/10.1038/nrn3961.

Merksamer, P. I. *et al.* (2013) 'The sirtuins, oxidative stress and aging: an emerging link', *Aging*. Impact Journals LLC, 5(3), pp. 144–150. doi: 10.18632/aging.100544.

Meske, V. *et al.* (2014) 'The autophagic defect in Niemann–Pick disease type C neurons differs from somatic cells and reduces neuronal viability', *Neurobiology of Disease*, 64, pp. 88–97. doi: https://doi.org/10.1016/j.nbd.2013.12.018.

Metallo, C. M. *et al.* (2011) 'Reductive glutamine metabolism by IDH1 mediates lipogenesis under hypoxia', *Nature*. Nature Publishing Group, a division of Macmillan Publishers Limited. All Rights Reserved., 481, p. 380. Available at: https://doi.org/10.1038/nature10602.

Methner, C. *et al.* (2014) 'Mitochondria selective S-nitrosation by mitochondria-targeted S-nitrosothiol protects against post-infarct heart failure in mouse hearts', *European journal of heart failure*. Wiley Online Library, 16(7), pp. 712–717.

Mijaljica, D., Prescott, M. and Devenish, R. (2011) *Microautophagy in mammalian cells Revisiting a 40-year-old conundrum*, *Autophagy*. doi: 10.4161/auto.7.7.14733.

Mitchell, S. J. *et al.* (2018) 'Nicotinamide improves aspects of healthspan, but not lifespan, in mice', *Cell metabolism*. Elsevier, 27(3), pp. 667–676.

Mizushima, N. *et al.* (2008) 'Autophagy fights disease through cellular self-digestion', *Nature*. Nature Publishing Group, 451, p. 1069. Available at: https://doi.org/10.1038/nature06639.

Mizushima, N., Noda, T. and Ohsumi, Y. (1999) 'Apg16p is required for the function of the Apg12p–Apg5p conjugate in the yeast autophagy pathway', *The EMBO journal*. John Wiley & Sons, Ltd, 18(14), pp. 3888–3896.

Molina, A. J. A. *et al.* (2009) 'Mitochondrial networking protects β-cells from nutrient-induced apoptosis', *Diabetes*. Am Diabetes Assoc, 58(10), pp. 2303–2315.

Montserrat, N. *et al.* (2011) 'Simple generation of human induced pluripotent stem cells using poly-beta-amino esters as the non-viral gene delivery system', *The Journal of biological chemistry*. 2011/02/01. American Society for Biochemistry and Molecular Biology, 286(14), pp. 12417–12428. doi: 10.1074/jbc.M110.168013.

Mookerjee, S. A. *et al.* (2015) 'The contributions of respiration and glycolysis to extracellular acid production', *Biochimica et Biophysica Acta (BBA) - Bioenergetics*. Elsevier, 1847(2), pp. 171–181. doi: 10.1016/J.BBABIO.2014.10.005.

Mookerjee, S. A. and Brand, M. D. (2015) 'Measurement and Analysis of Extracellular Acid Production to Determine Glycolytic Rate', *Journal of visualized experiments : JoVE*. MyJove Corporation, (106), pp. e53464–e53464. doi: 10.3791/53464.

Moreno-Gonzalez, I. and Soto, C. (2011) 'Misfolded protein aggregates: Mechanisms, structures and potential for disease transmission', *Seminars in Cell & Developmental Biology*, 22(5), pp. 482–487. doi: https://doi.org/10.1016/j.semcdb.2011.04.002.

Moreno-Lastres, D. *et al.* (2012) 'Mitochondrial Complex I Plays an Essential Role in Human Respirasome Assembly', *Cell Metabolism*, 15(3), pp. 324–335. doi: https://doi.org/10.1016/j.cmet.2012.01.015.

Morimoto, R. I. and Cuervo, A. M. (2014) 'Proteostasis and the Aging Proteome in Health and Disease', *The Journals of Gerontology: Series A*, 69(Suppl_1), pp. S33–S38. doi: 10.1093/gerona/glu049.

Mouchiroud, L. *et al.* (2013) 'The NAD+/Sirtuin Pathway Modulates Longevity through Activation of Mitochondrial UPR and FOXO Signaling', *Cell*, 154(2), pp. 430–441. doi: https://doi.org/10.1016/j.cell.2013.06.016.

Muñoz-Gámez, J. A. *et al.* (2009) 'PARP-1 is involved in autophagy induced by DNA damage', *Autophagy*. Taylor & Francis, 5(1), pp. 61–74. doi: 10.4161/auto.5.1.7272.

Murai, J. *et al.* (2012) 'Trapping of PARP1 and PARP2 by Clinical PARP Inhibitors', *Cancer Research*, 72(21), pp. 5588 LP – 5599. doi: 10.1158/0008-5472.CAN-12-2753.

Murata, S., Chiba, T. and Tanaka, K. (2003) 'CHIP: a quality-control E3 ligase collaborating with molecular chaperones', *The International Journal of Biochemistry & Cell Biology*, 35(5), pp. 572–578. doi: https://doi.org/10.1016/S1357-2725(02)00394-1.

Murray, J. *et al.* (2003) 'Oxidative Damage to Mitochondrial Complex I Due to Peroxynitrite identification of reactive tyrosines by mass spectrometry', *Journal of Biological Chemistry*. ASBMB, 278(39), pp. 37223–37230.

Nagi, M. *et al.* (2016) 'Iron-depletion promotes mitophagy to maintain mitochondrial integrity in pathogenic yeast Candida glabrata', *Autophagy*. Taylor & Francis, 12(8), pp. 1259–1271. doi: 10.1080/15548627.2016.1183080.

Nah, J., Yuan, J. and Jung, Y.-K. (2015) 'Autophagy in neurodegenerative diseases: from mechanism to therapeutic approach', *Molecules and cells*. 2015/04/20. Korean Society for Molecular and Cellular Biology, 38(5), pp. 381–389. doi: 10.14348/molcells.2015.0034.

Nakamura, K. (2013) 'α-Synuclein and mitochondria: partners in crime?', *Neurotherapeutics*. Springer, 10(3), pp. 391–399.

Narendra, D. *et al.* (2008) 'Parkin is recruited selectively to impaired mitochondria and promotes their autophagy', *The Journal of cell biology*. Rockefeller University Press, 183(5), pp. 795–803.

Narendra, D. P. *et al.* (2010) 'PINK1 is selectively stabilized on impaired mitochondria to activate Parkin', *PLoS biology*. Public Library of Science, 8(1), p. e1000298.

Nargund, A. M. *et al.* (2012) 'Mitochondrial Import Efficiency of ATFS-1 Regulates Mitochondrial UPR Activation', *Science*, 337(6094), pp. 587 LP – 590. doi: 10.1126/science.1223560.

Nazio, F. *et al.* (2019) 'Autophagy and cancer stem cells: molecular mechanisms and therapeutic applications', *Cell death and differentiation*. 2019/02/06. Nature Publishing Group UK, 26(4), pp. 690–702. doi: 10.1038/s41418-019-0292-y.

Neuspiel, M. *et al.* (2008) 'Cargo-Selected Transport from the Mitochondria to Peroxisomes Is Mediated by Vesicular Carriers', *Current Biology*, 18(2), pp. 102–108. doi: https://doi.org/10.1016/j.cub.2007.12.038.

Ni, H.-M., Williams, J. A. and Ding, W.-X. (2015) 'Mitochondrial dynamics and mitochondrial quality control', *Redox Biology*, 4, pp. 6–13. doi: https://doi.org/10.1016/j.redox.2014.11.006.

Nijman, S. M. B. *et al.* (2005) 'A genomic and functional inventory of deubiquitinating enzymes', *Cell*. Elsevier, 123(5), pp. 773–786.

Noda, N. N. *et al.* (2013) 'Structure of the Atg12–Atg5 conjugate reveals a platform for stimulating Atg8–PE conjugation', *EMBO reports*. John Wiley & Sons, Ltd, 14(2), pp. 206–211.

Novak, I. *et al.* (2010) 'Nix is a selective autophagy receptor for mitochondrial clearance', *EMBO reports*. John Wiley & Sons, Ltd, 11(1), pp. 45–51.

O'Neill, L. A. J., Kishton, R. J. and Rathmell, J. (2016) 'A guide to immunometabolism for immunologists', *Nature Reviews Immunology*. Nature Publishing Group, a division of Macmillan Publishers Limited. All Rights Reserved., 16, p. 553.

Obulesu, M. and Rao, D. M. (2010) 'DNA damage and impairment of DNA repair in Alzheimer's disease', *International Journal of Neuroscience*. Taylor & Francis, 120(6), pp. 397–403.

Okabe, K. *et al.* (2019) 'Implications of altered NAD metabolism in metabolic disorders', *Journal of Biomedical Science*, 26(1), p. 34. doi: 10.1186/s12929-019-0527-8.

Okano, S. *et al.* (2003) 'Spatial and Temporal Cellular Responses to Single-Strand Breaks in Human Cells', *Molecular and Cellular Biology*, 23(11), pp. 3974 LP – 3981. doi: 10.1128/MCB.23.11.3974-3981.2003.

Okatsu, K. *et al.* (2012) 'PINK1 autophosphorylation upon membrane potential dissipation is essential for Parkin recruitment to damaged mitochondria', *Nature Communications*. The Author(s), 3, p. 1016. Available at: https://doi.org/10.1038/ncomms2016.

Ong, S.-B. *et al.* (2010) 'Inhibiting mitochondrial fission protects the heart against ischemia/reperfusion injury', *Circulation*. Citeseer, 121(18), p. 2012.

Ordonez, M. P. *et al.* (2012) 'Disruption and therapeutic rescue of autophagy in a human neuronal model of Niemann Pick type C1', *Human Molecular Genetics*, 21(12), pp. 2651–2662. doi: 10.1093/hmg/dds090.

Orihuela, R., McPherson, C. A. and Harry, G. J. (2016) 'Microglial M1/M2 polarization and metabolic states', *British Journal of Pharmacology*. John Wiley & Sons, Ltd (10.1111), 173(4), pp. 649–665. doi: 10.1111/bph.13139.

Oroboros Instruments (2019) *Oroboros Instruments O2k Mitochondria and Cell Research*. Available at: https://wiki.oroboros.at/index.php/OROBOROS_INSTRUMENTS (Accessed: 19 August 2019).

Ory, D. S. *et al.* (2017) 'Intrathecal 2-hydroxypropyl-β-cyclodextrin decreases neurological disease progression in Niemann-Pick disease, type C1: a non-randomised, open-label, phase

1–2 trial', *The Lancet*. Elsevier, 390(10104), pp. 1758–1768.

Ory, D. S., Neugeboren, B. A. and Mulligan, R. C. (1996) 'A stable human-derived packaging cell line for production of high titer retrovirus/vesicular stomatitis virus G pseudotypes', *Proceedings of the National Academy of Sciences*, 93(21), pp. 11400 LP – 11406. doi: 10.1073/pnas.93.21.11400.

Owens, K. M. *et al.* (2011) 'Impaired OXPHOS complex III in breast cancer', *PloS one*. Public Library of Science, 6(8), p. e23846.

Pacheco, C. D., Kunkel, R. and Lieberman, A. P. (2007) 'Autophagy in Niemann–Pick C disease is dependent upon Beclin-1 and responsive to lipid trafficking defects', *Human Molecular Genetics*, 16(12), pp. 1495–1503. doi: 10.1093/hmg/ddm100.

Pacher, P. and Szabo, C. (2008) 'Role of the Peroxynitrite-Poly(ADP-Ribose) Polymerase Pathway in Human Disease', *The American Journal of Pathology*, 173(1), pp. 2–13. doi: https://doi.org/10.2353/ajpath.2008.080019.

Papandreou, I. *et al.* (2006) 'HIF-1 mediates adaptation to hypoxia by actively downregulating mitochondrial oxygen consumption', *Cell metabolism*. Elsevier, 3(3), pp. 187–197.

Paradies, G. *et al.* (2010) 'Oxidative stress, mitochondrial bioenergetics, and cardiolipin in aging', *Free Radical Biology and Medicine*, 48(10), pp. 1286–1295. doi: https://doi.org/10.1016/j.freeradbiomed.2010.02.020.

Park, J. H. *et al.* (2016) 'Nicotinamide mononucleotide inhibits post-ischemic NAD+ degradation and dramatically ameliorates brain damage following global cerebral ischemia', *Neurobiology of disease*. Elsevier, 95, pp. 102–110.

Park, W. D. *et al.* (2003) 'Identification of 58 novel mutations in Niemann-Pick disease type C: Correlation with biochemical phenotype and importance of PTC1-like domains in NPC1', *Human Mutation*. John Wiley & Sons, Ltd, 22(4), pp. 313–325. doi: 10.1002/humu.10255.

Parsons, R. B. *et al.* (2002) 'Expression of Nicotinamide N-Methyltransferase (E.C. 2.1.1.1) in the Parkinsonian Brain', *Journal of Neuropathology & Experimental Neurology*, 61(2), pp. 111–124. doi: 10.1093/jnen/61.2.111.

Patterson, M. C. *et al.* (2012) 'Recommendations for the diagnosis and management of Niemann–Pick disease type C: An update', *Molecular Genetics and Metabolism*, 106(3), pp. 330–344. doi: https://doi.org/10.1016/j.ymgme.2012.03.012.

Pearce, L. L. *et al.* (2005) 'Nitrosative stress results in irreversible inhibition of purified mitochondrial complexes I and III without modification of cofactors', *Nitric Oxide*, 13(4), pp. 254–263. doi: https://doi.org/10.1016/j.niox.2005.07.010.

Petrosillo, G. *et al.* (2008) 'Mitochondrial dysfunction in rat brain with aging: involvement of complex I, reactive oxygen species and cardiolipin', *Neurochemistry international*. Elsevier, 53(5), pp. 126–131.

Pfanner, N. *et al.* (2014) 'Uniform nomenclature for the mitochondrial contact site and cristae organizing system', *The Journal of Cell Biology*, 204(7), pp. 1083 LP – 1086. doi: 10.1083/jcb.201401006.

Pickrell, A. M. and Youle, R. J. (2015) 'The roles of PINK1, parkin, and mitochondrial fidelity in Parkinson's disease', *Neuron*. Elsevier, 85(2), pp. 257–273.

Pierzynowska, K. *et al.* (2018) 'Autophagy stimulation as a promising approach in treatment of neurodegenerative diseases', *Metabolic Brain Disease*, 33(4), pp. 989–1008. doi: 10.1007/s11011-018-0214-6.

Pineda, M., Walterfang, M. and Patterson, M. C. (2018) 'Miglustat in Niemann-Pick disease type C patients: a review', *Orphanet Journal of Rare Diseases*, 13(1), p. 140. doi: 10.1186/s13023-018-0844-0.

Pinson, B. *et al.* (2019) 'Dual control of NAD+ synthesis by purine metabolites in yeast', *eLife*. Edited by N. Barkai, A. G. Hinnebusch, and R. Rolfes. eLife Sciences Publications, Ltd, 8, p.

e43808. doi: 10.7554/eLife.43808.

Pinti, M. *et al.* (2014) 'Circulating mitochondrial DNA increases with age and is a familiar trait: Implications for "inflamm-aging"', *European journal of immunology*. Wiley Online Library, 44(5), pp. 1552–1562.

Pipalia, N. H. *et al.* (2017) 'Histone deacetylase inhibitors correct the cholesterol storage defect in most Niemann-Pick C1 mutant cells', *Journal of lipid research*. ASBMB, 58(4), pp. 695–708.

Pissios, P. (2017) 'Nicotinamide N-Methyltransferase: More Than a Vitamin B3 Clearance Enzyme', *Trends in Endocrinology & Metabolism*, 28(5), pp. 340–353. doi: https://doi.org/10.1016/j.tem.2017.02.004.

Pittelli, M. *et al.* (2010) 'Inhibition of nicotinamide phosphoribosyltransferase: cellular bioenergetics reveals a mitochondrial insensitive NAD pool', *The Journal of biological chemistry*. 2010/08/19. American Society for Biochemistry and Molecular Biology, 285(44), pp. 34106–34114. doi: 10.1074/jbc.M110.136739.

Ploumi, C., Daskalaki, I. and Tavernarakis, N. (2017) 'Mitochondrial biogenesis and clearance: a balancing act', *The FEBS journal*. Wiley Online Library, 284(2), pp. 183–195.

Pointer, C. B. and Klegeris, A. (2017) 'Cardiolipin in Central Nervous System Physiology and Pathology', *Cellular and Molecular Neurobiology*, 37(7), pp. 1161–1172. doi: 10.1007/s10571-016-0458-9.

Pontikis, C. C. *et al.* (2013) 'Cyclodextrin alleviates neuronal storage of cholesterol in Niemann-Pick C disease without evidence of detectable blood–brain barrier permeability', *Journal of inherited metabolic disease*. Springer, 36(3), pp. 491–498.

Praggastis, M. *et al.* (2015) 'A Murine Niemann-Pick C1 I1061T Knock-In Model Recapitulates the Pathological Features of the Most Prevalent Human Disease Allele', *The Journal of Neuroscience*, 35(21), pp. 8091 LP – 8106. doi: 10.1523/JNEUROSCI.4173-14.2015.

Probert, F. *et al.* (2017) 'NMR analysis reveals significant differences in the plasma metabolic profiles of Niemann Pick C1 patients, heterozygous carriers, and healthy controls', *Scientific reports*. Nature Publishing Group UK, 7(1), p. 6320. doi: 10.1038/s41598-017-06264-2.

Pryde, K. R., Taanman, J. W. and Schapira, A. H. (2016) 'A LON-ClpP Proteolytic Axis Degrades Complex I to Extinguish ROS Production in Depolarized Mitochondria', *Cell Reports*, 17(10), pp. 2522–2531. doi: https://doi.org/10.1016/j.celrep.2016.11.027.

Qu, X. *et al.* (2007) 'Autophagy Gene-Dependent Clearance of Apoptotic Cells during Embryonic Development', *Cell*. Elsevier, 128(5), pp. 931–946. doi: 10.1016/j.cell.2006.12.044.

Rabinovitch, R. C. *et al.* (2017) 'AMPK Maintains Cellular Metabolic Homeostasis through Regulation of Mitochondrial Reactive Oxygen Species', *Cell Reports*, 21(1), pp. 1–9. doi: https://doi.org/10.1016/j.celrep.2017.09.026.

Rabinowitz, J. D. and White, E. (2010) 'Autophagy and Metabolism', *Science*, 330(6009), pp. 1344 LP – 1348. doi: 10.1126/science.1193497.

Rajamohan, S. B. *et al.* (2009) 'SIRT1 Promotes Cell Survival under Stress by Deacetylation-Dependent Deactivation of Poly(ADP-Ribose) Polymerase 1', *Molecular and Cellular Biology*, 29(15), pp. 4116 LP – 4129. doi: 10.1128/MCB.00121-09.

Rajman, L., Chwalek, K. and Sinclair, D. A. (2018) 'Therapeutic Potential of NAD-Boosting Molecules: The In Vivo Evidence', *Cell Metabolism*, 27(3), pp. 529–547. doi: https://doi.org/10.1016/j.cmet.2018.02.011.

Rambold, A. S. *et al.* (2011) 'Tubular network formation protects mitochondria from autophagosomal degradation during nutrient starvation', *Proceedings of the National Academy of Sciences*, 108(25), pp. 10190 LP – 10195. doi: 10.1073/pnas.1107402108.

Ramsay, R. R. (2019) 'Electron carriers and energy conservation in mitochondrial respiration', *ChemTexts*. Springer, 5(2), p. 9.

Ran, F. A. *et al.* (2013) 'Genome engineering using the CRISPR-Cas9 system', *Nature protocols*. 2013/10/24, 8(11), pp. 2281–2308. doi: 10.1038/nprot.2013.143.

Al Rasheed, H., Rizwan, M. and Tarjan, G. (2018) 'Succinate Dehydrogenase Complex: An Updated Review.', *Archives of Pathology & Laboratory Medicine*, 142(12).

Ravikumar, B. *et al.* (2010) 'Regulation of Mammalian Autophagy in Physiology and Pathophysiology', *Physiological Reviews*. American Physiological Society, 90(4), pp. 1383–1435. doi: 10.1152/physrev.00030.2009.

Ray Chaudhuri, A. and Nussenzweig, A. (2017) 'The multifaceted roles of PARP1 in DNA repair and chromatin remodelling', *Nature Reviews Molecular Cell Biology*. Nature Publishing Group, a division of Macmillan Publishers Limited. All Rights Reserved., 18, p. 610. Available at: https://doi.org/10.1038/nrm.2017.53.

Reggiori, F. *et al.* (2004) 'The Atg1-Atg13 Complex Regulates Atg9 and Atg23 Retrieval Transport from the Pre-Autophagosomal Structure', *Developmental Cell*, 6(1), pp. 79–90. doi: https://doi.org/10.1016/S1534-5807(03)00402-7.

Reinherz, E. L. *et al.* (1980) 'Discrete stages of human intrathymic differentiation: analysis of normal thymocytes and leukemic lymphoblasts of T-cell lineage', *Proceedings of the National Academy of Sciences*. National Acad Sciences, 77(3), pp. 1588–1592.

Rhein, V. *et al.* (2009) 'Amyloid-β and tau synergistically impair the oxidative phosphorylation system in triple transgenic Alzheimer's disease mice', *Proceedings of the National Academy of Sciences*, 106(47), pp. 20057 LP – 20062. doi: 10.1073/pnas.0905529106.

Ribas, G. S. *et al.* (2012) 'Oxidative stress in Niemann-Pick type C patients: a protective role of N-butyl-deoxynojirimycin therapy', *International Journal of Developmental Neuroscience*, 30(6), pp. 439–444. doi: https://doi.org/10.1016/j.ijdevneu.2012.07.002.

Riffelmacher, T., Richter, F. C. and Simon, A. K. (2018) 'Autophagy dictates metabolism and differentiation of inflammatory immune cells', *Autophagy*. Taylor & Francis, 14(2), pp. 199–206. doi: 10.1080/15548627.2017.1362525.

Riss, T. L. *et al.* (2016) 'Cell viability assays'. Eli Lilly & Company and the National Center for Advancing Translational Sciences.

Robak, L. A. *et al.* (2017) 'Excessive burden of lysosomal storage disorder gene variants in Parkinson's disease', *Brain*, 140(12), pp. 3191–3203. doi: 10.1093/brain/awx285.

Roberts, P. *et al.* (2002) 'Piecemeal Microautophagy of Nucleus in Saccharomyces cerevisiae', *Molecular Biology of the Cell*. American Society for Cell Biology (mboc), 14(1), pp. 129–141. doi: 10.1091/mbc.e02-08-0483.

Robinson, B. H. *et al.* (1992) 'Nonviability of cells with oxidative defects in galactose medium: A screening test for affected patient fibroblasts', *Biochemical Medicine and Metabolic Biology*, 48(2), pp. 122–126. doi: https://doi.org/10.1016/0885-4505(92)90056-5.

Rocha, E. M., De Miranda, B. and Sanders, L. H. (2018) 'Alpha-synuclein: Pathology, mitochondrial dysfunction and neuroinflammation in Parkinson's disease', *Neurobiology of Disease*, 109, pp. 249–257. doi: https://doi.org/10.1016/j.nbd.2017.04.004.

Rogers, S. and Segal, S. (1981) 'Changing activities of galactose-metabolizing enzymes during perfusion of suckling-rat liver', *American Journal of Physiology-Endocrinology and Metabolism*. American Physiological Society, 240(3), pp. E333–E339. doi: 10.1152/ajpendo.1981.240.3.E333.

Rojo, M. *et al.* (2002) 'Membrane topology and mitochondrial targeting of mitofusins, ubiquitous mammalian homologs of the transmembrane GTPase Fzo', *Journal of Cell Science*, 115(8), pp. 1663 LP – 1674. Available at: http://jcs.biologists.org/content/115/8/1663.abstract.

Ross, C. A. and Poirier, M. A. (2005) 'What is the role of protein aggregation in neurodegeneration?', *Nature Reviews Molecular Cell Biology*. Nature Publishing Group, 6, p. 891. Available at: https://doi.org/10.1038/nrm1742.

Rossi, M. N. *et al.* (2009) 'Mitochondrial localization of PARP-1 requires interaction with mitofilin and is involved in the maintenance of mitochondrial DNA integrity', *Journal of Biological Chemistry*. ASBMB, 284(46), pp. 31616–31624.

Rossignol, R. *et al.* (2004) 'Energy Substrate Modulates Mitochondrial Structure and Oxidative Capacity in Cancer Cells', *Cancer Research*, 64(3), pp. 985 LP – 993. doi: 10.1158/0008-5472.CAN-03-1101.

Ruggiero, F. M. *et al.* (1992) 'Lipid composition in synaptic and nonsynaptic mitochondria from rat brains and effect of aging', *Journal of neurochemistry*. Wiley Online Library, 59(2), pp. 487–491.

Ruiz-Rodado, V. *et al.* (2014) '1H NMR-linked urinary metabolic profiling of Niemann-Pick Class C1 (NPC1) disease: Identification of potential new biomarkers using correlated component regression (CCR) and genetic algorithm (GA) analysis strategies', *Current Metabolomics*. Bentham Science Publishers, 2(2), pp. 88–121.

Ryan, K. *et al.* (2012) 'Post-translational oxidative modification and inactivation of mitochondrial complex I in epileptogenesis', *The Journal of neuroscience : the official journal of the Society for Neuroscience*. Society for Neuroscience, 32(33), pp. 11250–11258. doi: 10.1523/JNEUROSCI.0907-12.2012.

Saito, Y. *et al.* (2004) 'Aberrant Phosphorylation of α-Synuclein in Human Niemann-Pick Type C1 Disease', *Journal of Neuropathology & Experimental Neurology*, 63(4), pp. 323–328. doi: 10.1093/jnen/63.4.323.

Salek, R. M. *et al.* (2007) 'A metabolomic comparison of urinary changes in type 2 diabetes in mouse, rat, and human', *Physiological Genomics*. American Physiological Society, 29(2), pp. 99–108. doi: 10.1152/physiolgenomics.00194.2006.

Sánchez-Caballero, L., Guerrero-Castillo, S. and Nijtmans, L. (2016) 'Unraveling the complexity of mitochondrial complex I assembly: A dynamic process', *Biochimica et Biophysica Acta (BBA) - Bioenergetics*, 1857(7), pp. 980–990. doi: https://doi.org/10.1016/j.bbabio.2016.03.031.

Sanz, A. *et al.* (2010) 'Expression of the yeast NADH dehydrogenase Ndi1 in Drosophila confers increased lifespan independently of dietary restriction', *Proceedings of the National Academy of Sciences*. National Acad Sciences, 107(20), pp. 9105–9110.

Sarkar, S. *et al.* (2013) 'Impaired Autophagy in the Lipid-Storage Disorder Niemann-Pick Type C1 Disease', *Cell Reports*, 5(5), pp. 1302–1315. doi: https://doi.org/10.1016/j.celrep.2013.10.042.

Sarkar, S. (2013) 'Regulation of autophagy by mTOR-dependent and mTOR-independent pathways: autophagy dysfunction in neurodegenerative diseases and therapeutic application of autophagy enhancers', *Biochemical Society Transactions*, 41(5), pp. 1103 LP – 1130. doi: 10.1042/BST20130134.

Sauve, A. A. (2010) 'Sirtuin chemical mechanisms', *Biochimica et Biophysica Acta (BBA) - Proteins and Proteomics*, 1804(8), pp. 1591–1603. doi: https://doi.org/10.1016/j.bbapap.2010.01.021.

Scarpulla, R. C. (2011) 'Metabolic control of mitochondrial biogenesis through the PGC-1 family regulatory network', *Biochimica et Biophysica Acta (BBA) - Molecular Cell Research*, 1813(7), pp. 1269–1278. doi: https://doi.org/10.1016/j.bbamcr.2010.09.019.

Scatena, R. *et al.* (2004) 'Mitochondrial dysfunction by synthetic ligands of peroxisome proliferator activated receptors (PPARs)', *IUBMB life*. Wiley Online Library, 56(8), pp. 477–482.

Schägger, H. *et al.* (2004) 'Significance of respirasomes for the assembly/stability of human respiratory chain complex I', *Journal of Biological Chemistry*. ASBMB, 279(35), pp. 36349–36353.

Scheffler, I. E. (2015) 'Mitochondrial disease associated with complex I (NADH-CoQ

oxidoreductase) deficiency', *Journal of Inherited Metabolic Disease*, 38(3), pp. 405–415. doi: 10.1007/s10545-014-9768-6.

Scheibye-Knudsen, M. *et al.* (2012) 'Cockayne syndrome group B protein prevents the accumulation of damaged mitochondria by promoting mitochondrial autophagy', *The Journal of experimental medicine*. The Rockefeller University Press, 209(4), pp. 855–869. doi: 10.1084/jem.20111721.

Scheibye-Knudsen, M. *et al.* (2014) 'A High-Fat Diet and NAD+ Activate Sirt1 to Rescue Premature Aging in Cockayne Syndrome', *Cell Metabolism*, 20(5), pp. 840–855. doi: https://doi.org/10.1016/j.cmet.2014.10.005.

Scherz-Shouval, R. *et al.* (2007) 'Reactive oxygen species are essential for autophagy and specifically regulate the activity of Atg4', *The EMBO Journal*. John Wiley & Sons, Ltd, 26(7), pp. 1749–1760. doi: 10.1038/sj.emboj.7601623.

Schiavi, A. *et al.* (2015) 'Iron-starvation-induced mitophagy mediates lifespan extension upon mitochondrial stress in C. elegans', *Current Biology*. Elsevier, 25(14), pp. 1810–1822.

Schmidt, H. H. H. W. *et al.* (2015) 'Antioxidants in Translational Medicine', *Antioxidants & Redox Signaling*. Mary Ann Liebert, Inc., publishers, 23(14), pp. 1130–1143. doi: 10.1089/ars.2015.6393.

Schneider, J. L., Suh, Y. and Cuervo, A. M. (2014) 'Deficient chaperone-mediated autophagy in liver leads to metabolic dysregulation', *Cell metabolism*. Elsevier, 20(3), pp. 417–432.

Scialò, F. *et al.* (2016) 'Mitochondrial ROS Produced via Reverse Electron Transport Extend Animal Lifespan', *Cell Metabolism*, 23(4), pp. 725–734. doi: https://doi.org/10.1016/j.cmet.2016.03.009.

Sedlackova, L. and Korolchuk, V. I. (2018) 'Mitochondrial quality control as a key determinant of cell survival', *Biochimica et Biophysica Acta (BBA)-Molecular Cell Research*. Elsevier.

Seo, B. B. *et al.* (2000) 'Use of the NADH-Quinone Oxidoreductase (NDI1) Gene ofSaccharomyces cerevisiae as a Possible Cure for Complex I Defects in Human Cells', *Journal of Biological Chemistry*. ASBMB, 275(48), pp. 37774–37778.

Shah, R. C. *et al.* (2014) 'An evaluation of MSDC-0160, a prototype mTOT modulating insulin sensitizer, in patients with mild Alzheimer's disease', *Current Alzheimer Research*. Bentham Science Publishers, 11(6), pp. 564–573.

Shpilka, T. and Haynes, C. M. (2017) 'The mitochondrial UPR: mechanisms, physiological functions and implications in ageing', *Nature Reviews Molecular Cell Biology*. Nature Publishing Group, a division of Macmillan Publishers Limited. All Rights Reserved., 19, p. 109. Available at: https://doi.org/10.1038/nrm.2017.110.

Singh, C. K. *et al.* (2017) 'The Role of Sirtuins in Antioxidant and Redox Signaling', *Antioxidants & Redox Signaling*. Mary Ann Liebert, Inc., publishers, 28(8), pp. 643–661. doi: 10.1089/ars.2017.7290.

SKIDMORE, C. J. *et al.* (1979) 'The involvement of poly (ADP-ribose) polymerase in the degradation of NAD caused by γ-radiation and N-methyl-N-nitrosourea', *European journal of biochemistry*. Wiley Online Library, 101(1), pp. 135–142.

Smeitink, J., van den Heuvel, L. and DiMauro, S. (2001) 'The genetics and pathology of oxidative phosphorylation', *Nature Reviews Genetics*. Nature Publishing Group, 2(5), p. 342.

Smith, D. *et al.* (2009) 'Beneficial effects of anti-inflammatory therapy in a mouse model of Niemann-Pick disease type C1', *Neurobiology of Disease*, 36(2), pp. 242–251. doi: https://doi.org/10.1016/j.nbd.2009.07.010.

Snow, B. J. *et al.* (2010) 'A double-blind, placebo-controlled study to assess the mitochondria-targeted antioxidant MitoQ as a disease-modifying therapy in Parkinson's disease', *Movement Disorders*. John Wiley & Sons, Ltd, 25(11), pp. 1670–1674. doi: 10.1002/mds.23148.

Solaini, G. *et al.* (2010) 'Hypoxia and mitochondrial oxidative metabolism', *Biochimica et*

Biophysica Acta (BBA) - Bioenergetics, 1797(6), pp. 1171–1177. doi: https://doi.org/10.1016/j.bbabio.2010.02.011.

Song, Z. *et al.* (2007) 'OPA1 processing controls mitochondrial fusion and is regulated by mRNA splicing, membrane potential, and Yme1L', *The Journal of Cell Biology*, 178(5), pp. 749 LP – 755. doi: 10.1083/jcb.200704110.

Soubannier, V. *et al.* (2012) 'A Vesicular Transport Pathway Shuttles Cargo from Mitochondria to Lysosomes', *Current Biology*, 22(2), pp. 135–141. doi: https://doi.org/10.1016/j.cub.2011.11.057.

de Sousa, R. T. *et al.* (2015) 'Lithium increases leukocyte mitochondrial complex I activity in bipolar disorder during depressive episodes', *Psychopharmacology*, 232(1), pp. 245–250. doi: 10.1007/s00213-014-3655-6.

De Stefani, D. *et al.* (2011) 'A forty-kilodalton protein of the inner membrane is the mitochondrial calcium uniporter', *Nature*. Nature Publishing Group, 476(7360), p. 336.

Stein, L. R. and Imai, S. (2014) 'Specific ablation of Nampt in adult neural stem cells recapitulates their functional defects during aging', *The EMBO Journal*. John Wiley & Sons, Ltd, 33(12), pp. 1321–1340. doi: 10.1002/embj.201386917.

Stepien, G. *et al.* (1992) 'Differential expression of adenine nucleotide translocator isoforms in mammalian tissues and during muscle cell differentiation.', *Journal of Biological Chemistry*. ASBMB, 267(21), pp. 14592–14597.

Stolz, A., Ernst, A. and Dikic, I. (2014) 'Cargo recognition and trafficking in selective autophagy', *Nature Cell Biology*. Nature Publishing Group, a division of Macmillan Publishers Limited. All Rights Reserved., 16, p. 495. Available at: https://doi.org/10.1038/ncb2979.

Strauss, M. *et al.* (2008) 'Dimer ribbons of ATP synthase shape the inner mitochondrial membrane', *The EMBO journal*. John Wiley & Sons, Ltd, 27(7), pp. 1154–1160.

Strittmatter, W. J. and Roses, A. D. (1996) 'Apolipoprotein E and Alzheimer's disease', *Annual review of neuroscience*. Annual Reviews 4139 El Camino Way, PO Box 10139, Palo Alto, CA 94303-0139, USA, 19(1), pp. 53–77.

Strohecker, A. M. *et al.* (2013) 'Autophagy sustains mitochondrial glutamine metabolism and growth of BrafV600E–driven lung tumors', *Cancer discovery*. AACR, 3(11), pp. 1272–1285.

Sugiura, A. *et al.* (2014) 'A new pathway for mitochondrial quality control: mitochondrial-derived vesicles', *The EMBO Journal*, 33(19), pp. 2142 LP – 2156. doi: 10.15252/embj.201488104.

Sun, F. *et al.* (2012) 'Biochemical issues in estimation of cytosolic free NAD/NADH ratio', *PLoS One*. Public Library of Science, 7(5), p. e34525.

Sun, N. *et al.* (2015) 'Measuring in vivo mitophagy', *Molecular cell*. Elsevier, 60(4), pp. 685–696.

Sun, Y. and Grabowski, G. A. (2010) 'Impaired autophagosomes and lysosomes in neuronopathic Gaucher disease', *Autophagy*. Taylor & Francis, 6(5), pp. 648–649.

Sung, E.-A. *et al.* (2017) 'Generation of patient specific human neural stem cells from Niemann-Pick disease type C patient-derived fibroblasts', *Oncotarget*. Impact Journals LLC, 8(49), pp. 85428–85441. doi: 10.18632/oncotarget.19976.

Suzuki, K. *et al.* (2007) 'Hierarchy of Atg proteins in pre-autophagosomal structure organization', *Genes to Cells*. John Wiley & Sons, Ltd (10.1111), 12(2), pp. 209–218. doi: 10.1111/j.1365-2443.2007.01050.x.

Sweeney, P. *et al.* (2017) 'Protein misfolding in neurodegenerative diseases: implications and strategies', *Translational Neurodegeneration*, 6(1), p. 6. doi: 10.1186/s40035-017-0077-5.

Takamura, A. *et al.* (2011) 'Autophagy-deficient mice develop multiple liver tumors', *Genes & development*. Cold Spring Harbor Laboratory Press, 25(8), pp. 795–800. doi:

10.1101/gad.2016211.

Tanaka, A. *et al.* (2010) 'Proteasome and p97 mediate mitophagy and degradation of mitofusins induced by Parkin', *The Journal of Cell Biology*, 191(7), pp. 1367 LP – 1380. doi: 10.1083/jcb.201007013.

Tanaka, K. and Matsuda, N. (2014) 'Proteostasis and neurodegeneration: The roles of proteasomal degradation and autophagy', *Biochimica et Biophysica Acta (BBA) - Molecular Cell Research*, 1843(1), pp. 197–204. doi: https://doi.org/10.1016/j.bbamcr.2013.03.012.

Tanik, S. A. *et al.* (2013) 'Lewy Body-like α-Synuclein Aggregates Resist Degradation and Impair Macroautophagy', *Journal of Biological Chemistry*. American Society for Biochemistry and Molecular Biology, 288(21), pp. 15194–15210. doi: 10.1074/JBC.M113.457408.

Tasset, I. and Cuervo, A. M. (2016) 'Role of chaperone-mediated autophagy in metabolism', *The FEBS journal*. Wiley Online Library, 283(13), pp. 2403–2413.

Taylor, E. R. *et al.* (2003) 'Reversible glutathionylation of complex I increases mitochondrial superoxide formation', *Journal of Biological Chemistry*. ASBMB, 278(22), pp. 19603–19610.

Tekirdag, K. and Cuervo, A. M. (2018) 'Chaperone-mediated autophagy and endosomal microautophagy: Jointed by a chaperone', *Journal of Biological Chemistry*. ASBMB, 293(15), pp. 5414–5424.

Thameem Dheen, S., Kaur, C. and Ling, E.-A. (2007) 'Microglial activation and its implications in the brain diseases', *Current medicinal chemistry*. Bentham Science Publishers, 14(11), pp. 1189–1197.

Theurey, P. and Pizzo, P. (2018) 'The Aging Mitochondria', *Genes* . doi: 10.3390/genes9010022.

Thumm, M. *et al.* (1994) 'Isolation of autophagocytosis mutants of Saccharomyces cerevisiae', *FEBS Letters*. John Wiley & Sons, Ltd, 349(2), pp. 275–280. doi: 10.1016/0014-5793(94)00672-5.

Tong, X., Zhao, F. and Thompson, C. B. (2009) 'The molecular determinants of de novo nucleotide biosynthesis in cancer cells', *Current Opinion in Genetics & Development*, 19(1), pp. 32–37. doi: https://doi.org/10.1016/j.gde.2009.01.002.

Torres, S. *et al.* (2017) 'Lysosomal and Mitochondrial Liaisons in Niemann-Pick Disease ', *Frontiers in Physiology* , p. 982. Available at: https://www.frontiersin.org/article/10.3389/fphys.2017.00982.

Tsukada, M. and Ohsumi, Y. (1993) 'Isolation and characterization of autophagy-defective mutants of Saccharomyces cerevisiae', *FEBS Letters*. John Wiley & Sons, Ltd, 333(1–2), pp. 169–174. doi: 10.1016/0014-5793(93)80398-E.

Tsukamoto, S. *et al.* (2008) 'Autophagy is essential for preimplantation development of mouse embryos', *Science*. American Association for the Advancement of Science, 321(5885), pp. 117–120.

Unsay, J. D. *et al.* (2013) 'Cardiolipin Effects on Membrane Structure and Dynamics', *Langmuir*. American Chemical Society, 29(51), pp. 15878–15887. doi: 10.1021/la402669z.

Valentin-Vega, Y. A. *et al.* (2012) 'Mitochondrial dysfunction in ataxia-telangiectasia', *Blood*, 119(6), pp. 1490 LP – 1500. doi: 10.1182/blood-2011-08-373639.

Vanier, M. T. (2010) 'Niemann-Pick disease type C', *Orphanet Journal of Rare Diseases*, 5(1), p. 16. doi: 10.1186/1750-1172-5-16.

Vanier, M. T. and Latour, P. (2015) 'Chapter 18 - Laboratory diagnosis of Niemann–Pick disease type C: The filipin staining test', in Platt, F. and Platt, N. B. T.-M. in C. B. (eds) *Lysosomes and Lysosomal Diseases*. Academic Press, pp. 357–375. doi: https://doi.org/10.1016/bs.mcb.2014.10.028.

Vázquez, M. C. *et al.* (2012) *Oxidative Stress: A Pathogenic Mechanism for Niemann-Pick*

Type C Disease, *Oxidative medicine and cellular longevity*. doi: 10.1155/2012/205713.

van de Ven, R. A. H., Santos, D. and Haigis, M. C. (2017) 'Mitochondrial Sirtuins and Molecular Mechanisms of Aging', *Trends in Molecular Medicine*, 23(4), pp. 320–331. doi: https://doi.org/10.1016/j.molmed.2017.02.005.

Verdin, E. (2015) 'NAD⁺ in aging, metabolism, and neurodegeneration', *Science*, 350(6265), pp. 1208 LP – 1213. doi: 10.1126/science.aac4854.

Villalba, J. M. and Alcaín, F. J. (2012) 'Sirtuin activators and inhibitors', *BioFactors (Oxford, England)*. 2012/06/25, 38(5), pp. 349–359. doi: 10.1002/biof.1032.

Vincow, E. S. *et al.* (2013) 'The PINK1-Parkin pathway promotes both mitophagy and selective respiratory chain turnover in vivo', *Proceedings of the National Academy of Sciences of the United States of America*. 2013/03/18. National Academy of Sciences, 110(16), pp. 6400–6405. doi: 10.1073/pnas.1221132110.

Vogel, C. and Marcotte, E. M. (2012) 'Insights into the regulation of protein abundance from proteomic and transcriptomic analyses', *Nature Reviews Genetics*. Nature Publishing Group, a division of Macmillan Publishers Limited. All Rights Reserved., 13, p. 227. Available at: https://doi.org/10.1038/nrg3185.

Vogel, R. O. *et al.* (2007) 'Identification of Mitochondrial Complex I Assembly Intermediates by Tracing Tagged NDUFS3 Demonstrates the Entry Point of Mitochondrial Subunits', *Journal of Biological Chemistry* , 282(10), pp. 7582–7590. Available at: http://www.jbc.org/content/282/10/7582.abstract.

Van Vranken, J. G. *et al.* (2015) 'Protein-mediated assembly of succinate dehydrogenase and its cofactors', *Critical Reviews in Biochemistry and Molecular Biology*. Taylor & Francis, 50(2), pp. 168–180. doi: 10.3109/10409238.2014.990556.

Wakade, C. *et al.* (2014) 'Upregulation of GPR109A in Parkinson's disease', *PloS one*. Public Library of Science, 9(10), pp. e109818–e109818. doi: 10.1371/journal.pone.0109818.

Walkley, S. U. and Suzuki, K. (2004) 'Consequences of NPC1 and NPC2 loss of function in mammalian neurons', *Biochimica et Biophysica Acta (BBA) - Molecular and Cell Biology of Lipids*, 1685(1), pp. 48–62. doi: https://doi.org/10.1016/j.bbalip.2004.08.011.

Wallace, D. C. (2005) 'A mitochondrial paradigm of metabolic and degenerative diseases, aging, and cancer: a dawn for evolutionary medicine', *Annual review of genetics*, 39, pp. 359–407. doi: 10.1146/annurev.genet.39.110304.095751.

Wang, W. *et al.* (2015) 'Parkinson's disease–associated mutant VPS35 causes mitochondrial dysfunction by recycling DLP1 complexes', *Nature Medicine*. Nature Publishing Group, a division of Macmillan Publishers Limited. All Rights Reserved., 22, p. 54. Available at: https://doi.org/10.1038/nm.3983.

Wang, X. *et al.* (2016) 'Nicotinamide mononucleotide protects against β-amyloid oligomer-induced cognitive impairment and neuronal death', *Brain Research*, 1643, pp. 1–9. doi: https://doi.org/10.1016/j.brainres.2016.04.060.

Wassif, C. A. *et al.* (2016) 'High incidence of unrecognized visceral/neurological late-onset Niemann-Pick disease, type C1, predicted by analysis of massively parallel sequencing data sets', *Genetics in medicine : official journal of the American College of Medical Genetics*. 2015/03/12, 18(1), pp. 41–48. doi: 10.1038/gim.2015.25.

Watmough, N. J. and Frerman, F. E. (2010) 'The electron transfer flavoprotein: Ubiquinone oxidoreductases', *Biochimica et Biophysica Acta (BBA) - Bioenergetics*, 1797(12), pp. 1910–1916. doi: https://doi.org/10.1016/j.bbabio.2010.10.007.

Watson, A. J. M., Askew, J. N. and Benson, R. S. P. (1995) 'Poly(adenosine diphosphate ribose) polymerase inhibition prevents necrosis induced by H2O2 but not apoptosis', *Gastroenterology*, 109(2), pp. 472–482. doi: https://doi.org/10.1016/0016-5085(95)90335-6.

Watt, I. N. *et al.* (2010) 'Bioenergetic cost of making an adenosine triphosphate molecule in

animal mitochondria', *Proceedings of the National Academy of Sciences*. National Acad Sciences, 107(39), pp. 16823–16827.

Webb, A. E. and Brunet, A. (2014) 'FOXO transcription factors: key regulators of cellular quality control', *Trends in Biochemical Sciences*, 39(4), pp. 159–169. doi: https://doi.org/10.1016/j.tibs.2014.02.003.

Weinberg, S. E. and Chandel, N. S. (2014) 'Targeting mitochondria metabolism for cancer therapy', *Nature Chemical Biology*. Nature Publishing Group, a division of Macmillan Publishers Limited. All Rights Reserved., 11, p. 9. Available at: https://doi.org/10.1038/nchembio.1712.

Welchman, R. L., Gordon, C. and Mayer, R. J. (2005) 'Ubiquitin and ubiquitin-like proteins as multifunctional signals', *Nature Reviews Molecular Cell Biology*. Nature Publishing Group, 6, p. 599. Available at: https://doi.org/10.1038/nrm1700.

Wesselborg, S. and Stork, B. (2015) 'Autophagy signal transduction by ATG proteins: from hierarchies to networks', *Cellular and Molecular Life Sciences*, 72(24), pp. 4721–4757. doi: 10.1007/s00018-015-2034-8.

Westermann, B. (2010) 'Mitochondrial fusion and fission in cell life and death', *Nature Reviews Molecular Cell Biology*. Nature Publishing Group, a division of Macmillan Publishers Limited. All Rights Reserved., 11, p. 872. Available at: https://doi.org/10.1038/nrm3013.

Westphal, C. H., Dipp, M. A. and Guarente, L. (2007) 'A therapeutic role for sirtuins in diseases of aging?', *Trends in Biochemical Sciences*, 32(12), pp. 555–560. doi: https://doi.org/10.1016/j.tibs.2007.09.008.

Whitworth, A. J. and Pallanck, L. J. (2017) 'PINK1/Parkin mitophagy and neurodegeneration—what do we really know in vivo?', *Current opinion in genetics & development*. Elsevier, 44, pp. 47–53.

Wiley, C. D. *et al.* (2016) 'Mitochondrial Dysfunction Induces Senescence with a Distinct Secretory Phenotype', *Cell Metabolism*, 23(2), pp. 303–314. doi: https://doi.org/10.1016/j.cmet.2015.11.011.

Williams, A. C. and Ramsden, D. B. (2005) 'Autotoxicity, methylation and a road to the prevention of Parkinson's disease', *Journal of Clinical Neuroscience*, 12(1), pp. 6–11. doi: https://doi.org/10.1016/j.jocn.2004.10.002.

Winklhofer, K. F., Tatzelt, J. and Haass, C. (2008) 'The two faces of protein misfolding: gain- and loss-of-function in neurodegenerative diseases', *The EMBO Journal*, 27(2), pp. 336 LP – 349. doi: 10.1038/sj.emboj.7601930.

Wong, E. and Cuervo, A. M. (2010) 'Autophagy gone awry in neurodegenerative diseases', *Nature Neuroscience*. Nature Publishing Group, 13, p. 805. Available at: https://doi.org/10.1038/nn.2575.

Woo, H. A. *et al.* (2003) 'Reversible Oxidation of the Active Site Cysteine of Peroxiredoxins to Cysteine Sulfinic Acid: IMMUNOBLOT DETECTION WITH ANTIBODIES SPECIFIC FOR THE HYPEROXIDIZED CYSTEINE-CONTAINING SEQUENCE ', *Journal of Biological Chemistry* , 278(48), pp. 47361–47364. doi: 10.1074/jbc.C300428200.

Woś, M. *et al.* (2016) 'Mitochondrial dysfunction in fibroblasts derived from patients with Niemann-Pick type C disease', *Archives of Biochemistry and Biophysics*, 593, pp. 50–59. doi: https://doi.org/10.1016/j.abb.2016.02.012.

Xia, Q. *et al.* (2008) 'Proteomic identification of novel proteins associated with Lewy bodies', *Frontiers in bioscience : a journal and virtual library*, 13, pp. 3850–3856. Available at: https://www.ncbi.nlm.nih.gov/pubmed/18508479.

Xu, P. *et al.* (2009) 'Quantitative Proteomics Reveals the Function of Unconventional Ubiquitin Chains in Proteasomal Degradation', *Cell*, 137(1), pp. 133–145. doi: https://doi.org/10.1016/j.cell.2009.01.041.

Yaku, K. *et al.* (2018) 'NAD Metabolism in Cancer Therapeutics', *Frontiers in oncology*. Frontiers Media S.A., 8, p. 622. doi: 10.3389/fonc.2018.00622.

Yamamoto, H. *et al.* (2012) 'Atg9 vesicles are an important membrane source during early steps of autophagosome formation', *The Journal of Cell Biology*, 198(2), pp. 219 LP – 233. doi: 10.1083/jcb.201202061.

Yamamoto, H. *et al.* (2014) 'Statistical hypothesis testing of factor loading in principal component analysis and its application to metabolite set enrichment analysis', *BMC Bioinformatics*, 15(1), p. 51. doi: 10.1186/1471-2105-15-51.

Yamamoto, T. *et al.* (2014) 'Nicotinamide mononucleotide, an intermediate of NAD+ synthesis, protects the heart from ischemia and reperfusion', *PloS one*. Public Library of Science, 9(6), p. e98972.

Yambire, K. F. *et al.* (2019) 'Mitochondrial biogenesis is transcriptionally repressed in lysosomal lipid storage diseases', *eLife*. eLife Sciences Publications Limited, 8, p. e39598.

Yang, H. *et al.* (2007) 'Nutrient-sensitive mitochondrial NAD+ levels dictate cell survival', *Cell*. Elsevier, 130(6), pp. 1095–1107.

Yin, F. *et al.* (2016) 'Energy metabolism and inflammation in brain aging and Alzheimer's disease', *Free Radical Biology and Medicine*, 100, pp. 108–122. doi: https://doi.org/10.1016/j.freeradbiomed.2016.04.200.

Yoshii, S. R. *et al.* (2016) 'Systemic analysis of Atg5-null mice rescued from neonatal lethality by transgenic ATG5 expression in neurons', *Developmental cell*. Elsevier, 39(1), pp. 116–130.

Yoshikawa, S. *et al.* (2012) 'Structural studies on bovine heart cytochrome c oxidase', *Biochimica et Biophysica Acta (BBA) - Bioenergetics*, 1817(4), pp. 579–589. doi: https://doi.org/10.1016/j.bbabio.2011.12.012.

Yoshikawa, S. and Shimada, A. (2015) 'Reaction mechanism of cytochrome c oxidase', *Chemical reviews*. ACS Publications, 115(4), pp. 1936–1989.

Youdim, M. B. H. and Arraf, Z. (2004) 'Prevention of MPTP (N-methyl-4-phenyl-1, 2, 3, 6-tetrahydropyridine) dopaminergic neurotoxicity in mice by chronic lithium: involvements of Bcl-2 and Bax', *Neuropharmacology*. Elsevier, 46(8), pp. 1130–1140.

Yu, D. *et al.* (2014) 'Niemann–Pick disease type C: induced pluripotent stem cell–derived neuronal cells for modeling neural disease and evaluating drug efficacy', *Journal of biomolecular screening*. SAGE Publications Sage CA: Los Angeles, CA, 19(8), pp. 1164–1173.

Yu, T. and Lieberman, A. P. (2013) 'Npc1 acting in neurons and glia is essential for the formation and maintenance of CNS myelin', *PLoS genetics*. Public Library of Science, 9(4), p. e1003462.

Yu, W. *et al.* (2005) 'Altered Cholesterol Metabolism in Niemann-Pick Type C1 Mouse Brains Affects Mitochondrial Function', *Journal of Biological Chemistry*. American Society for Biochemistry and Molecular Biology, 280(12), pp. 11731–11739. doi: 10.1074/JBC.M412898200.

Zaidi, S. *et al.* (2014) 'The role of key residues in structure, function, and stability of cytochrome-c', *Cellular and molecular life sciences*. Springer, 71(2), pp. 229–255.

Zampieri, S. *et al.* (2009) 'Oxidative stress in NPC1 deficient cells: protective effect of allopregnanolone', *Journal of cellular and molecular medicine*. 2008/09/04. John Wiley & Sons, Ltd, 13(9B), pp. 3786–3796. doi: 10.1111/j.1582-4934.2008.00493.x.

Zhang, J. and Liu, Q. (2015) 'Cholesterol metabolism and homeostasis in the brain', *Protein & Cell*, 6(4), pp. 254–264. doi: 10.1007/s13238-014-0131-3.

Zhang, J. and Ney, P. A. (2009) 'Role of BNIP3 and NIX in cell death, autophagy, and mitophagy', *Cell death and differentiation*. Nature Publishing Group, 16(7), p. 939.

Zhang, L. *et al.* (2015) 'Modulation of mitochondrial complex I activity averts cognitive decline

in multiple animal models of familial Alzheimer's Disease', *EBioMedicine*. Elsevier, 2(4), pp. 294–305. doi: 10.1016/j.ebiom.2015.03.009.

Zhang, T. *et al.* (2016) 'Global Analysis of Cellular Protein Flux Quantifies the Selectivity of Basal Autophagy', *Cell Reports*, 14(10), pp. 2426–2439. doi: https://doi.org/10.1016/j.celrep.2016.02.040.

Zhao, Y. *et al.* (2015) 'SoNar, a highly responsive NAD+/NADH sensor, allows high-throughput metabolic screening of anti-tumor agents', *Cell metabolism*. Elsevier, 21(5), pp. 777–789.

Zhao, Y. G. and Zhang, H. (2019) 'Autophagosome maturation: An epic journey from the ER to lysosomes', *J Cell Biol*. Rockefeller University Press, 218(3), pp. 757–770.

Zhao, Y. J. *et al.* (2011) 'Cytosolic CD38 protein forms intact disulfides and is active in elevating intracellular cyclic ADP-ribose', *Journal of Biological Chemistry*. ASBMB, 286(25), pp. 22170–22177.

Zhao, Y. J. *et al.* (2015) 'Determinants of the membrane orientation of a calcium signaling enzyme CD38', *Biochimica et Biophysica Acta (BBA) - Molecular Cell Research*, 1853(9), pp. 2095–2103. doi: https://doi.org/10.1016/j.bbamcr.2014.10.028.

Zhao, Y. J., Lam, C. M. C. and Lee, H. C. (2012) 'The membrane-bound enzyme CD38 exists in two opposing orientations', *Sci. Signal.* American Association for the Advancement of Science, 5(241), pp. ra67–ra67.

Zhong, Y. *et al.* (2009) 'Distinct regulation of autophagic activity by Atg14L and Rubicon associated with Beclin 1–phosphatidylinositol-3-kinase complex', *Nature cell biology*. Nature Publishing Group, 11(4), p. 468.

Zhong, Y. *et al.* (2015) 'Application of mitochondrial pyruvate carrier blocker UK5099 creates metabolic reprogram and greater stem-like properties in LnCap prostate cancer cells in vitro', *Oncotarget*. Impact Journals LLC, 6(35), pp. 37758–37769. doi: 10.18632/oncotarget.5386.

Zhu, J., Vinothkumar, K. R. and Hirst, J. (2016) 'Structure of mammalian respiratory complex I', *Nature*. Macmillan Publishers Limited, part of Springer Nature. All rights reserved., 536, p. 354. Available at: https://doi.org/10.1038/nature19095.

Zhu, X.-H. *et al.* (2015) 'In vivo NAD assay reveals the intracellular NAD contents and redox state in healthy human brain and their age dependences', *Proceedings of the National Academy of Sciences*. National Acad Sciences, 112(9), pp. 2876–2881.

Zong, S. *et al.* (2018) 'Structure of the intact 14-subunit human cytochrome c oxidase', *Cell Research*, 28(10), pp. 1026–1034. doi: 10.1038/s41422-018-0071-1.

Zorov, D. B., Juhaszova, M. and Sollott, S. J. (2006) 'Mitochondrial ROS-induced ROS release: An update and review', *Biochimica et Biophysica Acta (BBA) - Bioenergetics*, 1757(5), pp. 509–517. doi: https://doi.org/10.1016/j.bbabio.2006.04.029.